H-78184B

PHYSICS

AUBURN UNIVERSITY

AUBURN, ALABAMA

SURFACE ANALYSIS OF SPACE TELESCOPE MATERIAL SPECIMENS
(H-78184B)

Final Report prepared for
GEORGE C. MARSHALL SPACE FLIGHT CENTER
Marshall Space Flight Center, AL 35812
June 15, 1985
by

Albert Thomas Fromhold
Department of Physics
Auburn University, AL 36849

SURFACE ANALYSIS OF SPACE TELESCOPE MATERIAL SPECIMENS (H-78184B)

FINAL REPORT
(June 15, 1985)

Albert Thomas Fromhold, Jr.
Department of Physics
Auburn University, AL 36849

Prepared for

George C. Marshall Space Flight Center
Marshall Space Flight Center, Alabama 35812

FINAL REPORT

NASA Contract H-78184B

entitled

"Surface Analysis of Space Telescope Material Specimens"

Principal Investigator: Dr. Albert T. Fromhold, Jr.
Physics Department
Auburn University, AL 36849

Co-Investigator: Dr. Kasra Daneshvar
Physics Department
Auburn University, AL 36849

ABSTRACT

Qualitative and quantitative data on Space Telescope materials which were exposed to low earth orbital atomic oxygen in a controlled experiment during the 41-G (STS-17) mission were obtained utilizing the experimental techniques of Rutherford backscattering (RBS), particle induced x-ray emission (PIXE), and ellipsometry (ELL). The techniques employed were chosen with a view towards appropriateness for the sample in question, after consultation with NASA scientific personnel who provided the material specimens. A group of eight samples and their controls selected by NASA scientists were measured before and after flight. Information reported herein include specimen surface characterization by ellipsometry techniques, a determination of the thickness of the evaporated metal specimens by RBS, and a determination of trace impurity species present on and within the surface by PIXE. The work described was undertaken for a firm-fixed price of $9900, which included use of the experimental facilities of Auburn University. The imputed costs to Auburn University greatly exceeded this amount.

INTRODUCTION

Experimental studies were made on eight flight metal specimens and on the corresponding eight control metal specimens both before the STS-17 (41-G) shuttle mission and also after flight. These data are discussed in detail in this report, which is divided into sections entitled Visual Observations, Ellipsometry Data, Rutherford Backscattering Measurements, and Proton-Induced X-Ray Emission. The conclusions reached on the basis of each of these techniques are listed in that section of the report. Recommendations for future studies are listed at the end of the report.

The purpose of the measurements described in this report was to ascertain the effects of exposure of the metal specimens to the space ambient in low earth orbit. The primary reactive species during exposure is the atomic oxygen produced by ultraviolet decomposition of the low pressure molecular oxygen which otherwise would be present at that altitude.

The data obtained in this study are for various metal specimens chosen by NASA scientists for this study. The specimens were evaporated layers of silver, gold, palladium, platinum, nickel, copper, aluminum, and chromium on metal substrates. The nominal thicknesses of the layers ranged from 500 to 5000 A. More quantitative values for the thicknesses were deduced in this study.

VISUAL OBSERVATIONS AFTER FLIGHT

Silver:

The control sample had a milky white appearance. The flight sample had a brownish color with more texture to it than the control sample. There were sharp differences in the appearance of the silver surface underneath the tabs holding the flight sample, since the tabs protected the underlying silver. Specifically, there were interference color rings proceeding outward in a concentric elliptical pattern, indicating a successively thicker surface layer as one proceeds from the most protected part of the silver surface towards the fully exposed part of that surface. There were no such interference colors under the tabs of the control sample.

Gold:

There were no visual differences between the control and flight specimens.

Palladium:

Although the differences in appearance of the control and flight specimens were slight, nevertheless the flight sample appeared less bright, and had a more milky tint.

Platinum:

There were no visual differences between the flight and control specimens.

Nickel:

There were no visual differences between the flight and control specimens.

Copper:

The flight specimen had a brown-colored appearance relative to the control specimen. Underneath the tabs holding the flight specimen, however, where the copper surface was protected from exposure, the surface had the same appearance as the surface of the control specimen.

Aluminum:

The flight sample may have a slightly more milky appearance than the control specimen.

Chromium:

There were no visual differences between the flight and control specimens.

ELLIPSOMETRY DATA

Introduction

A complete set of optical constant data were measured on the eight flight metal specimens and on the corresponding eight control metal specimens both before the STS-17 (41-G) shuttle mission and also after flight. These data, which are listed in Table 1, are discussed in detail in this section The purpose of the measurements was to ascertain the effects of exposure of the metal specimens to the space ambient in low earth orbit. The primary reactive species during exposure is the atomic oxygen produced by ultraviolet decomposition of the low pressure molecular oxygen which otherwise would be present at that altitude.

The data obtained in this study are presented in a series of bar graphs depicting the value of the optical refractive index n and the optical absorption coefficient k for the various metal specimens chosen by NASA scientists for this study. The specimens were evaporated layers of silver, gold, palladium, platinum, nickel, copper, aluminum, and chromium on metal substrates. The nominal thicknesses of the layers ranged from 500 to 5000 A, with more quantitative values for the thicknesses as deduced from our RBS data listed in Table 2. The intense mercury green line (5461 A) was employed for the measurements.

Experimental Results from Ellipsometry

In order to facilitate the interpretation of the data, it is worthwhile to describe the several types of information which are contained in the figures, and explain how this information can be extracted readily from the three different types of figure utilized. First of all, let us describe our so-called "standard" plot, an example of which is given in Fig. 1. A standard plot contains eight individual bars on a graph. Each standard plot is for one optical constant on one sample taken either prior to flight or following the flight. The optical refractive index or the optical absorption coefficient which is represented by each of the eight bars in a standard plot will be described more specifically below. Such a plot can depict either the refractive index n or the absorption coefficient k for a given elemental metal, and all data on the plot are either pre-flight or else post-flight.

Such standard plots as described above are presented in pairs in a large number of figures in this report for the purpose of drawing comparisons and obtaining other information. In each plot, data are presented for two samples of the same elemental metal. Data prior to flight for the two samples are designated as A and B, respectively.

One of the two samples was subsequenntly flown and exposed on the STS-17 mission, this sample being the one represented as B. The other of the two samples, namely the one represented as A, is the control. Post-flight data on these two samples are designated by F for the flight sample (B before flight) and C for the control sample (A before flight). Thus we have the correlation:

	BEFORE FLIGHT		AFTER FLIGHT
SAMPLE:	A	=========>	C
SAMPLE:	B	=========>	F

A given standard plot contains either A,B data or else C,F data, but is restricted to either n data or k data. On a given figure containing two such standard plots, four types of figure based on the various combinations would therefore be possible. However, we have found it useful to restrict the figures to the following three combinations.

	BEFORE FLIGHT		AFTER FLIGHT
n:	A,B	+	C,F
	+		
k:	A,B	+	C,F

The main purposes of the various figures will now be explained. Standard plot pairs illustrating n and k (n,k pairs) for a given metal before flight (A,B) indicates the overall quality of the samples, since at that point in time the data for the two specimens of a given metal should not differ in any essential way. Eight figures (Figs. 2 through 9) illustrate these results for the eight elemental metals utilized in this study.

On the other hand, standard plot pairs illustrating either n or else k for a given elemental metal before and after the flight serve two important purposes. First of all, comparison of the A and C data demonstrates the aging effect on the optical constants during the several weeks time period spanning the STS-17 mission. This aging effect must of course be factored into any changes noted in the flight sample during this period. Comparison of the B and F data in juxtaposition with the A and C data then allows one to deduce

the specific effects of exposure during the shuttle flight on the metal specimen in question. There are AB,CF plot pairs for each of the two optical constants of a given metal. With 8 different elemental metals, this gives rise to 16 figures which will be discussed below in this report.

Other types of figures are also used in this report to deduce important correlations and inclusions from the ellipsometry data. Some of these figures are made up of plots which are averages of the data presented in the standard plots. Before these figures can be explained, it is necessary to describe in greater detail the actual data contained in a given standard plot. To do this, it is helpful to refer to a specific standard plot. Fig. 1 gives the refractive index data for the two samples of chromium before the flight. The letters A and B denote the sample in question. Two of the four bars for sample A give the results of two independent determinations (labeled a and b) for a given position on the sample surface, and the other two bars for sample A give the results of two independent determinations (again labeled a and b) for a different position on the sample surface. The two positions on the sample surface are labeled 1 and 2, respectively. Good agreement between the a,b data for a given position gives confidence in the experimental precision of the measurement; good agreement between the data for positions 1 and 2 gives us confidence that the surface of the sample is homogeneous. (The sample surface actually includes the region of penetration of the light wave, which typically can be 500 A into the bulk of the metal.) The need for precision requires no explanation. The need for surface homogeneity is less specific since it is based on several considerations, one being general confidence in good sample preparation and another being the pragmatic consideration that there is no way to preserve an accurate memory of the area measured after the sample is removed from the ellipsometer. That is, the measurement does not mark the area physically, so once the sample was removed from the ellipsometer and subsequently returned for remeasurement, one must rely on the fact that the values obtained are characteristic of any part of the surface. In summary, agreement between the data labeled A.1a and A.1b demonstrates measurement precision, as also would the agreement between the data labeled A.2a and A.2b. Agreement between the A.1 and A.2 data demonstrates sample homogeneity. Exactly analogous statements can be made for the B data shown in the same standard plot, since that data is the corresponding data for the second of the two samples. Agreement between the A and B data gives us the required confidence that prior to the shuttle flight the control and flight samples are essentially the same, and if not exactly the same, at least we quantify the differences between the two samples. This represents a basic requirement for drawing meaningful conclusions by comparing the data on the two

samples after flight. It can be inferred from the standard plot for the refractive index of chromium shown in Fig. 1, for example, that the data are precise (compare A.1a and A.1b, compare A.2a and A.2b, compare B.1a and B.1b, and compare B.2a and B.2b), the surface is homogeneous (cf. A.1 and A.2 data, and also B.1 and B.2 data), and the two samples are essential identical in optical properties (compare A data with B data). It is clear that these conclusions bear the restriction that they are limited to the refractive index data, so it is necessary to make a similar comparison of the absorption coefficient data.

Each of the eight figures (Figs. 2 through 9) thus gives us in an analogous way a more or less complete picture of the optical quality of the sample it represents. It may be noted from these figures that the experimental precision is excellent for all eight specimens, and the surface homogeneity varies from excellent for Cr, Pt, Pd, and Al to very good for Cu, Pd, Au, and Ag. As might be expected, there is somewhat more variation in the sample-to-sample data for a given metal, though as already noted the data for the chromium samples are in excellent agreement. The sample to sample agreement for Au, Pd, and Ni is quite good, as can be noted from Figs. 3, 4, and 6 that for copper and aluminum is relatively good, as can be noted from Figs. 7 and 8. For Pt the agreement is quite good for the refractive index but there is a sample to sample difference of about 15% for the absorption coefficient (see Fig. 5). For silver (see Fig. 2) the agreement for the absorption coefficient from sample to sample is within about 5%, but there is a factor of 2 difference in the refractive index between the two samples. Although this difference is somewhat surprising, such differences are not uncommon in the literature. (For example, values which have been cited for the refractive index of silver vary from 0.066 to 0.240 to 3 at wavelength 6328 A.) More importantly, our observed difference turned out to be of the same order as the aging effect, which in turn was relatively small compared to the much larger changes which occurred upon exposure to the shuttle environment in orbit.

Figures 10 through 25 depict the effects of the shuttle flight exposure on the samples. Each figure contains two standard plots for the same optical constant of the same elemental metal. The standard plot in the upper half of the figure shows the pre-flight data, and the standard plot in the lower half of the figure shows the post-flight data. A study of these figures shows that by far the greatest changes which can be attributed to exposure to space environment occur for silver (see Figs. 10 and 11), these changes being very large for both the refractive index and for the absorption coefficient. Figures 14, 15, 20, 21, 24, and 25 show that changes in both optical constants because of space exposure also occur for palladium, copper, and chromium,

although the effects are not as large as for silver, and likewise but to a somewhat lesser extent in gold and aluminum. There was also a change in the refractive index of platinum (Fig. 16), but this was of the same order as the sample to sample variation in the absorption coefficient of platinum prior to flight (Fig. 17). Thus it can be said that all eight metals show some effects which can be attributed to flight exposure. These effects are analyzed somewhat more quantitatively below.

Utilizing the fact that the precision of the measurements taken on a given area of each sample at a given time was extremely good, an averaging of these data was carried out and plots were made in which the averaged data for the two spatial sites on a given sample are given as adjoining bars. Also included in this new series of plots are both A,B and C,F data for either n or else k. This type of plot differs of course from the standard plots described above and utilized to this point. On a given figure we include both the n data plot (upper half) and the k data plot (lower half of the figure). These results for the 8 elemental metals are shown in Figs. 26 through 33. A comparison of the A and C data in a given plot shows, for example, the aging effects in the control specimen over the weeks spanning the mission, whereas a corresponding comparison of the B and F data includes aging but shows especially the much larger effects produced by flight. It can be noted from Fig. 26 that the aging effect on the refractive index of silver was a factor of 2, as noted by comparing the A and C data, whereas the corresponding change due to exposure (including aging) of the flight sample was a factor of 8. It can be noted from Fig. 33 that chromium also underwent a significant aging effect. Nickel, copper, and aluminum also exhibited aging effects (see Figs. 30 through 32), whereas no aging effects could be noted for gold (see Fig. 27 and only minor aging occurred in palladium and platinum (Figs. 28 and 29).

A comparison of the A and B data in these plots (Figs. 26 through 33) also shows convincingly that the sample to sample variations are significantly smaller than the variations produced by exposure during flight as indicated by a comparison of the C and F data. For example, Fig. 27 for gold shows small sample to sample variations in n and k compared to the changes in n and k which can be attributed to flight exposure.

To emphasize the especially large space exposure effects observed for silver relative to the other metals, a separate figure (Fig. 34 shows the flight sample results for the refractive index for both gold (upper half) and silver (lower half of the figure). The 10% or so variation in n for gold due to flight exposure seems rather small compared to the factor of 8 or so variation in n for silver during the same flight exposure.

The data presented in the adjoining bars in Figs. 26 through 33 discussed above clearly demonstrate that we do not need to worry about nonhomogeneity in the surface of a given sample. Thus the data for a given sample taken at a given time can be averaged, and these averaged data can be used to make a closer comparison between data taken on a given metal specimen before and after flight. This gives us our finest representation of the effects of flight exposure on each of the elemental metals. In this third type of graph, the data for n or for k for a given sample are presented as adjoining bars, one bar denoting the pre-flight measurements and the other denoting the post-flight measurements. On a given plot, the data for both samples of a given elemental metal are given so that one has a comparison of the pre-flight and post-flight data on the flight specimen with the corresponding data on the control specimen. The n plot is then given as the upper half of the figure and the k plot is given as the lower half of the figure. These eight figures for the eight elemental metals are Figs. 35 through 42. By examining carefully these figures, one can see that the adjoining bars for the control specimen (denoted in this third type of plot as C before flight and C' after flight) do not differ very much from one another, thus showing that aging effects are really quite unimportant with the possible exception of n for silver. On the contrary, the adjoining bars for the flight specimen (denoted as F before flight and F' following flight) demonstrate the experimentally significant changes which occurred in the flight specimen during the STS-17 mission.

Although this completes our discussion of the ellipsometer results, it is interesting to show composite figures for the optical constants for the entire series of elemental metals in this study. Figures 43 through 46 show these data for both n and k before the flight and after the flight. One cannot help but note how much the optical constants differ from metal to metal, differences which are generally far greater that the variations from sample to sample of the same elemental metal and the variations which can be attributed to exposure to space environment. The exception to this general observation is silver, which under space exposure takes on optical characteristics which could be typical of some entirely different metal.

RUTHERFORD BACKSCATTERING MEASUREMENTS

Introduction

The objectives of the RBS measurements were to determine the sample thickness before flight as an independent check on the thickness deduced from the evaporation monitor, and to ascertain whether any significant surface layers were formed during flight or whether any significant decreases in thickness due to surface erosion occurred during flight. Figure 47 illustrates the sample thicknesses obtained prior to and following the flight. These thicknesses are also listed in Table 2. A comparison of the RBS data taken after flight with that taken before flight shows some differences, but these differences are for the most part not systematic enough or sufficiently large to be considered statistically significant, with the possible exception of silver where a 40% increase in thickness was indicated for the flight specimen.

The primary RBS data are given in Figs. 48 through 79. These figures were used to obtain the thicknesses shown in Fig. 47, and in addition, they illustrate a number of interesting qualitative effects.

RBS Results for Silver:

The RBS spectrum for the Ag control and flight samples before the flight are shown in Figs. 48 and 49. The width of the tall peak on the right side of the figure is used to deduce the thickness of the silver layer. (These are the thicknesses which are listed in Table 2; note that they are initially in the range of 2300 angstroms.) The portion of the spectrum to the left in the figure is produced by the substrate, which in the present case is aluminum,as confirmed by the PIXE data. The spectra of the two samples can be noted to be essentially the same at this point in time, namely, prior to the shuttle flight. The corresponding spectra measured after the flight are shown in Figs. 50 and 51. Notice first of all that the two spectra after the flight are qualitatively quite different. Then note by comparison of Figs. 50 and 51 after the flight with corresponding data before the flight (Figs. 48 and 49) that the control sample manifests the same qualitative spectra before and after flight, whereas the flight sample manifests quite different qualitative spectra before and after the flight. The conclusion, of course, is that exposure of the silver to the atomic oxygen atmosphere in low earth orbit produces large changes in the silver. A comparison of the spectra after flight (Figs. 50 and 51) shows three distinct effects:

(a) The flight spectrum indicates a silver layer which is thicker physically than that of the control specimen.

(b) The region of the flight spectrum produced by the silver is rounded instead of being squared off, which indicates nonhomogeneity of the silver near the interfaces.

(c) The portion of the flight spectrum produced by the substrate is more rounded than that of the control specimen, which indicates the presence of oxygen in the silver.

The thicknesses of the flight and control samples obtained from the after-flight spectra are listed in Table 2. The ratio of the thicknesses obtained before and after flight for the two samples (viz., control and flight specimens) are also given in the table. The numbers indicate that the flight sample is approximately 40% thicker after flight, which is attributed principally to the oxidation of the silver in the atomic oxygen atmosphere.

RBS Results for Gold:

The RBS spectrum for the Au control and flight samples before the flight are shown in Figs. 52 and 53. The width of the tall peak on the right side of the figure can be noted to be much greater than that for silver. This width is used to deduce the thickness of the metal layer. These thicknesses, which are listed in Table 2, are in the range of 5000 angstroms. The portion of the spectrum to the left in the figure is again produced by the substrate, which in the present case is also aluminum (cf. PIXE Results). The spectra of the two samples can be noted to be essentially the same at this point in time, namely, prior to the shuttle flight. The corresponding spectra measured after the flight are shown in Figs. 54 and 55. Notice that in this particular case of gold the two spectra after the flight are qualitatively the same as before flight. Furthermore, except for the signal to noise ratio, which is determined by the integration time and does not reflect any intrinsic property of the samples, the spectra after the shuttle flight are qualitatively no different than the spectra before the flight. This contrasts markedly with the case of silver, where the flight specimen manifested a quite different appearance following exposure during flight. The conclusion for gold, then, is that exposure to the atomic oxygen atmosphere in low earth orbit produced almost no change detectable by RBS. The thicknesses of the flight and control samples obtained from the after-flight spectra are listed in Table 2. The ratio of the thicknesses obtained before and after flight for the two samples (viz., control and flight specimens) are also given in this table. The numbers verify that almost no change occurred during flight.

RBS Results for Palladium:

The RBS spectrum for the Pd control and flight samples before the flight are shown in Figs. 56 and 57. The width of the tall peak on the right side of the figure can be noted to be much greater than that of most of the other samples. This width yields thicknesses in the range of 6000 angstroms, as can be noted from Table 2. The portion of the spectrum to the left in the figure is again produced by the substrate, which in the present case is again aluminum. The spectra of the two samples can be noted to be essentially the same at this point in time, namely, prior to the shuttle flight. The corresponding spectra measured after the flight are shown in Figs. 58 and 59. Notice that as in the case of gold, the two spectra after the flight for palladium are qualitatively the same as before flight. Furthermore, there are no qualitative differences in the spectra which can be attributed to the flight. Table 2 shows no thickness differences produced by flight to within a precision better than 5%. The conclusion for palladium, then, is the same as that for gold, namely that exposure to the atomic oxygen atmosphere in low earth orbit produced almost no change detectable by RBS.

RBS Results for Platinum:

The RBS spectrum for the Pt control and flight samples before the flight are shown in Figs. 60 and 61. The width of the tall peak on the right side of the figure is not very large, and this is reflected in the sample thicknesses deduced (viz., approximately 500 angstroms). (These thicknesses are listed in table 2.) The substrate is again aluminum. The spectra of the two samples can be noted to be essentially the same. The corresponding spectra measured after the flight are shown in Figs. 62 and 63. Notice that, as in the case of gold, the two spectra after the flight are qualitatively the same as before flight, except for the irrelevant matter of the difference in the signal to noise ratios because of the different integration times. As contrasted to the case of gold, however, there is an increase in the measured thickness of the flight sample relative to the control sample: Whereas the ratio of the thickness of the two samples (flight to control) prior to flight was 1.002, the corresponding ratio after flight was found to be 1.211. (See Table 2.) The conclusion is that the atomic oxygen atmosphere in low earth orbit produced a change in the platinum sample thickness which was detectable by RBS. The PIXE data also lead to this same conclusion.

RBS Results for Nickel:

The RBS spectrum for the Ni control and flight samples before the flight are shown in Figs. 64 and 65. The width of the tall peak on the right side of the figure gives the sample thicknesses listed in Table 2. The thicknesses are in the range of 2000 angstroms. The portion of the spectrum to the left in the figure is again produced by the substrate, which in the present case is again aluminum. The spectra of the two samples can be noted to be essentially the same at this point in time, namely, prior to the shuttle flight. The corresponding spectra measured after the flight are shown in Figs. 66 and 67. Notice that two spectra after the flight for palladium are qualitatively similar to those before flight. However, careful examination indicates that there is a qualitative difference in the region of the spectrum to the left (i.e., the substrate produced portion) which can be attributed to the flight. Specifically, it can be noted that the spectrum edge in the flight specimen is more rounded after flight that that of the control specimen, which indicates an interdiffusion at the interface. Table 2 shows no thickness differences produced by flight to within a precision better than 5%. Note also from Fig. 67 for the flight specimen after flight that there is a bump in the spectrum between the Ni and the substrate portions. This indicates some element in the Cr, Mn, Fe weight range lighter than nickel is present on the surface of the flight sample which is not on the control specimen. This conclusion is confirmed by the PIXE data.

RBS Results for Copper:

The RBS spectrum for the Cu control and flight samples before the flight are shown in Figs. 68 and 69. The widths of each small peak on the right side of the figure is used to deduce the thickness of the metal layers. The thicknesses, as listed in Table 2, are of the order of 2000 angstroms. The substrate is again aluminum. The spectra of the two samples can be noted to be essentially the same. The corresponding spectra measured after the flight are shown in Figs. 70 and 71. Notice that the two spectra after the flight are qualitatively the same as before flight. Furthermore, except for the signal to noise ratio, the spectra after the shuttle flight are qualitatively no different than the spectra before the flight. Table 2 shows that within 5% precision there is no change in the thickness produced by flight. As for the case of gold, the conclusion is that exposure to the atomic oxygen atmosphere in low earth orbit produced almost no change detectable by RBS. This was an unexpected finding, because visually the flight sample looked darker than the control sample after flight (cf. Visual Observations Section).

RBS Results for Aluminum:

The RBS results for aluminum were not as definitive as for the other metals, as can be appreciated by looking at the spectra before flight (Figs. 72 and 73) and after flight (Figs. 74 and 75). Because the peaks are not well pronounced, there was great difficulty in obtain good estimates for the sample thickness. The source of the difficulty was the substrate material, namely stainless steel, which is heavier than aluminum so that the Al peak is superimposed on the substrate spectrum. From Table 2, it can be noted that no definitive thicknesses were obtained before flight, whereas the data taken after the flight gave thicknesses in the 1100 to 1300 angstrom range. There were no qualitative differences, apart from signal to noise ratio, to be noted in the spectra of the two samples taken before and after flight.

RBS Results for Chromium:

Figures 76 and 77 illustrate the RBS data for Cr for the control and flight specimens before flight. Qualitatively there is no difference to be noted in the spectra. The thicknesses as listed in Table 2 are in the range of 800 angstroms. Figures 78 and 79 show the corresponding spectra after the flight. Qualitatively there are no differences to be noted in the portion of the spectrum due to the chromium but note from Fig. 79 that there is a bump on the substrate portion of the spectrum for the flight sample. This indicates that the flight sample has an oxygen concentration which is not present in the control sample. This is most likely in the form of an oxide greater than 100 angstroms in thickness on the surface of the chromium. Although both the flight specimen and the control specimen appear to have decreased in thickness over the period of time spanning the flight, but with such thin metal films, it is difficult to access whether this is a real effect or simply due to lack of precision in the measurements.

PROTON-INDUCED X-RAY EMISSION

Introduction

The objectives of the PIXE measurements were to provide an independent confirmation of the specimen elemental metal, to ascertain the major impurity metals, and to see what trace impurities are present on the sample surfaces after the flight. In particular it was considered likely that the trace impurities on the surface might be different for the flight and control specimens due to the chemical reactions with atomic oxygen which were possible for the flight specimens.

The primary PIXE data are given in Figs. 80 through 95. The trace metals indicated by the spectra are indicated on each figure in question, and a summary of the results for each metal specimen is given in the discussion below. The conclusions to be reached are that the evaporated metal films did contain significant impurity metal concentrations, and there were differences in the trace impurities on the sample surfaces depending upon whether or not the sample was a flight or a control sample. The amount of information obtained is large in volume and varied in nature, so the reader is invited to extract the particular information which has a bearing on his particular question at the moment.

Shown in Fig. 96 is the Iron 55 calibration curve utilized in the data analysis.

Experimental Results

PIXE Results for Silver:

The x-ray spectrum for the Ag control sample is shown in Fig. 80 and that for the corresponding flight sample is shown in Fig. 81. Impurities to be noted from the spectrum are Si and Mn. The substrate material is primarily Al. The ratio of the x-ray line intensity of the flight sample to that of the control sample was found to be 1.21, which is indicative of the relative number of Ag atoms in these two metal films. The conclusion is that the flight sample has more Ag than the control sample. This is in qualitative agreement with the RBS results, which gave 1.42 as the corresponding ratio.

PIXE Results for Gold:

The x-ray spectrum for the Au control sample is shown in Fig. 82 and that for the corresponding flight sample is shown in Fig. 83. The substrate material is primarily Al. The ratio of the x-ray line intensity of the flight sample to that of the control sample was found to be 1.Ø5. The conclusion is that, within experimental error, the flight sample has approximately the same amount of Au as the control sample.

PIXE Results for Palladium:

The x-ray spectrum for the Pd control sample is shown in Fig. 84 and that for the corresponding flight sample is shown in Fig. 85. The one impurity to be noted from the spectrum is Cr. The substrate material is primarily Al. The ratio of the x-ray line intensity of the flight sample to that of the control sample was approximately 1, indicating that the flight and control samples contained essentially the same amounts of palladium. There were, however, approximately 4Ø% fewer Cr impurity atoms on the control sample than on the flight sample.

PIXE Results for Platinum:

The x-ray spectrum for the Pt control sample is shown in Fig. 86 and that for the Pt flight sample is shown in Fig. 87. The substrate material is primarily Al. The ratio of the x-ray line intensity of the flight sample to that of the control sample was found to be 1.14. The conclusion is that the flight sample has more Pt than the control sample. This is in qualitative agreement with the RBS results, which gave 1.21 as the corresponding ratio.

PIXE Results for Nickel:

The x-ray spectrum for the Ni control sample is shown in Fig. 88 and that for the corresponding flight sample is shown in Fig. 89. Impurities to be noted from the spectrum are very low concentrations of Cr, Fe, and Mn. The substrate material is primarily Al. The ratio of the x-ray line intensity of the flight sample to that of the control sample did not indicate any differences between the control and flight specimens.

PIXE Results for Copper:

The x-ray spectrum for the Cu control sample is shown in Fig. 90 and that for the Cu flight sample is shown in Fig. 91. Impurities to be noted from the spectrum are Si, S, Cr, Fe, and Ni. The substrate material is primarily Al. The ratio of the x-ray line intensity of the flight sample to that of the control sample was found to be approximately 1, so the flight sample had the same number of Cu atoms as the control sample.

PIXE Results for Aluminum:

The x-ray spectrum for the Al control sample is shown in Fig. 92 and that for the corresponding flight sample is shown in Fig. 93. Impurities to be noted from the spectrum are S, Cr, Fe, and Ni. The substrate material is stainless steel. The ratio of the x-ray line intensity of the flight sample to that of the control sample was found to be 0.85, which indicates that the flight sample has fewer Cr atoms than the control sample. The Cr, Fe, and Ni concentrations were the same for the flight and control samples, which is to be expected since the substrate is stainless steel. The S concentration was lower by 15% in the flight sample, the same as the difference in the amount of Al in the two films.

PIXE Results for Chromium:

The x-ray spectrum for the Cr control sample is shown in Fig. 94 and that for the corresponding flight sample is shown in Fig. 95. The substrate material is primarily Al. The ratio of the x-ray line intensity of the flight sample to that of the control sample was found to be 1.07, indicating that the flight sample had somewhat more Cr atoms that the control specimen. An impurity to be noted from the spectrum is Cu, which decreased by about 15% for the flight specimen relative to the control specimen.

Comments:

It may be noted that the spectra for the flight and control specimens of a given metal often have a different signal to noise ratio. This is not due to any fundamental difference in the two specimens, but instead is to the fact that the exposure time to the proton beam was notexactly the same for the two. This was taken into account in the normalization process in reducing the data. Probably this does lead to some greater uncertainty in the results than might be the case had the exposure times been chosen to be exactly the same.

The depth of the sample region probed is also of interest when studying the data. The fall-off distance of the proton beam in the silver specimens, for example, is estimated to be approximately 1000 angstroms.

It should be noted that PIXE does not detect the extremely light mass elements, such as carbon, oxygen, and fluorine. It may be safely said that no elements lighter than fluorine appear in the spectra.

RECOMMENDATIONS FOR FUTURE STUDIES

It is recommended that a series of measurements be carried out on carefully prepared single crystals of copper, silver and nickel of at least two crystal orientations. It would be advisable to utilize at least three different temperatures.

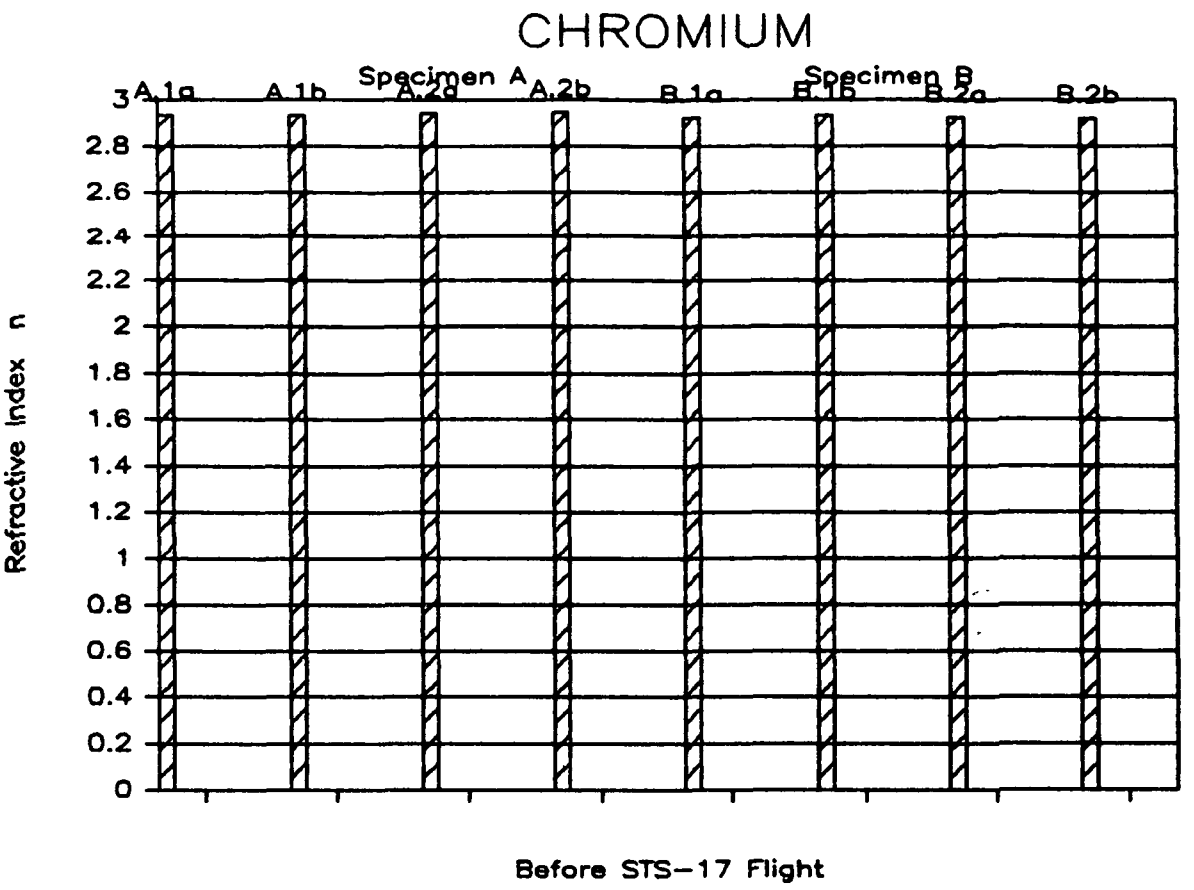

Fig. 1. Ellipsometry Data
(Standard Plot)

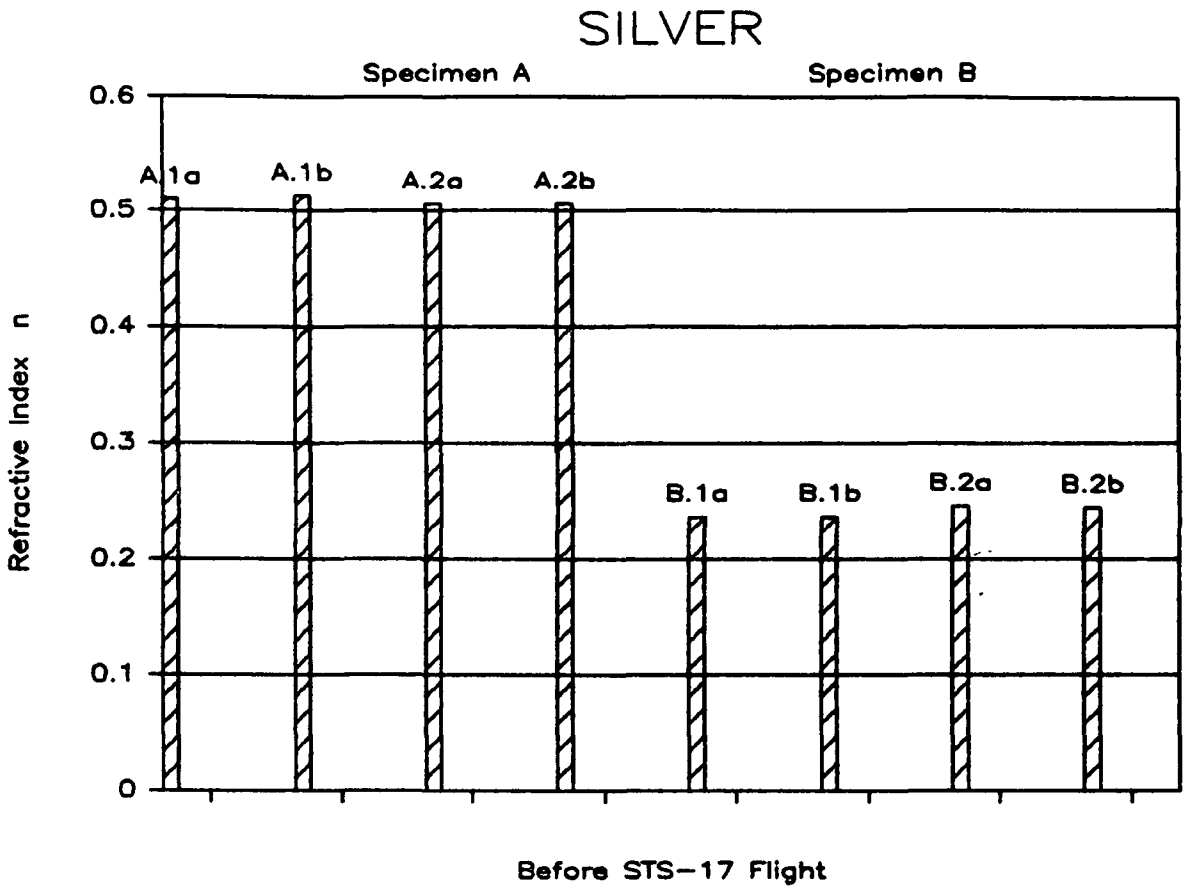
SILVER
Specimen A
Specimen B
0.6
0.5
0.4
0.3
0.2
0.1
0
A.1a
A.1b
A.2a
A.2b
B.1a
B.1b
B.2a
B.2b
Refractive Index n
Before STS-17 Flight

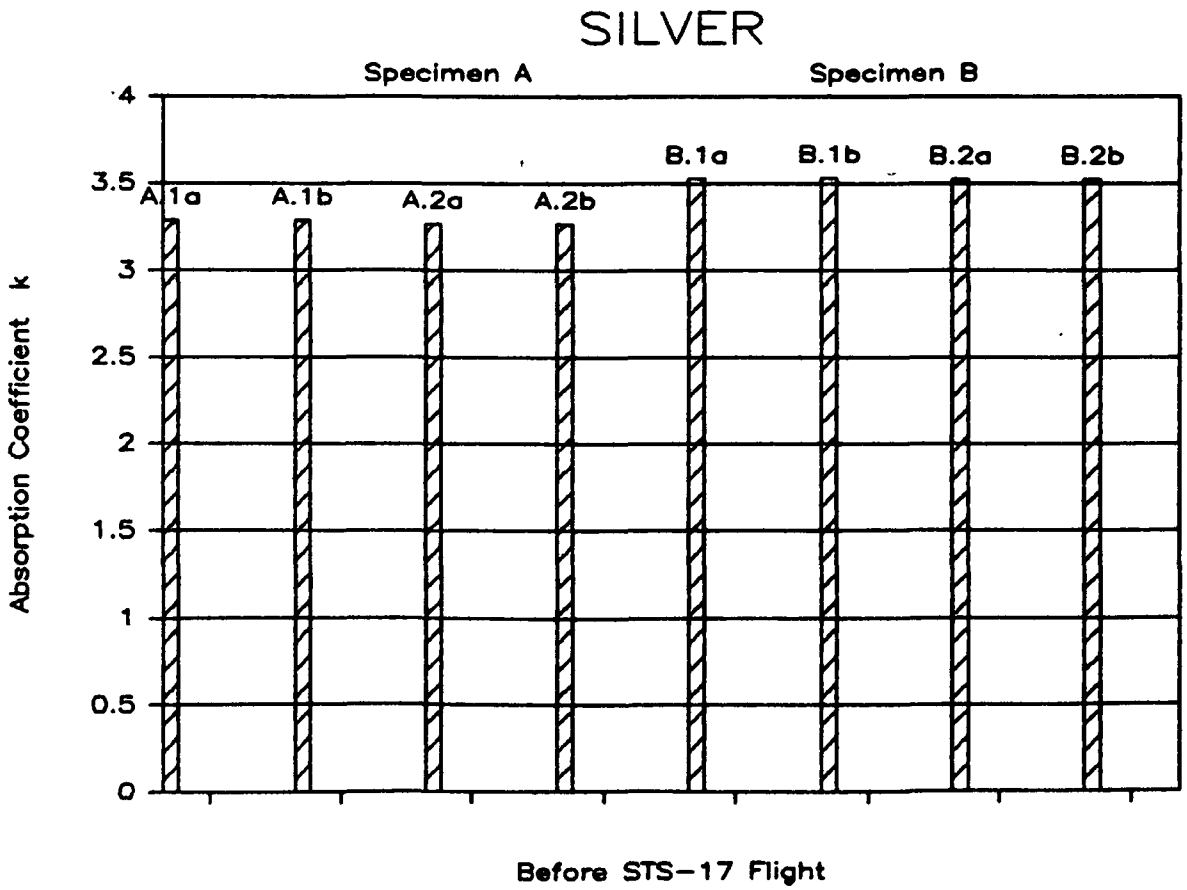
SILVER
Specimen A
Specimen B
4
3.5
3
2.5
2
1.5
1
0.5
0
A.1a
A.1b
A.2a
A.2b
B.1a
B.1b
B.2a
B.2b
Absorption Coefficient k
Before STS-17 Flight

Fig. 2

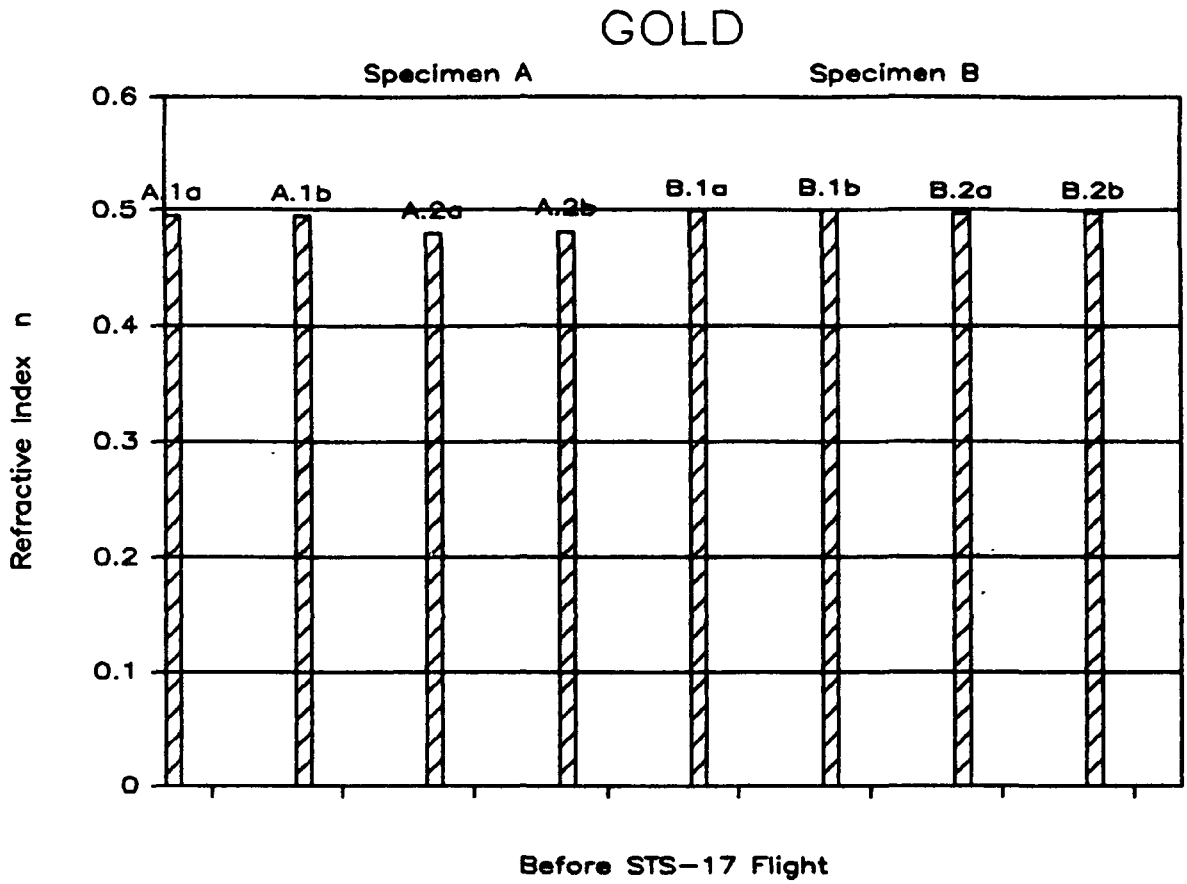
GOLD
Specimen A
Specimen B
0.6
0.5
0.4
0.3
0.2
0.1
0
A.1a
A.1b
A.2a
A.2b
B.1a
B.1b
B.2a
B.2b
Refractive Index n
Before STS-17 Flight

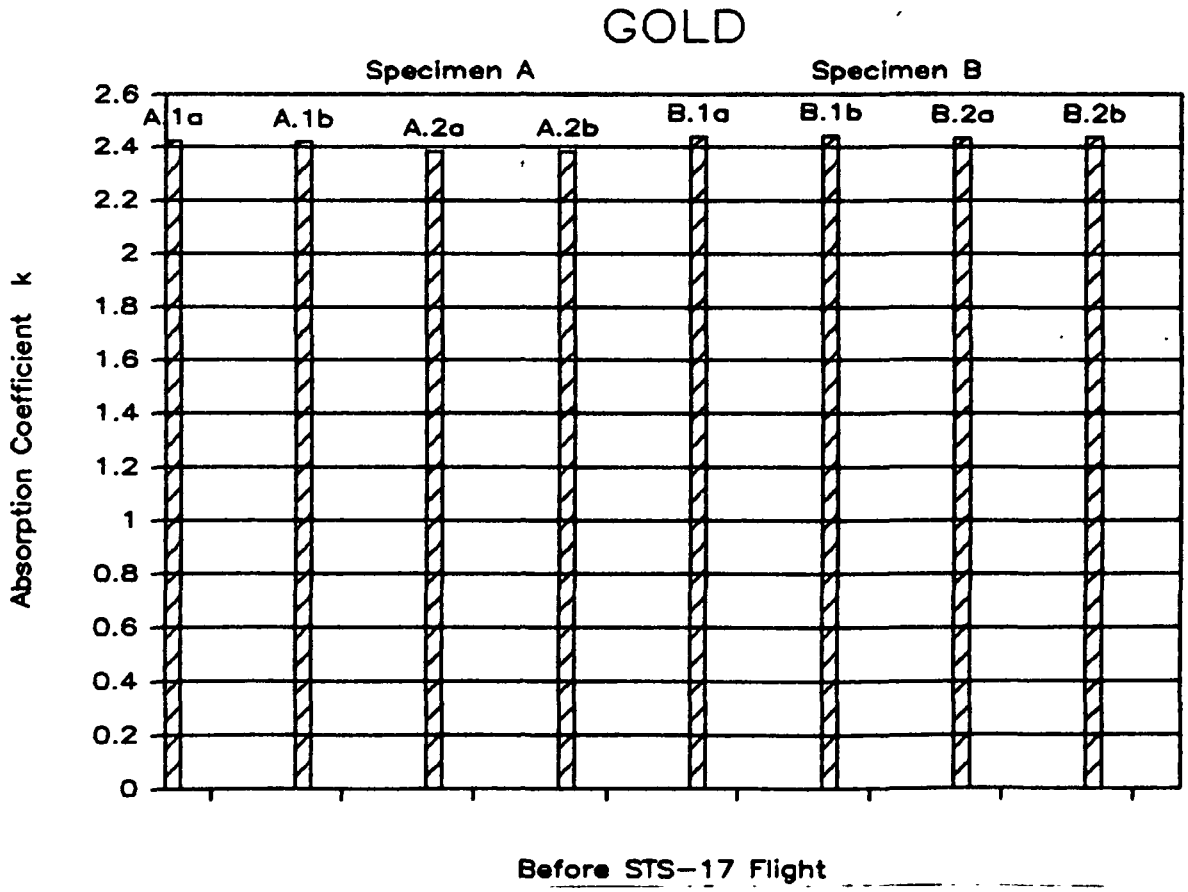
GOLD
Specimen A
Specimen B
2.6
2.4
2.2
2
1.8
1.6
1.4
1.2
1
0.8
0.6
0.4
0.2
0
A.1a
A.1b
A.2a
A.2b
B.1a
B.1b
B.2a
B.2b
Absorption Coefficient k
Before STS-17 Flight

Fig. 3

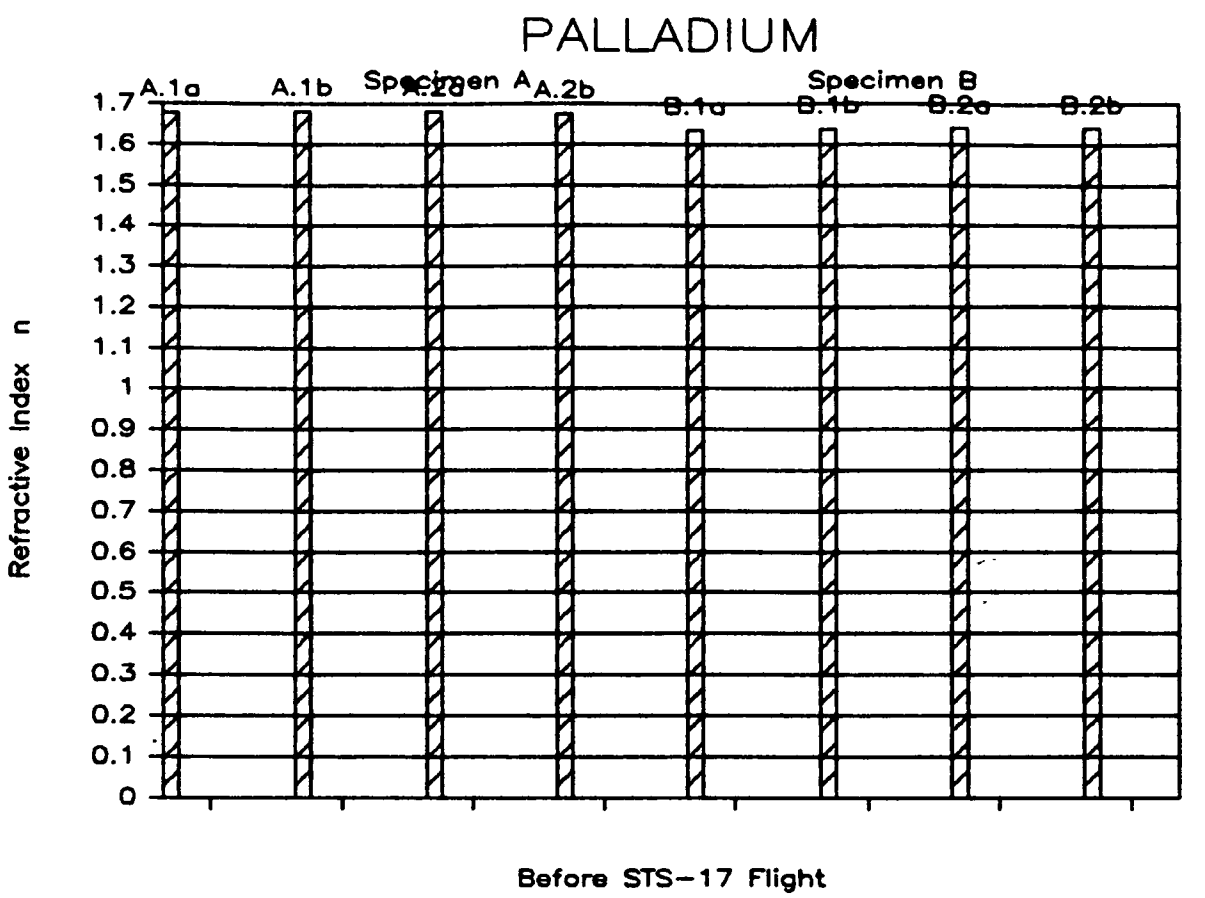
PALLADIUM
Specimen A
Specimen B
A.1a
A.1b
A.2a
A.2b
B.1a
B.1b
B.2a
B.2b
1.7
1.6
1.5
1.4
1.3
1.2
1.1
1
0.9
0.8
0.7
0.6
0.5
0.4
0.3
0.2
0.1
0
Refractive Index n
Before STS-17 Flight

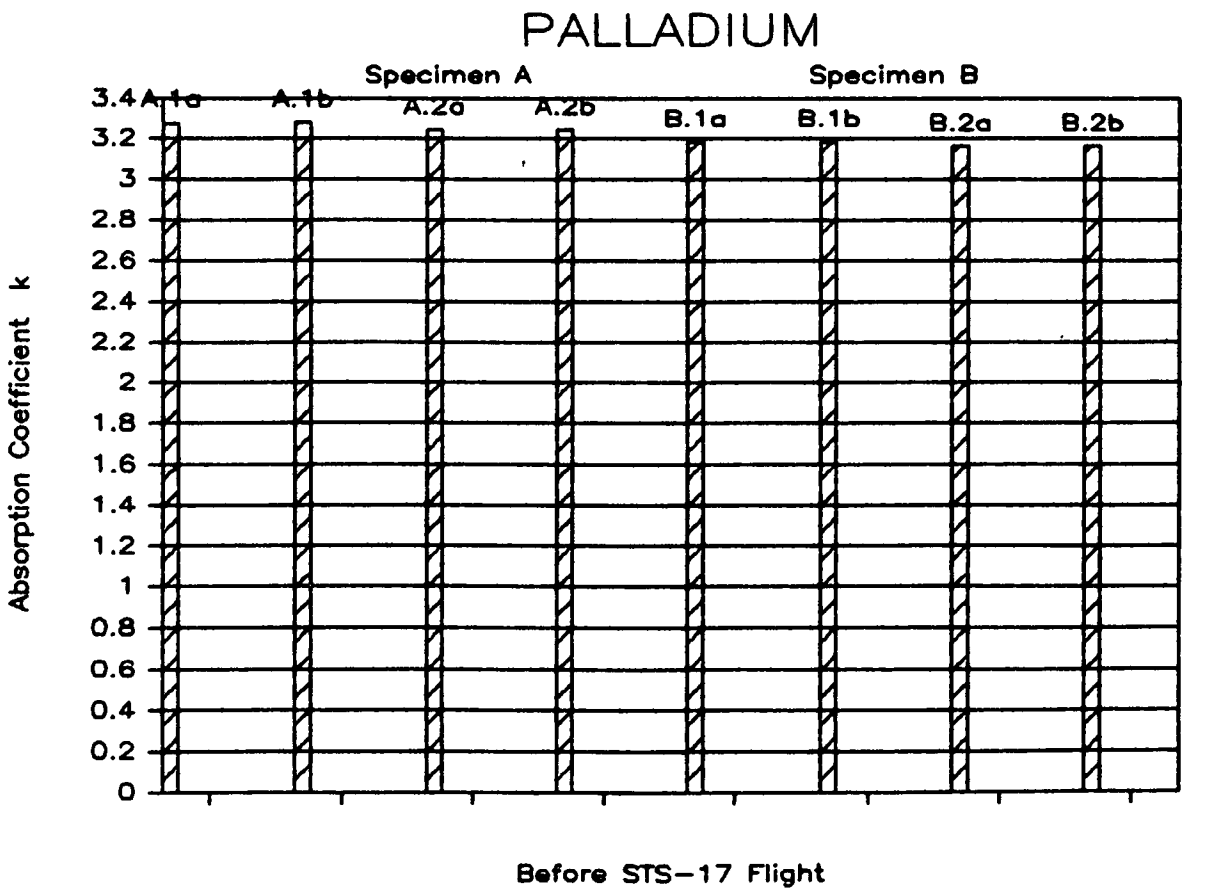
PALLADIUM
Specimen A
Specimen B
A.1a
A.1b
A.2a
A.2b
B.1a
B.1b
B.2a
B.2b
3.4
3.2
3
2.8
2.6
2.4
2.2
2
1.8
1.6
1.4
1.2
1
0.8
0.6
0.4
0.2
0
Absorption Coefficient k
Before STS-17 Flight

Fig. 4

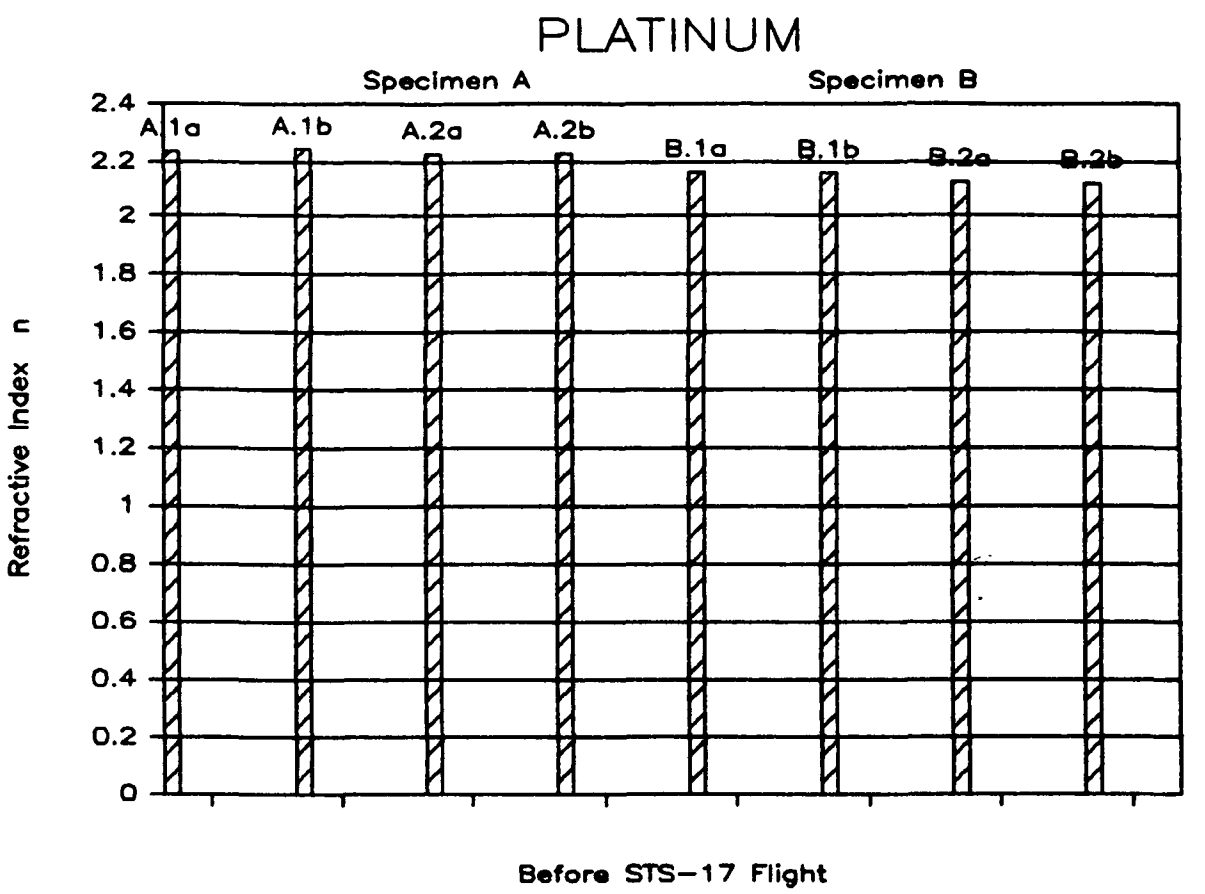
PLATINUM
Specimen A
Specimen B
A.1a
A.1b
A.2a
A.2b
B.1a
B.1b
B.2a
B.2b
2.4
2.2
2
1.8
1.6
1.4
1.2
1
0.8
0.6
0.4
0.2
0
Refractive Index n
Before STS-17 Flight

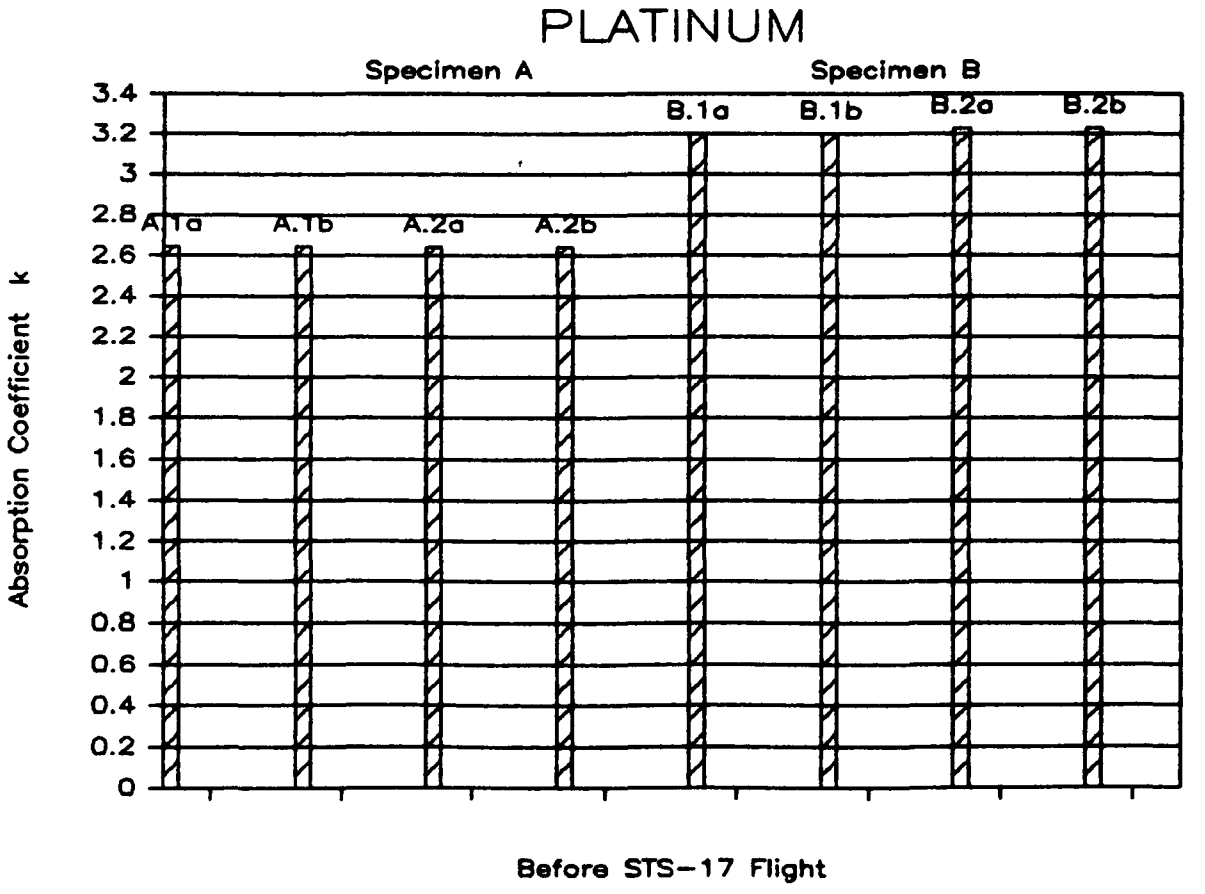
PLATINUM
Specimen A
Specimen B
A.1a
A.1b
A.2a
A.2b
B.1a
B.1b
B.2a
B.2b
3.4
3.2
3
2.8
2.6
2.4
2.2
2
1.8
1.6
1.4
1.2
1
0.8
0.6
0.4
0.2
0
Absorption Coefficient k
Before STS-17 Flight

Fig. 5

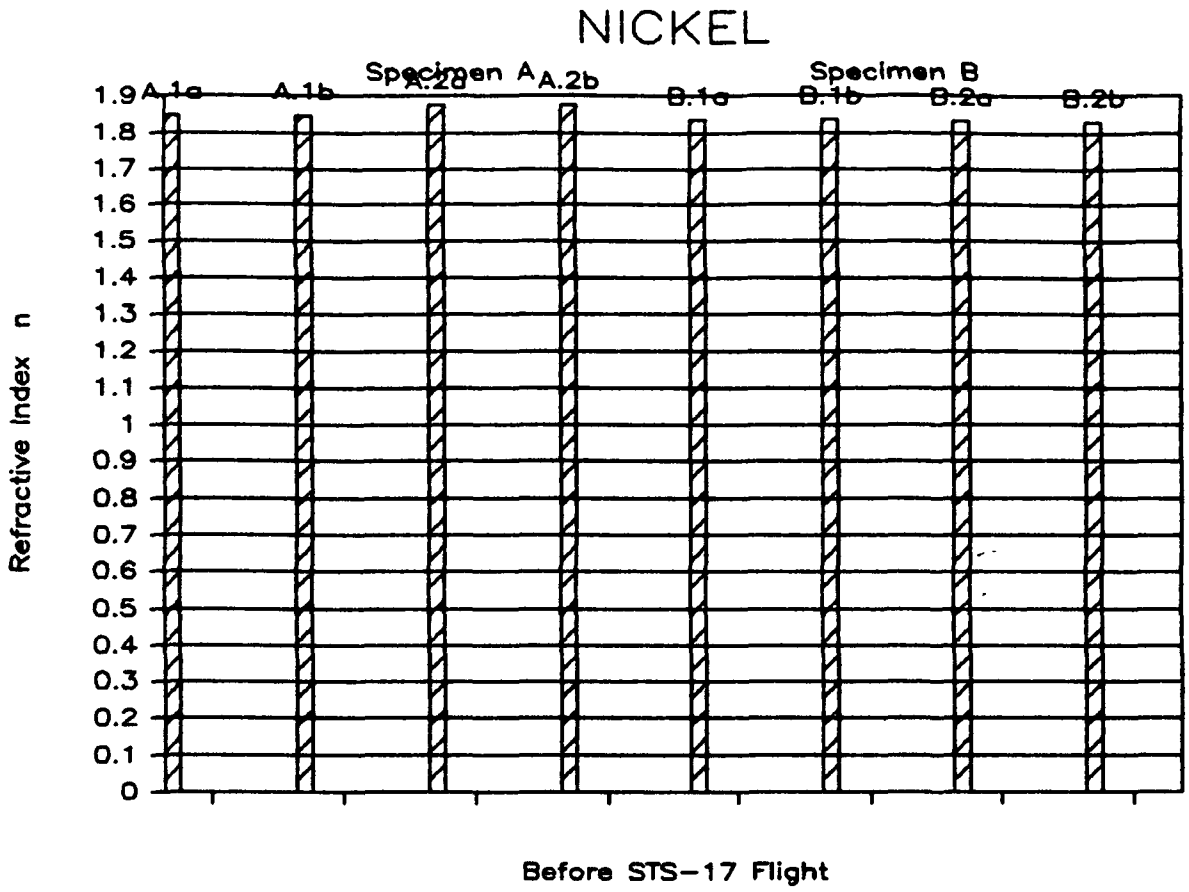
NICKEL
Specimen A
Specimen B
A.1a
A.1b
A.2a
A.2b
B.1a
B.1b
B.2a
B.2b
Refractive Index n
1.9
1.8
1.7
1.6
1.5
1.4
1.3
1.2
1.1
1
0.9
0.8
0.7
0.6
0.5
0.4
0.3
0.2
0.1
0
Before STS-17 Flight

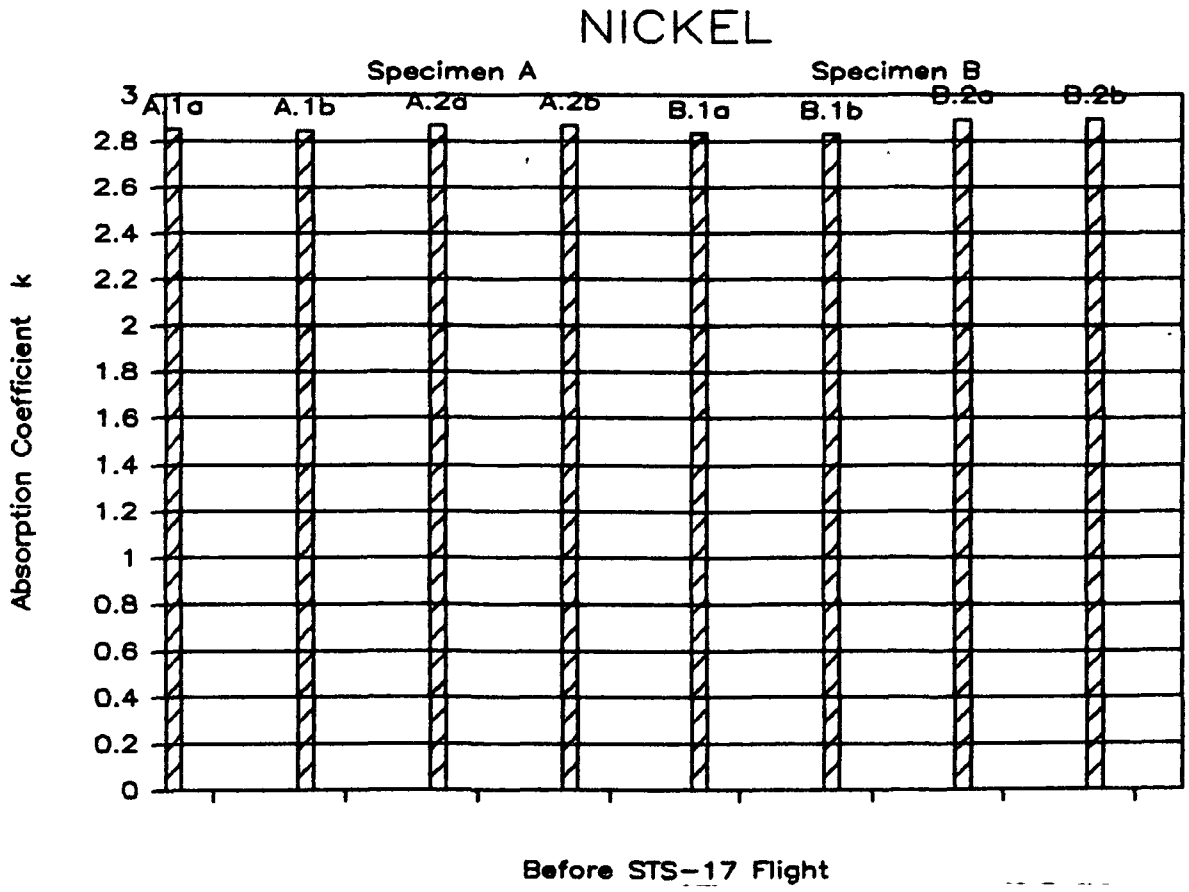
NICKEL
Specimen A
Specimen B
A.1a
A.1b
A.2a
A.2b
B.1a
B.1b
B.2a
B.2b
Absorption Coefficient k
3
2.8
2.6
2.4
2.2
2
1.8
1.6
1.4
1.2
1
0.8
0.6
0.4
0.2
0
Before STS-17 Flight

Fig. 6

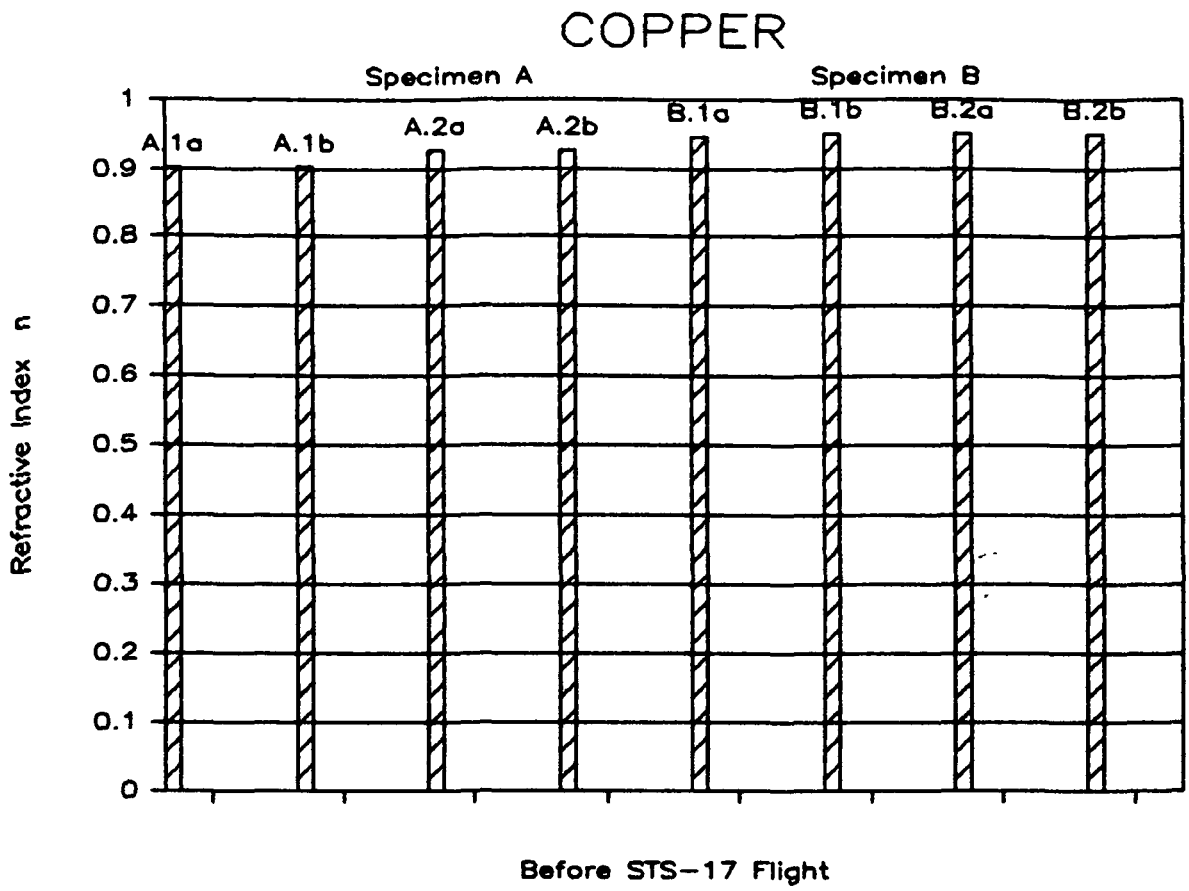
COPPER
Specimen A
Specimen B
A.1a
A.1b
A.2a
A.2b
B.1a
B.1b
B.2a
B.2b
Refractive Index n
1
0.9
0.8
0.7
0.6
0.5
0.4
0.3
0.2
0.1
0
Before STS-17 Flight

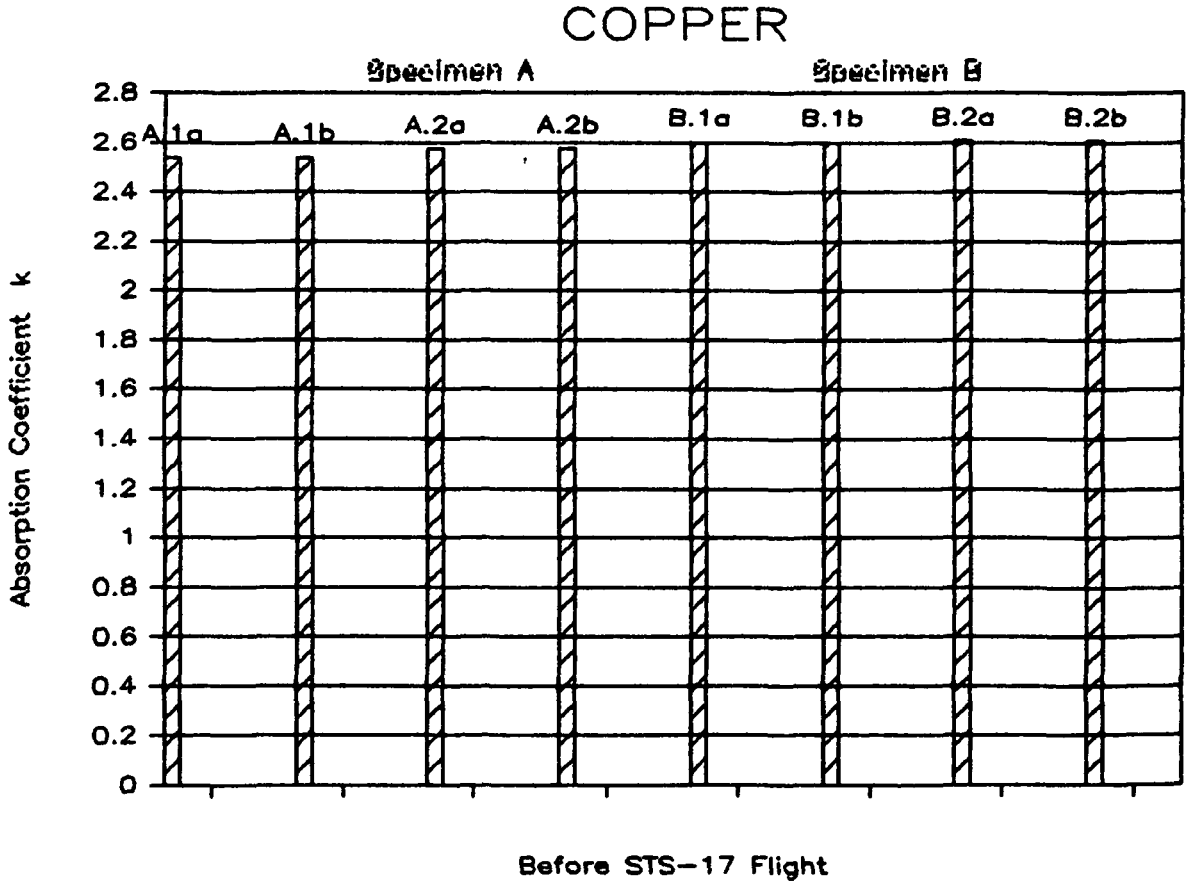
COPPER
Specimen A
Specimen B
A.1a
A.1b
A.2a
A.2b
B.1a
B.1b
B.2a
B.2b
Absorption Coefficient k
2.8
2.6
2.4
2.2
2
1.8
1.6
1.4
1.2
1
0.8
0.6
0.4
0.2
0
Before STS-17 Flight

Fig. 7

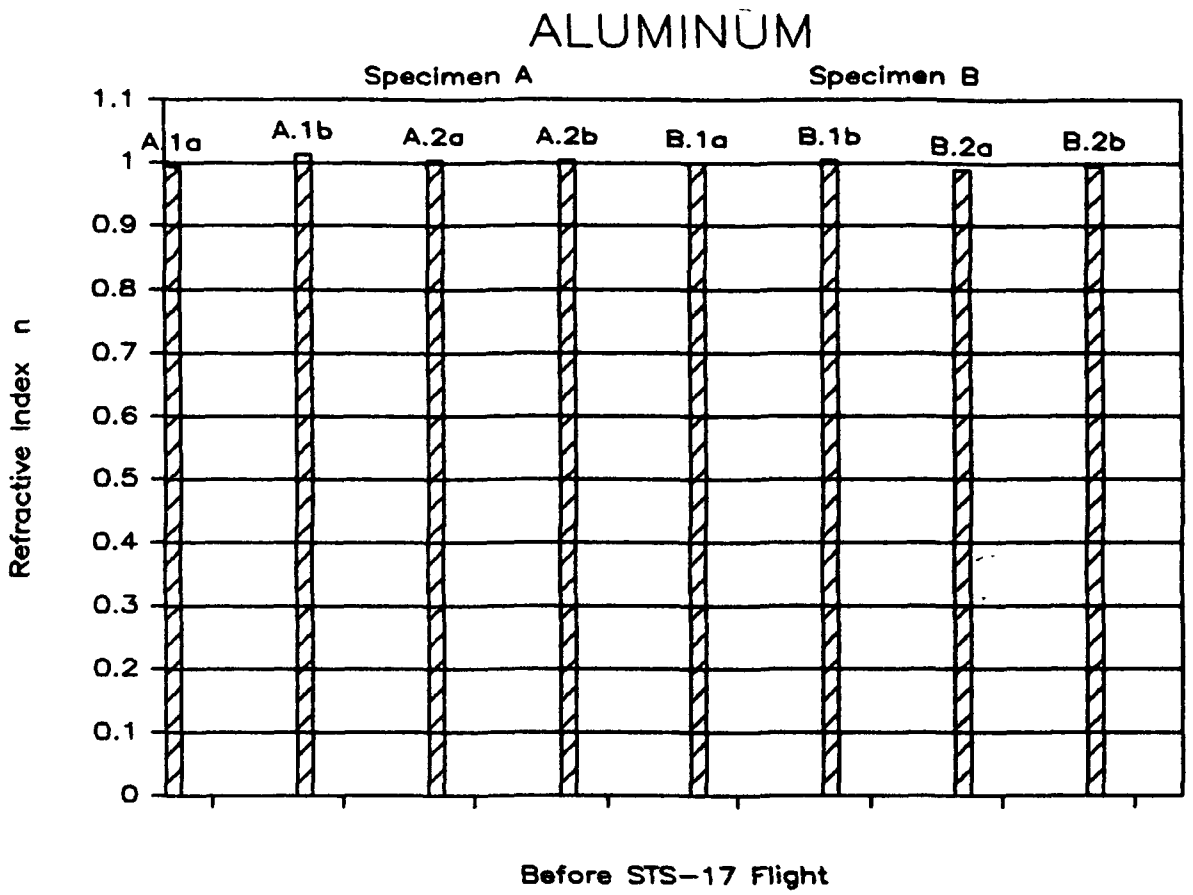
ALUMINUM
Specimen A
Specimen B
A.1a
A.1b
A.2a
A.2b
B.1a
B.1b
B.2a
B.2b
1.1
1
0.9
0.8
0.7
0.6
0.5
0.4
0.3
0.2
0.1
0
Refractive Index n
Before STS-17 Flight

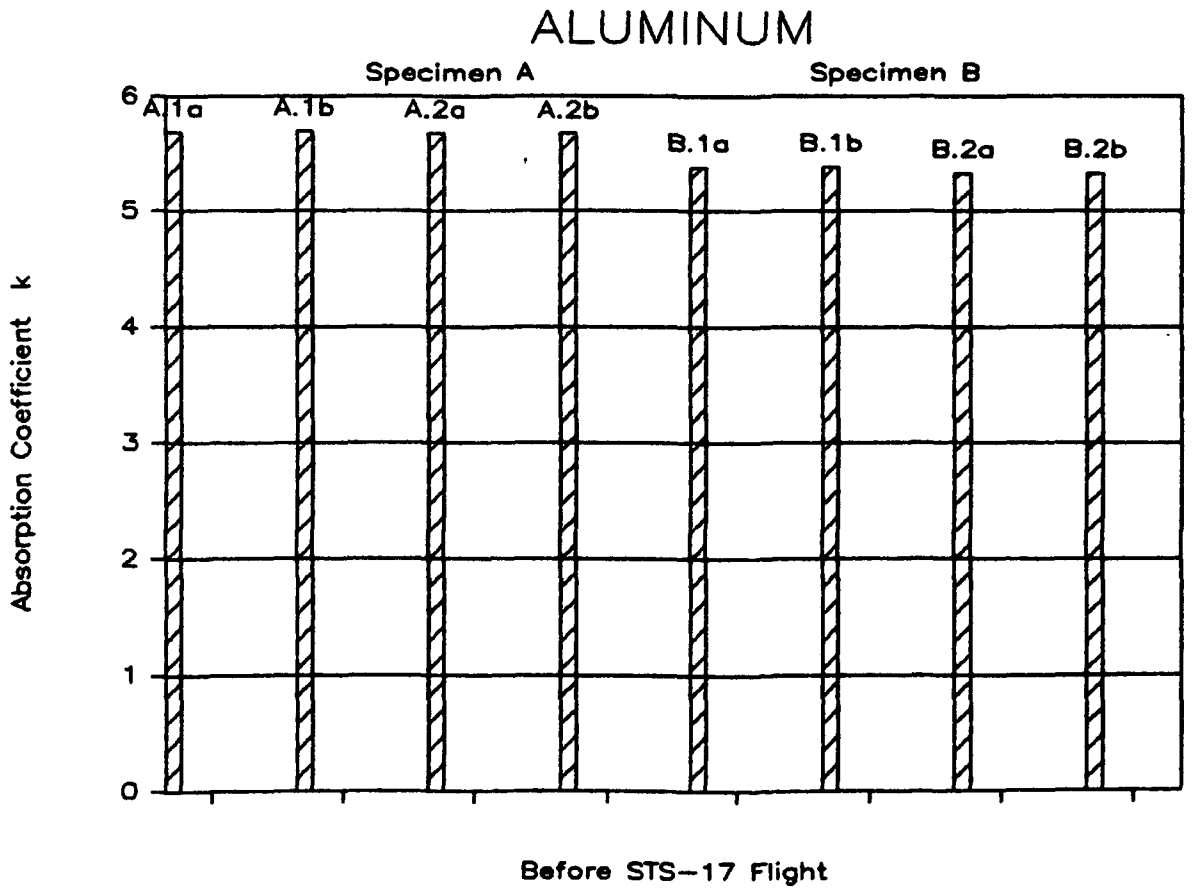
ALUMINUM
Specimen A
Specimen B
A.1a
A.1b
A.2a
A.2b
B.1a
B.1b
B.2a
B.2b
6
5
4
3
2
1
0
Absorption Coefficient k
Before STS-17 Flight

Fig. 8

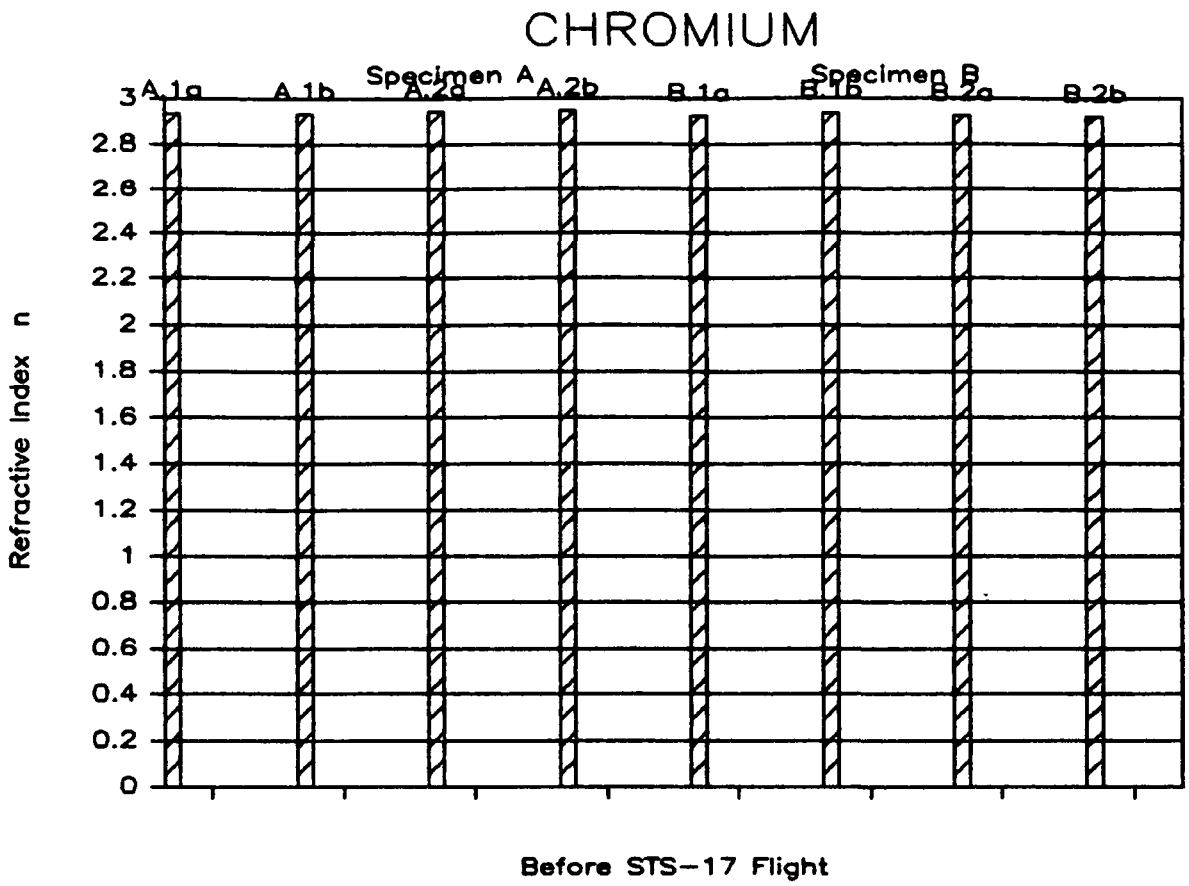
CHROMIUM
Specimen A
Specimen B
A.1a
A.1b
A.2a
A.2b
B.1a
B.1b
B.2a
B.2b
3
2.8
2.6
2.4
2.2
2
1.8
1.6
1.4
1.2
1
0.8
0.6
0.4
0.2
0
Refractive Index n
Before STS-17 Flight

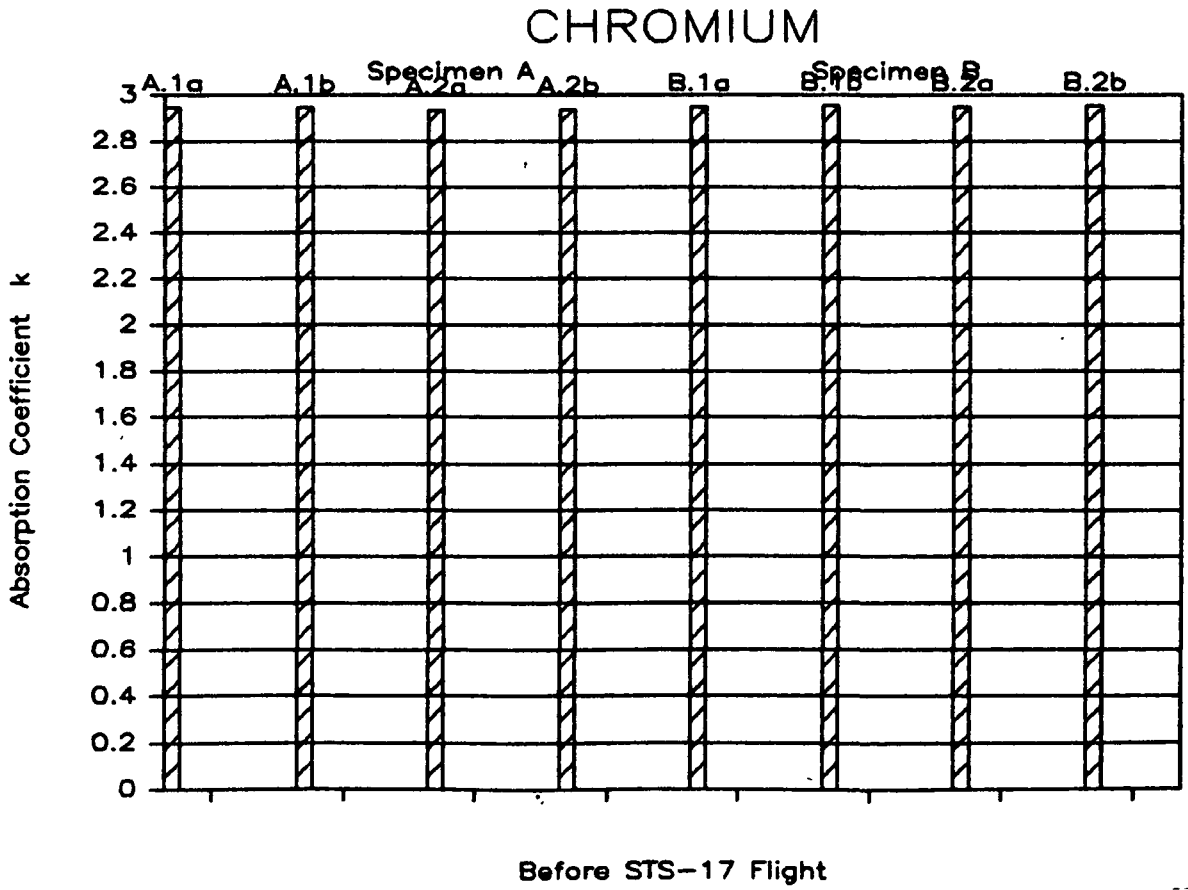
CHROMIUM
Specimen A
Specimen B
A.1a
A.1b
A.2a
A.2b
B.1a
B.1b
B.2a
B.2b
3
2.8
2.6
2.4
2.2
2
1.8
1.6
1.4
1.2
1
0.8
0.6
0.4
0.2
0
Absorption Coefficient k
Before STS-17 Flight

Fig. 9

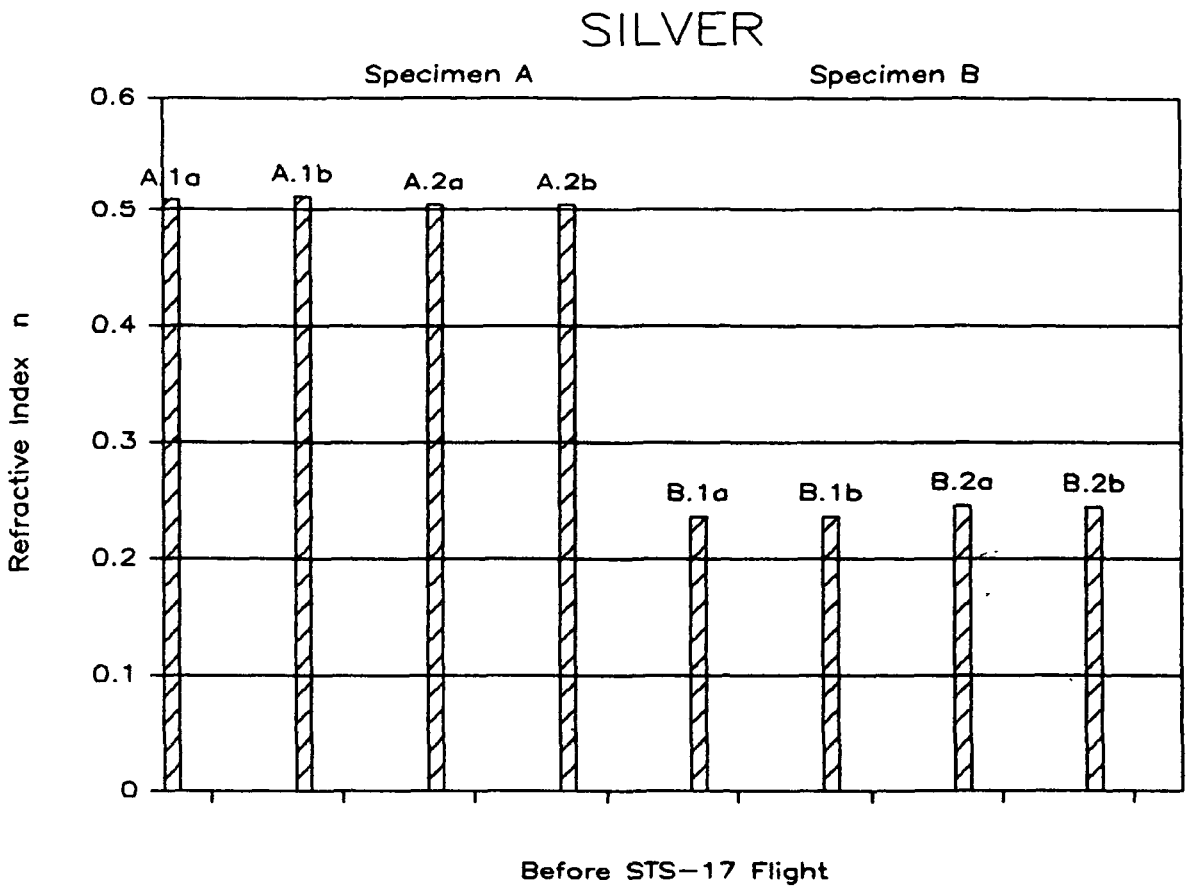
SILVER
Specimen A
Specimen B
0.6
0.5
0.4
0.3
0.2
0.1
0
A.1a
A.1b
A.2a
A.2b
B.1a
B.1b
B.2a
B.2b
Refractive Index n
Before STS-17 Flight

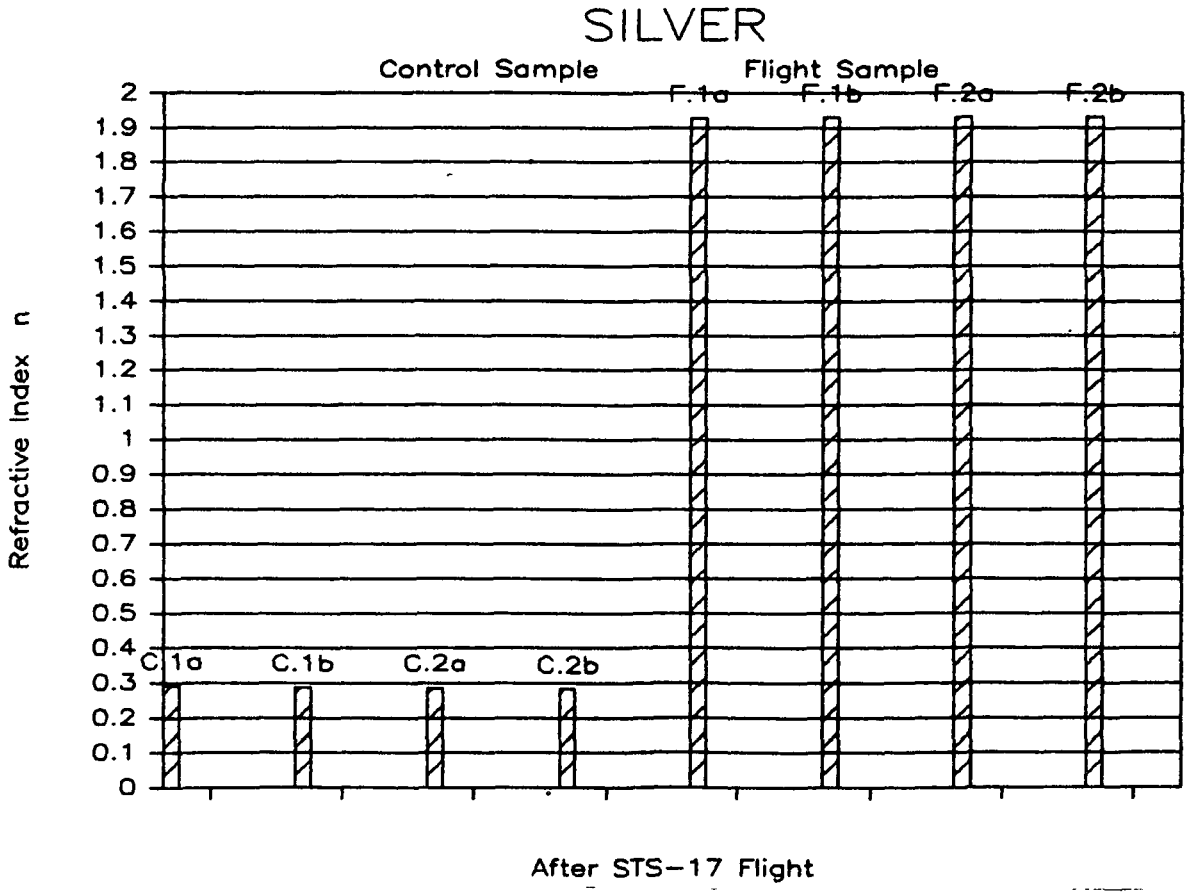
SILVER
Control Sample
Flight Sample
2
1.9
1.8
1.7
1.6
1.5
1.4
1.3
1.2
1.1
1
0.9
0.8
0.7
0.6
0.5
0.4
0.3
0.2
0.1
0
C.1a
C.1b
C.2a
C.2b
F.1a
F.1b
F.2a
F.2b
Refractive Index n
After STS-17 Flight

Fig. 10

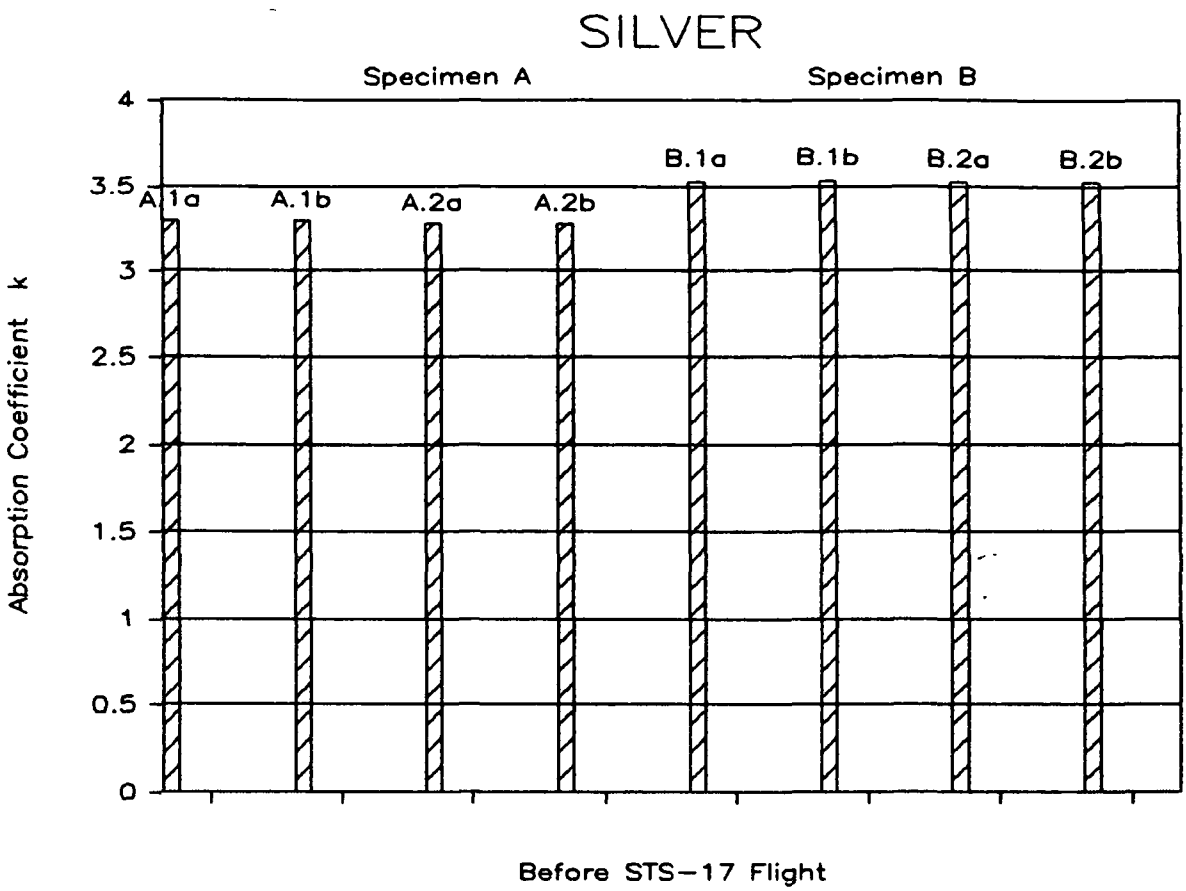
SILVER
Specimen A
Specimen B
A.1a
A.1b
A.2a
A.2b
B.1a
B.1b
B.2a
B.2b
Absorption Coefficient k
4
3.5
3
2.5
2
1.5
1
0.5
0
Before STS–17 Flight

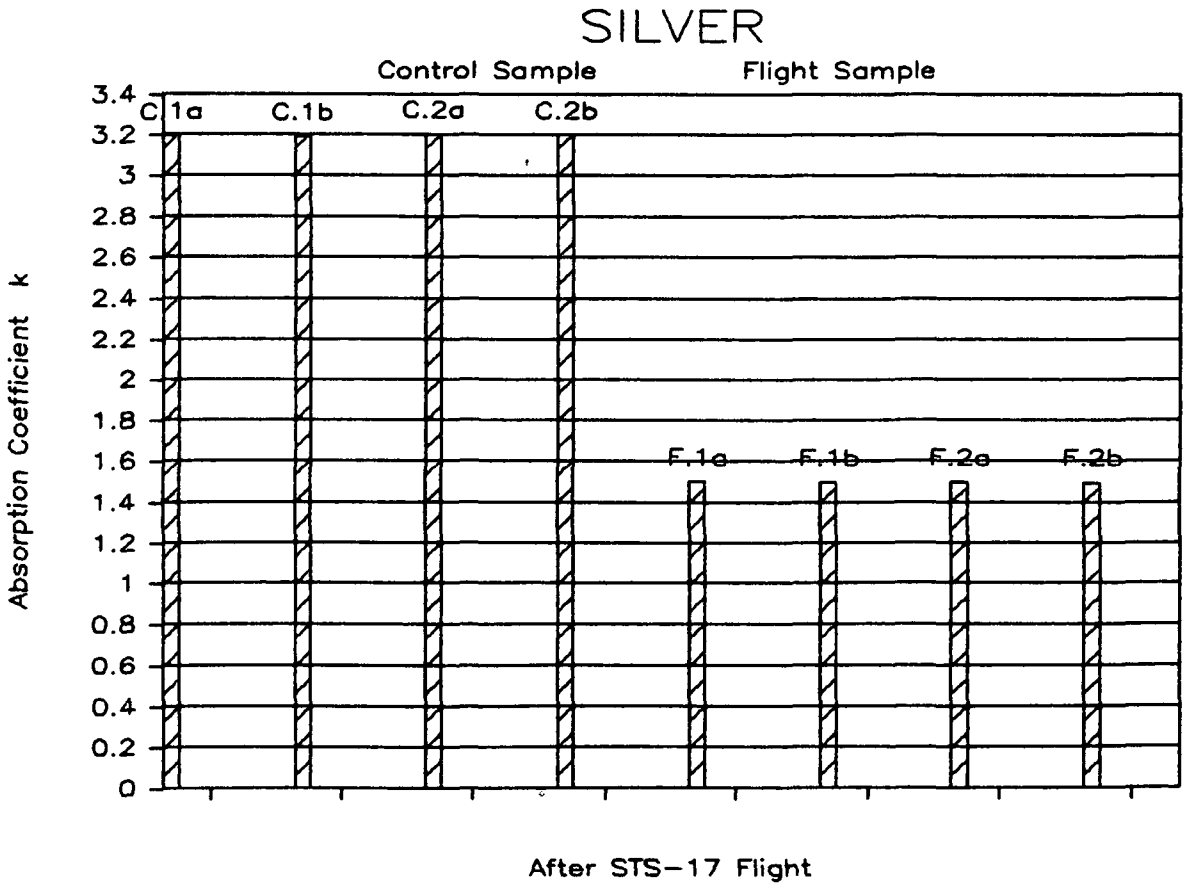
SILVER
Control Sample
Flight Sample
C.1a
C.1b
C.2a
C.2b
F.1a
F.1b
F.2a
F.2b
Absorption Coefficient k
3.4
3.2
3
2.8
2.6
2.4
2.2
2
1.8
1.6
1.4
1.2
1
0.8
0.6
0.4
0.2
0
After STS–17 Flight

Fig. 11

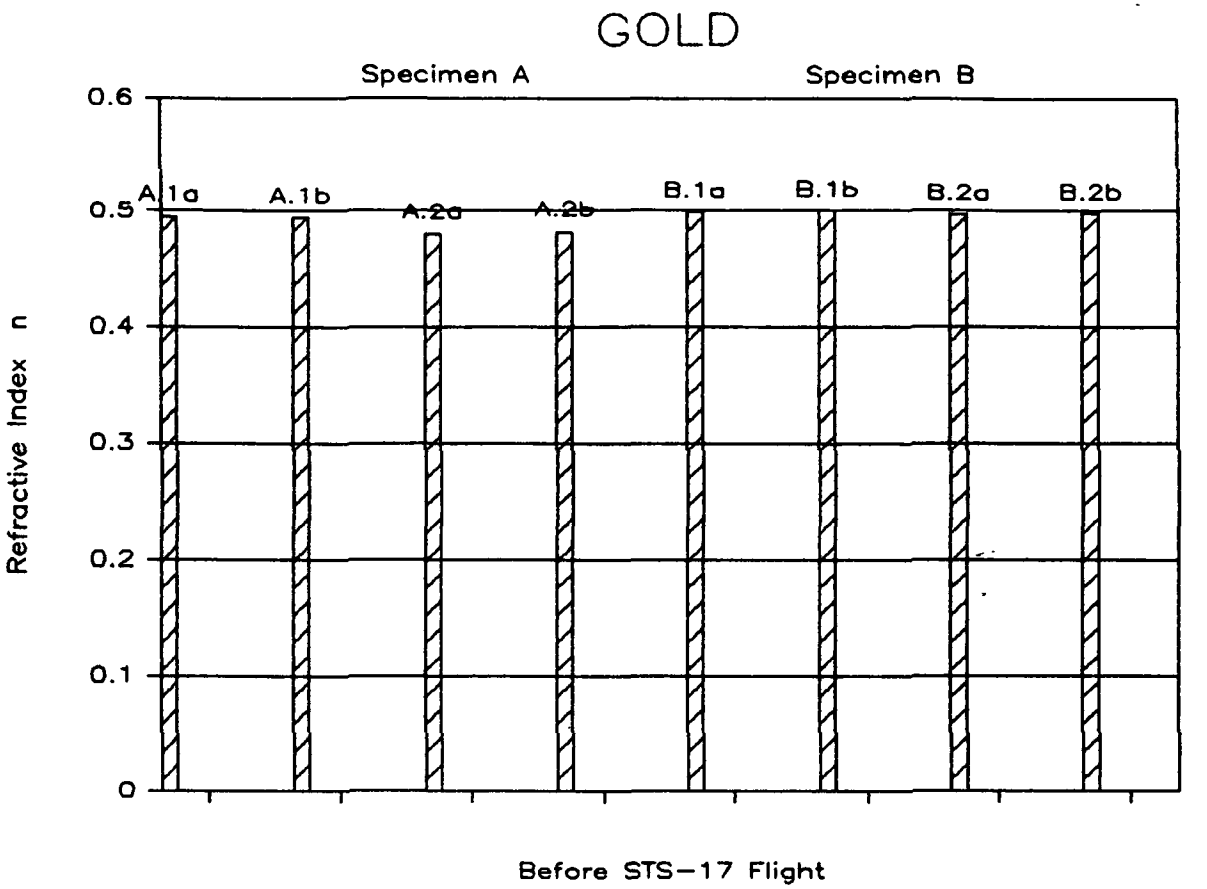
GOLD
Specimen A
Specimen B
0.6
0.5
0.4
0.3
0.2
0.1
0
A.1a
A.1b
A.2a
A.2b
B.1a
B.1b
B.2a
B.2b
Refractive Index n
Before STS-17 Flight

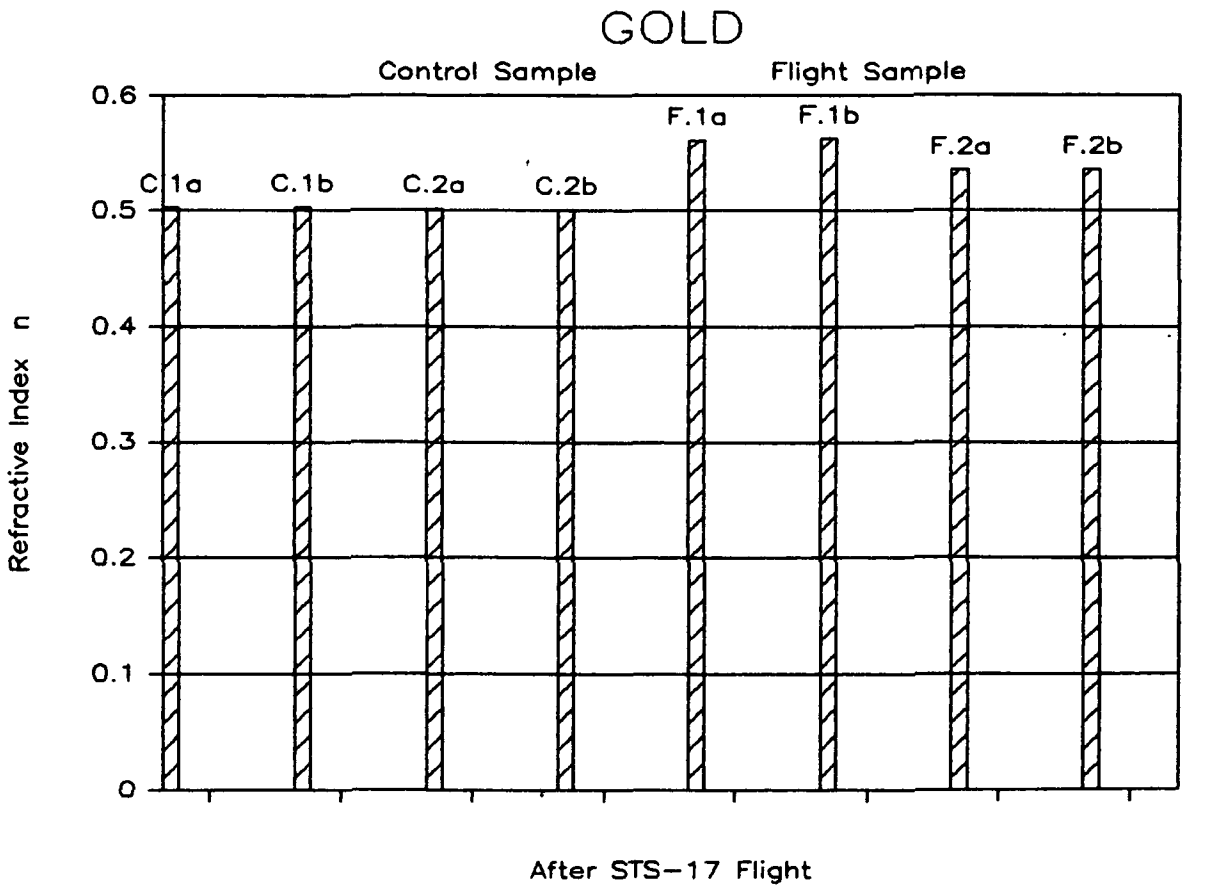
GOLD
Control Sample
Flight Sample
0.6
0.5
0.4
0.3
0.2
0.1
0
C.1a
C.1b
C.2a
C.2b
F.1a
F.1b
F.2a
F.2b
Refractive Index n
After STS-17 Flight

Fig. 12

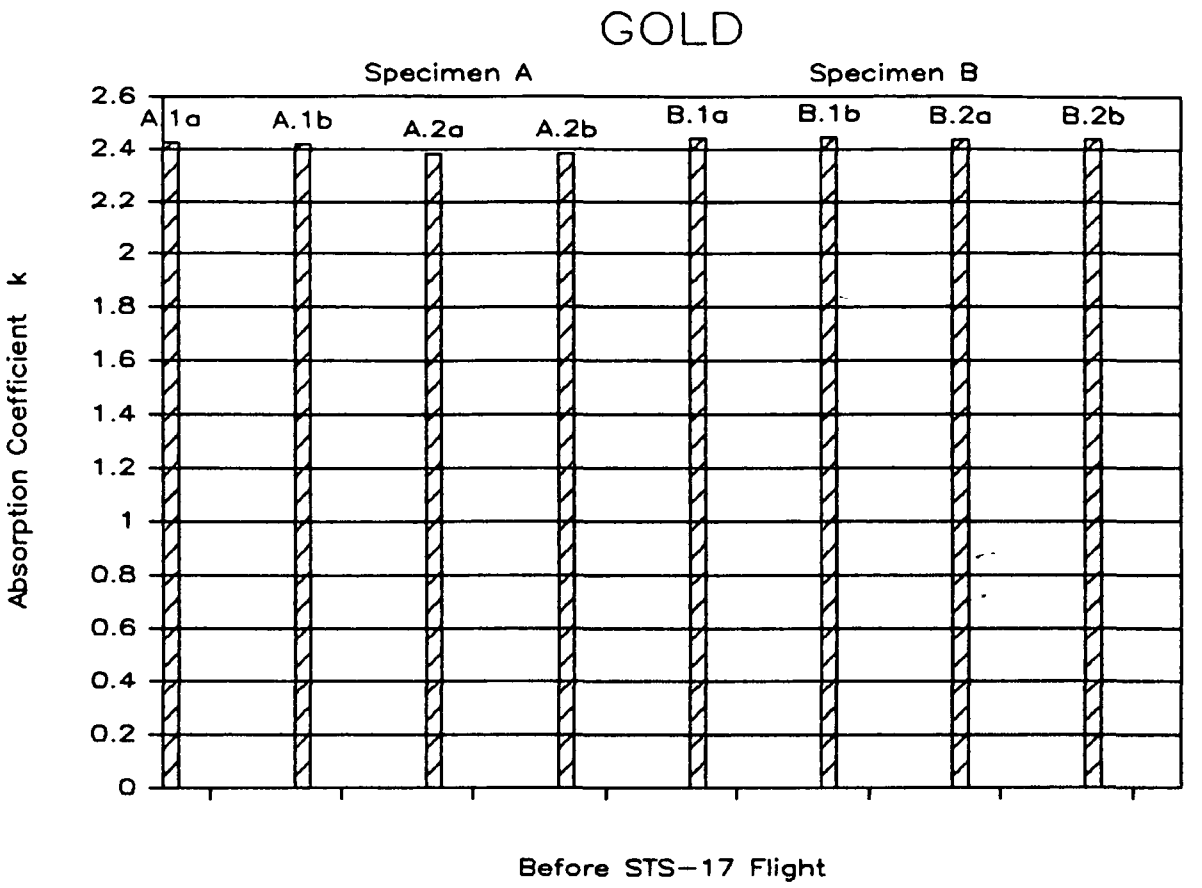
GOLD
Specimen A
Specimen B
A.1a
A.1b
A.2a
A.2b
B.1a
B.1b
B.2a
B.2b
2.6
2.4
2.2
2
1.8
1.6
1.4
1.2
1
0.8
0.6
0.4
0.2
0
Absorption Coefficient k
Before STS-17 Flight

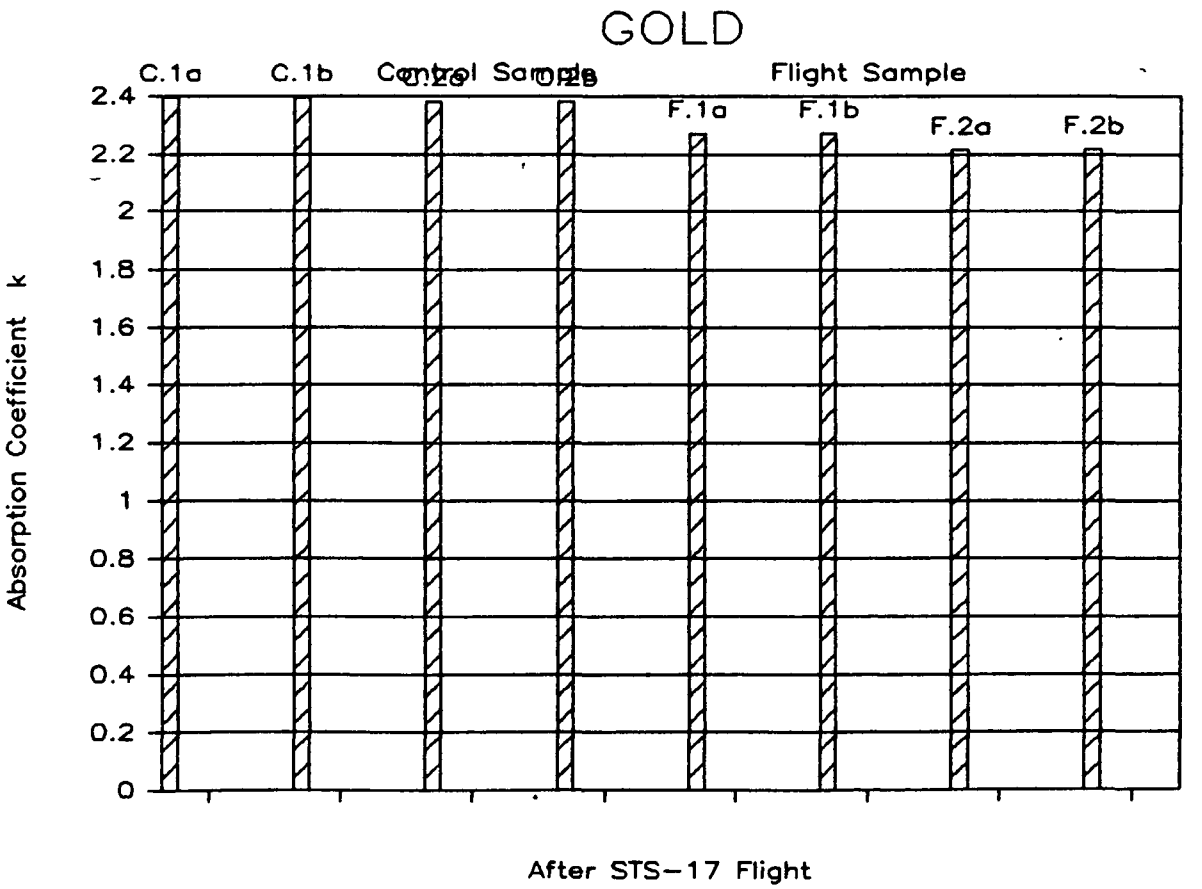
GOLD
C.1a
C.1b
Control Sample
Flight Sample
F.1a
F.1b
F.2a
F.2b
2.4
2.2
2
1.8
1.6
1.4
1.2
1
0.8
0.6
0.4
0.2
0
Absorption Coefficient k
After STS-17 Flight

Fig. 13

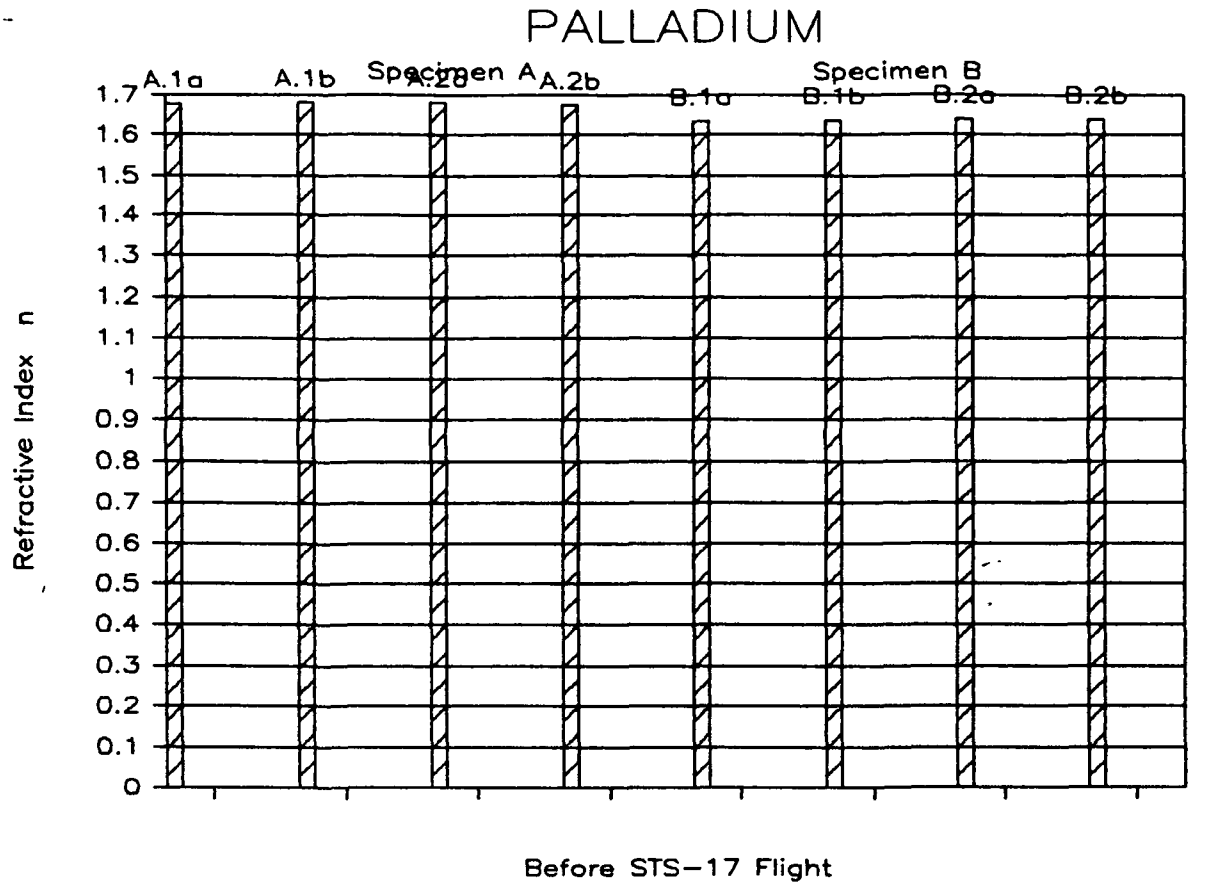
PALLADIUM
Specimen A
Specimen B
A.1a
A.1b
A.2a
A.2b
B.1a
B.1b
B.2a
B.2b
Refractive Index n
1.7
1.6
1.5
1.4
1.3
1.2
1.1
1
0.9
0.8
0.7
0.6
0.5
0.4
0.3
0.2
0.1
0
Before STS–17 Flight

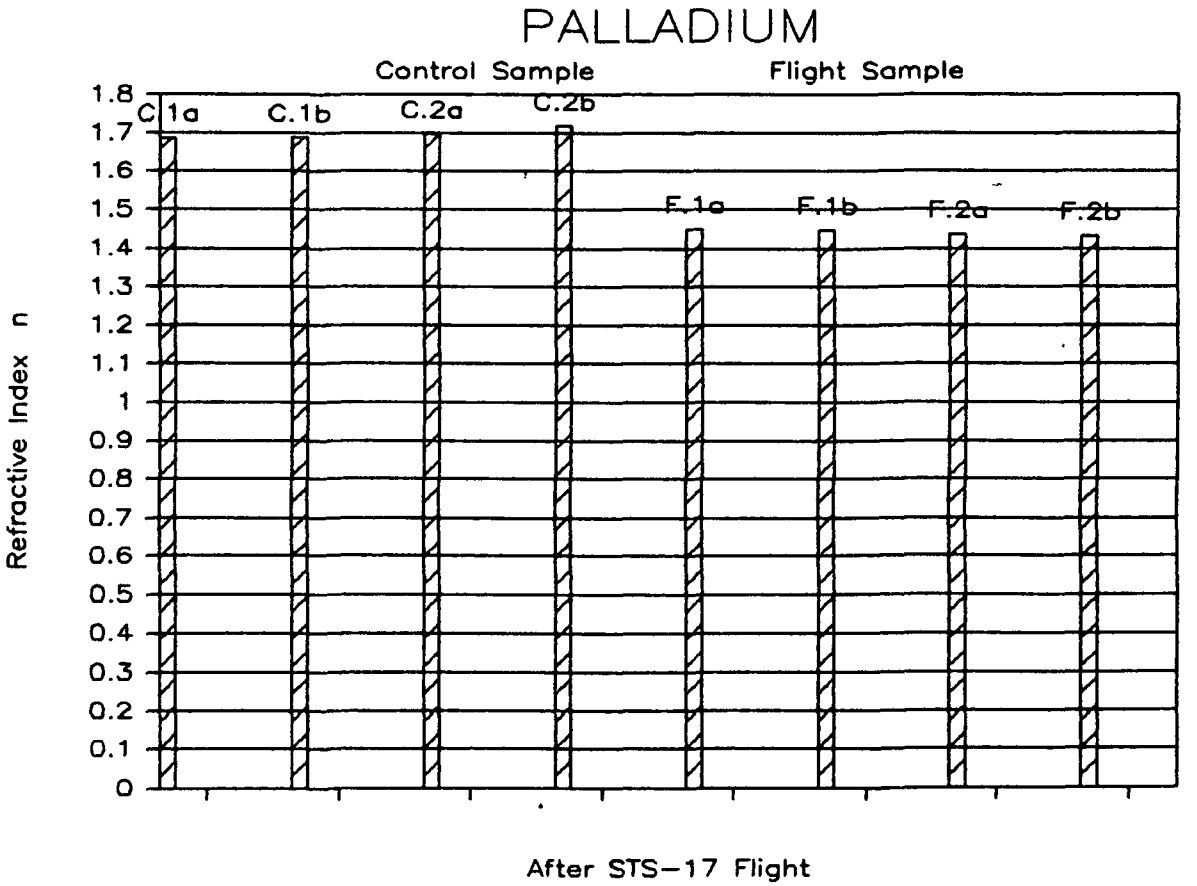
PALLADIUM
Control Sample
Flight Sample
C.1a
C.1b
C.2a
C.2b
F.1a
F.1b
F.2a
F.2b
Refractive Index n
1.8
1.7
1.6
1.5
1.4
1.3
1.2
1.1
1
0.9
0.8
0.7
0.6
0.5
0.4
0.3
0.2
0.1
0
After STS–17 Flight

Fig. 14

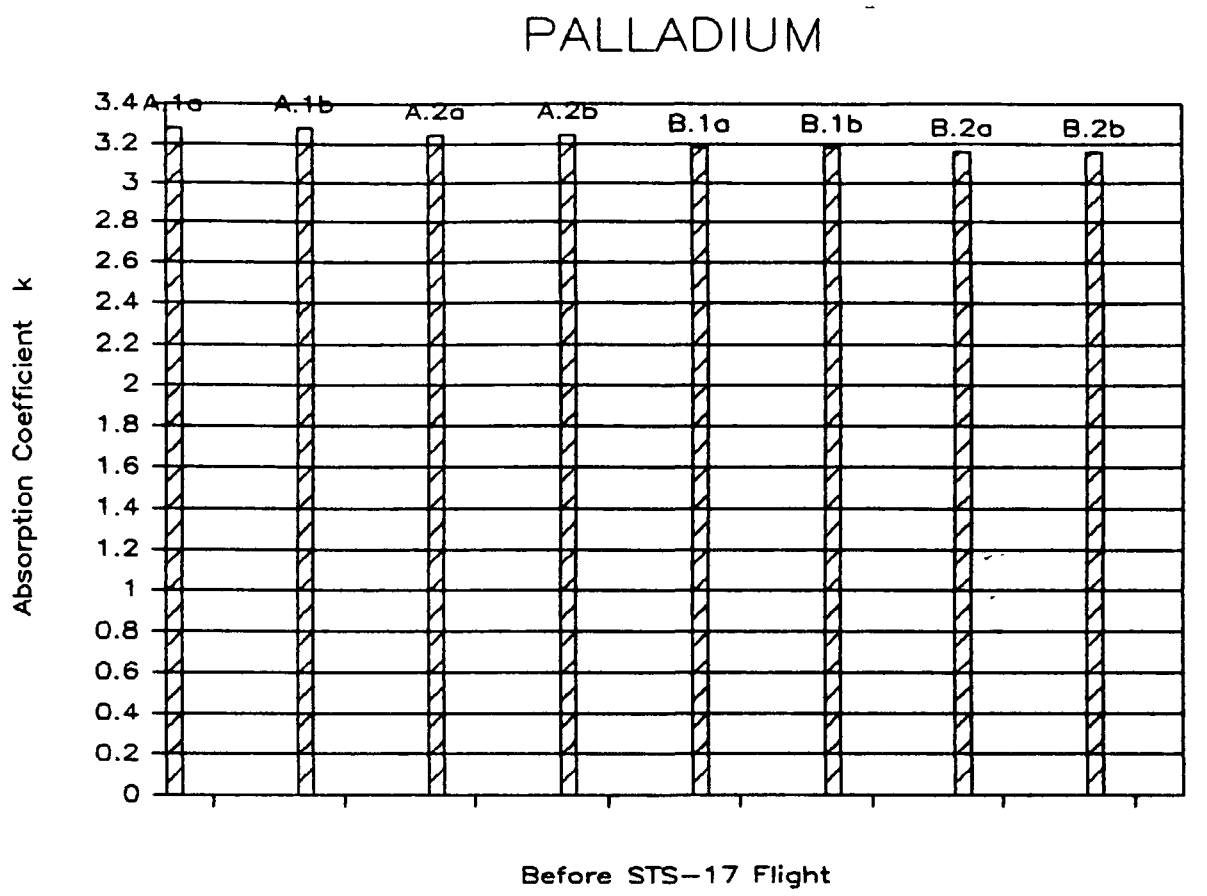
PALLADIUM
A.1a
A.1b
A.2a
A.2b
B.1a
B.1b
B.2a
B.2b
3.4
3.2
3
2.8
2.6
2.4
2.2
2
1.8
1.6
1.4
1.2
1
0.8
0.6
0.4
0.2
0
Absorption Coefficient k
Before STS-17 Flight

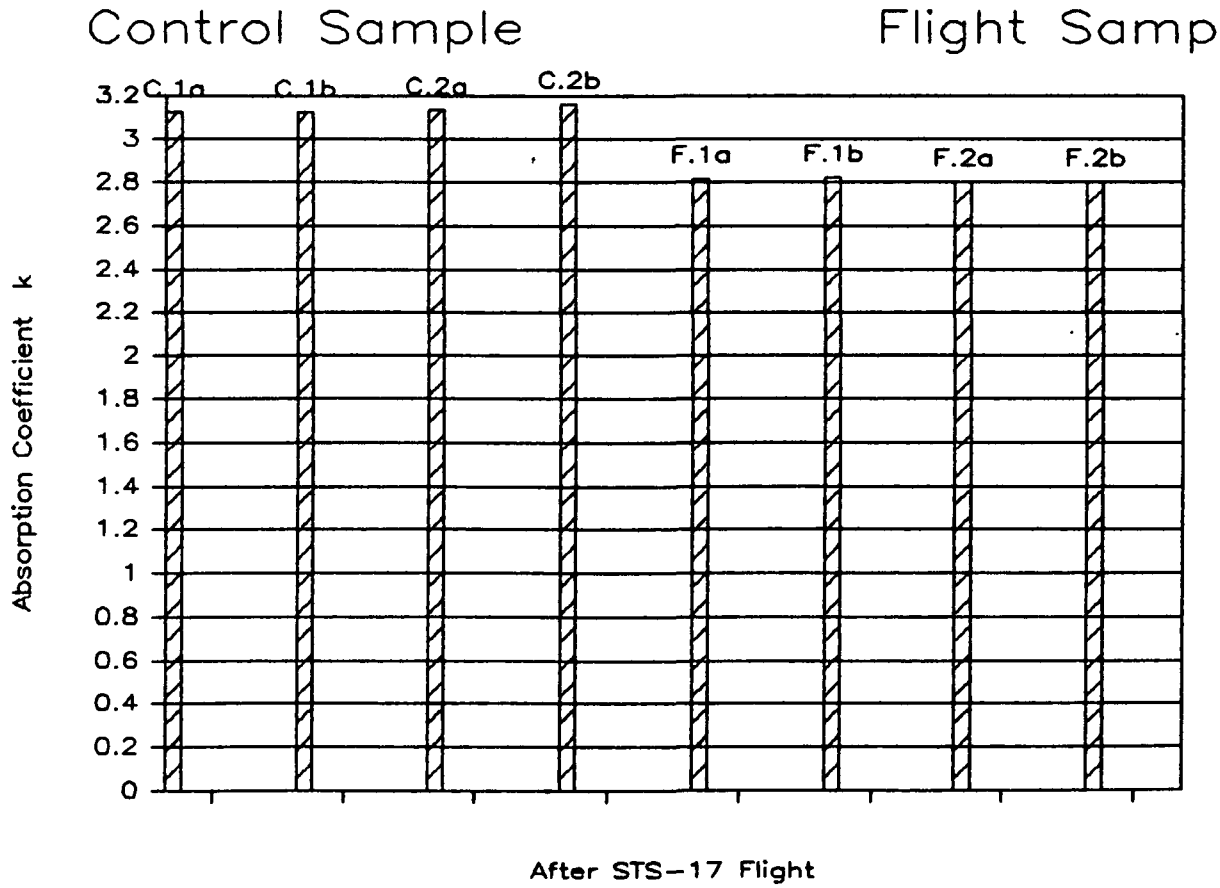
Control Sample
Flight Sample
C.1a
C.1b
C.2a
C.2b
F.1a
F.1b
F.2a
F.2b
3.2
3
2.8
2.6
2.4
2.2
2
1.8
1.6
1.4
1.2
1
0.8
0.6
0.4
0.2
0
Absorption Coefficient k
After STS-17 Flight

Fig. 15

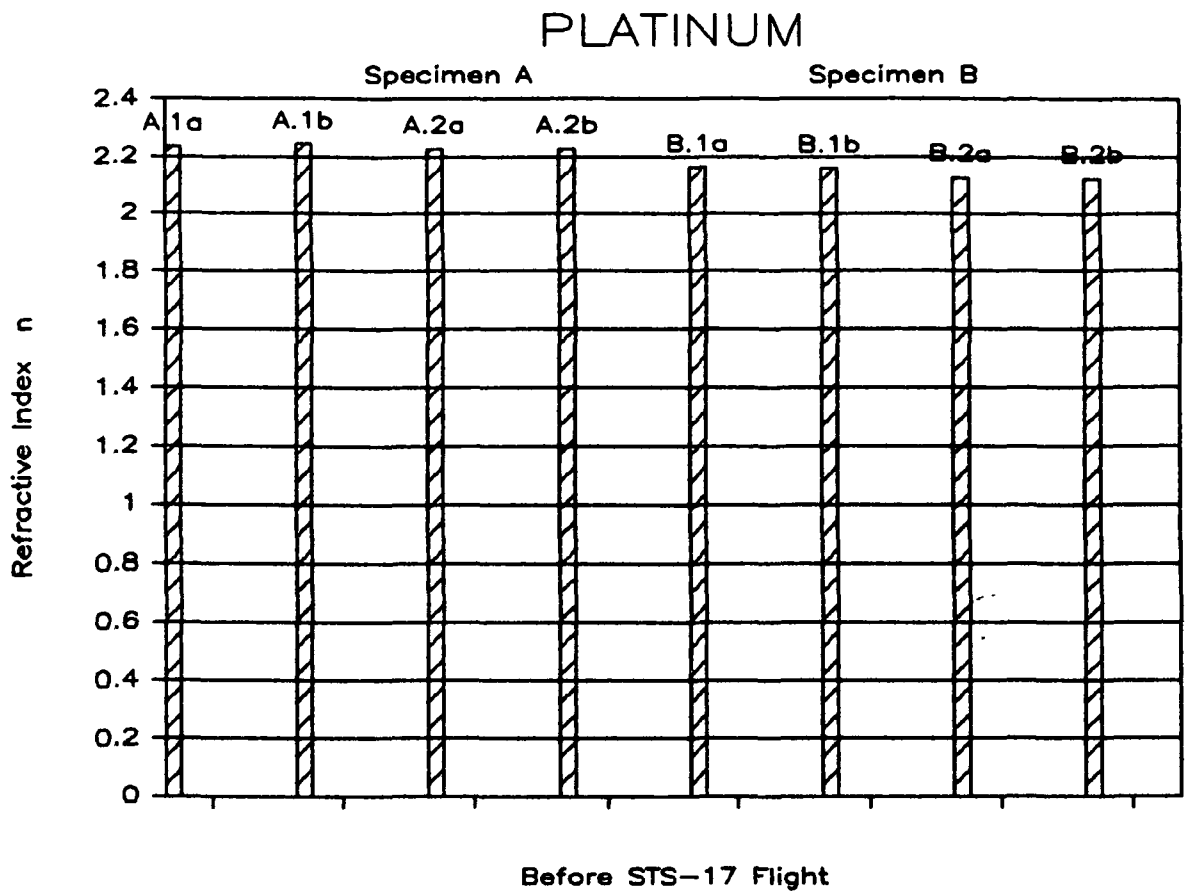
PLATINUM
Specimen A
Specimen B
A.1a
A.1b
A.2a
A.2b
B.1a
B.1b
B.2a
B.2b
2.4
2.2
2
1.8
1.6
1.4
1.2
1
0.8
0.6
0.4
0.2
0
Refractive Index n
Before STS–17 Flight

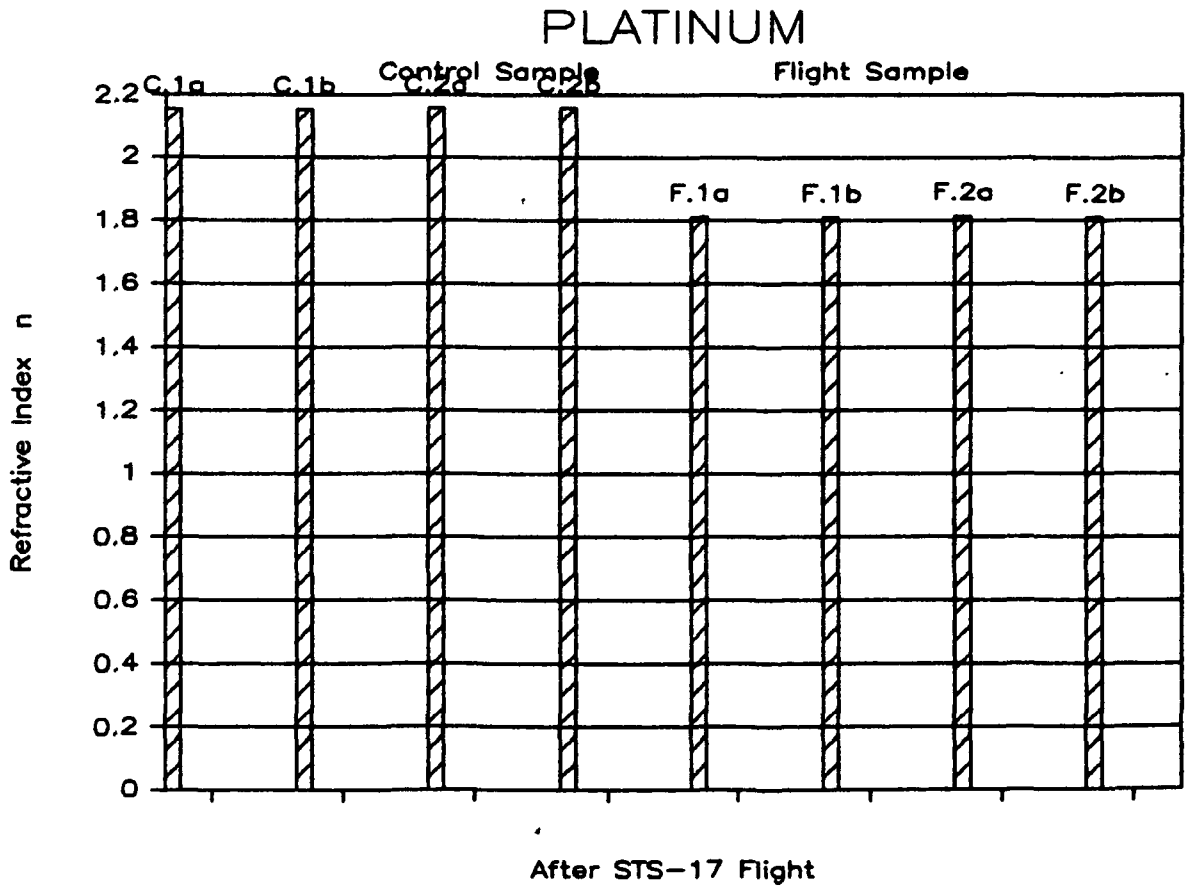
PLATINUM
Control Sample
Flight Sample
C.1a
C.1b
C.2a
C.2b
F.1a
F.1b
F.2a
F.2b
2.2
2
1.8
1.6
1.4
1.2
1
0.8
0.6
0.4
0.2
0
Refractive Index n
After STS–17 Flight

Fig. 16

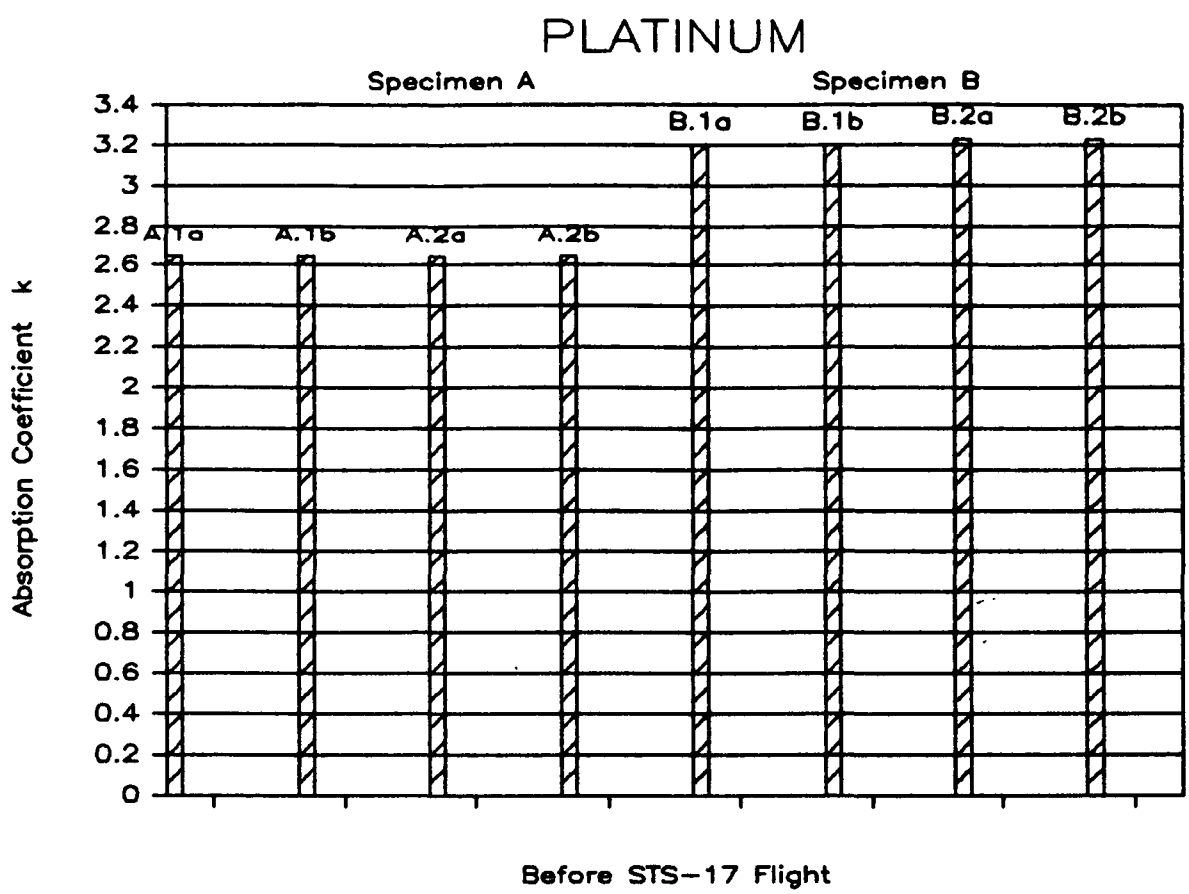
PLATINUM
Specimen A
Specimen B
A.1a
A.1b
A.2a
A.2b
B.1a
B.1b
B.2a
B.2b
Absorption Coefficient k
3.4
3.2
3
2.8
2.6
2.4
2.2
2
1.8
1.6
1.4
1.2
1
0.8
0.6
0.4
0.2
0
Before STS-17 Flight

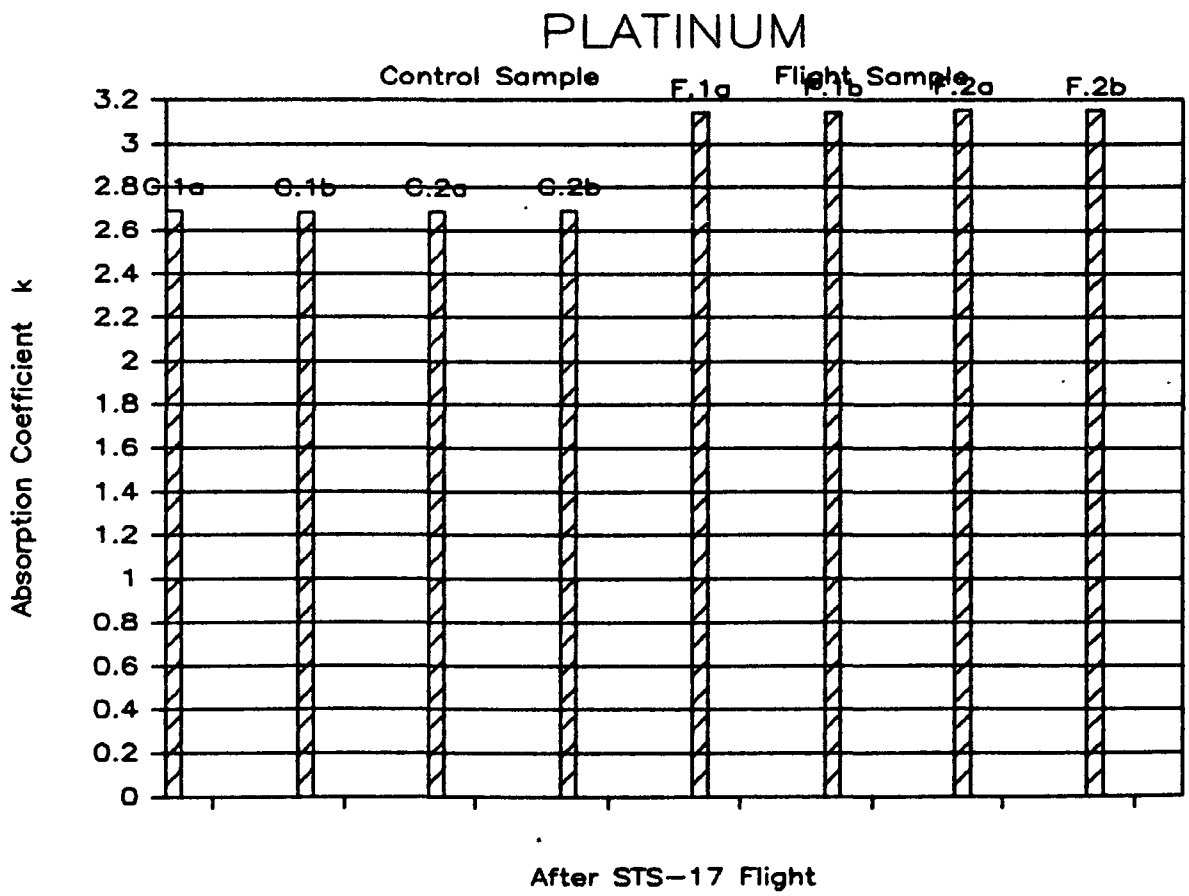
PLATINUM
Control Sample
Flight Sample
C.1a
C.1b
C.2a
C.2b
F.1a
F.1b
F.2a
F.2b
Absorption Coefficient k
3.2
3
2.8
2.6
2.4
2.2
2
1.8
1.6
1.4
1.2
1
0.8
0.6
0.4
0.2
0
After STS-17 Flight

Fig. 17

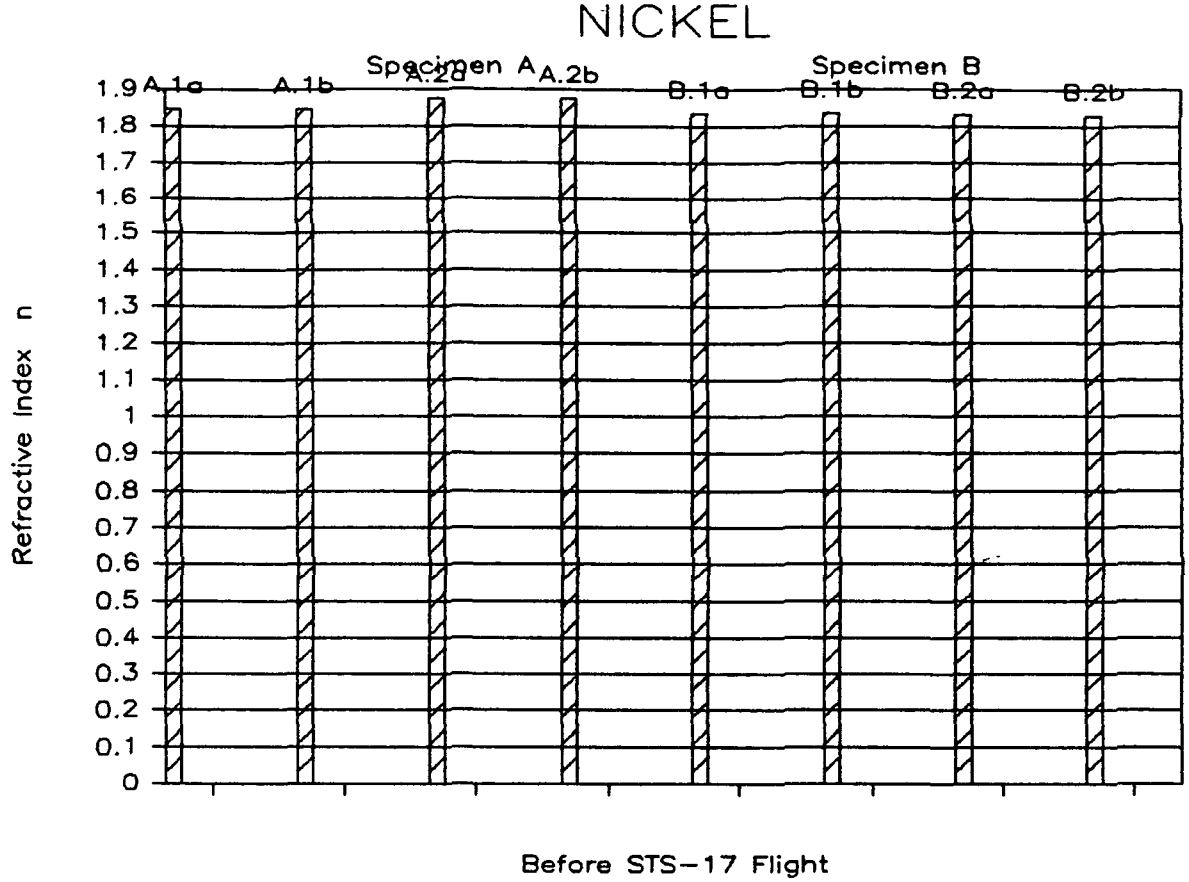
NICKEL
Specimen A
Specimen B
A.1a
A.1b
A.2a
A.2b
B.1a
B.1b
B.2a
B.2b
1.9
1.8
1.7
1.6
1.5
1.4
1.3
1.2
1.1
1
0.9
0.8
0.7
0.6
0.5
0.4
0.3
0.2
0.1
0
Refractive Index n
Before STS-17 Flight

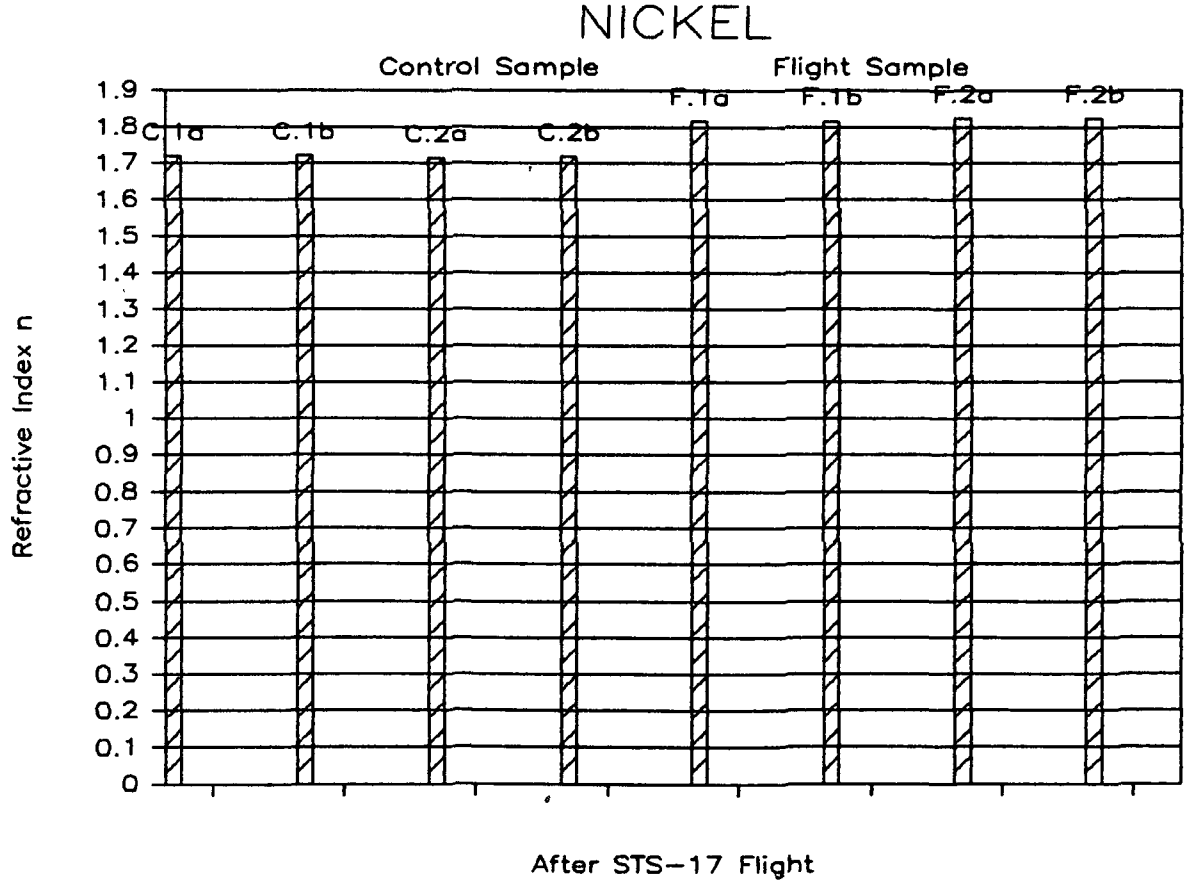
NICKEL
Control Sample
Flight Sample
C.1a
C.1b
C.2a
C.2b
F.1a
F.1b
F.2a
F.2b
1.9
1.8
1.7
1.6
1.5
1.4
1.3
1.2
1.1
1
0.9
0.8
0.7
0.6
0.5
0.4
0.3
0.2
0.1
0
Refractive Index n
After STS-17 Flight

Fig. 18

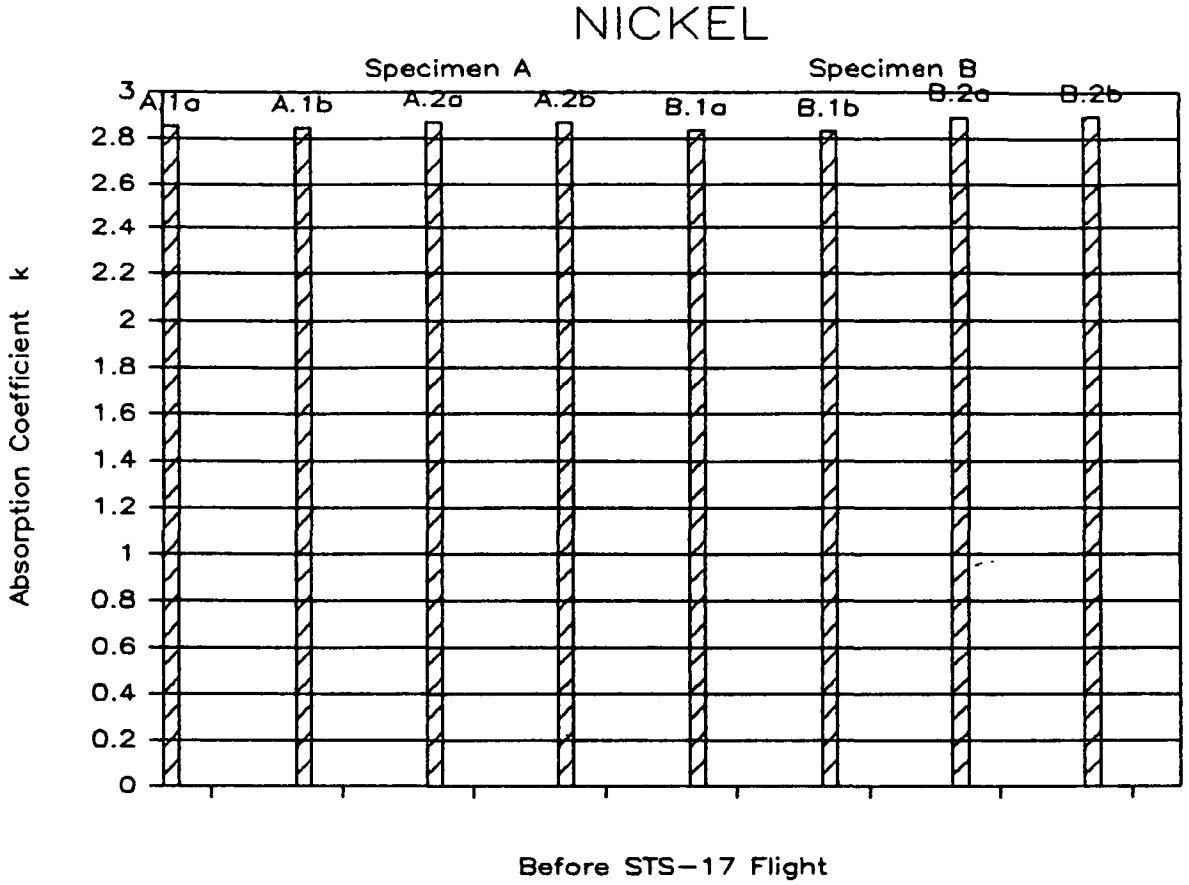
NICKEL
Specimen A
Specimen B
A.1a
A.1b
A.2a
A.2b
B.1a
B.1b
B.2a
B.2b
Absorption Coefficient k
3
2.8
2.6
2.4
2.2
2
1.8
1.6
1.4
1.2
1
0.8
0.6
0.4
0.2
0
Before STS-17 Flight

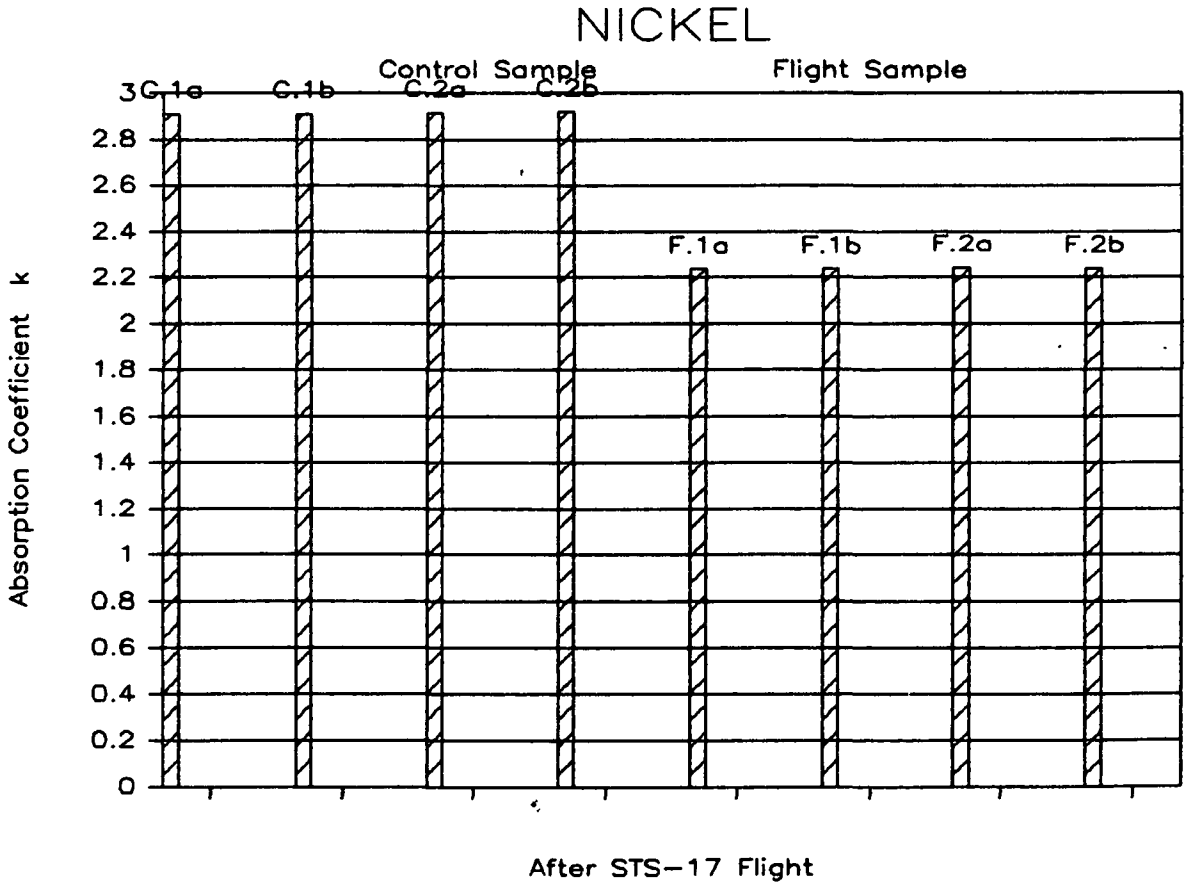
NICKEL
Control Sample
Flight Sample
C.1a
C.1b
C.2a
C.2b
F.1a
F.1b
F.2a
F.2b
Absorption Coefficient k
3
2.8
2.6
2.4
2.2
2
1.8
1.6
1.4
1.2
1
0.8
0.6
0.4
0.2
0
After STS-17 Flight

Fig. 19

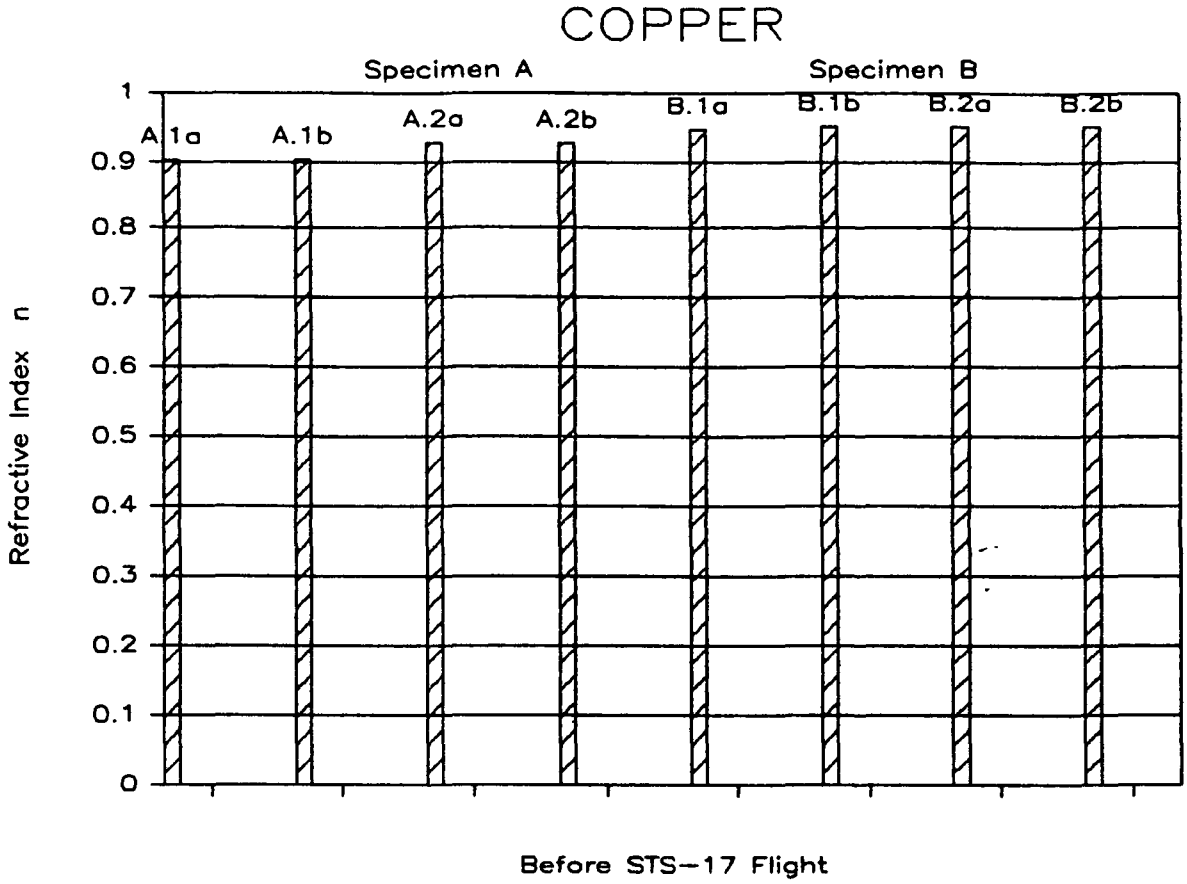
COPPER
Specimen A
Specimen B
A.1a
A.1b
A.2a
A.2b
B.1a
B.1b
B.2a
B.2b
Refractive Index n
1
0.9
0.8
0.7
0.6
0.5
0.4
0.3
0.2
0.1
0
Before STS-17 Flight

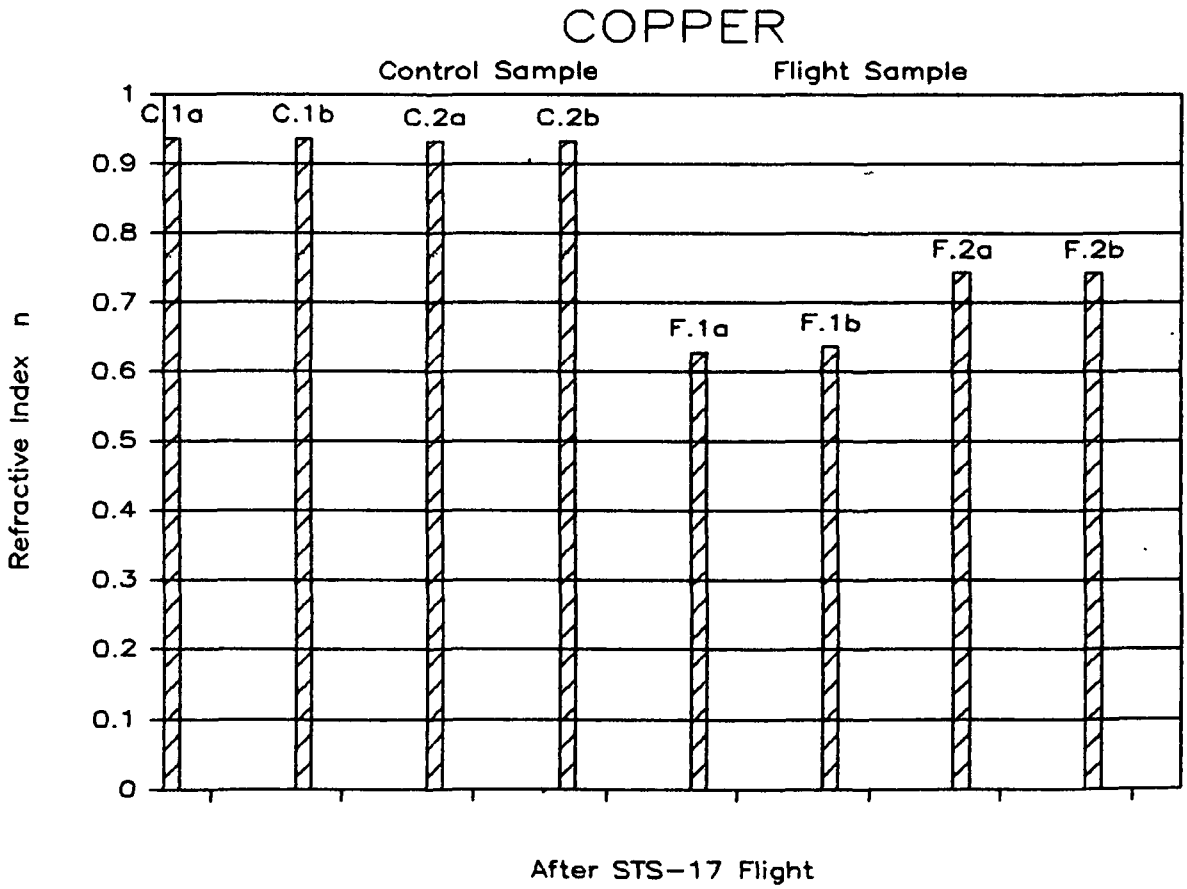
COPPER
Control Sample
Flight Sample
C.1a
C.1b
C.2a
C.2b
F.1a
F.1b
F.2a
F.2b
Refractive Index n
1
0.9
0.8
0.7
0.6
0.5
0.4
0.3
0.2
0.1
0
After STS-17 Flight

Fig. 20

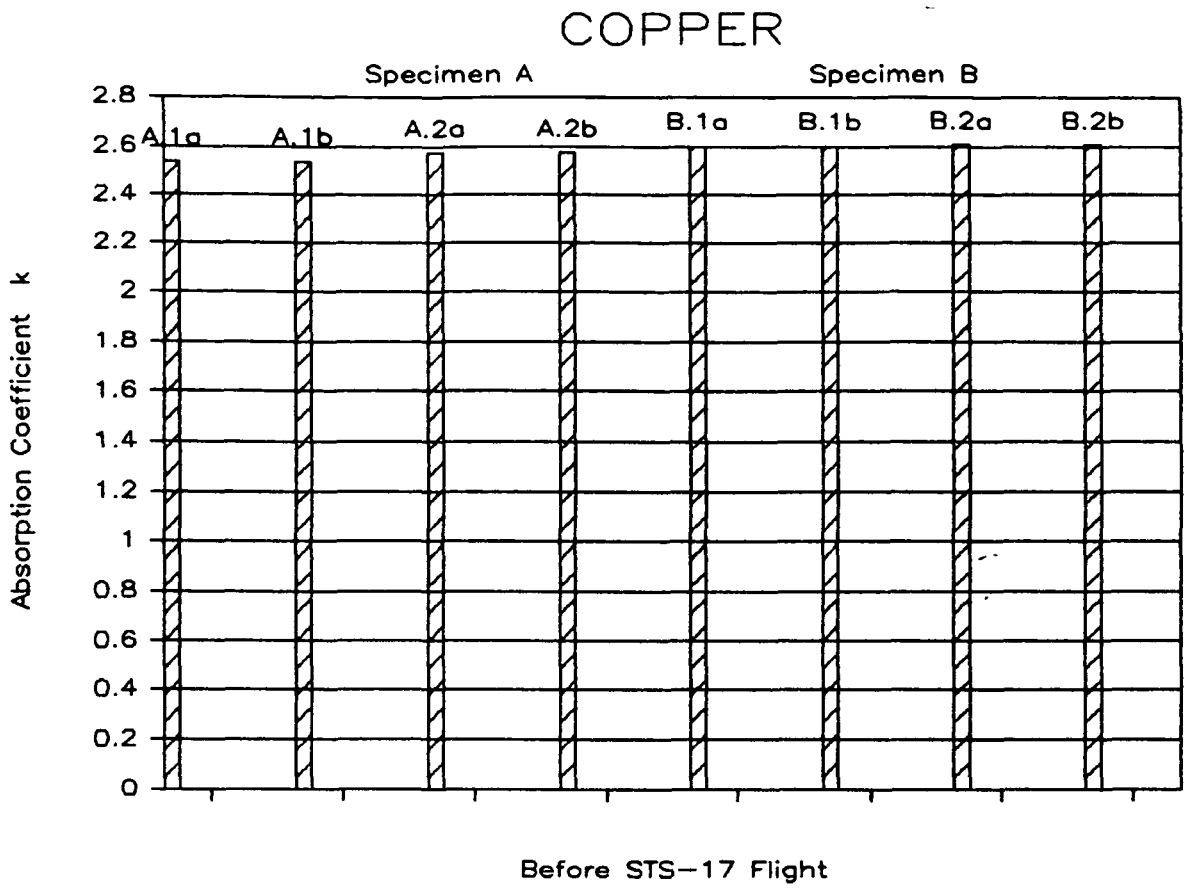
COPPER
Specimen A
Specimen B
A.1a
A.1b
A.2a
A.2b
B.1a
B.1b
B.2a
B.2b
Absorption Coefficient k
2.8
2.6
2.4
2.2
2
1.8
1.6
1.4
1.2
1
0.8
0.6
0.4
0.2
0
Before STS—17 Flight

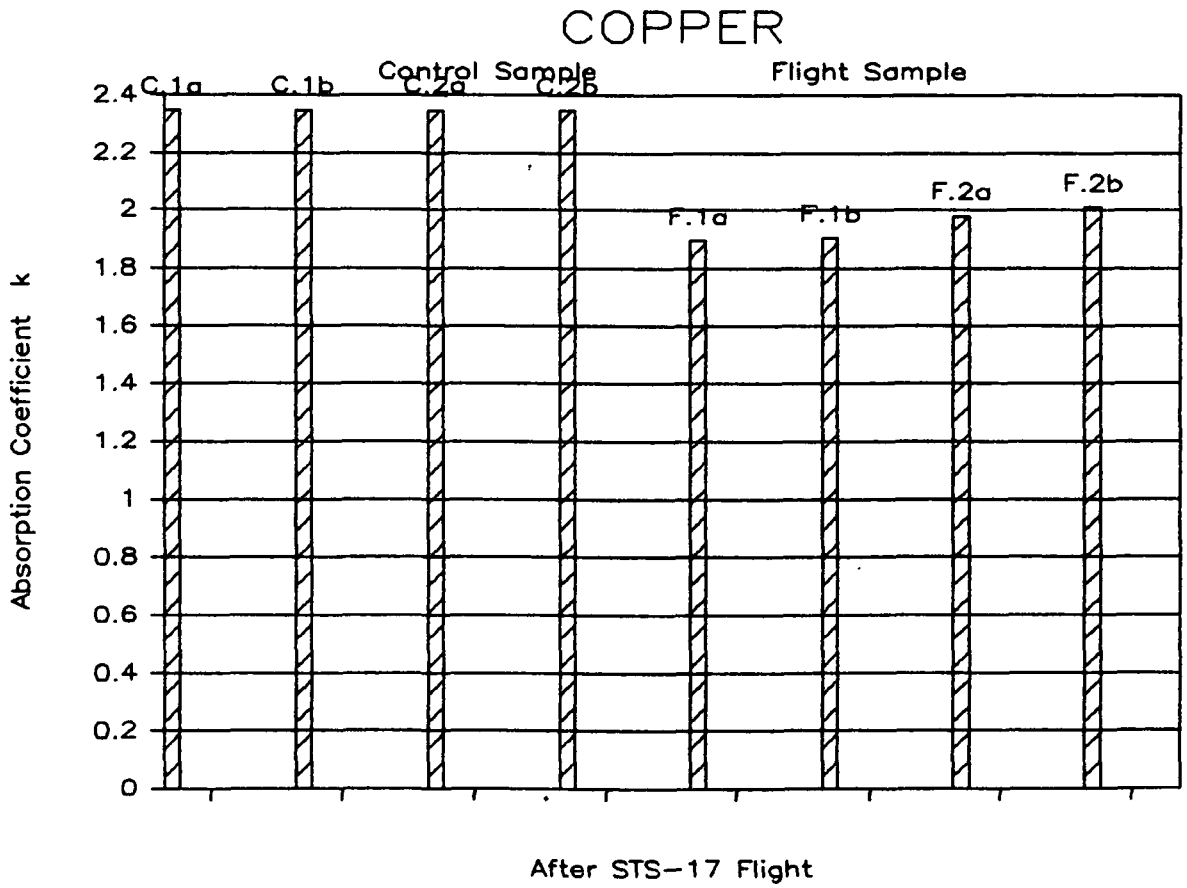
COPPER
Control Sample
Flight Sample
C.1a
C.1b
C.2a
C.2b
F.1a
F.1b
F.2a
F.2b
Absorption Coefficient k
2.4
2.2
2
1.8
1.6
1.4
1.2
1
0.8
0.6
0.4
0.2
0
After STS—17 Flight

Fig. 21

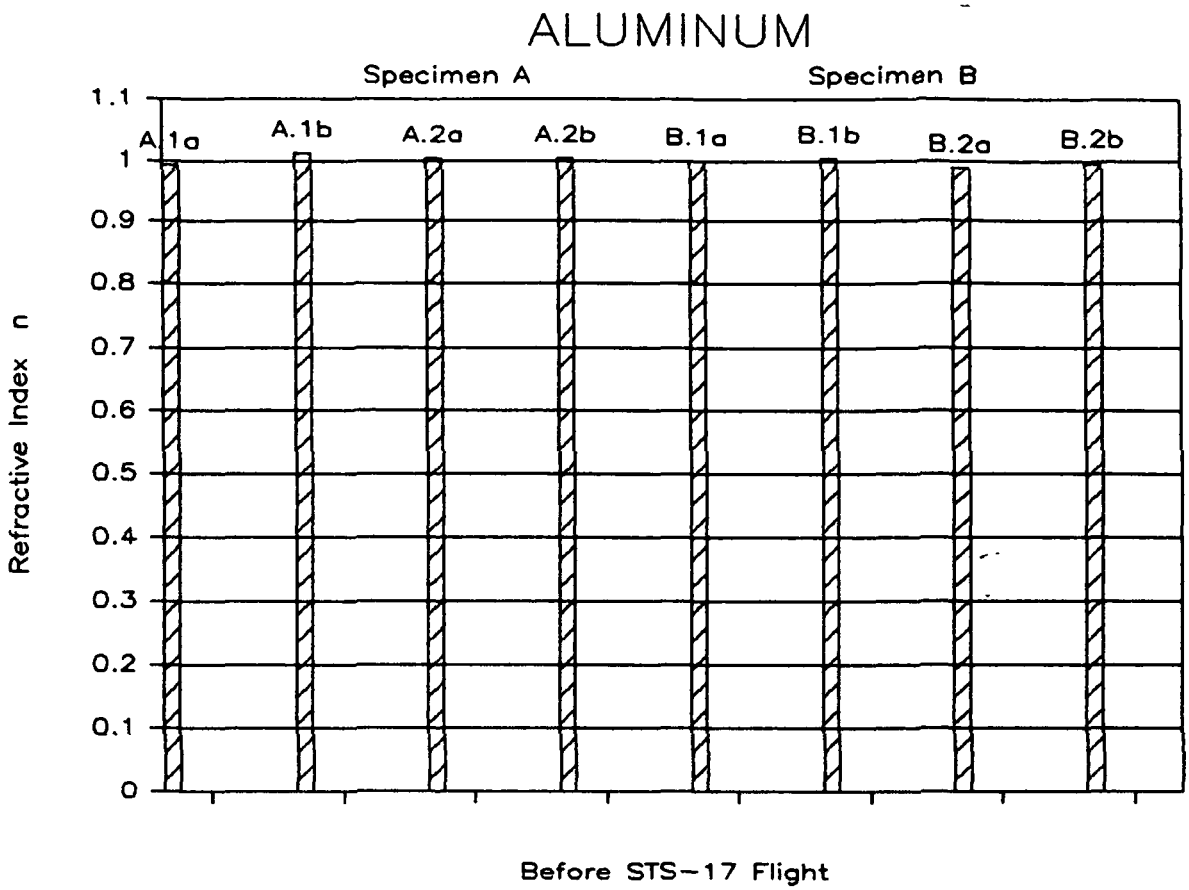
ALUMINUM
Specimen A
Specimen B
A.1a
A.1b
A.2a
A.2b
B.1a
B.1b
B.2a
B.2b
Refractive Index n
1.1
1
0.9
0.8
0.7
0.6
0.5
0.4
0.3
0.2
0.1
0
Before STS-17 Flight

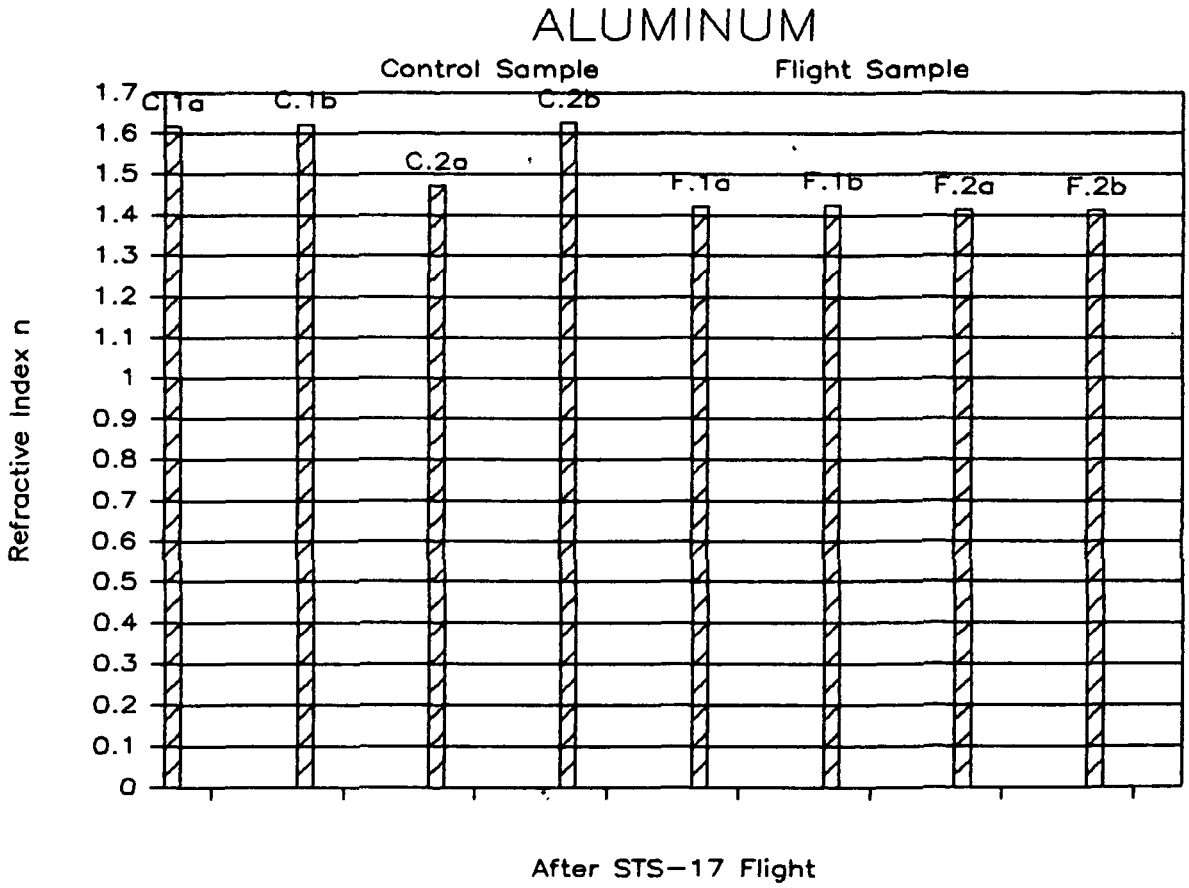
ALUMINUM
Control Sample
Flight Sample
C.1a
C.1b
C.2a
C.2b
F.1a
F.1b
F.2a
F.2b
Refractive Index n
1.7
1.6
1.5
1.4
1.3
1.2
1.1
1
0.9
0.8
0.7
0.6
0.5
0.4
0.3
0.2
0.1
0
After STS-17 Flight

Fig. 22

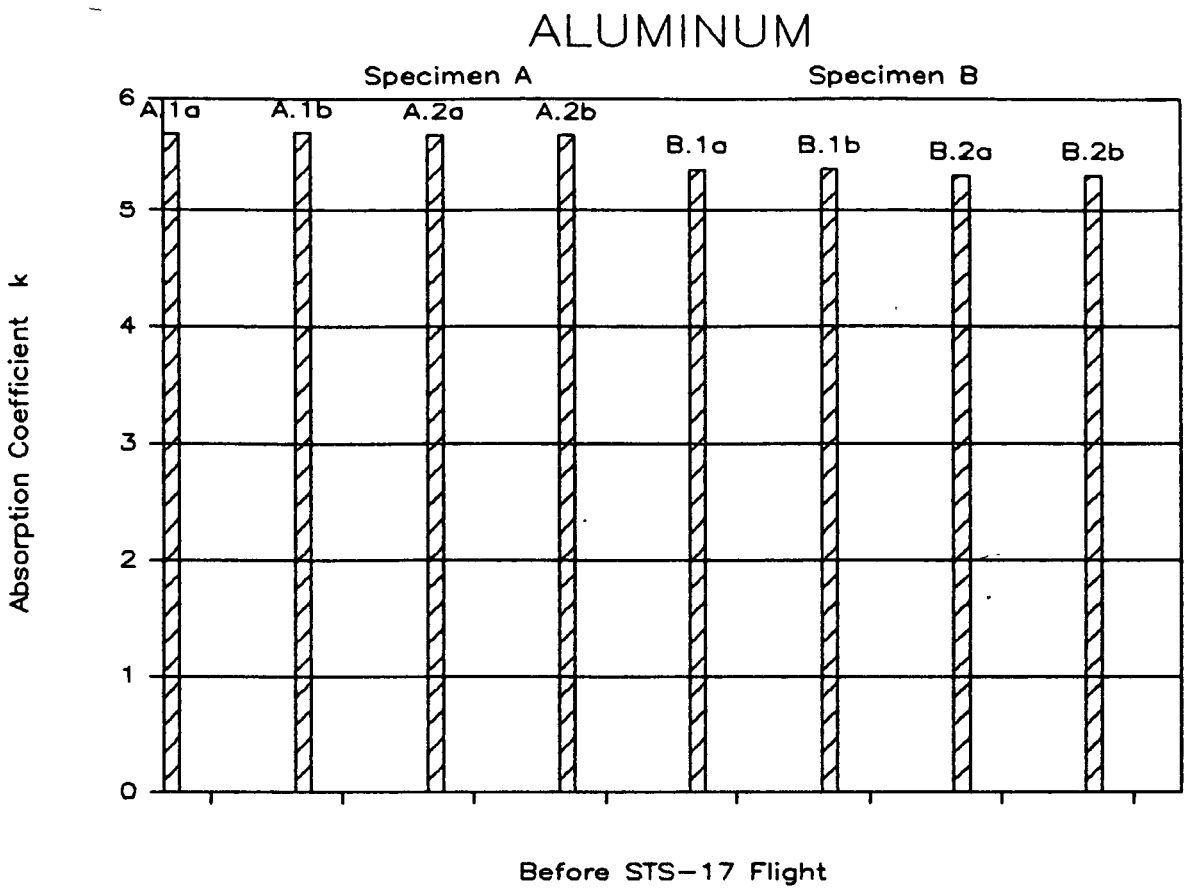
ALUMINUM
Specimen A
Specimen B
A.1a
A.1b
A.2a
A.2b
B.1a
B.1b
B.2a
B.2b
Absorption Coefficient k
0
1
2
3
4
5
6
Before STS-17 Flight

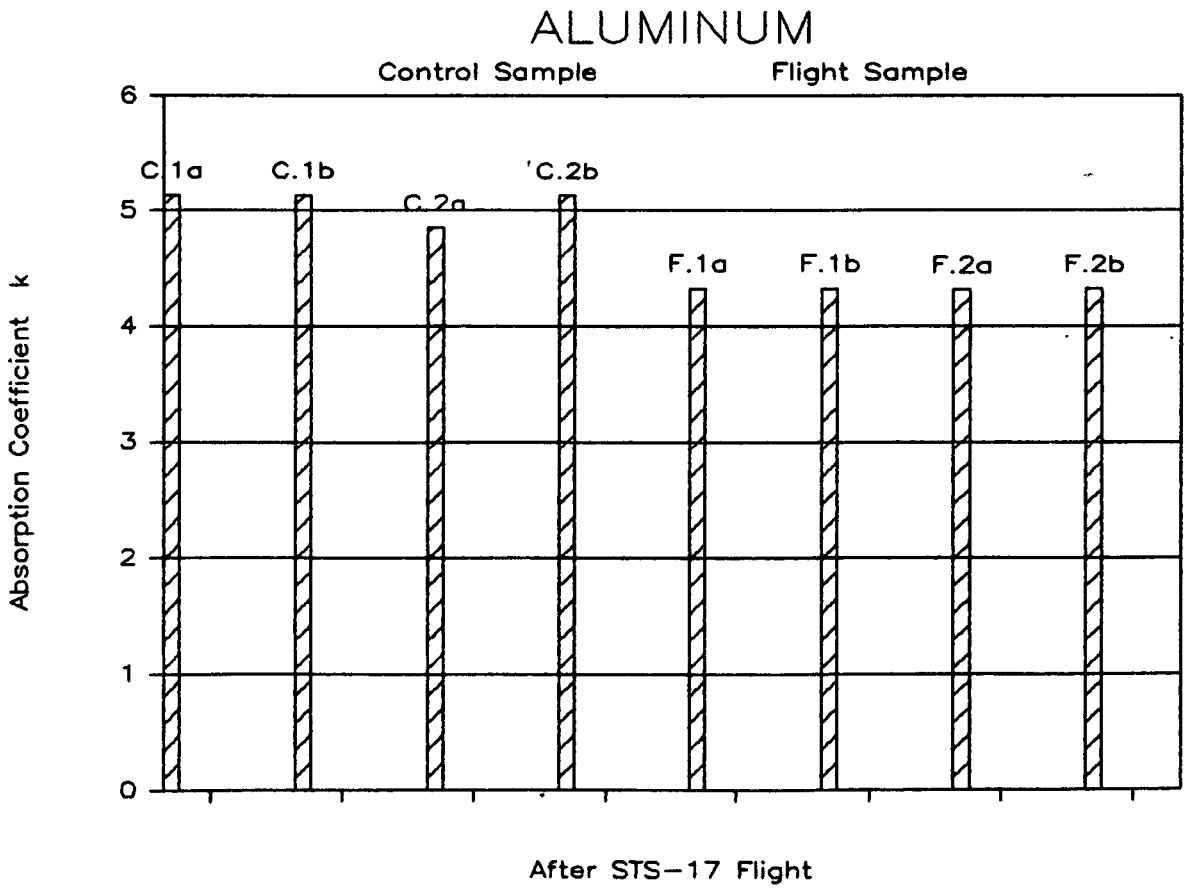
ALUMINUM
Control Sample
Flight Sample
C.1a
C.1b
C.2a
C.2b
F.1a
F.1b
F.2a
F.2b
Absorption Coefficient k
0
1
2
3
4
5
6
After STS-17 Flight

Fig. 23

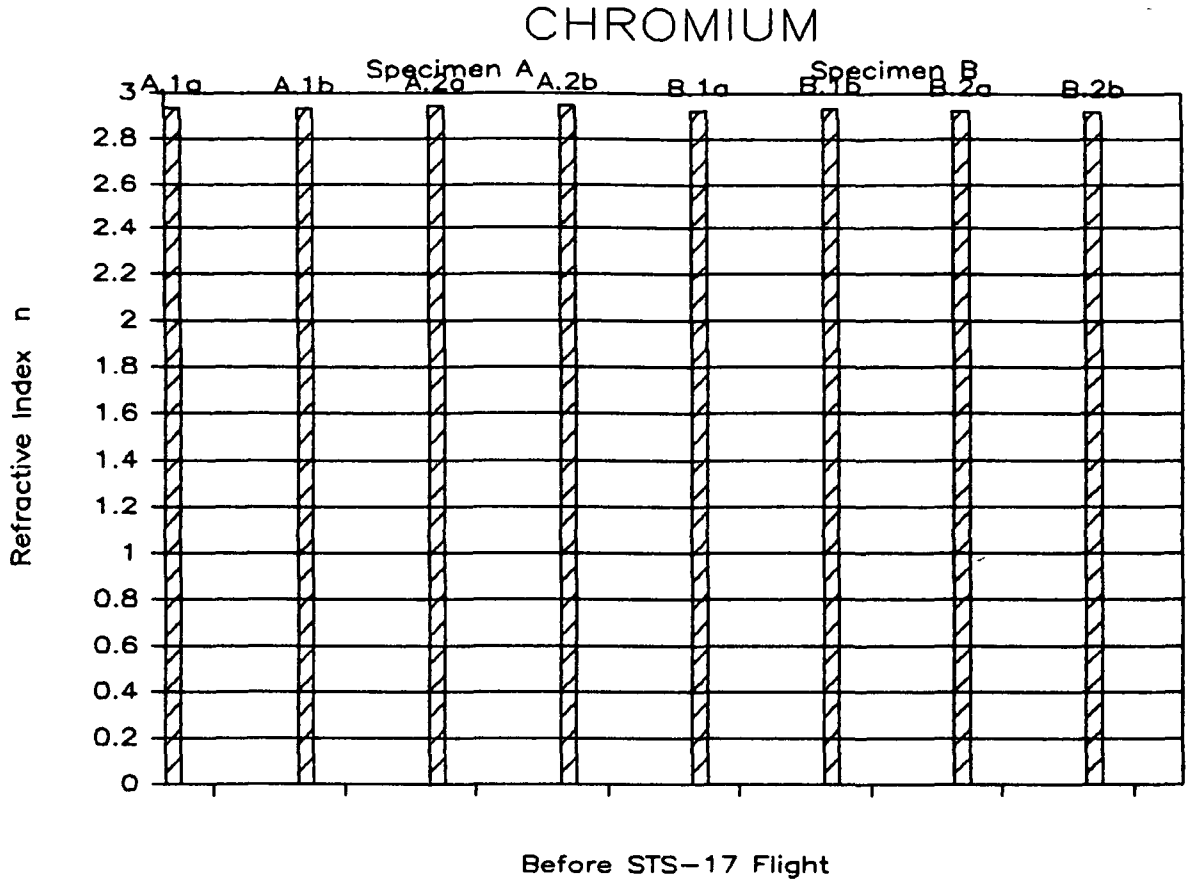
CHROMIUM
Specimen A
Specimen B
A.1a
A.1b
A.2a
A.2b
B.1a
B.1b
B.2a
B.2b
3
2.8
2.6
2.4
2.2
2
1.8
1.6
1.4
1.2
1
0.8
0.6
0.4
0.2
0
Refractive Index n
Before STS-17 Flight

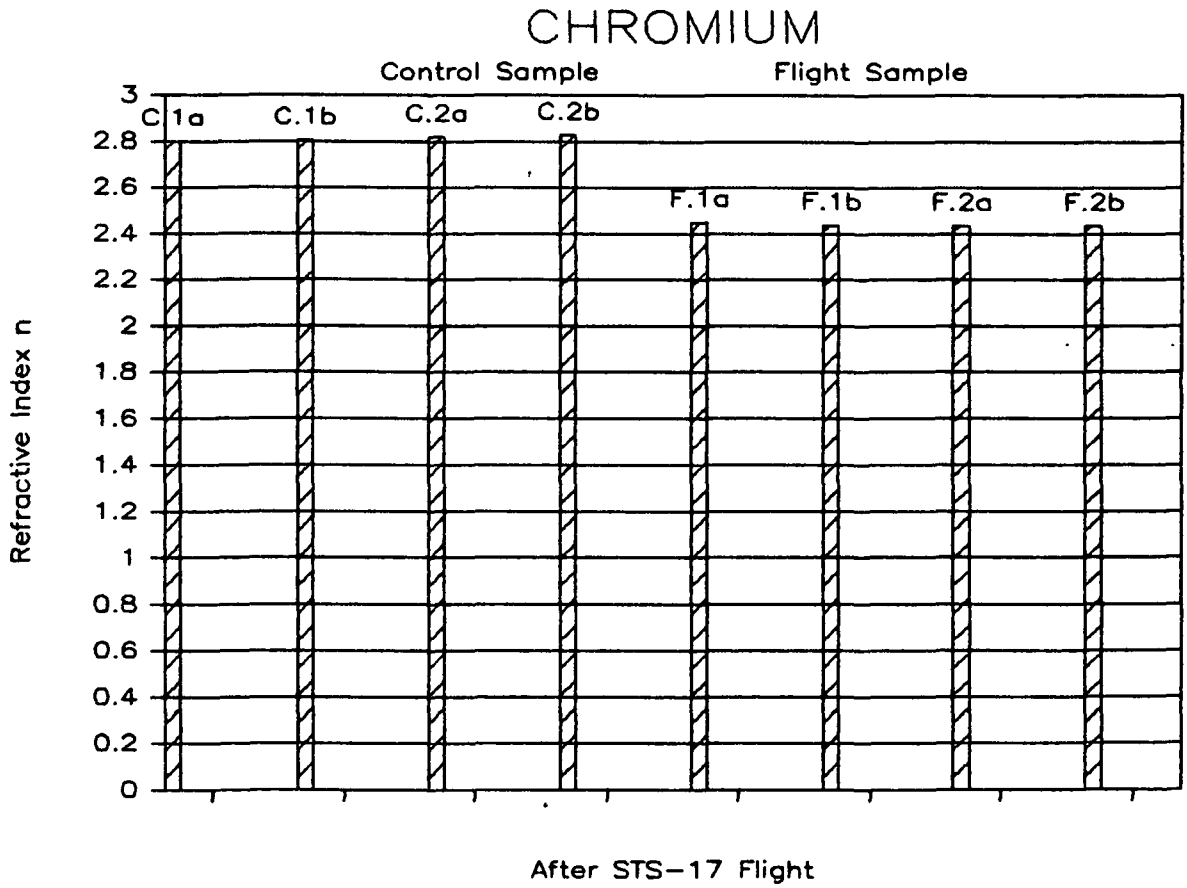
CHROMIUM
Control Sample
Flight Sample
C.1a
C.1b
C.2a
C.2b
F.1a
F.1b
F.2a
F.2b
3
2.8
2.6
2.4
2.2
2
1.8
1.6
1.4
1.2
1
0.8
0.6
0.4
0.2
0
Refractive Index n
After STS-17 Flight

Fig. 24

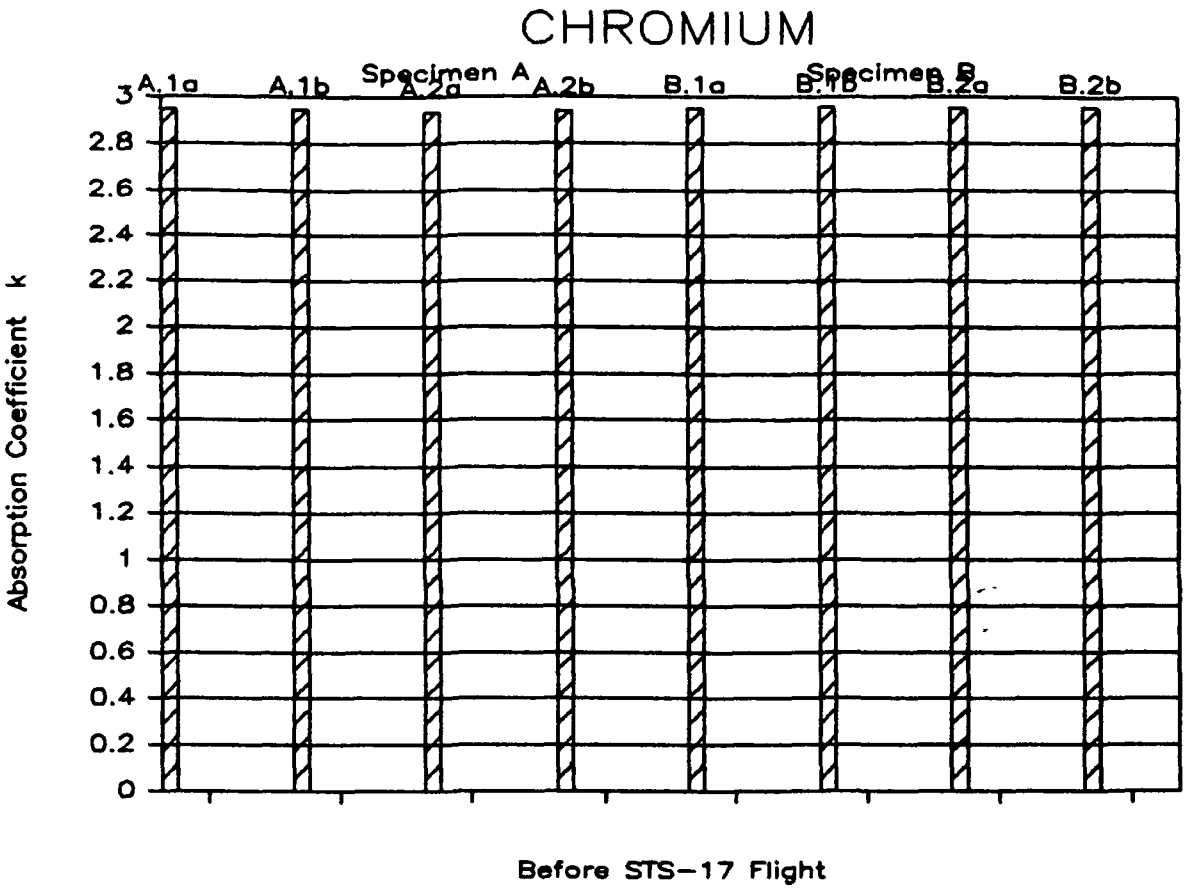
CHROMIUM
Specimen A
Specimen B
A.1a
A.1b
A.2a
A.2b
B.1a
B.1b
B.2a
B.2b
Absorption Coefficient k
3
2.8
2.6
2.4
2.2
2
1.8
1.6
1.4
1.2
1
0.8
0.6
0.4
0.2
0
Before STS–17 Flight

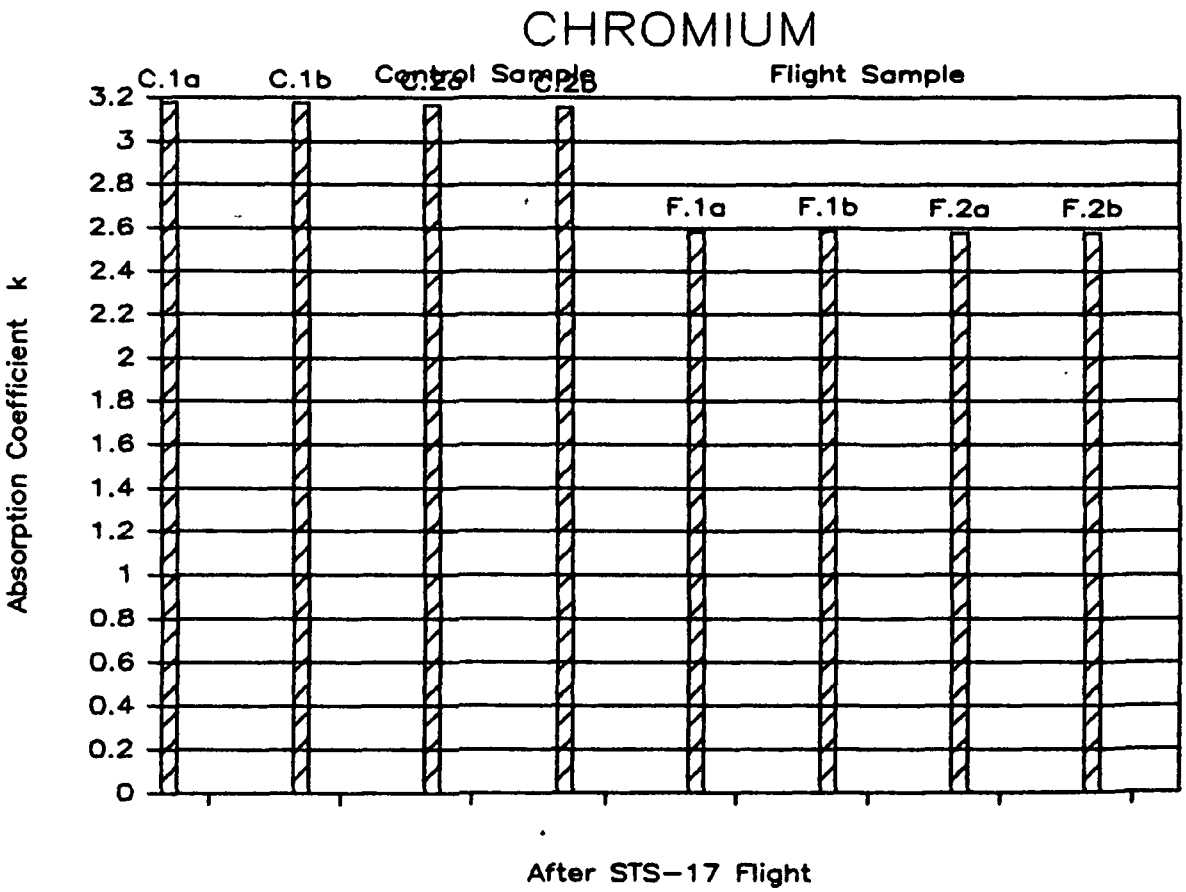
CHROMIUM
Control Sample
Flight Sample
C.1a
C.1b
C.2a
C.2b
F.1a
F.1b
F.2a
F.2b
Absorption Coefficient k
3.2
3
2.8
2.6
2.4
2.2
2
1.8
1.6
1.4
1.2
1
0.8
0.6
0.4
0.2
0
After STS–17 Flight

Fig. 25

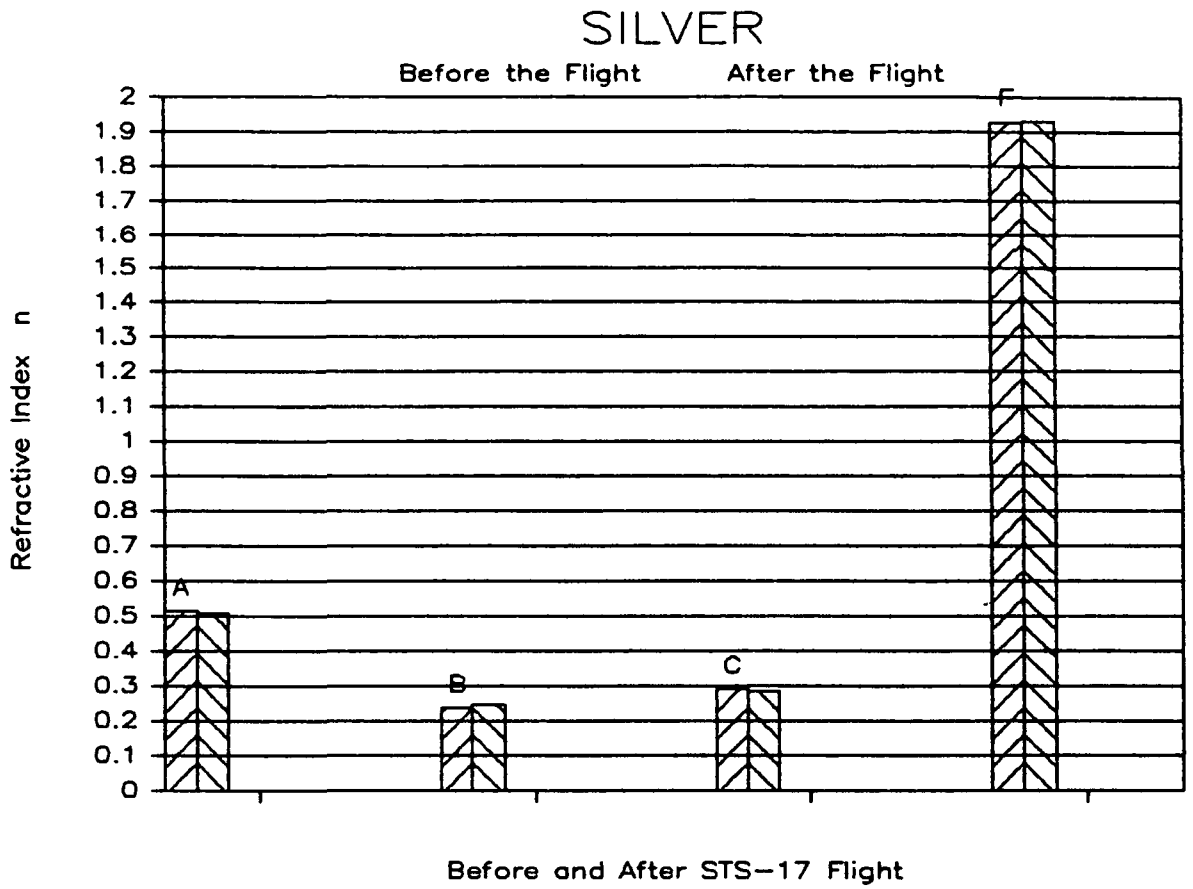
SILVER
Before the Flight
After the Flight
Refractive Index n
2
1.9
1.8
1.7
1.6
1.5
1.4
1.3
1.2
1.1
1
0.9
0.8
0.7
0.6
0.5
0.4
0.3
0.2
0.1
0
A
B
C
F
Before and After STS-17 Flight

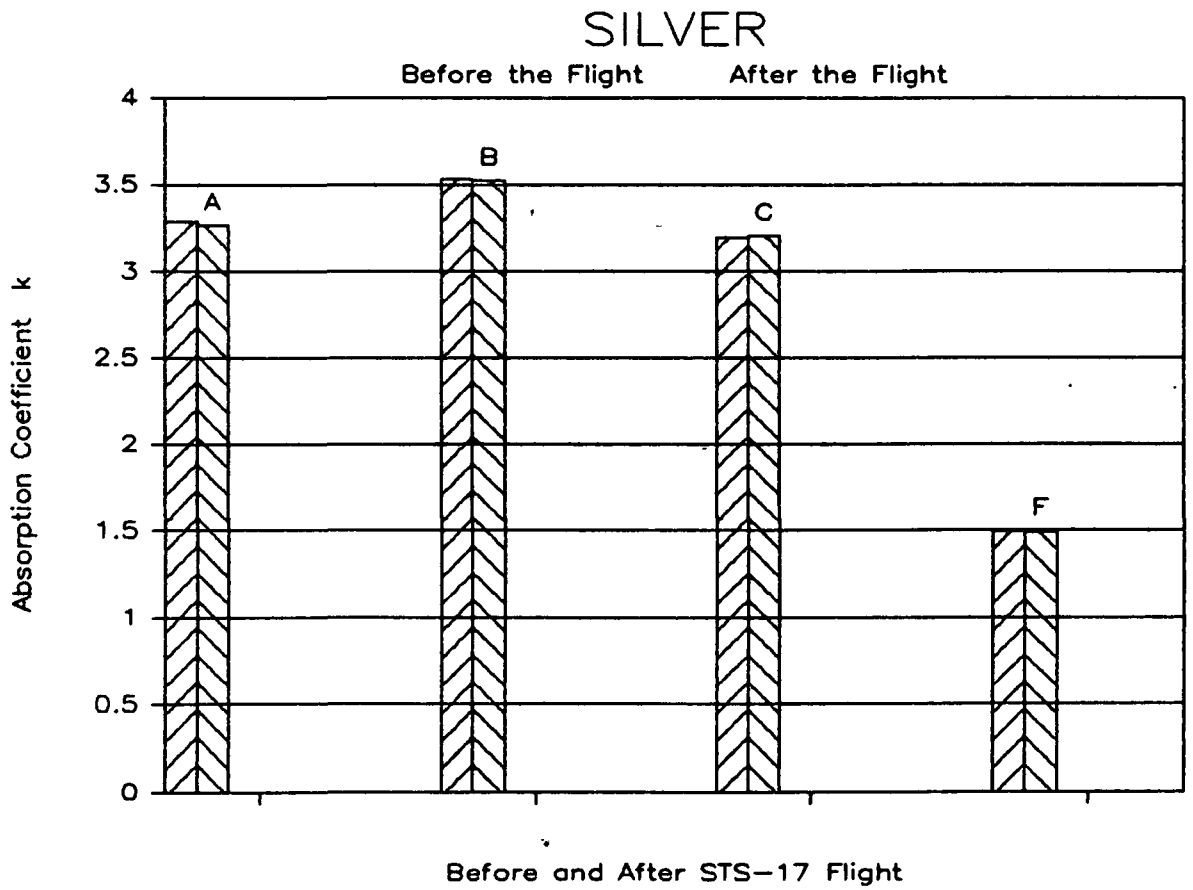
SILVER
Before the Flight
After the Flight
Absorption Coefficient k
4
3.5
3
2.5
2
1.5
1
0.5
0
A
B
C
F
Before and After STS-17 Flight

Fig. 26

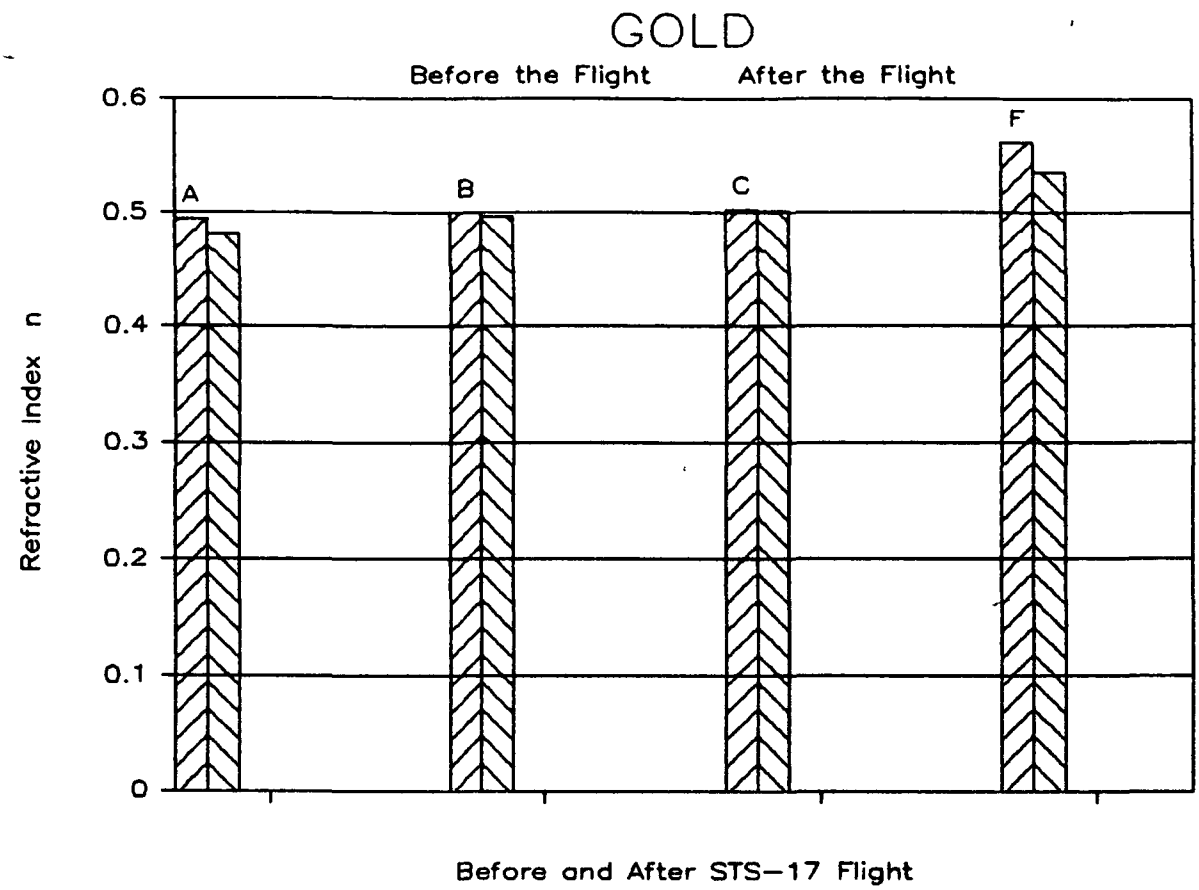
GOLD
Before the Flight
After the Flight
Refractive Index n
0.6
0.5
0.4
0.3
0.2
0.1
0
A
B
C
F
Before and After STS-17 Flight

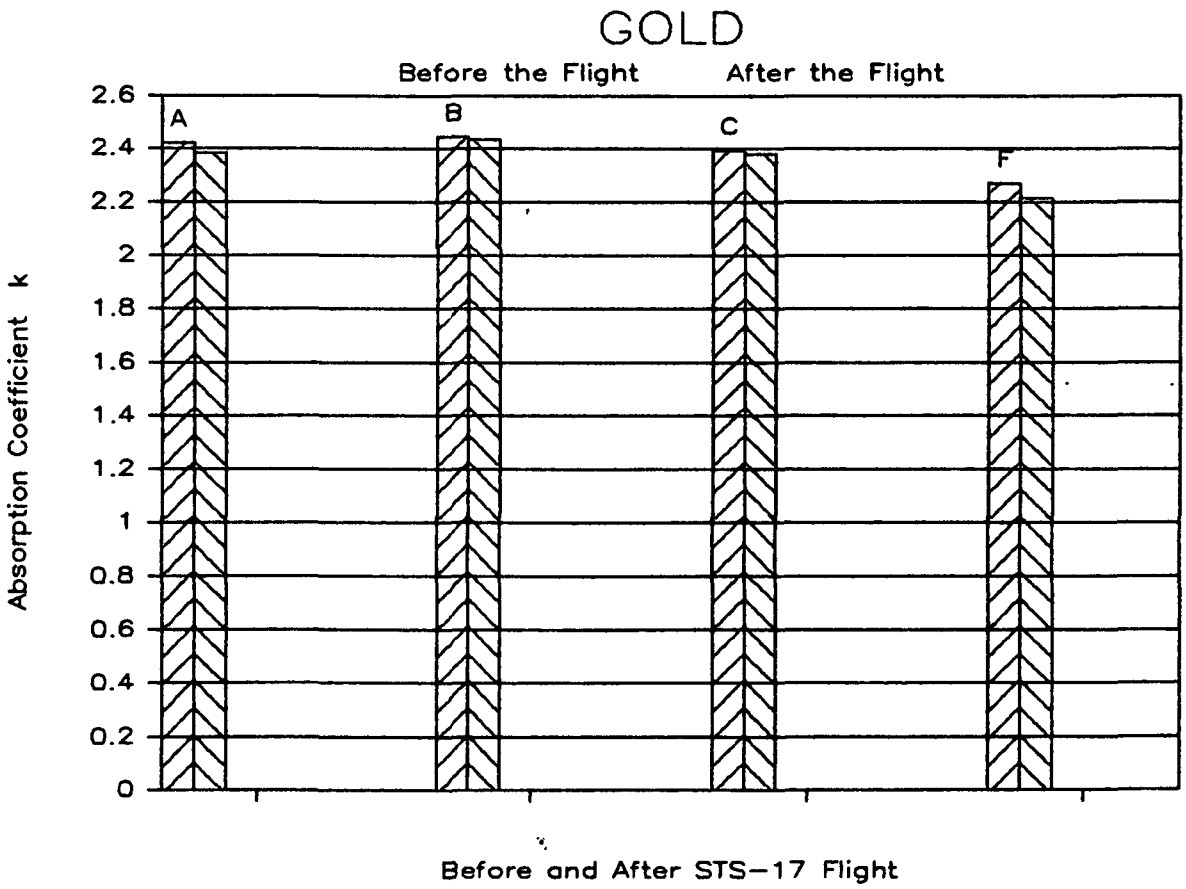
GOLD
Before the Flight
After the Flight
Absorption Coefficient k
2.6
2.4
2.2
2
1.8
1.6
1.4
1.2
1
0.8
0.6
0.4
0.2
0
A
B
C
F
Before and After STS-17 Flight

Fig. 27

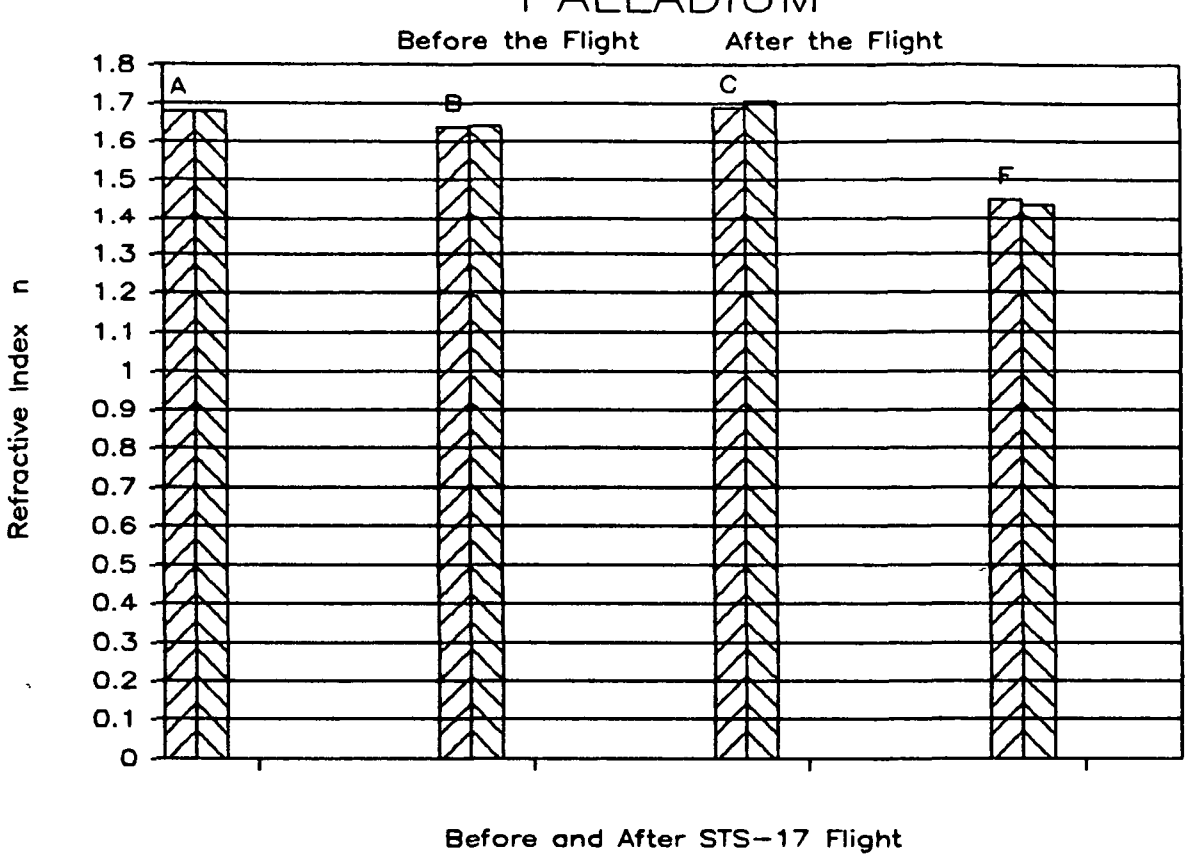
PALLADIUM
Before the Flight
After the Flight
Refractive Index n
1.8
1.7
1.6
1.5
1.4
1.3
1.2
1.1
1
0.9
0.8
0.7
0.6
0.5
0.4
0.3
0.2
0.1
0
A
B
C
F
Before and After STS-17 Flight

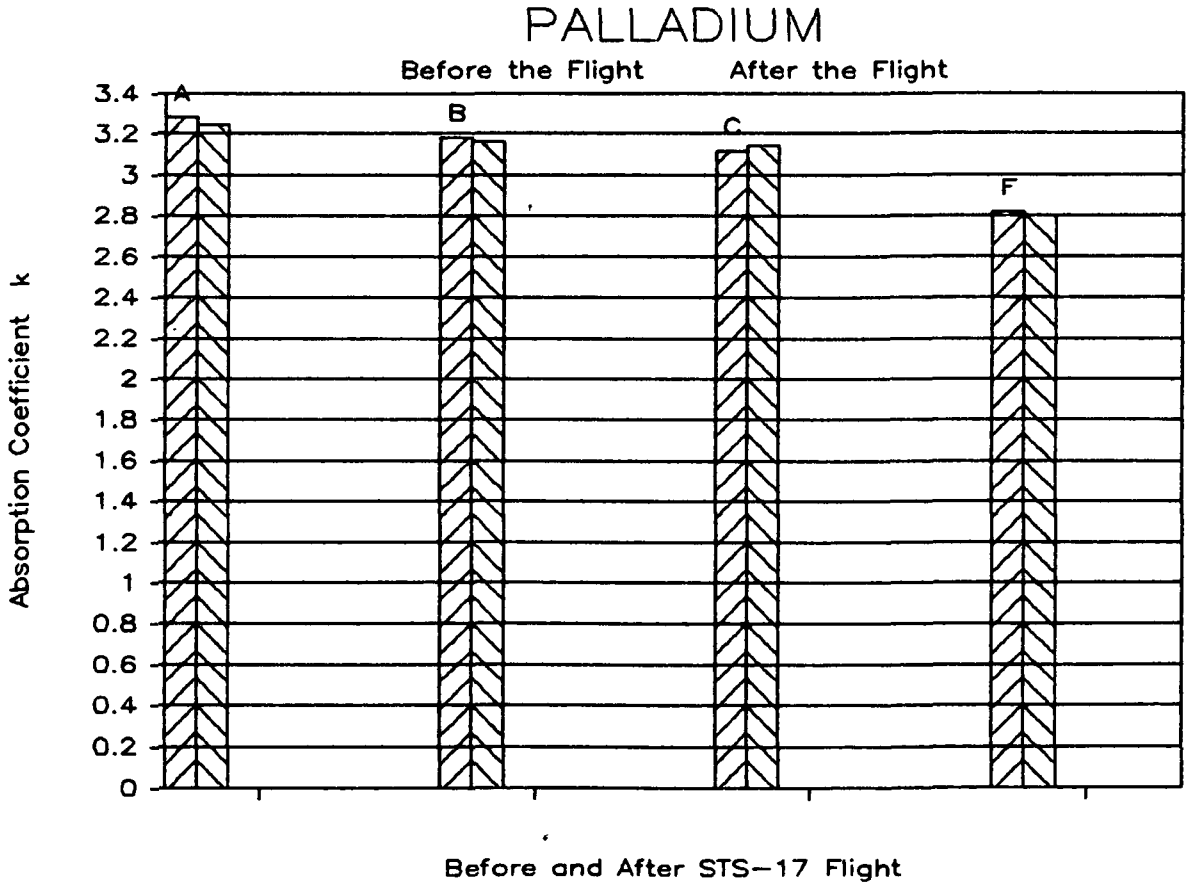
PALLADIUM
Before the Flight
After the Flight
Absorption Coefficient k
3.4
3.2
3
2.8
2.6
2.4
2.2
2
1.8
1.6
1.4
1.2
1
0.8
0.6
0.4
0.2
0
A
B
C
F
Before and After STS-17 Flight

Fig. 28

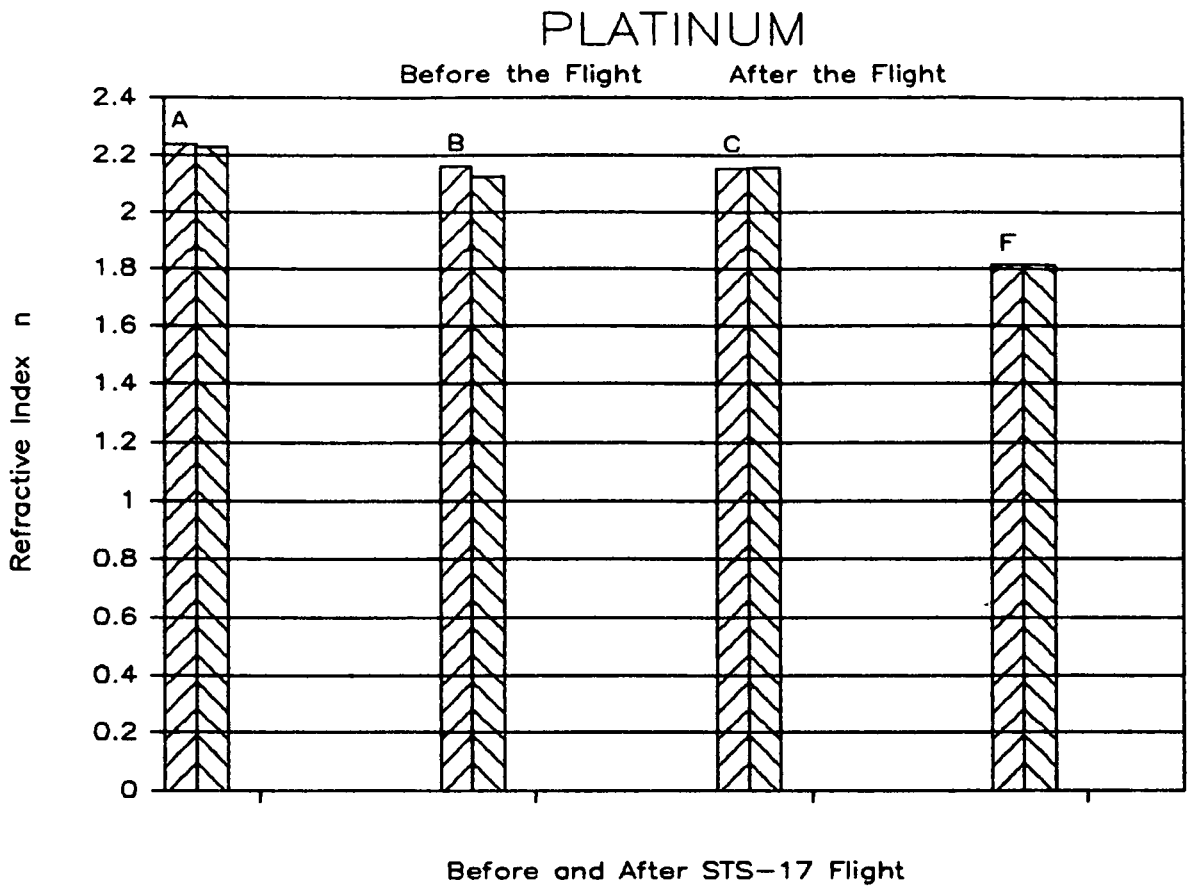
PLATINUM
Before the Flight
After the Flight
Refractive Index n
2.4
2.2
2
1.8
1.6
1.4
1.2
1
0.8
0.6
0.4
0.2
0
A
B
C
F
Before and After STS-17 Flight

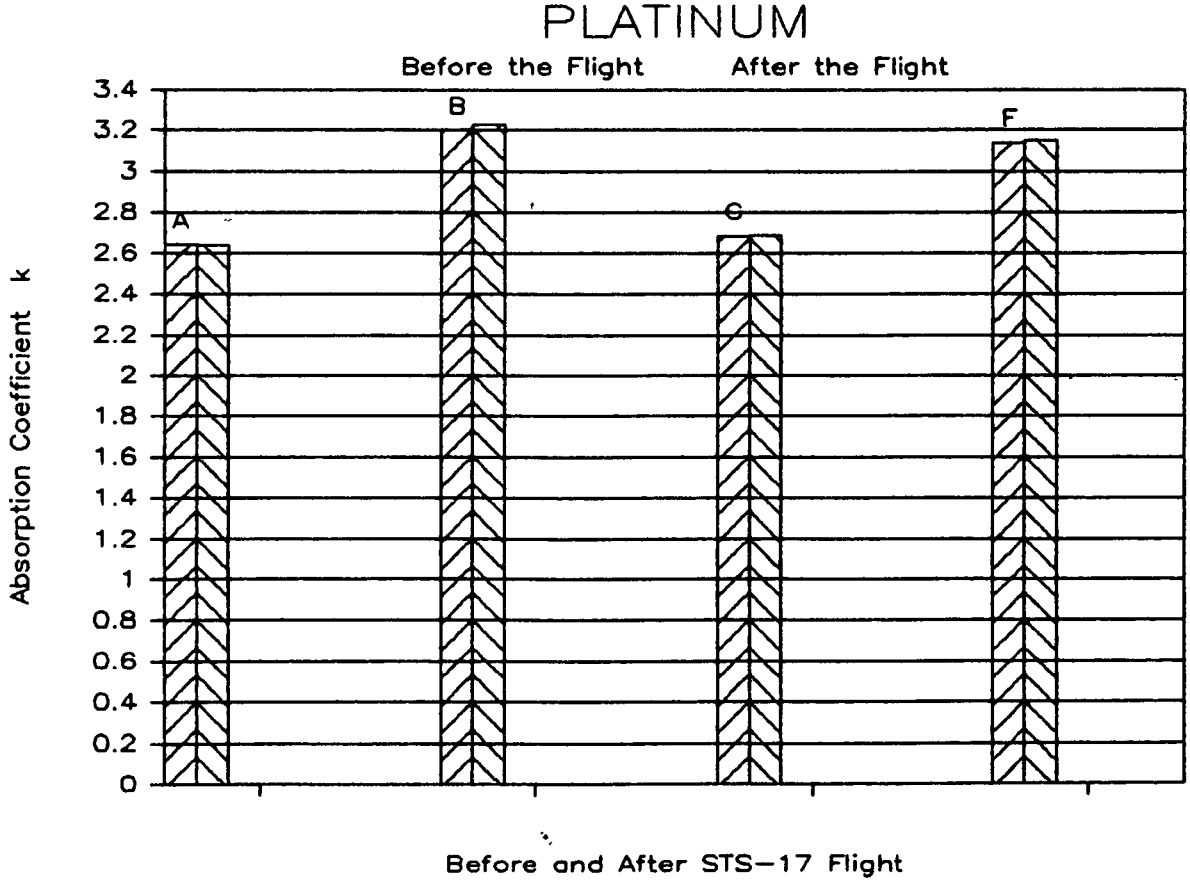
PLATINUM
Before the Flight
After the Flight
Absorption Coefficient k
3.4
3.2
3
2.8
2.6
2.4
2.2
2
1.8
1.6
1.4
1.2
1
0.8
0.6
0.4
0.2
0
A
B
C
F
Before and After STS-17 Flight

Fig. 29

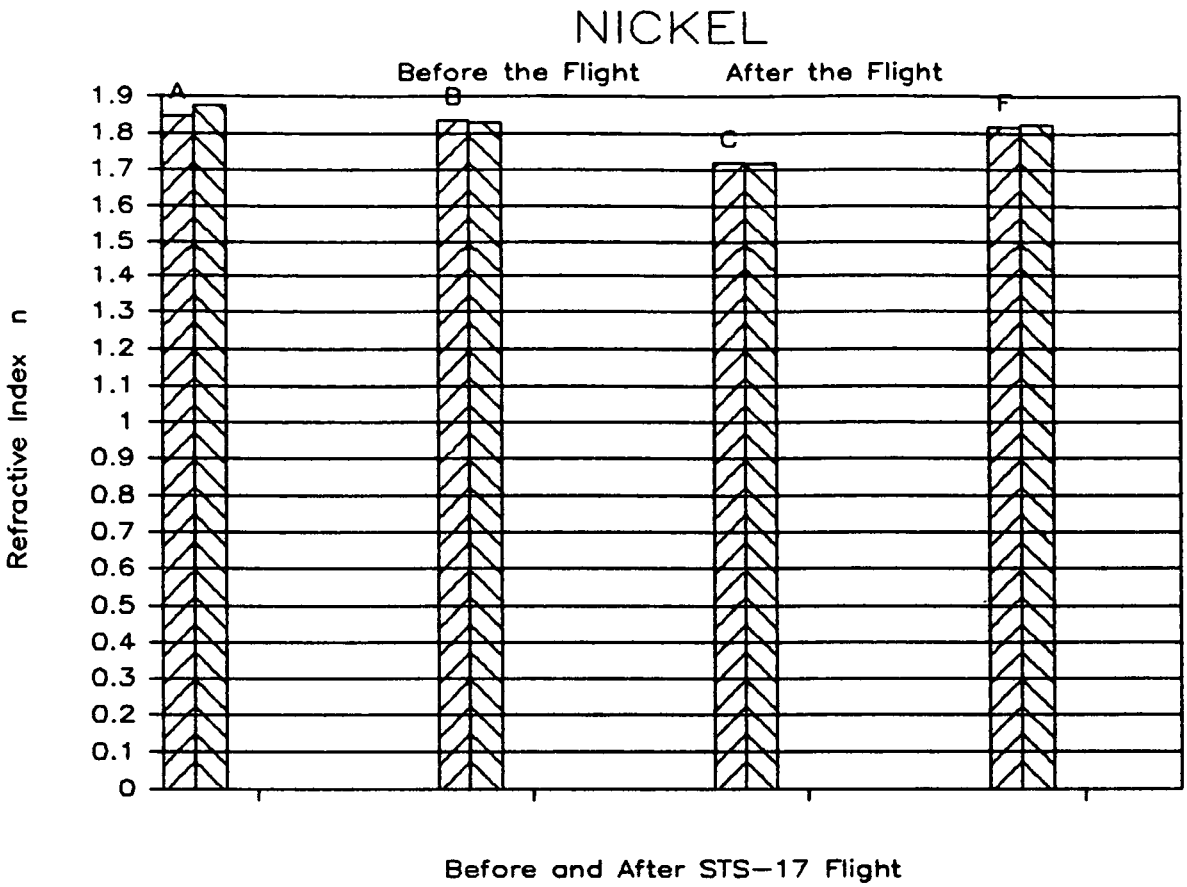
NICKEL
Before the Flight
After the Flight
A
B
C
F
1.9
1.8
1.7
1.6
1.5
1.4
1.3
1.2
1.1
1
0.9
0.8
0.7
0.6
0.5
0.4
0.3
0.2
0.1
0
Refractive Index n
Before and After STS-17 Flight

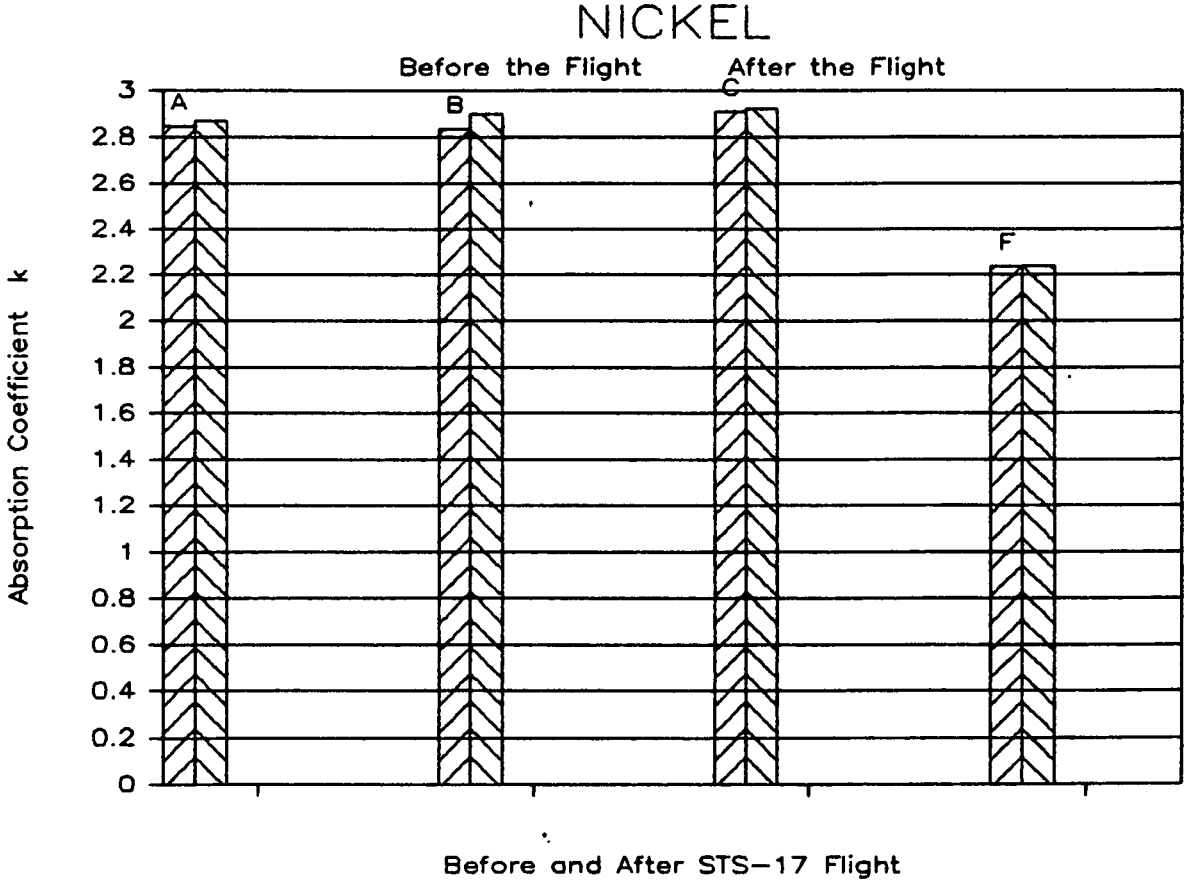
NICKEL
Before the Flight
After the Flight
A
B
C
F
3
2.8
2.6
2.4
2.2
2
1.8
1.6
1.4
1.2
1
0.8
0.6
0.4
0.2
0
Absorption Coefficient k
Before and After STS-17 Flight

Fig. 30

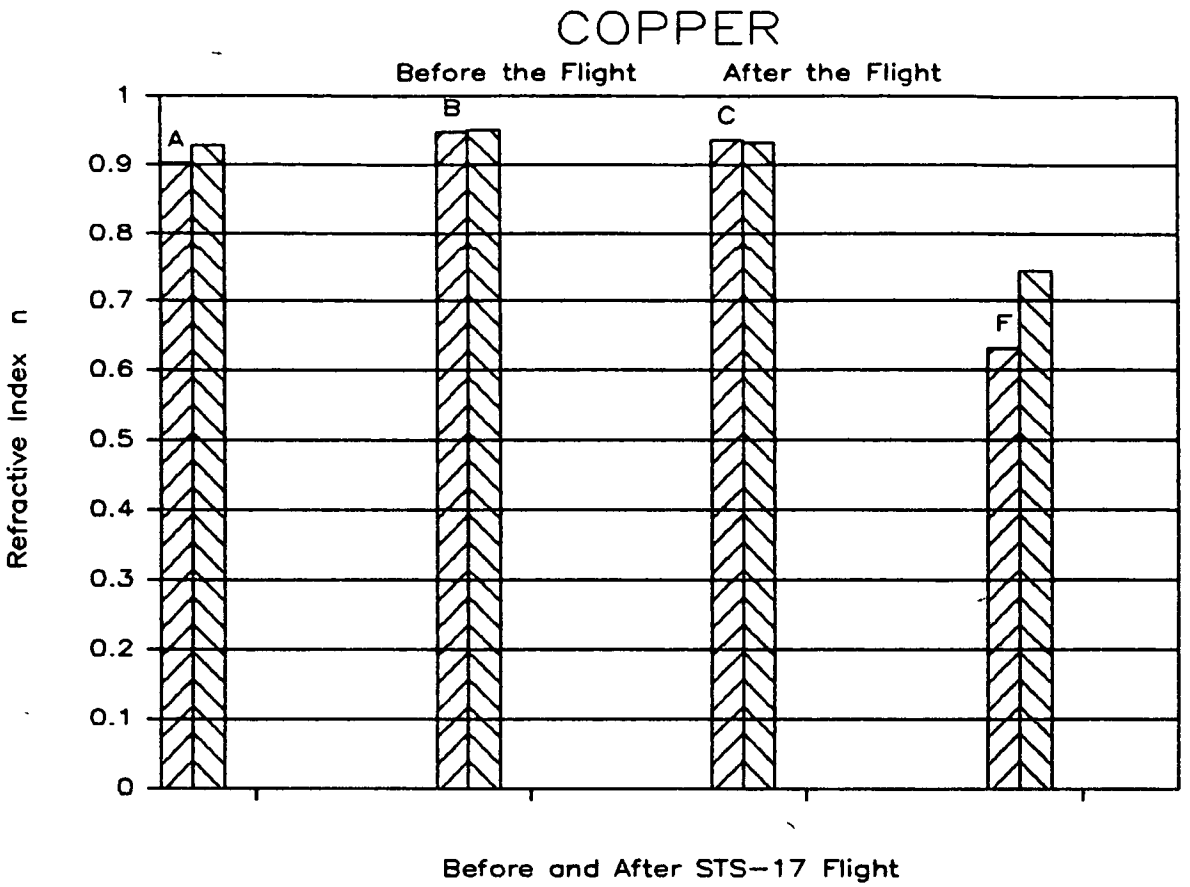

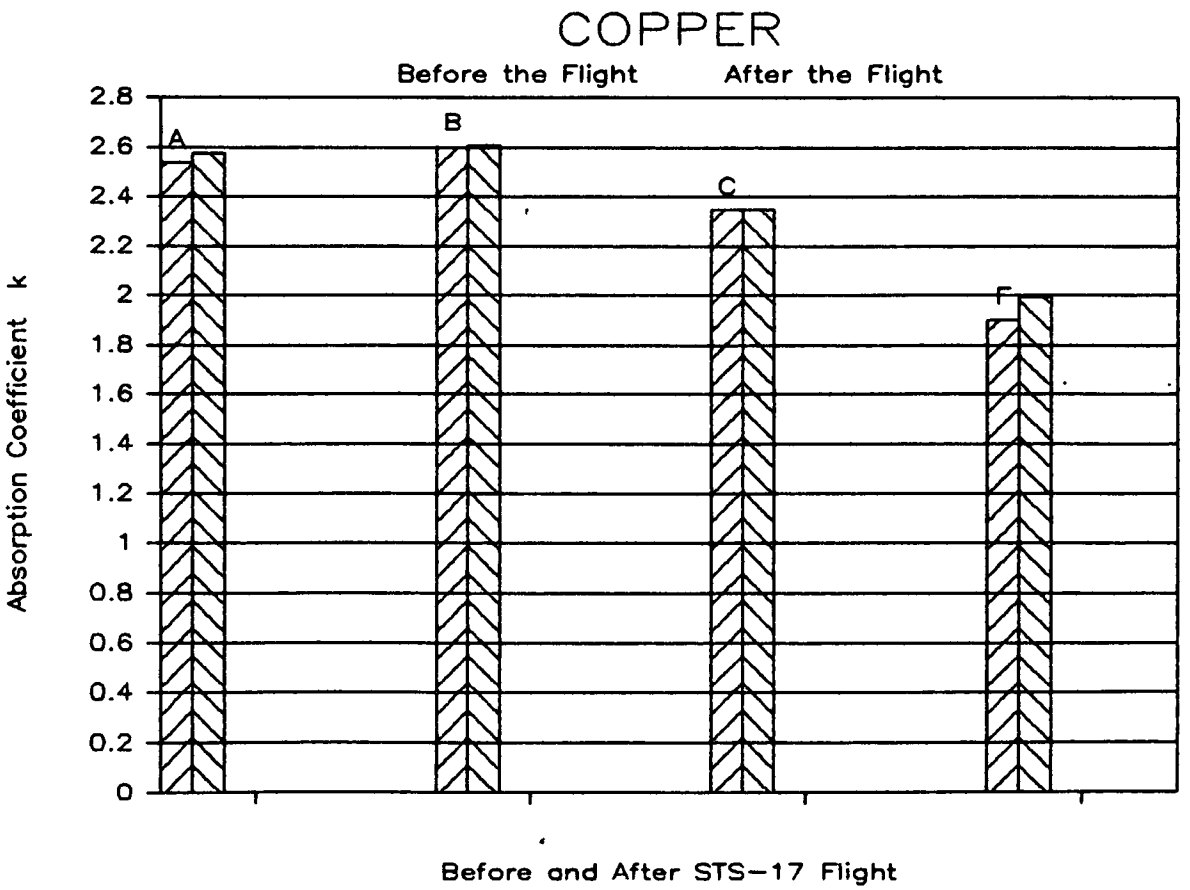

Fig. 31 Ellipsometry Data

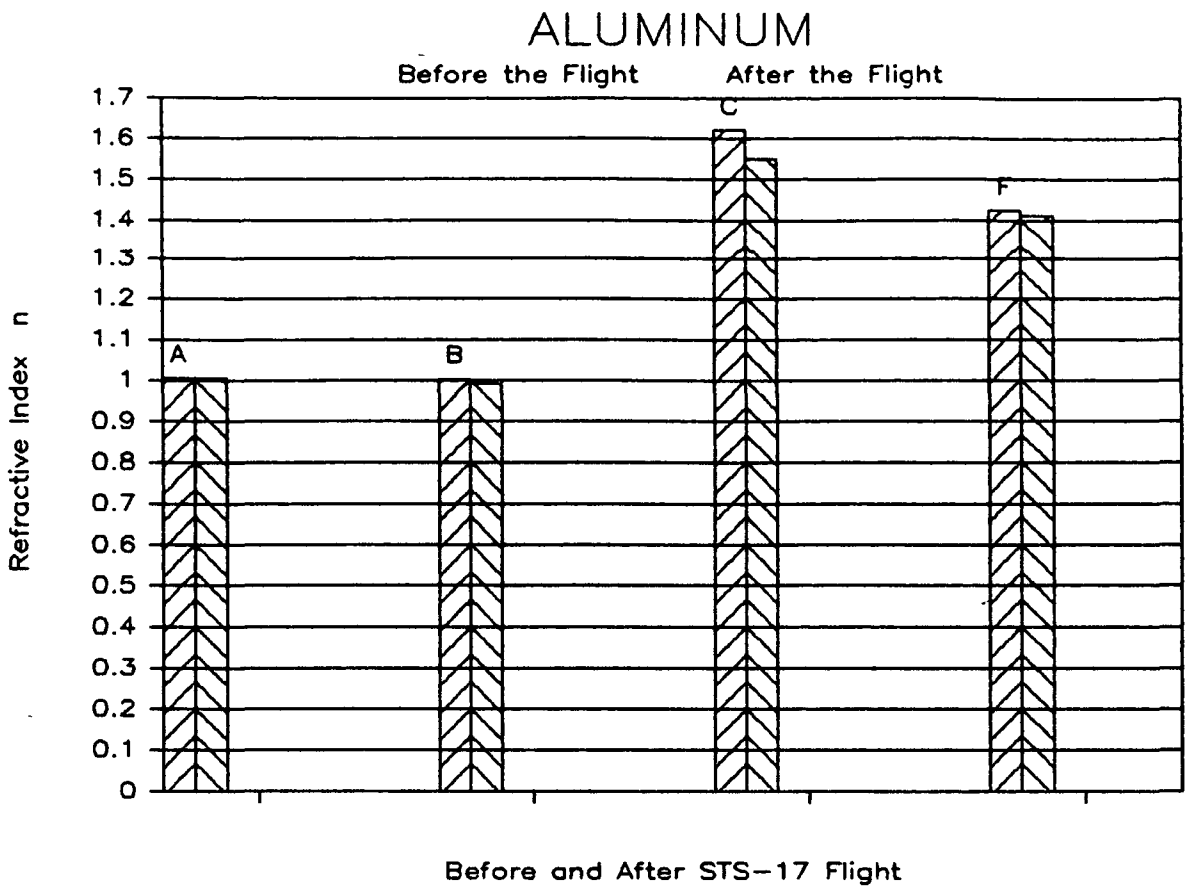
ALUMINUM
Before the Flight
After the Flight
Refractive Index n
1.7
1.6
1.5
1.4
1.3
1.2
1.1
1
0.9
0.8
0.7
0.6
0.5
0.4
0.3
0.2
0.1
0
A
B
C
F
Before and After STS-17 Flight

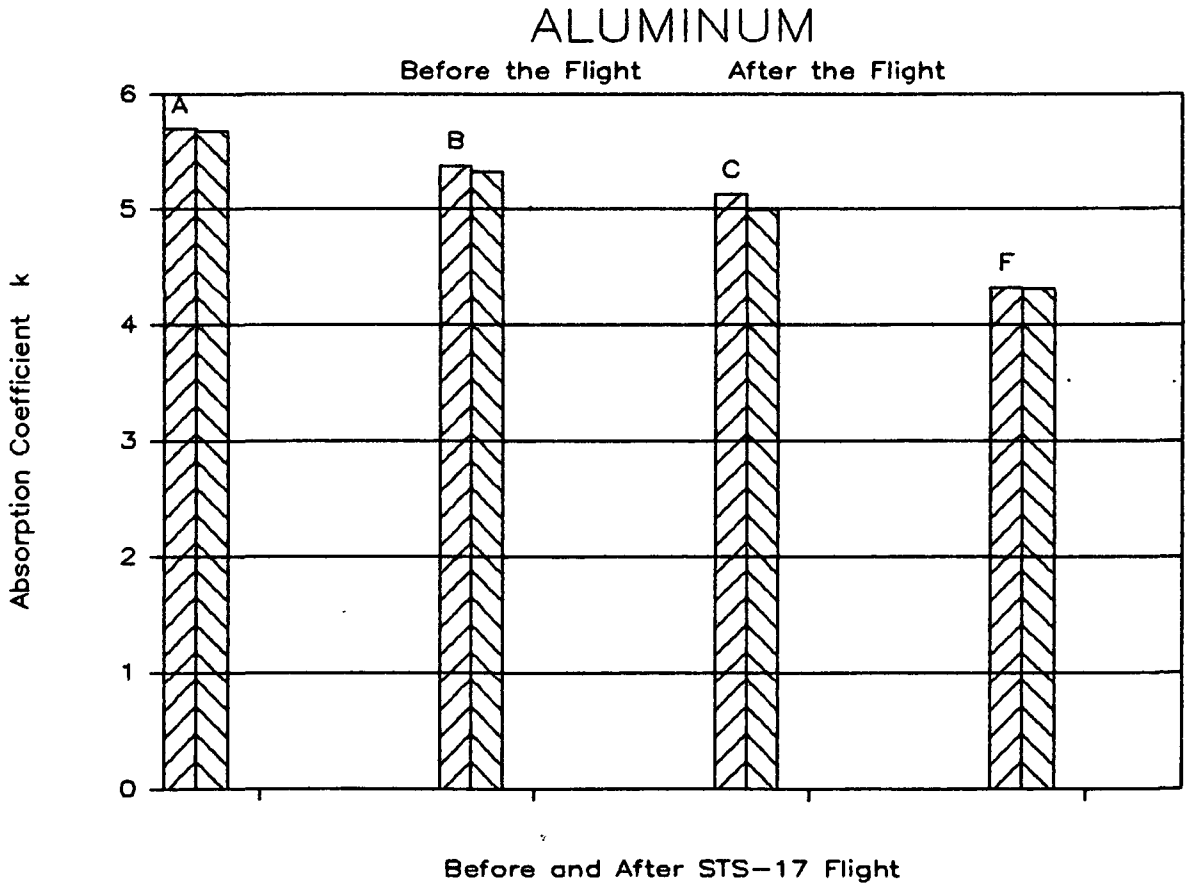
ALUMINUM
Before the Flight
After the Flight
Absorption Coefficient k
6
5
4
3
2
1
0
A
B
C
F
Before and After STS-17 Flight

Fig. 32

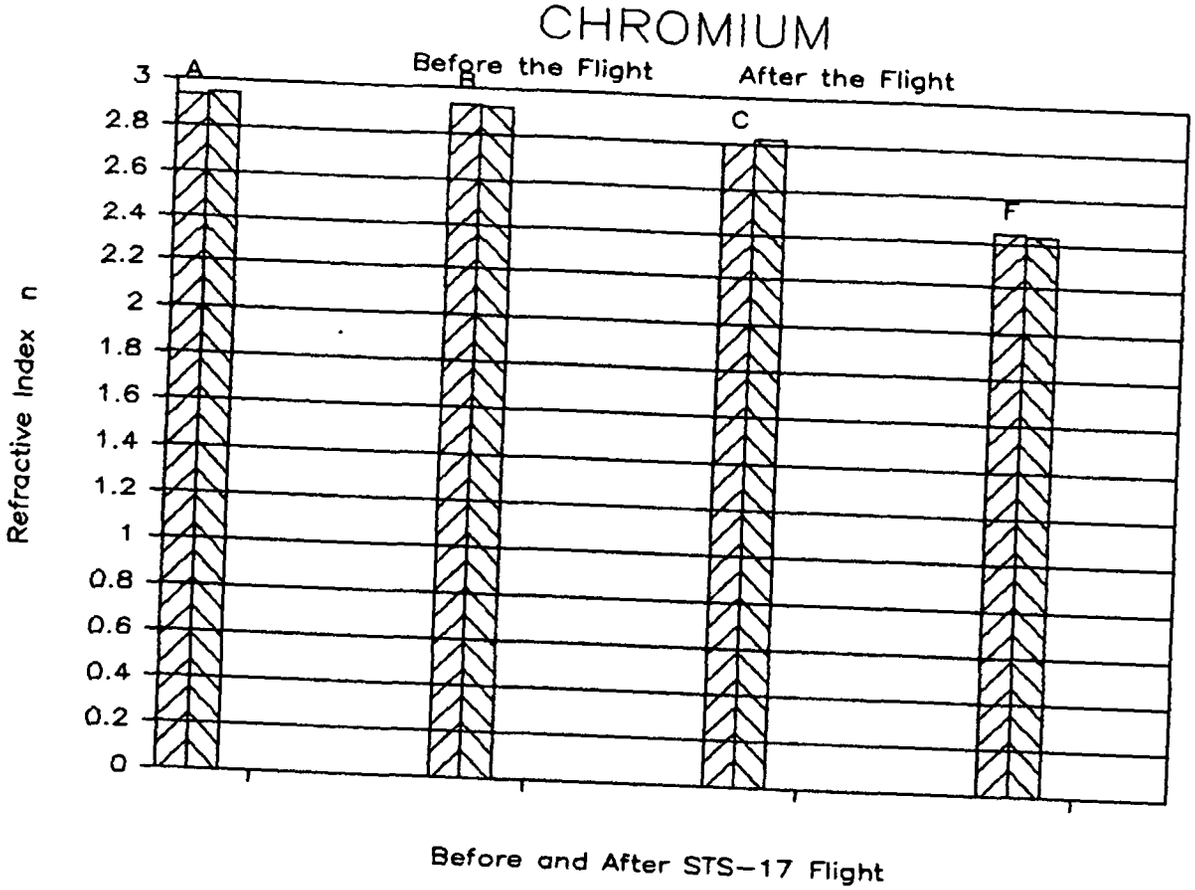
CHROMIUM
Before the Flight
After the Flight
A
B
C
F
Refractive Index n
3
2.8
2.6
2.4
2.2
2
1.8
1.6
1.4
1.2
1
0.8
0.6
0.4
0.2
0
Before and After STS-17 Flight

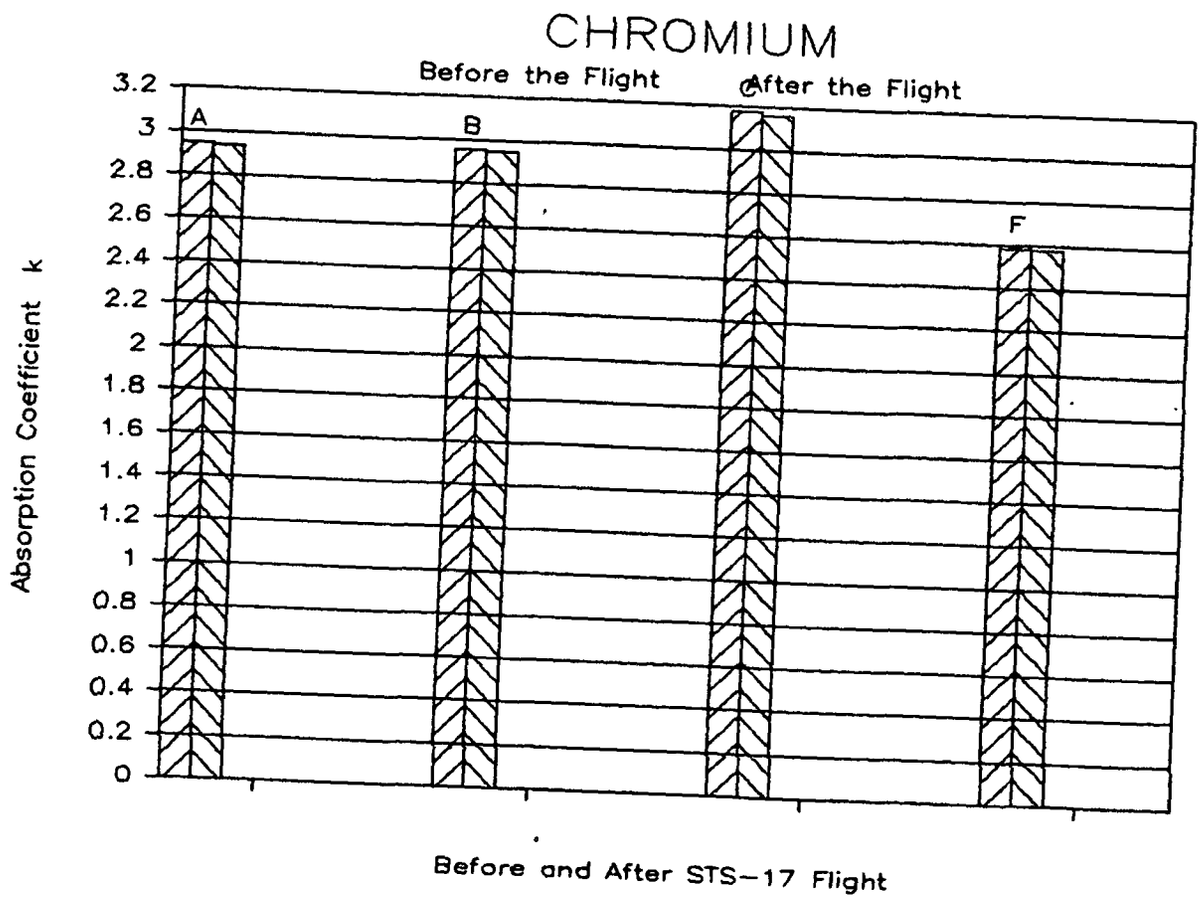
CHROMIUM
Before the Flight
After the Flight
A
B
C
F
Absorption Coefficient k
3.2
3
2.8
2.6
2.4
2.2
2
1.8
1.6
1.4
1.2
1
0.8
0.6
0.4
0.2
0
Before and After STS-17 Flight

Fig. 33

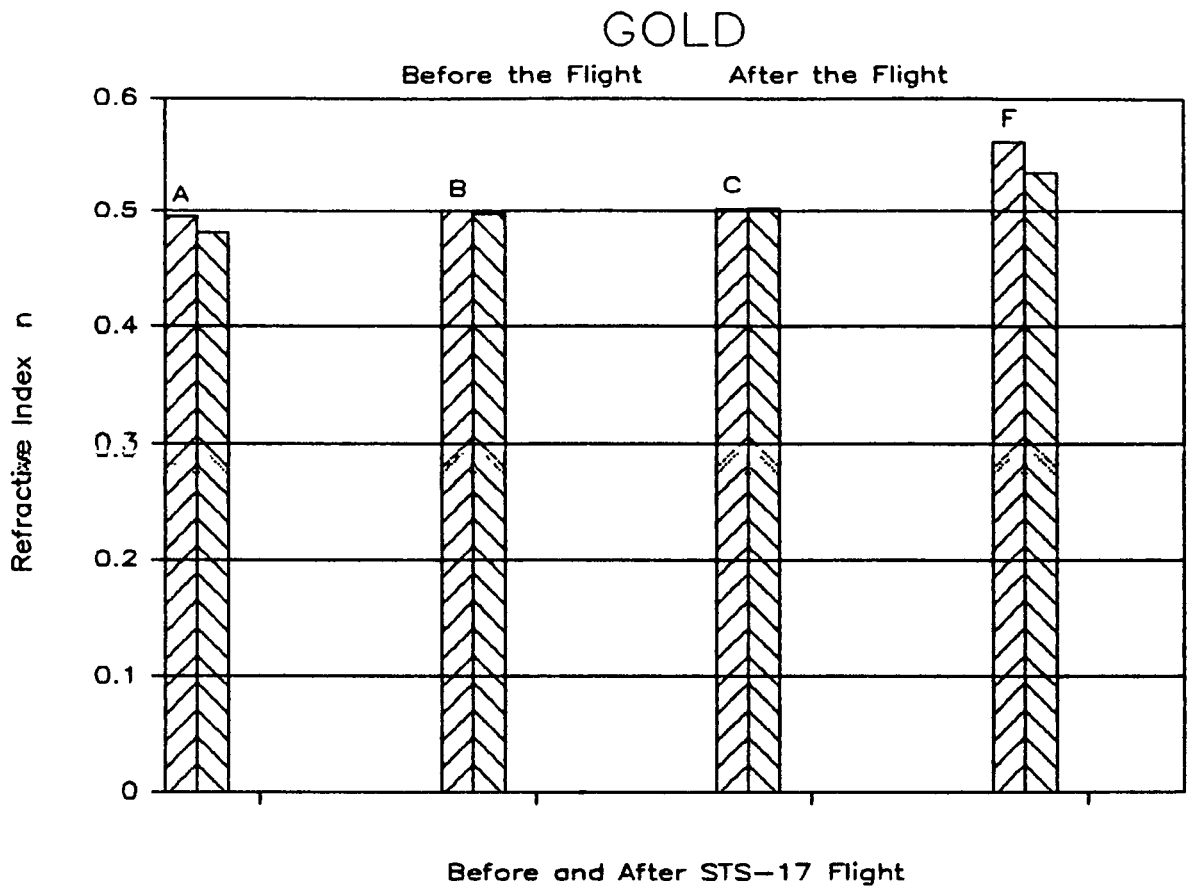
GOLD
Before the Flight
After the Flight
Refractive Index n
0.6
0.5
0.4
0.3
0.2
0.1
0
A
B
C
F
Before and After STS-17 Flight

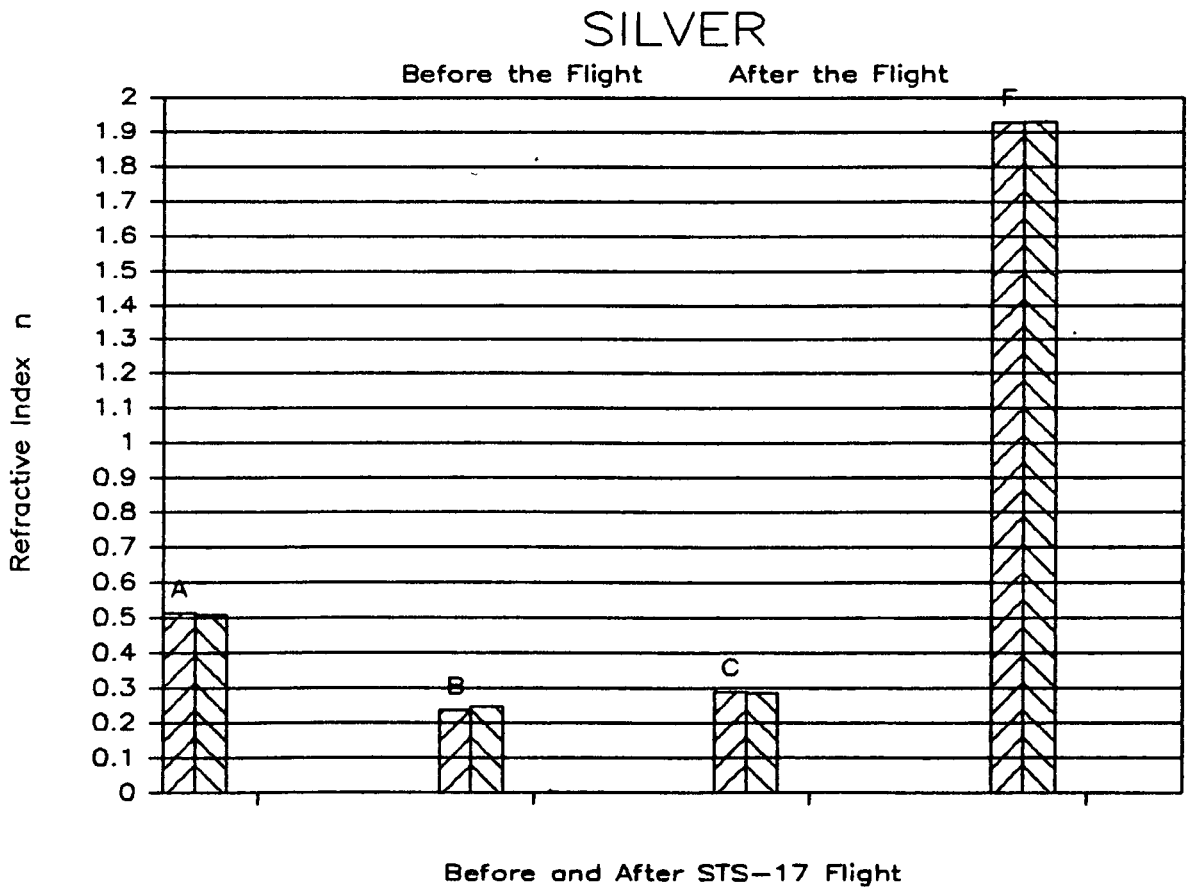
SILVER
Before the Flight
After the Flight
Refractive Index n
2
1.9
1.8
1.7
1.6
1.5
1.4
1.3
1.2
1.1
1
0.9
0.8
0.7
0.6
0.5
0.4
0.3
0.2
0.1
0
A
B
C
F
Before and After STS-17 Flight

Fig. 34

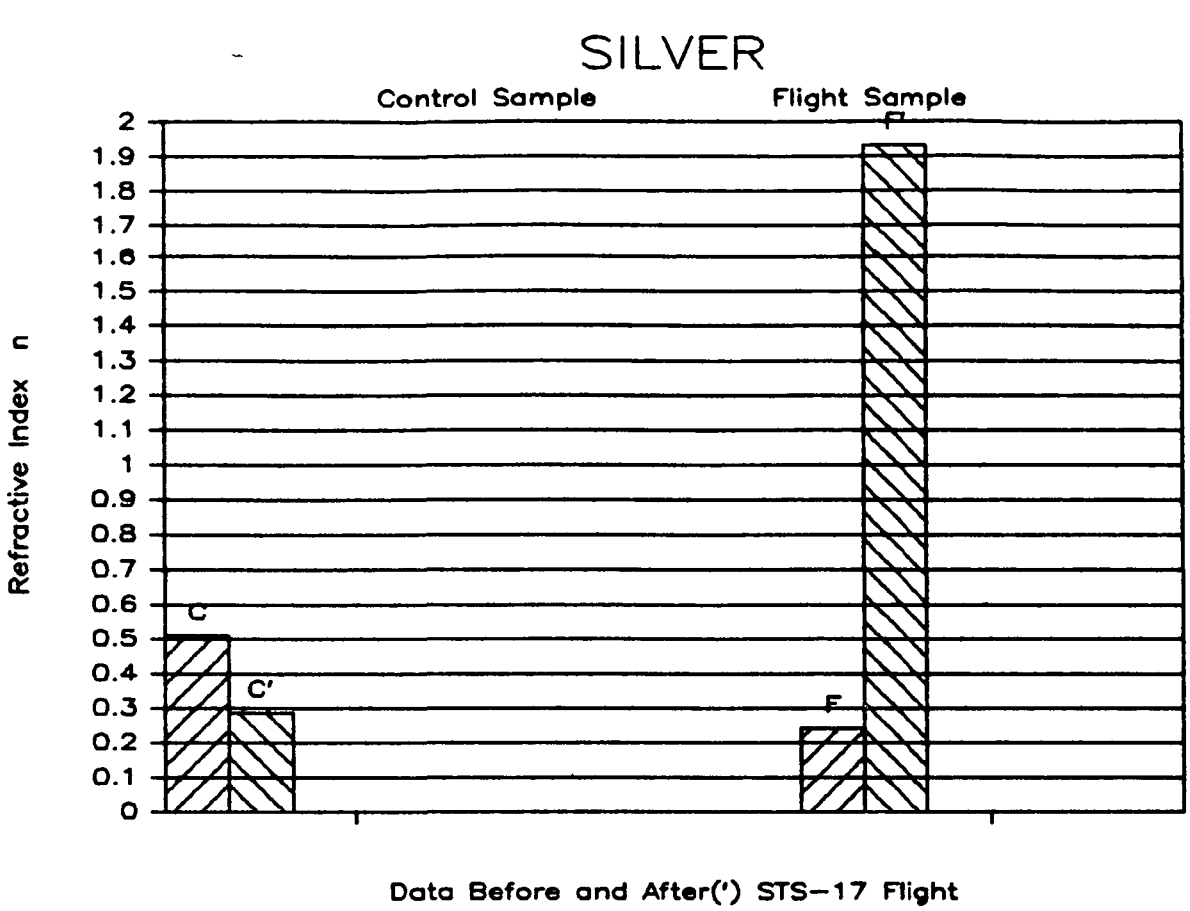
SILVER
Control Sample
Flight Sample
Refractive Index n
2
1.9
1.8
1.7
1.6
1.5
1.4
1.3
1.2
1.1
1
0.9
0.8
0.7
0.6
0.5
0.4
0.3
0.2
0.1
0
C
C'
F
F'
Data Before and After(') STS-17 Flight

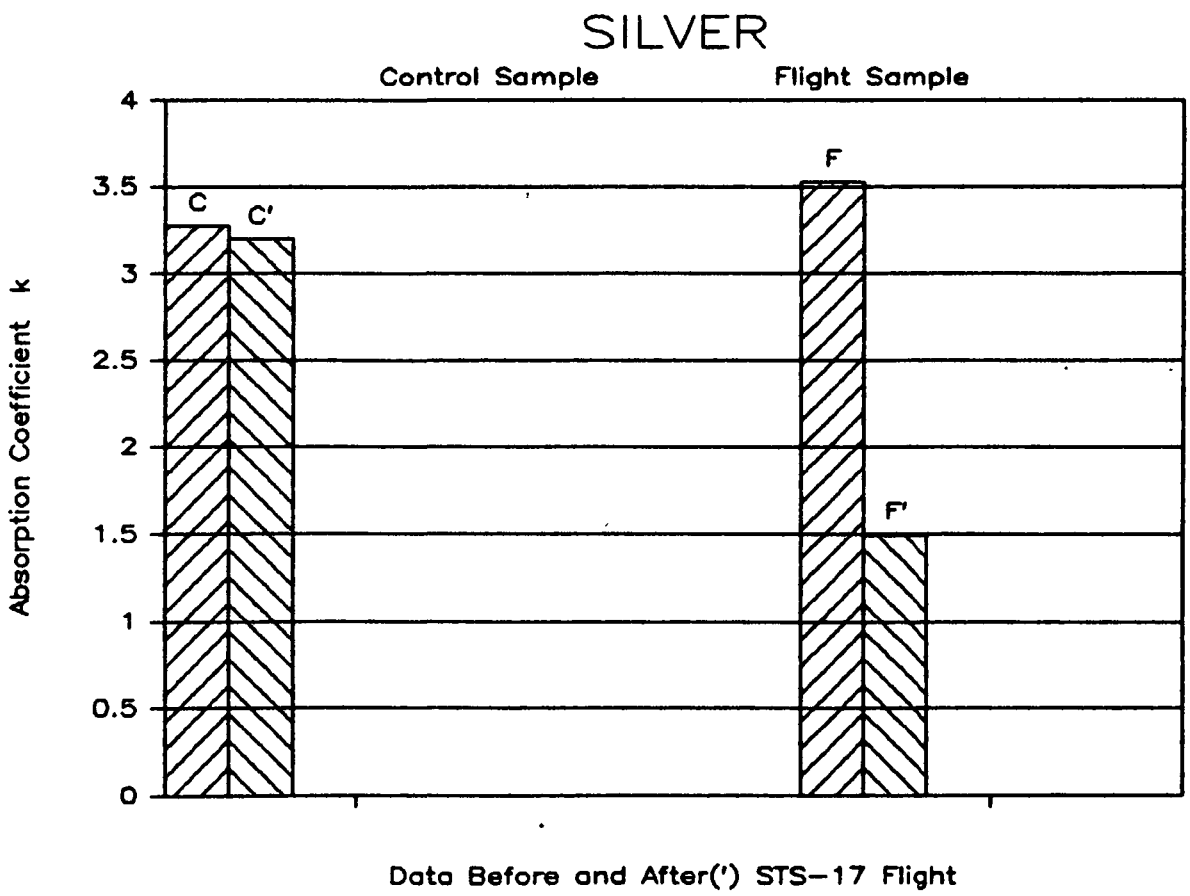
SILVER
Control Sample
Flight Sample
Absorption Coefficient k
4
3.5
3
2.5
2
1.5
1
0.5
0
C
C'
F
F'
Data Before and After(') STS-17 Flight

Fig. 35

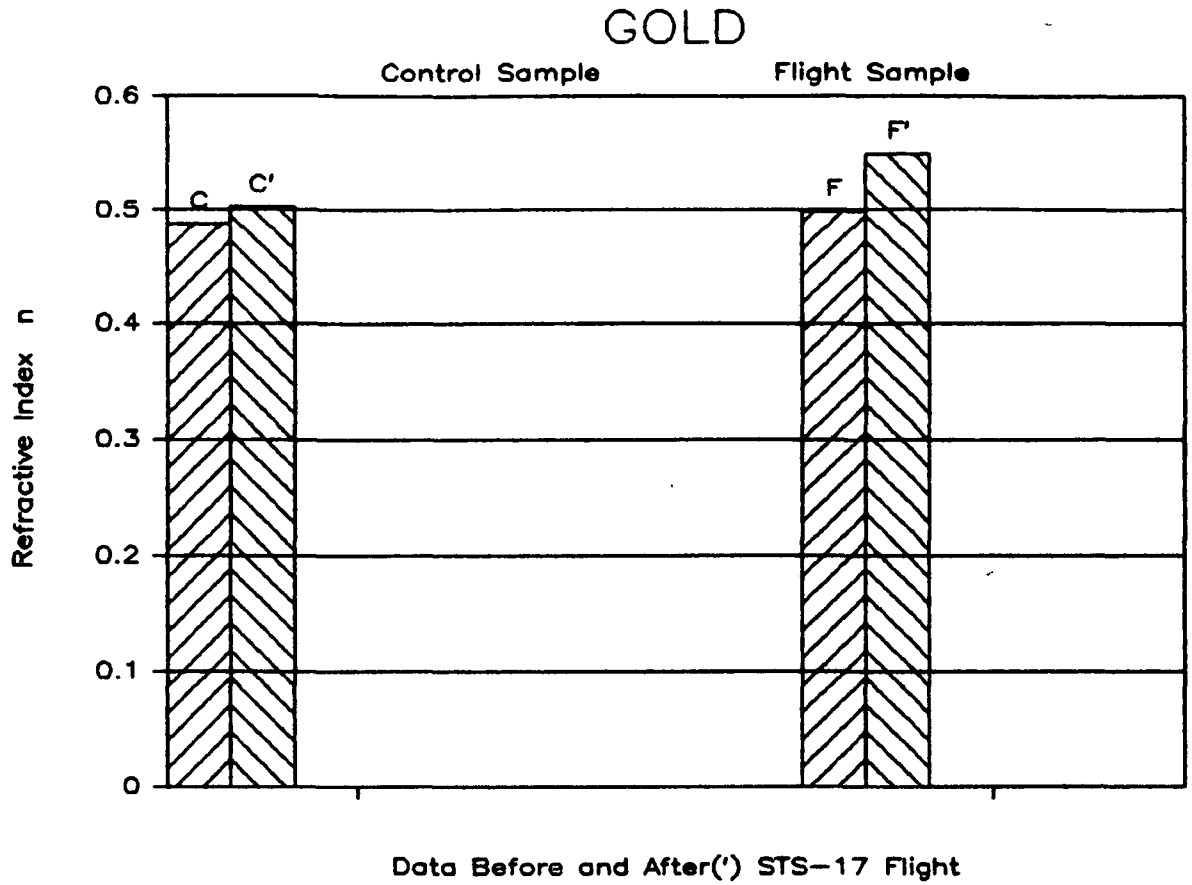
GOLD
Control Sample
Flight Sample
0.6
0.5
0.4
0.3
0.2
0.1
0
C
C'
F
F'
Refractive Index n
Data Before and After(') STS-17 Flight

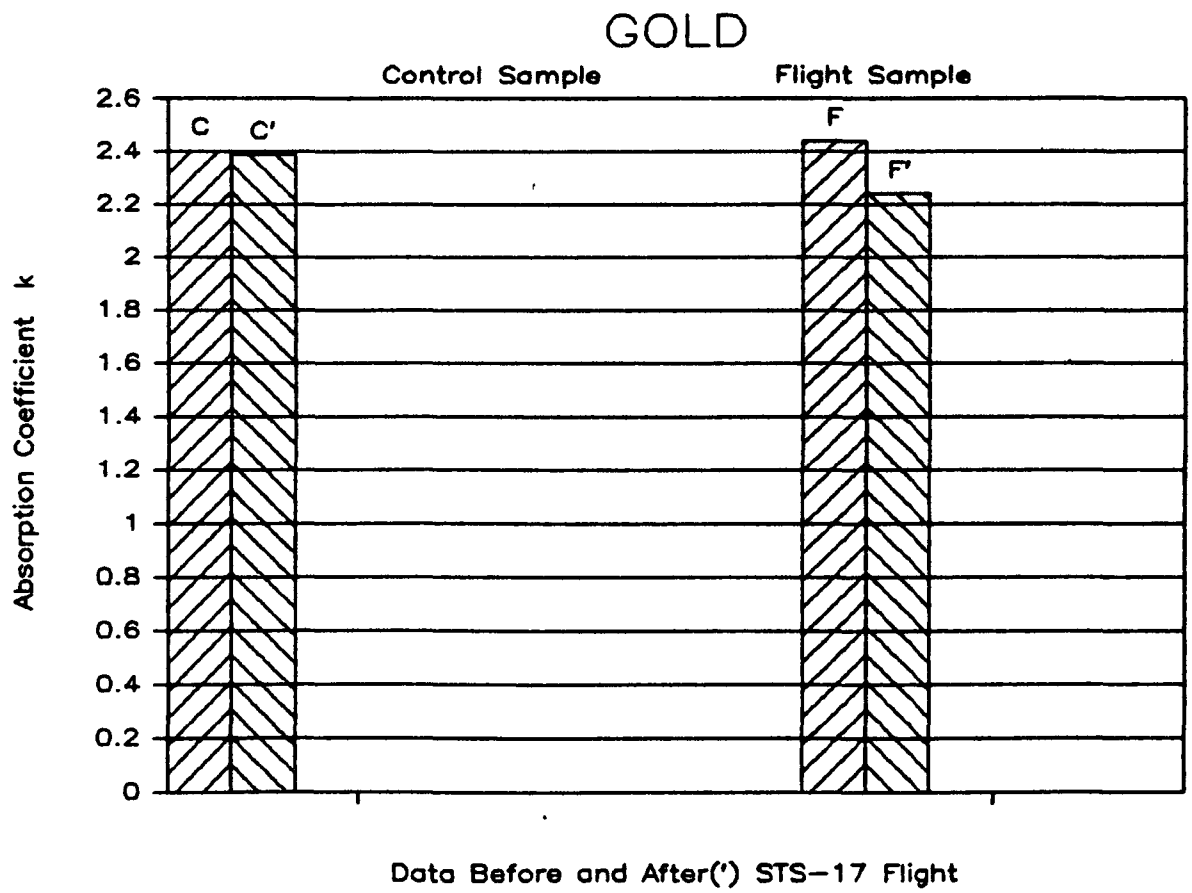
GOLD
Control Sample
Flight Sample
2.6
2.4
2.2
2
1.8
1.6
1.4
1.2
1
0.8
0.6
0.4
0.2
0
C
C'
F
F'
Absorption Coefficient k
Data Before and After(') STS-17 Flight

Fig. 36

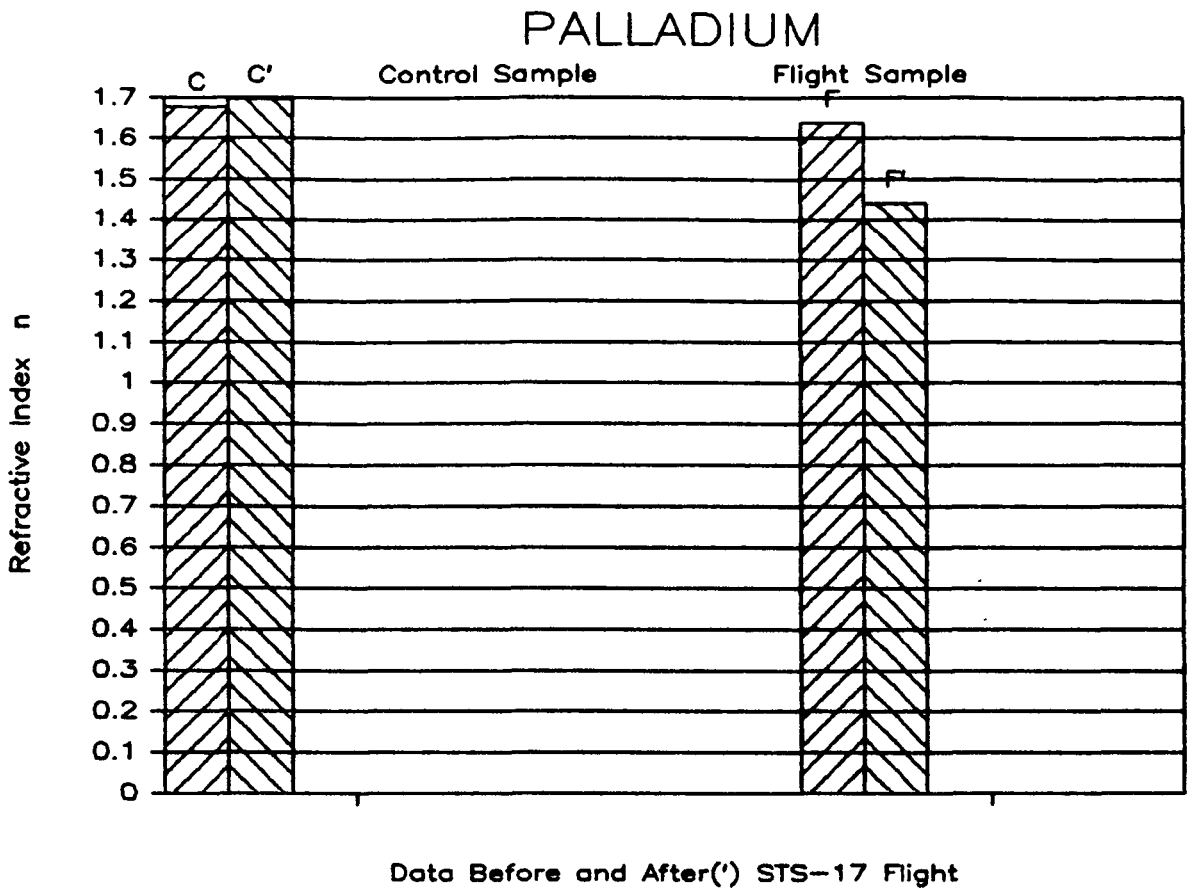
PALLADIUM
Control Sample
Flight Sample
C
C'
F
F'
Refractive Index n
1.7
1.6
1.5
1.4
1.3
1.2
1.1
1
0.9
0.8
0.7
0.6
0.5
0.4
0.3
0.2
0.1
0
Data Before and After(') STS-17 Flight

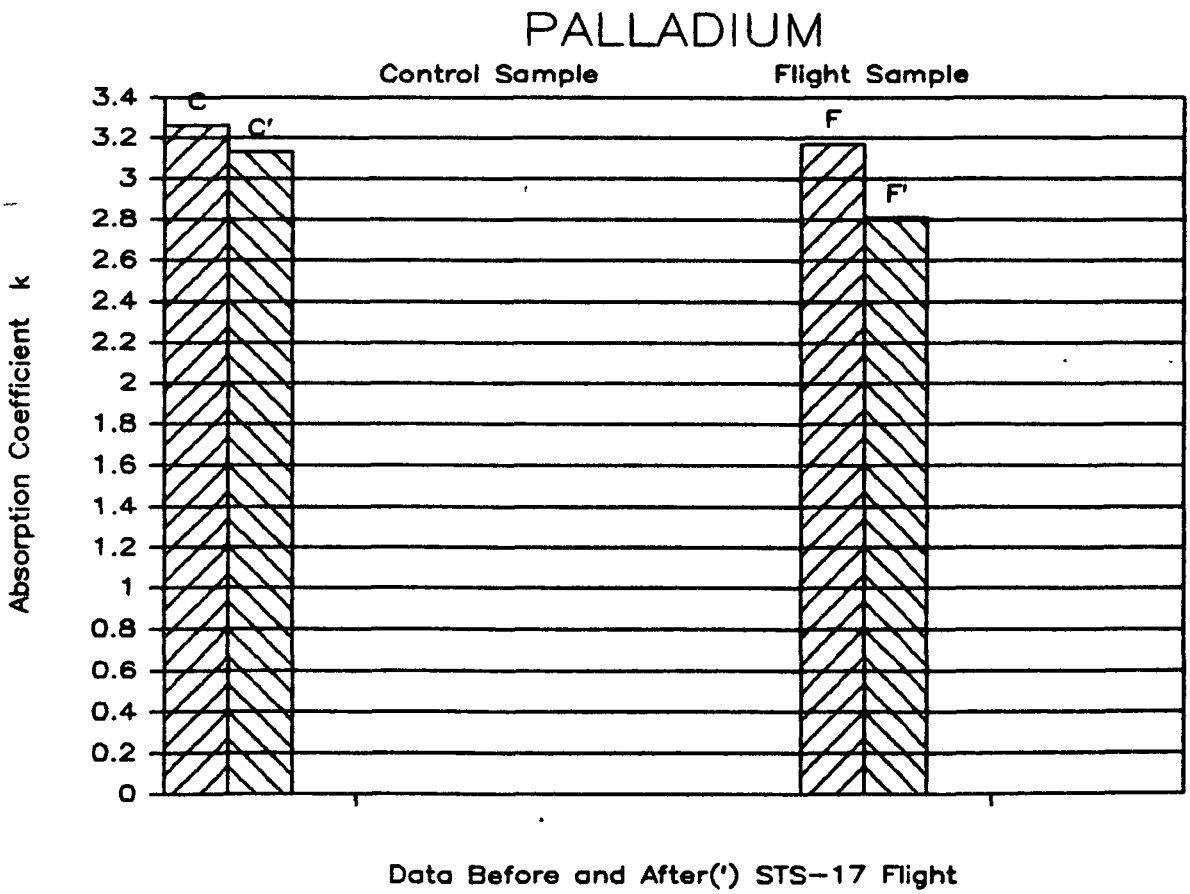
PALLADIUM
Control Sample
Flight Sample
C
C'
F
F'
Absorption Coefficient k
3.4
3.2
3
2.8
2.6
2.4
2.2
2
1.8
1.6
1.4
1.2
1
0.8
0.6
0.4
0.2
0
Data Before and After(') STS-17 Flight

Fig. 37

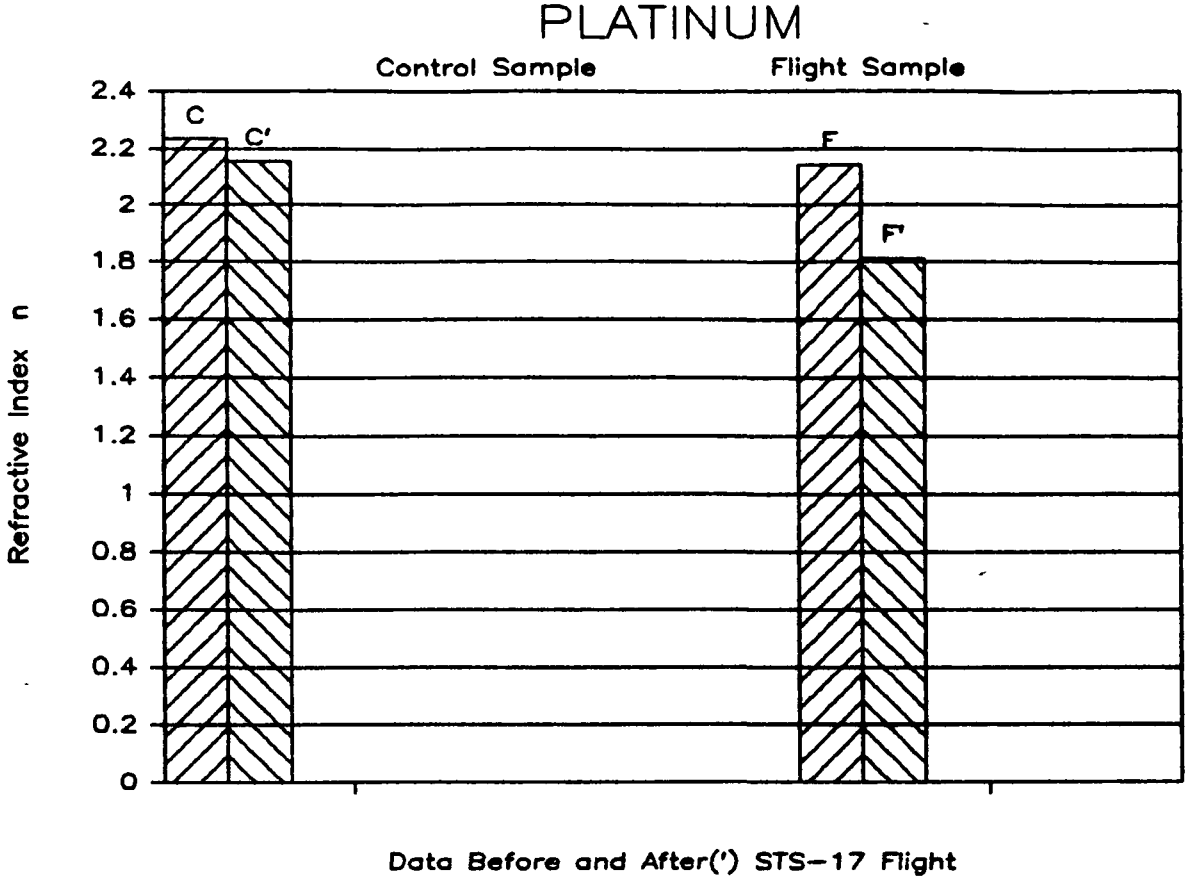
PLATINUM
Control Sample
Flight Sample
C
C'
F
F'
2.4
2.2
2
1.8
1.6
1.4
1.2
1
0.8
0.6
0.4
0.2
0
Refractive Index n
Data Before and After(') STS-17 Flight

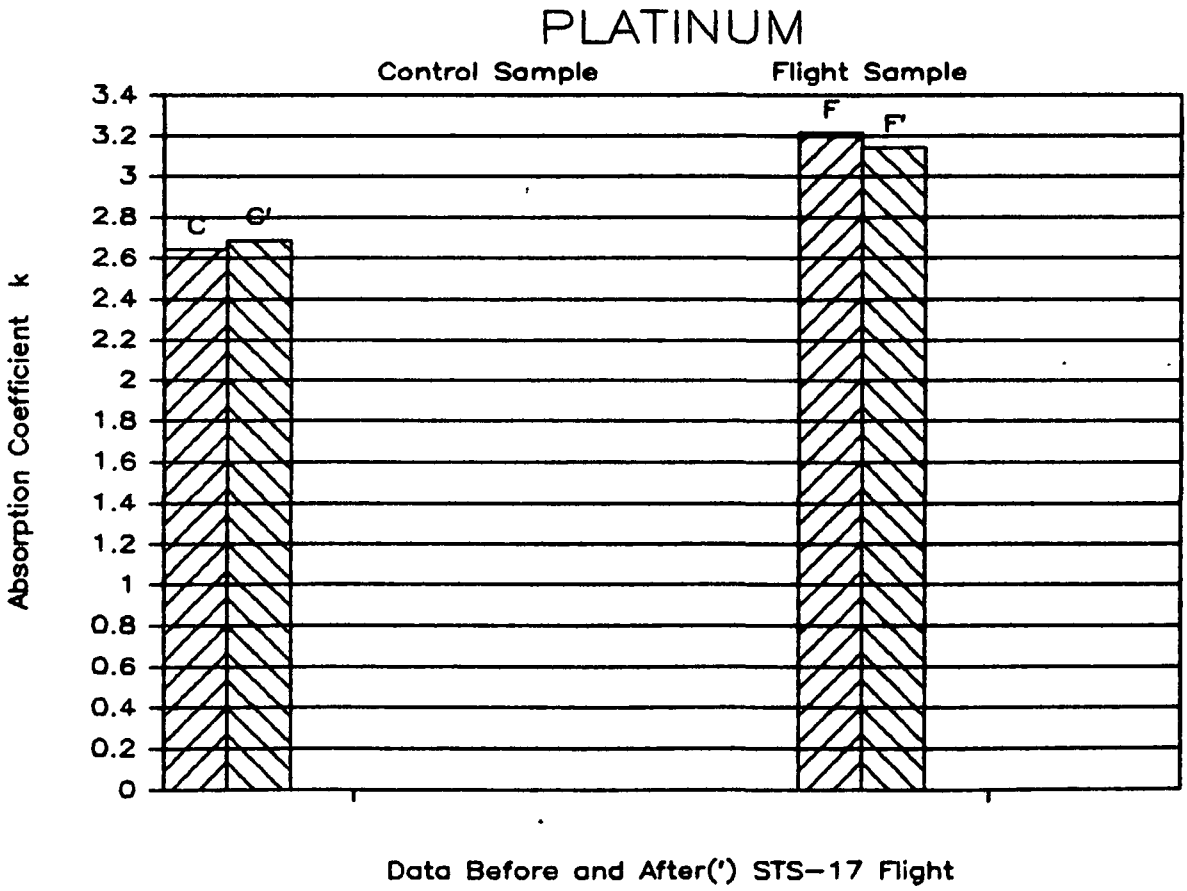
PLATINUM
Control Sample
Flight Sample
C
C'
F
F'
3.4
3.2
3
2.8
2.6
2.4
2.2
2
1.8
1.6
1.4
1.2
1
0.8
0.6
0.4
0.2
0
Absorption Coefficient k
Data Before and After(') STS-17 Flight

Fig. 38

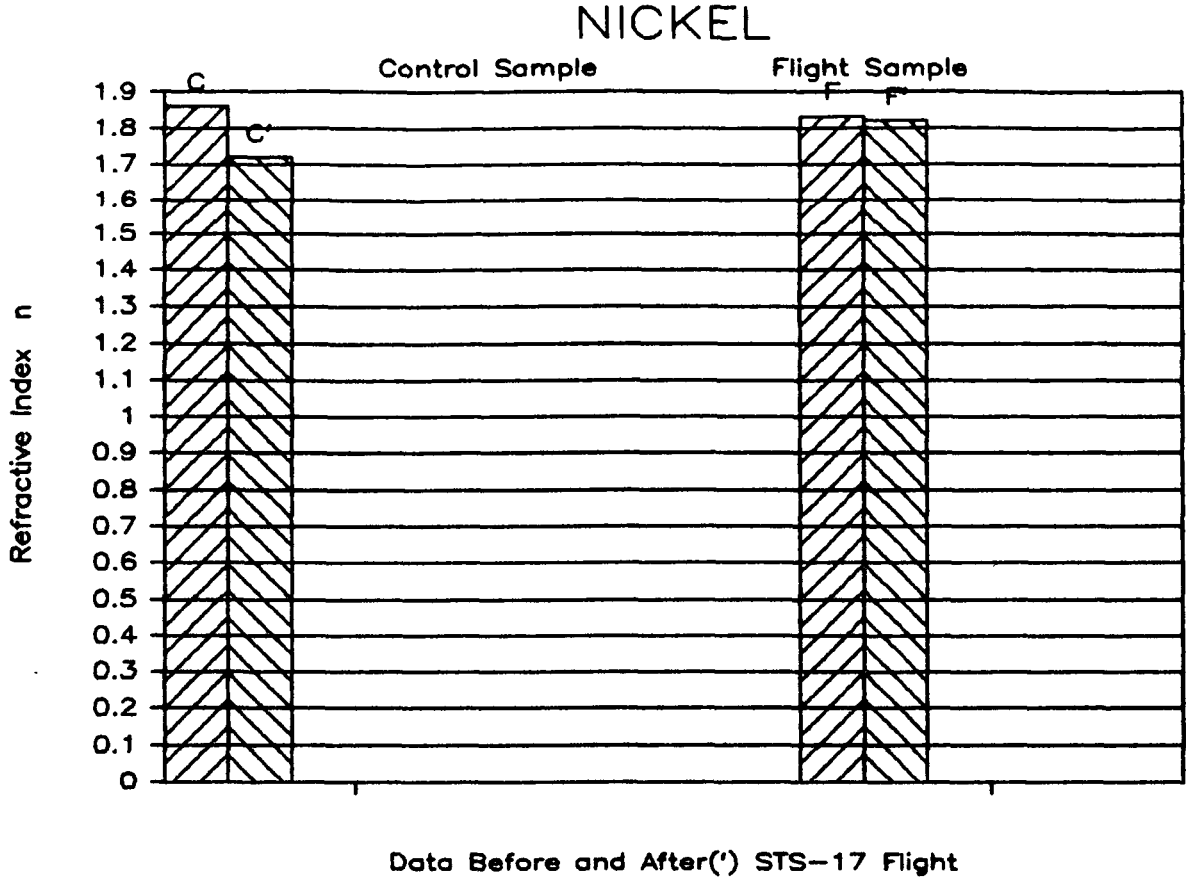
NICKEL
Control Sample
Flight Sample
C
C'
F
F'
Refractive Index n
1.9
1.8
1.7
1.6
1.5
1.4
1.3
1.2
1.1
1
0.9
0.8
0.7
0.6
0.5
0.4
0.3
0.2
0.1
0
Data Before and After(') STS-17 Flight

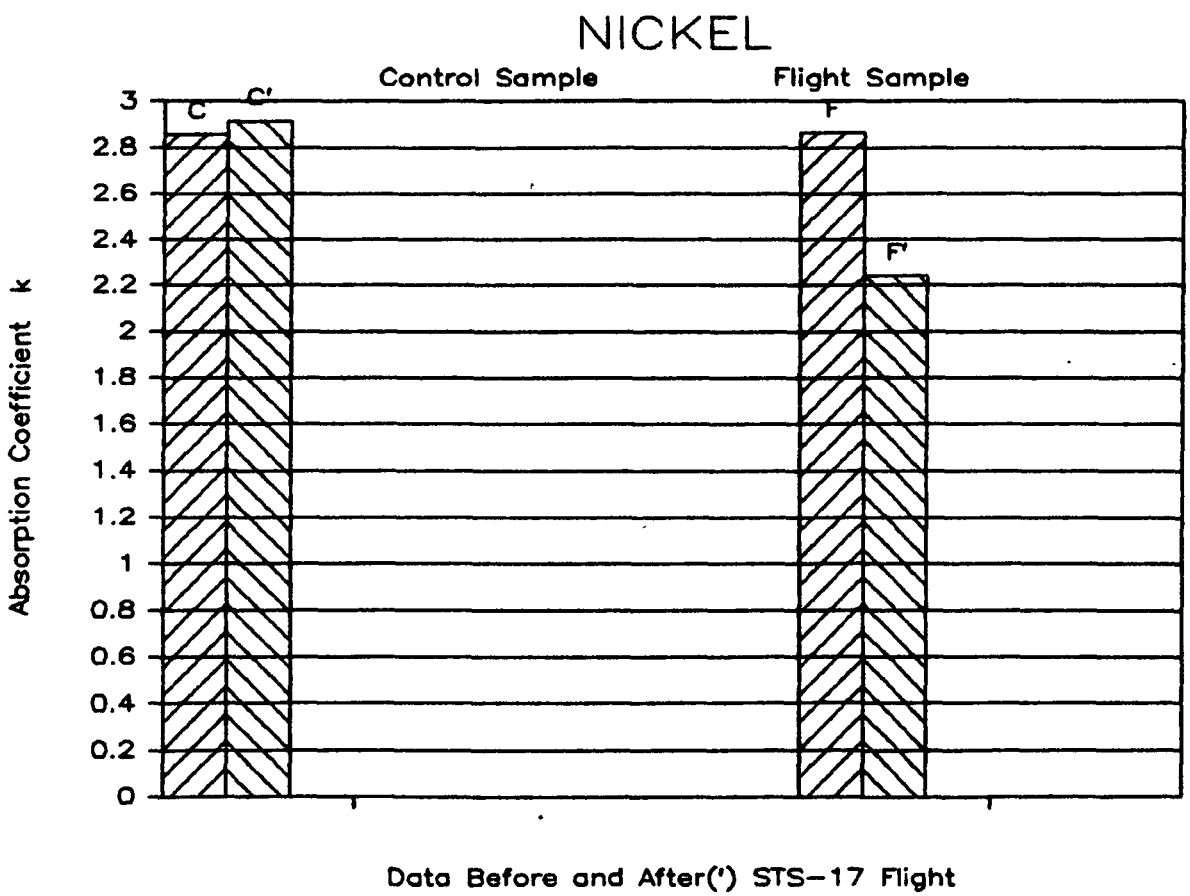
NICKEL
Control Sample
Flight Sample
C
C'
F
F'
Absorption Coefficient k
3
2.8
2.6
2.4
2.2
2
1.8
1.6
1.4
1.2
1
0.8
0.6
0.4
0.2
0
Data Before and After(') STS-17 Flight

Fig. 39

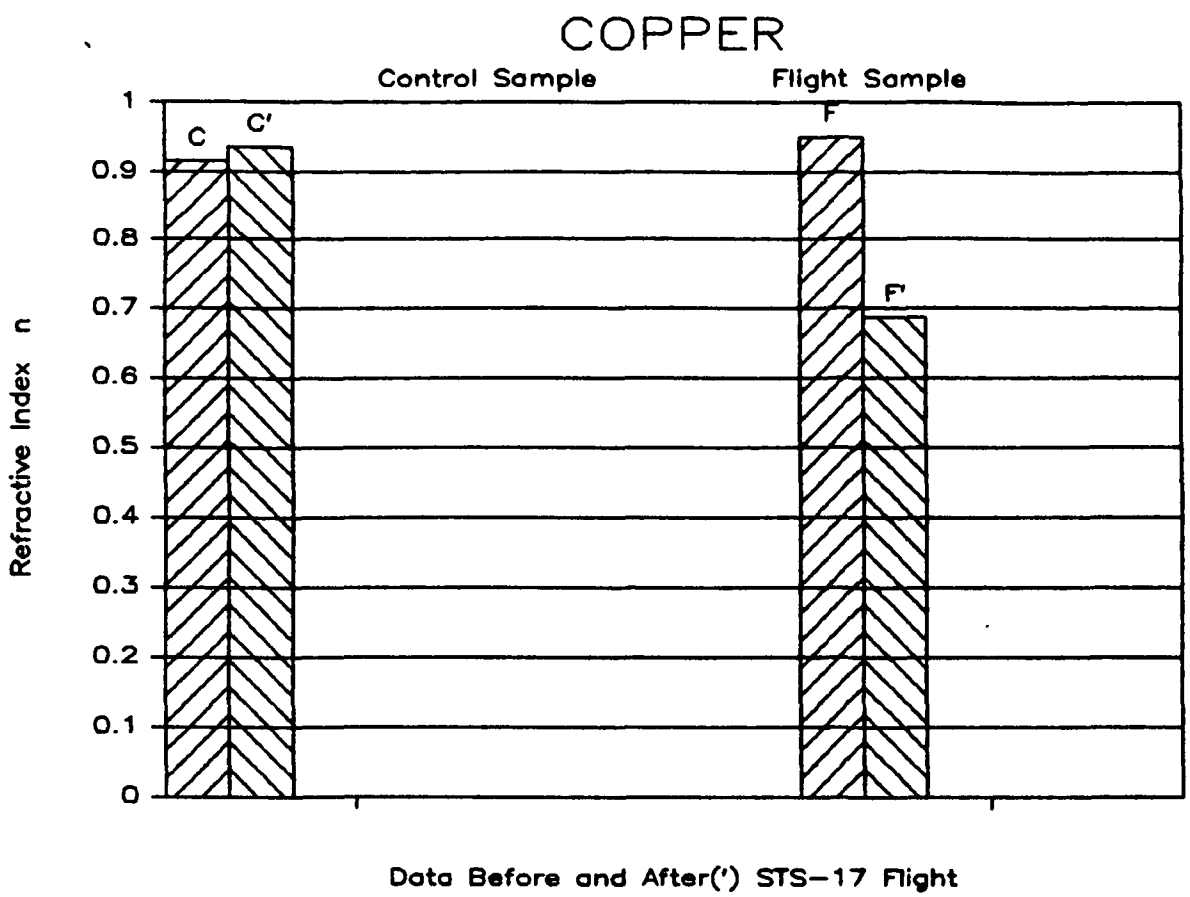
COPPER
Control Sample
Flight Sample
C
C'
F
F'
Refractive Index n
1
0.9
0.8
0.7
0.6
0.5
0.4
0.3
0.2
0.1
0
Data Before and After(') STS-17 Flight

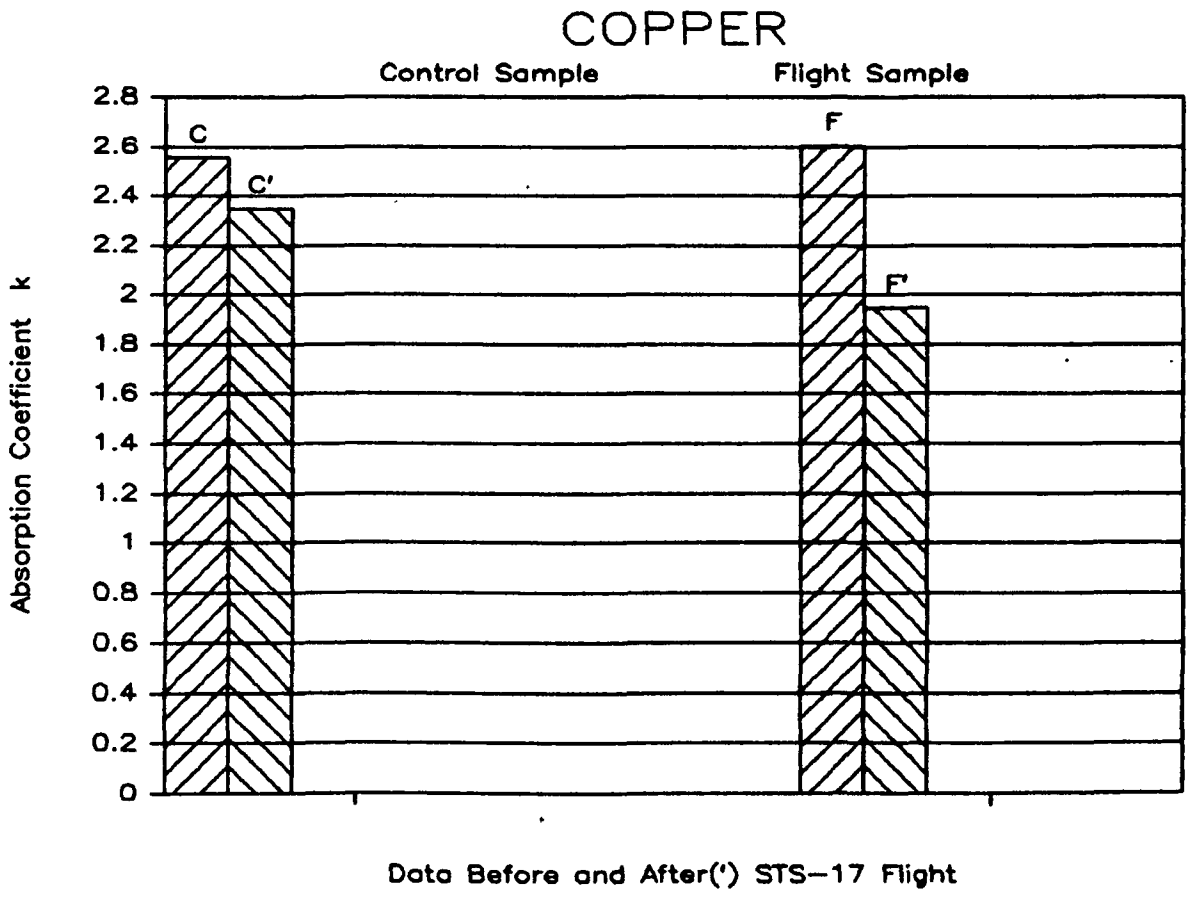
COPPER
Control Sample
Flight Sample
C
C'
F
F'
Absorption Coefficient k
2.8
2.6
2.4
2.2
2
1.8
1.6
1.4
1.2
1
0.8
0.6
0.4
0.2
0
Data Before and After(') STS-17 Flight

Fig. 40

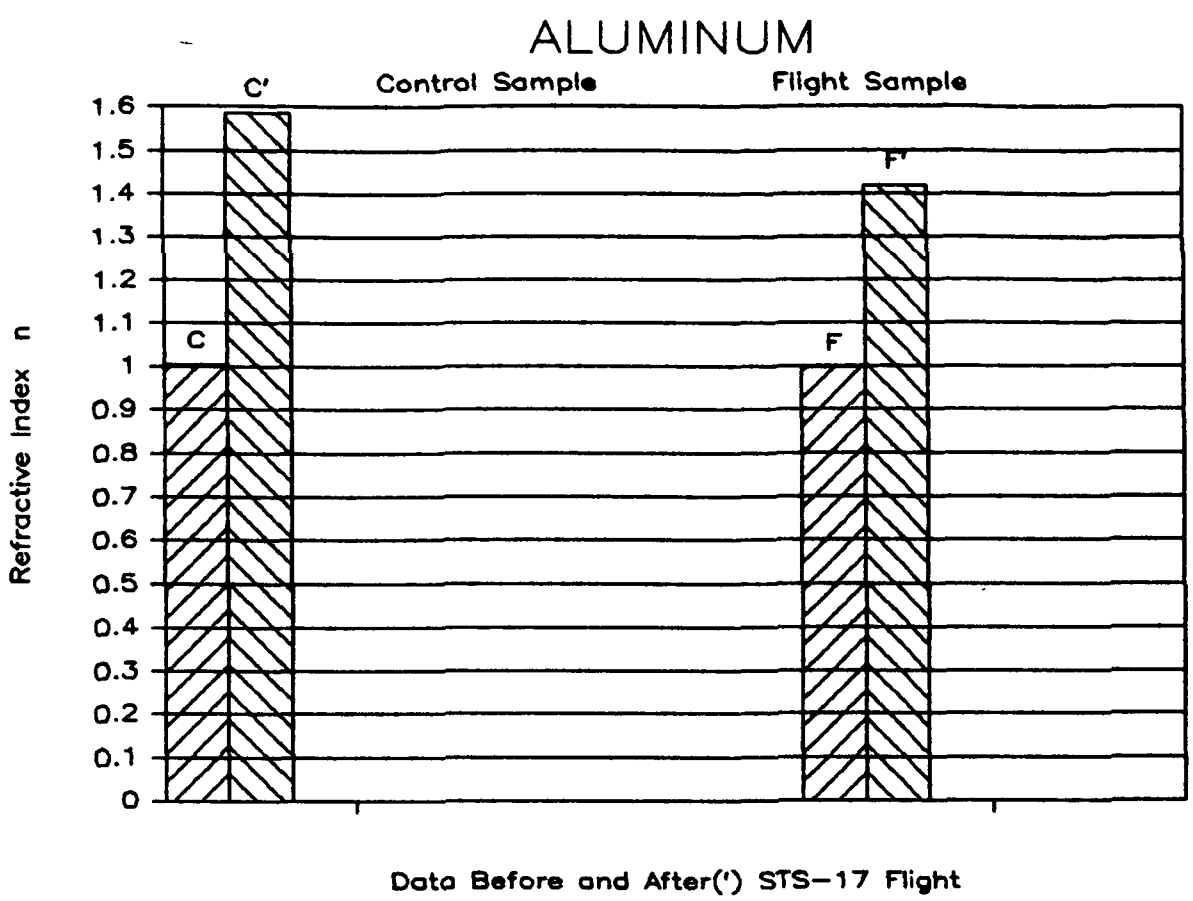

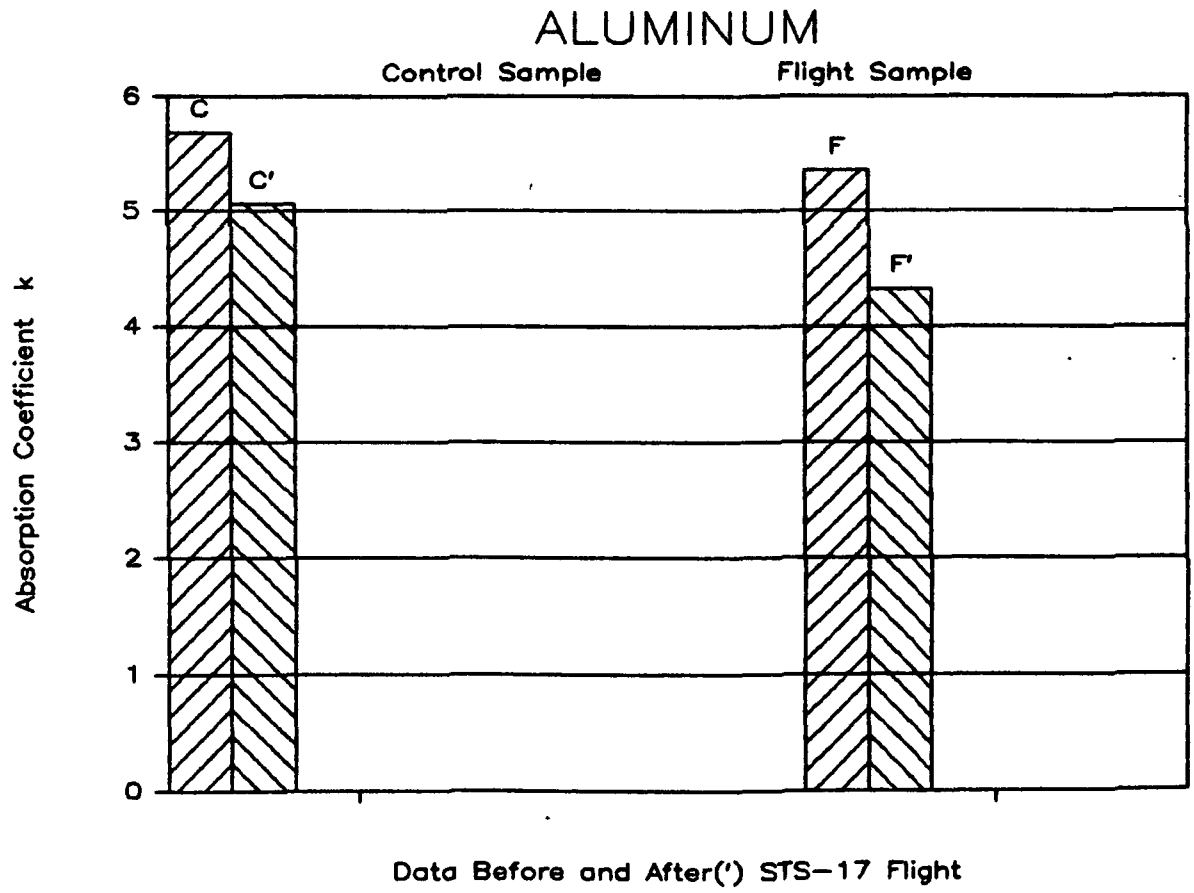

Fig. 41 Ellipsometry Data

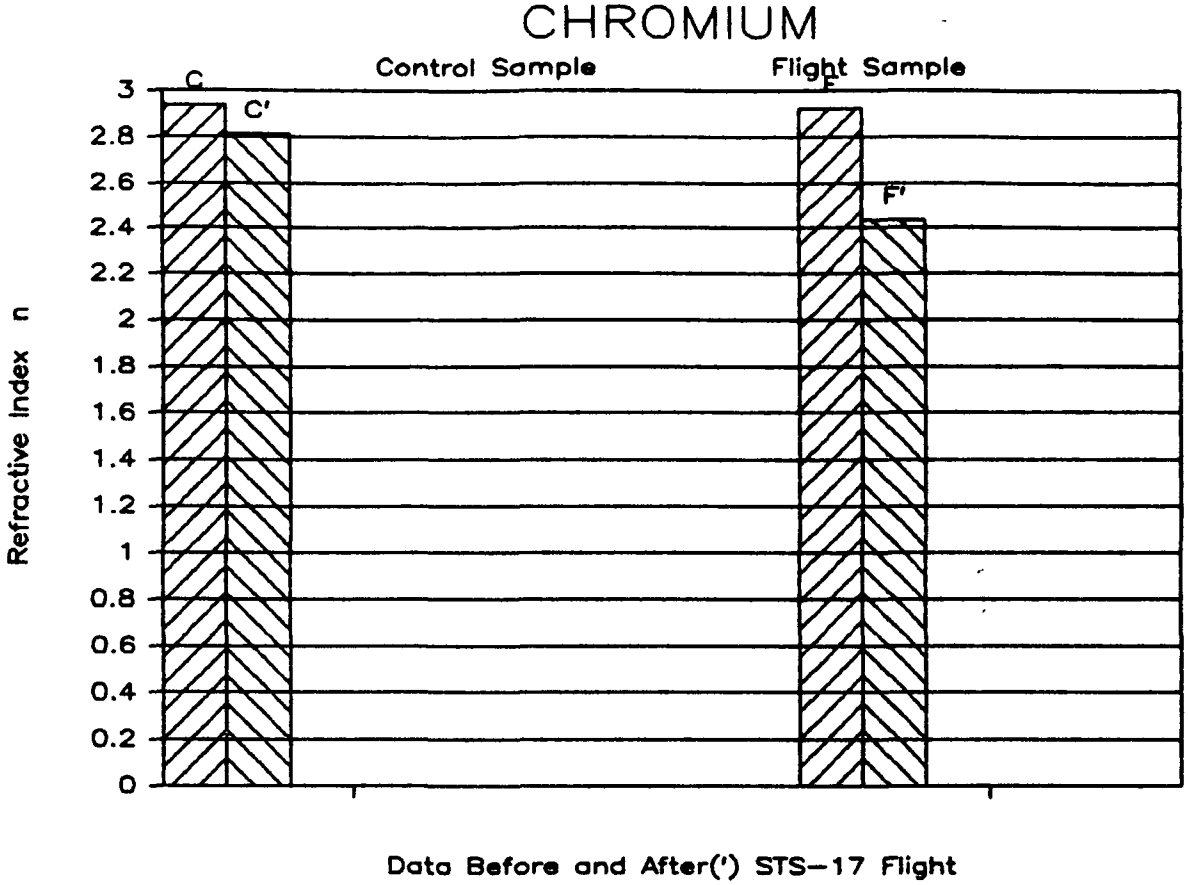
CHROMIUM
Control Sample
Flight Sample
C
C'
F
F'
Refractive Index n
3
2.8
2.6
2.4
2.2
2
1.8
1.6
1.4
1.2
1
0.8
0.6
0.4
0.2
0
Data Before and After(') STS-17 Flight

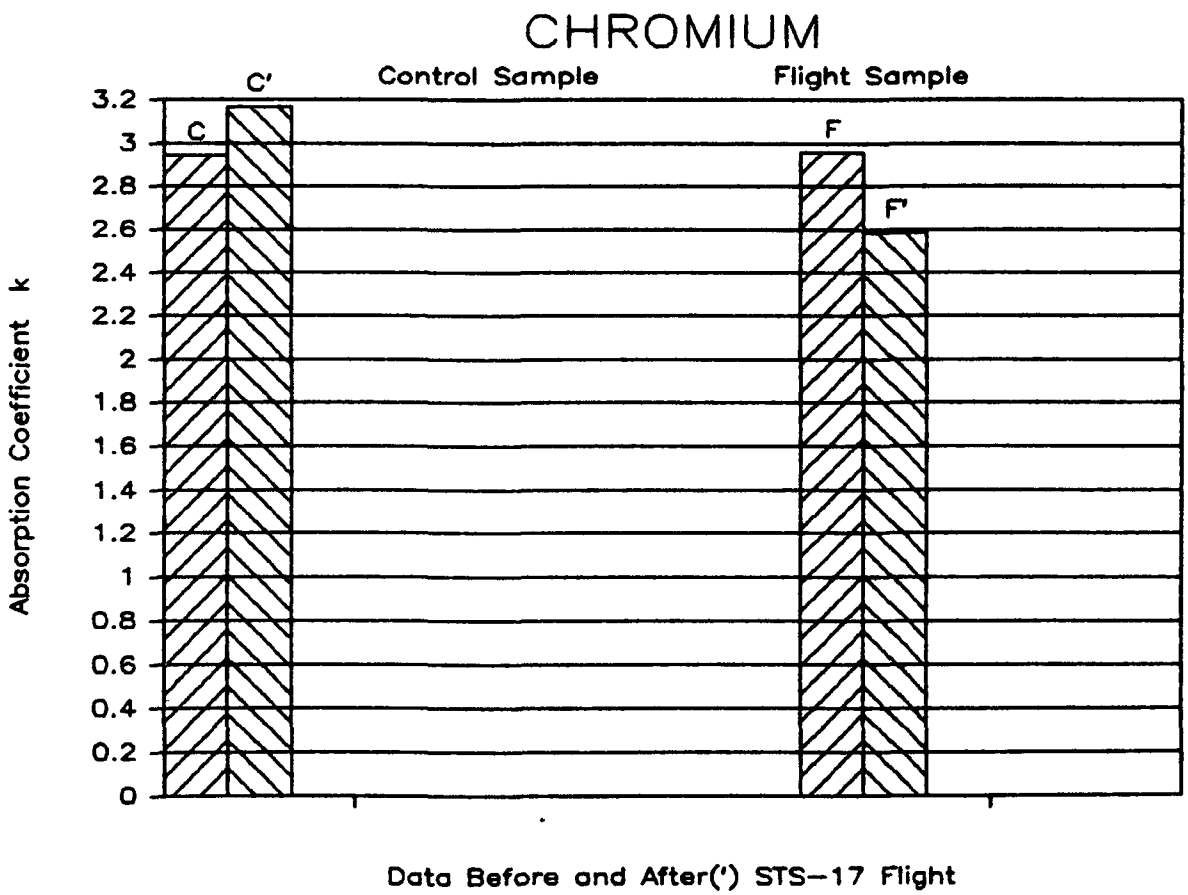
CHROMIUM
Control Sample
Flight Sample
C'
C
F
F'
Absorption Coefficient k
3.2
3
2.8
2.6
2.4
2.2
2
1.8
1.6
1.4
1.2
1
0.8
0.6
0.4
0.2
0
Data Before and After(') STS-17 Flight

42

Fig. 42

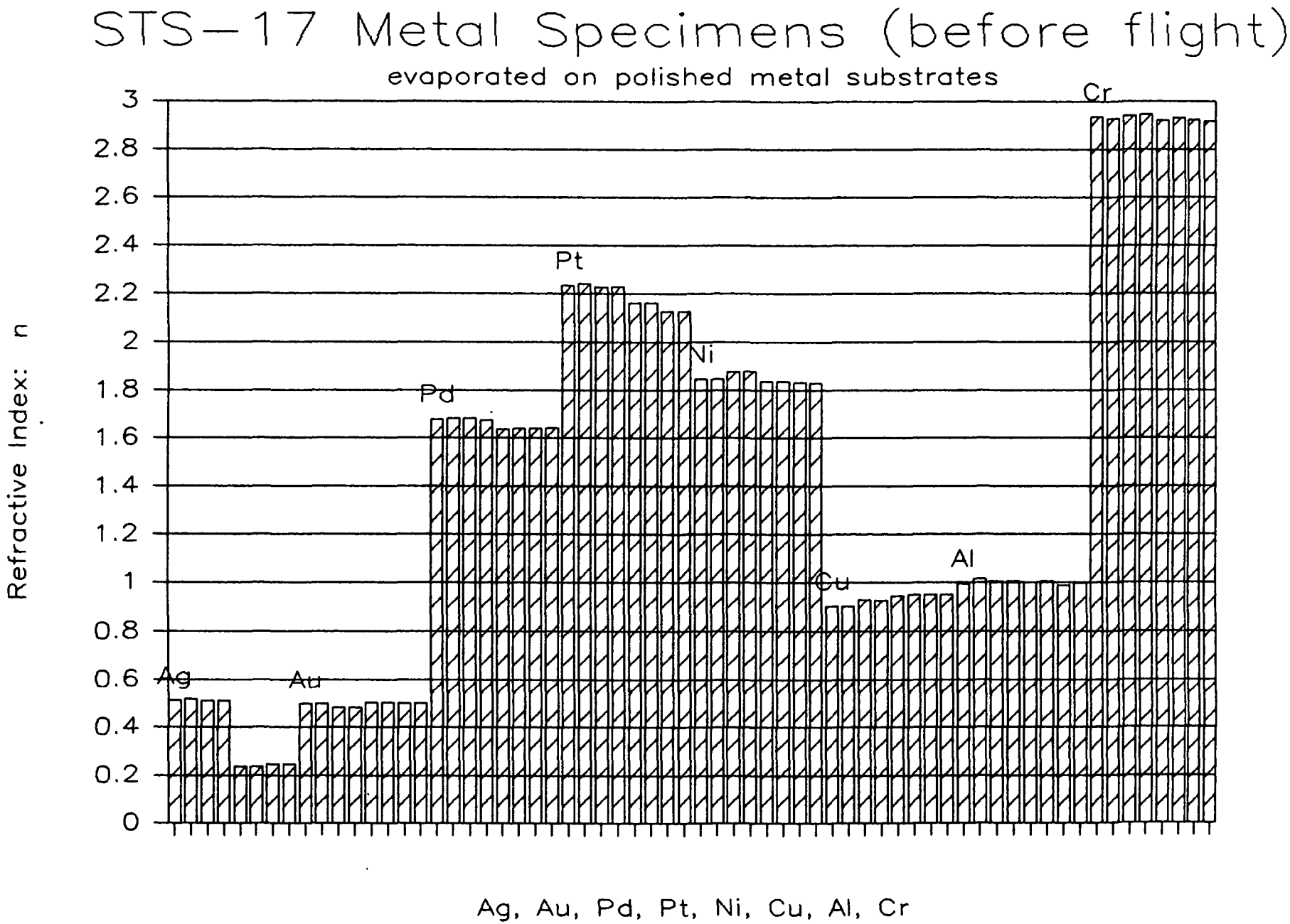
STS-17 Metal Specimens (before flight)
evaporated on polished metal substrates
Refractive Index: n
3
2.8
2.6
2.4
2.2
2
1.8
1.6
1.4
1.2
1
0.8
0.6
0.4
0.2
0
Ag
Au
Pd
Pt
Ni
Cu
Al
Cr
Ag, Au, Pd, Pt, Ni, Cu, Al, Cr

Fig. 43

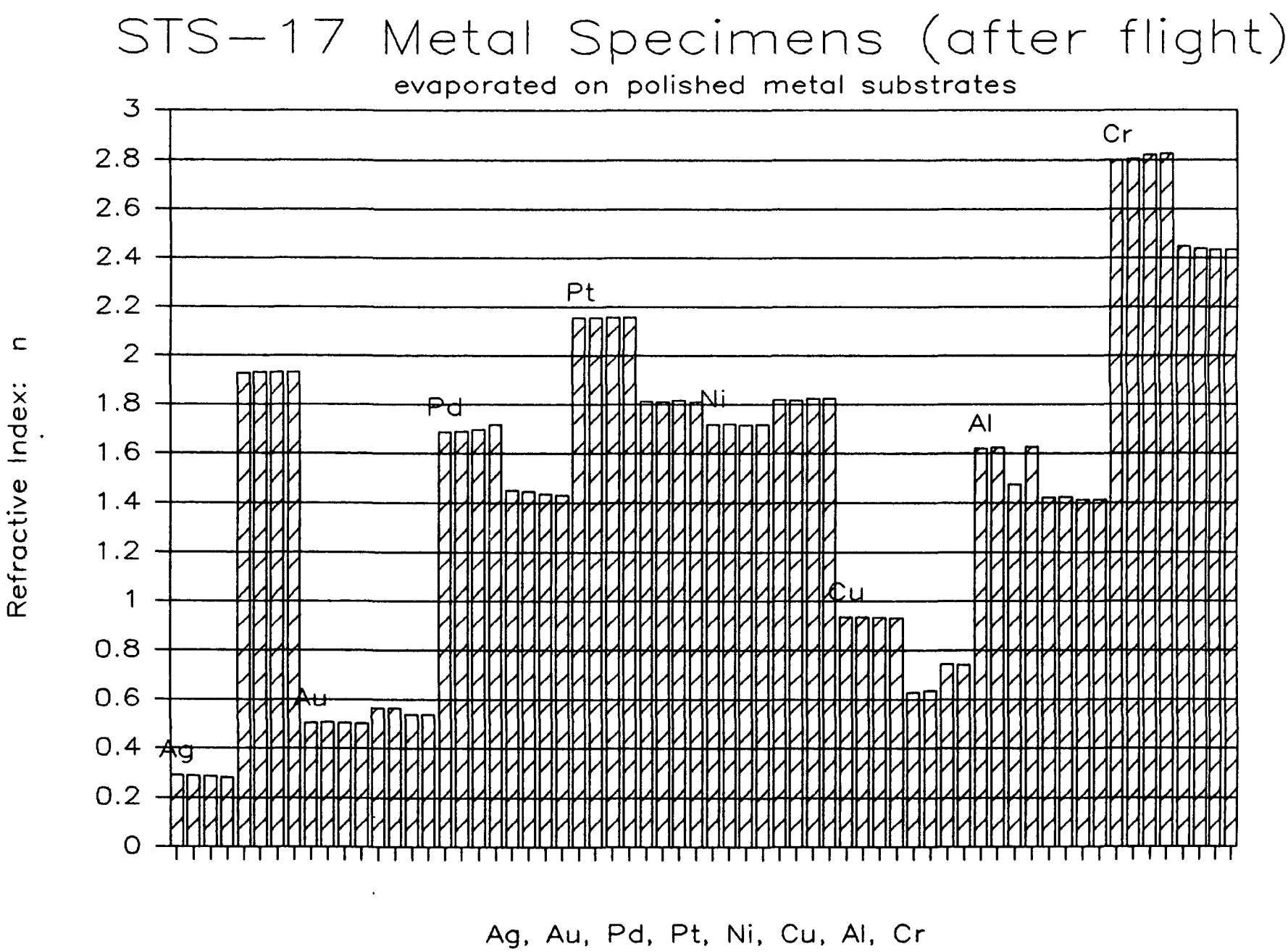
STS-17 Metal Specimens (after flight)
evaporated on polished metal substrates
Refractive Index: n
3
2.8
2.6
2.4
2.2
2
1.8
1.6
1.4
1.2
1
0.8
0.6
0.4
0.2
0
Ag
Au
Pd
Pt
Ni
Cu
Al
Cr
Ag, Au, Pd, Pt, Ni, Cu, Al, Cr

Fig. 44

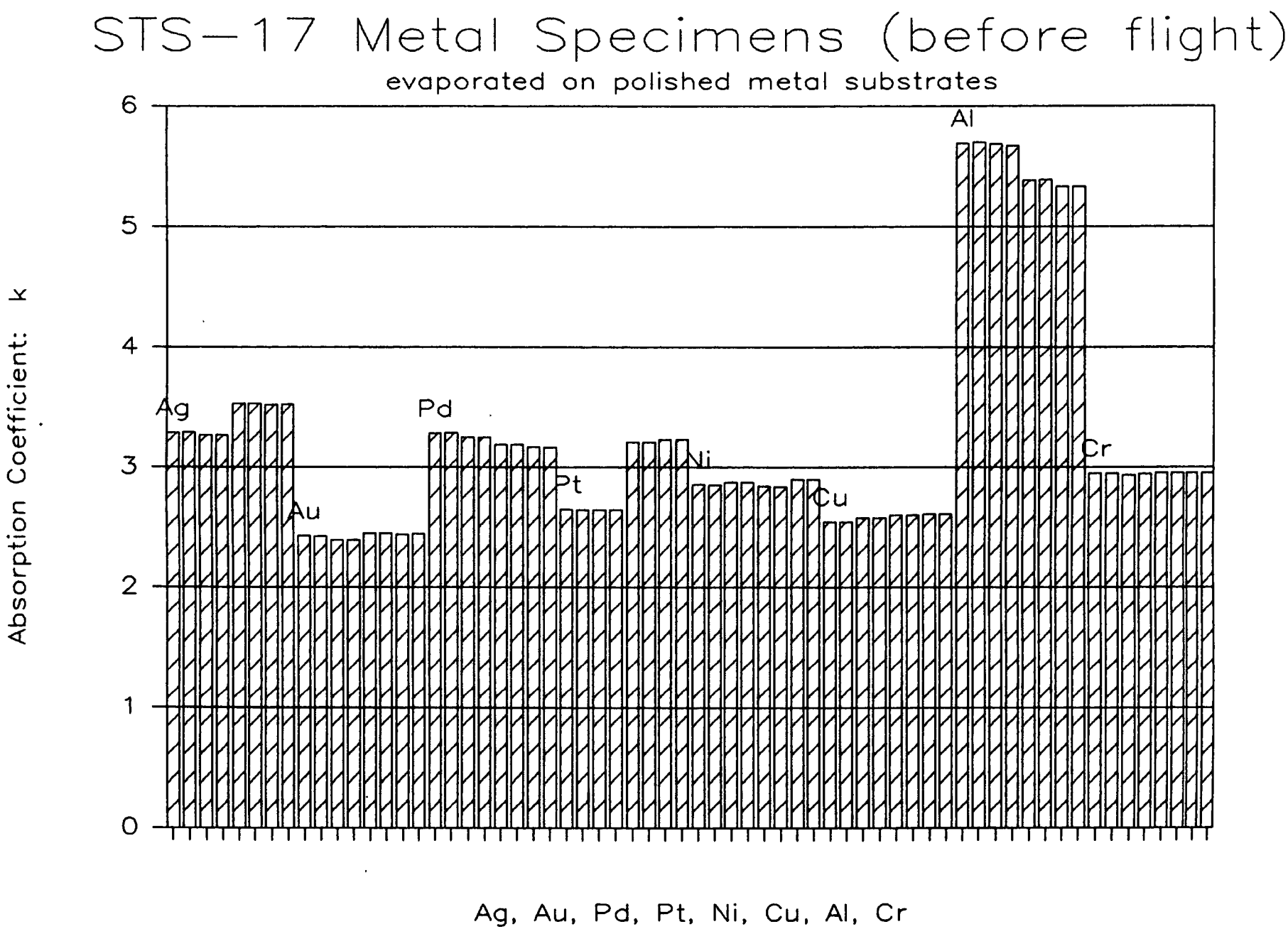
STS–17 Metal Specimens (before flight)
evaporated on polished metal substrates
Absorption Coefficient: k
6
5
4
3
2
1
0
Ag
Au
Pd
Pt
Ni
Cu
Al
Cr
Ag, Au, Pd, Pt, Ni, Cu, Al, Cr

Fig. 45

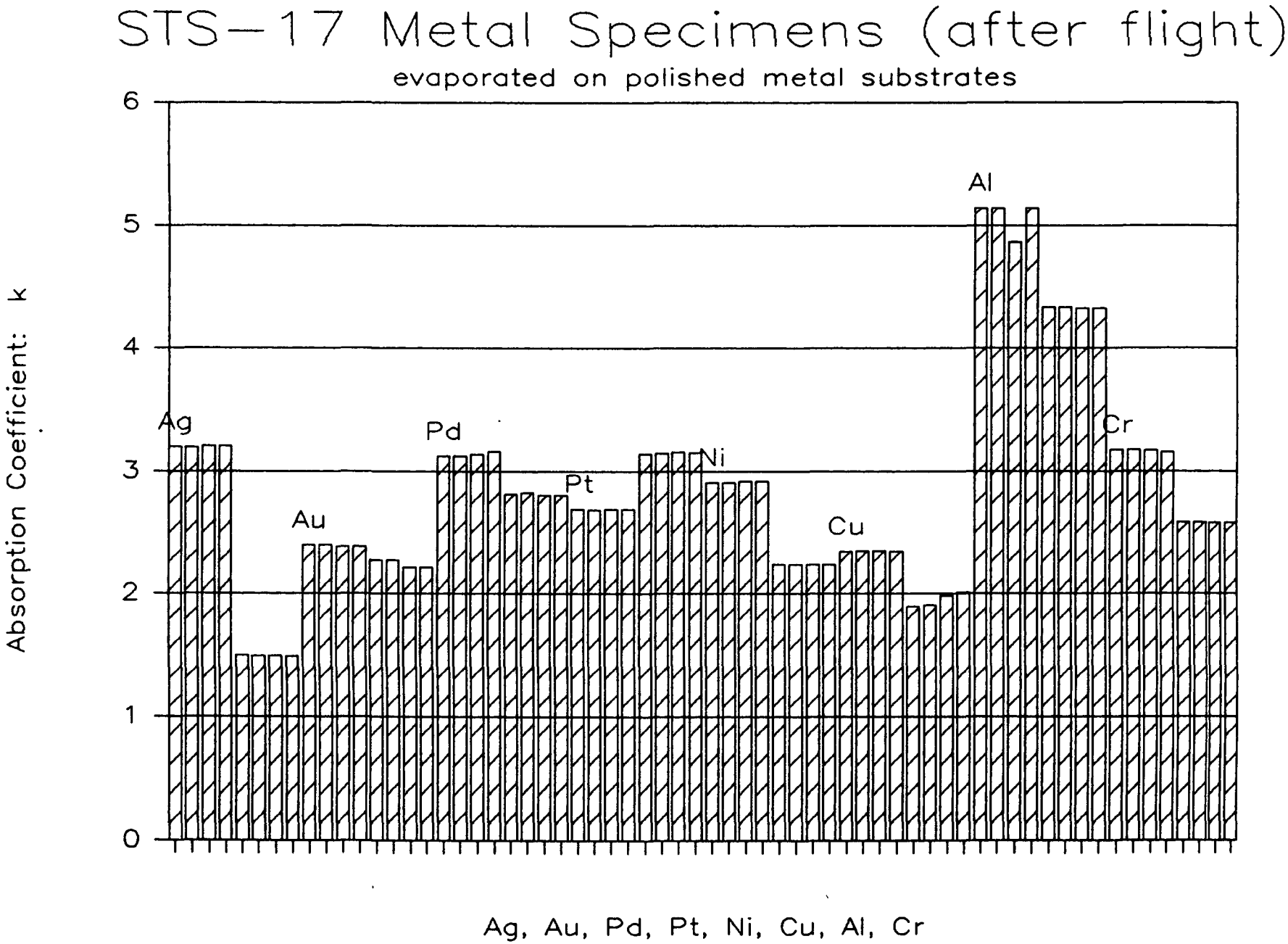
STS-17 Metal Specimens (after flight)
evaporated on polished metal substrates
Absorption Coefficient: k
6
5
4
3
2
1
0
Ag
Au
Pd
Pt
Ni
Cu
Al
Cr
Ag, Au, Pd, Pt, Ni, Cu, Al, Cr

Fig. 46

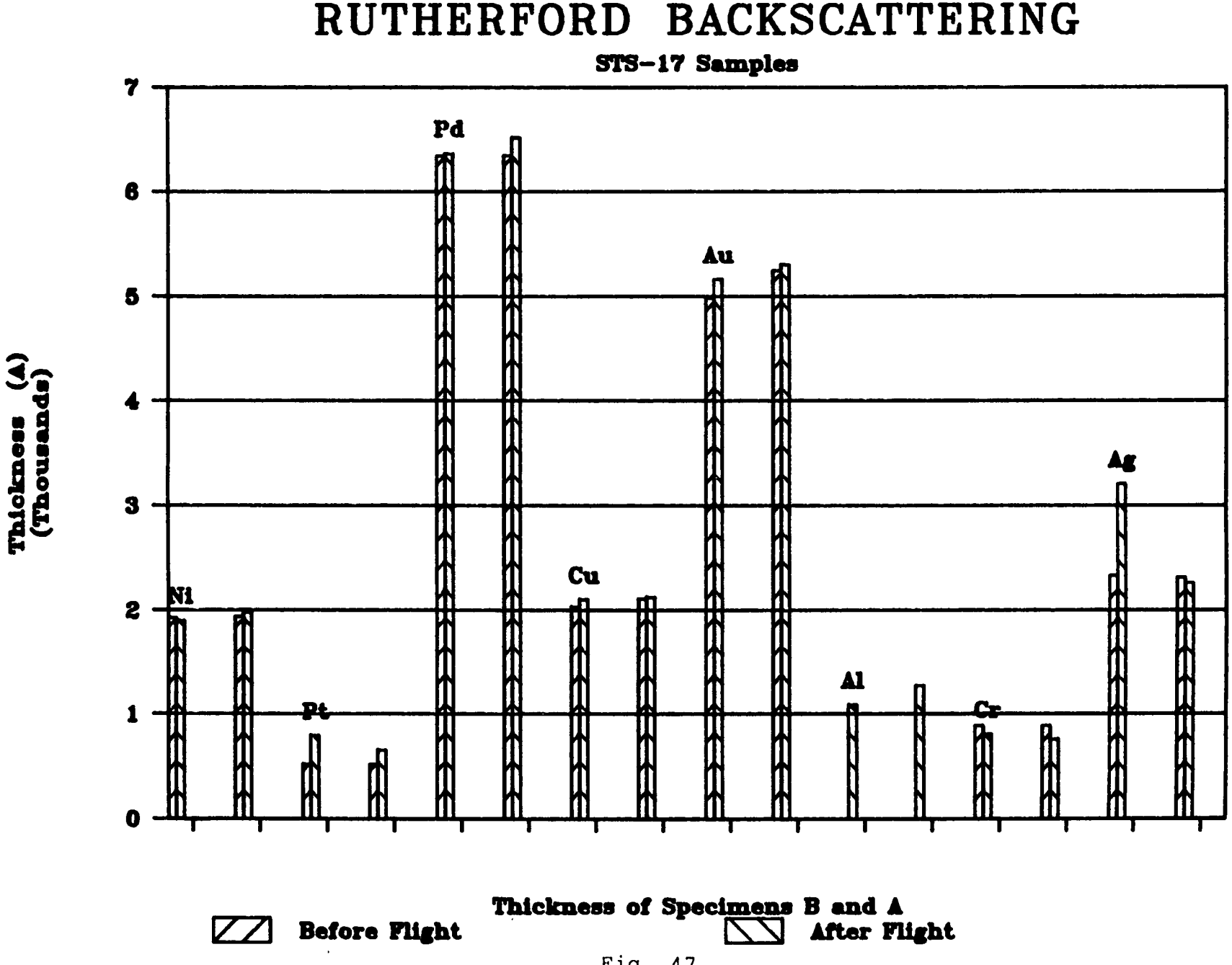
RUTHERFORD BACKSCATTERING
STS-17 Samples
Thickness (A)
(Thousands)
7
6
5
4
3
2
1
0
Ni
Pt
Pd
Cu
Au
Al
Cr
Ag
Thickness of Specimens B and A
Before Flight
After Flight

Fig. 47

Ag 6061-A

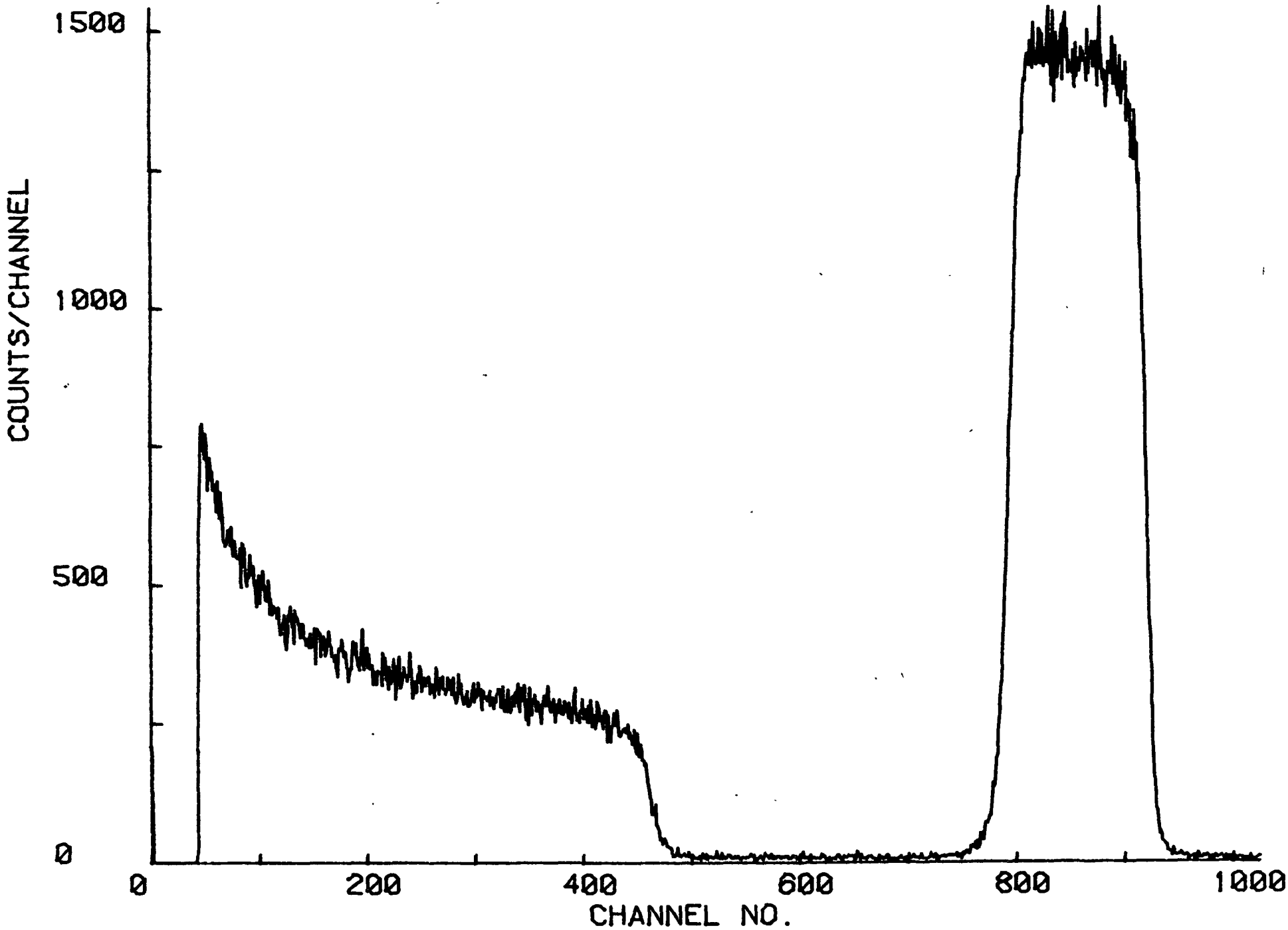

Fig. 48 Ag RBS Spectrum - Specimen A

lg 6061-15

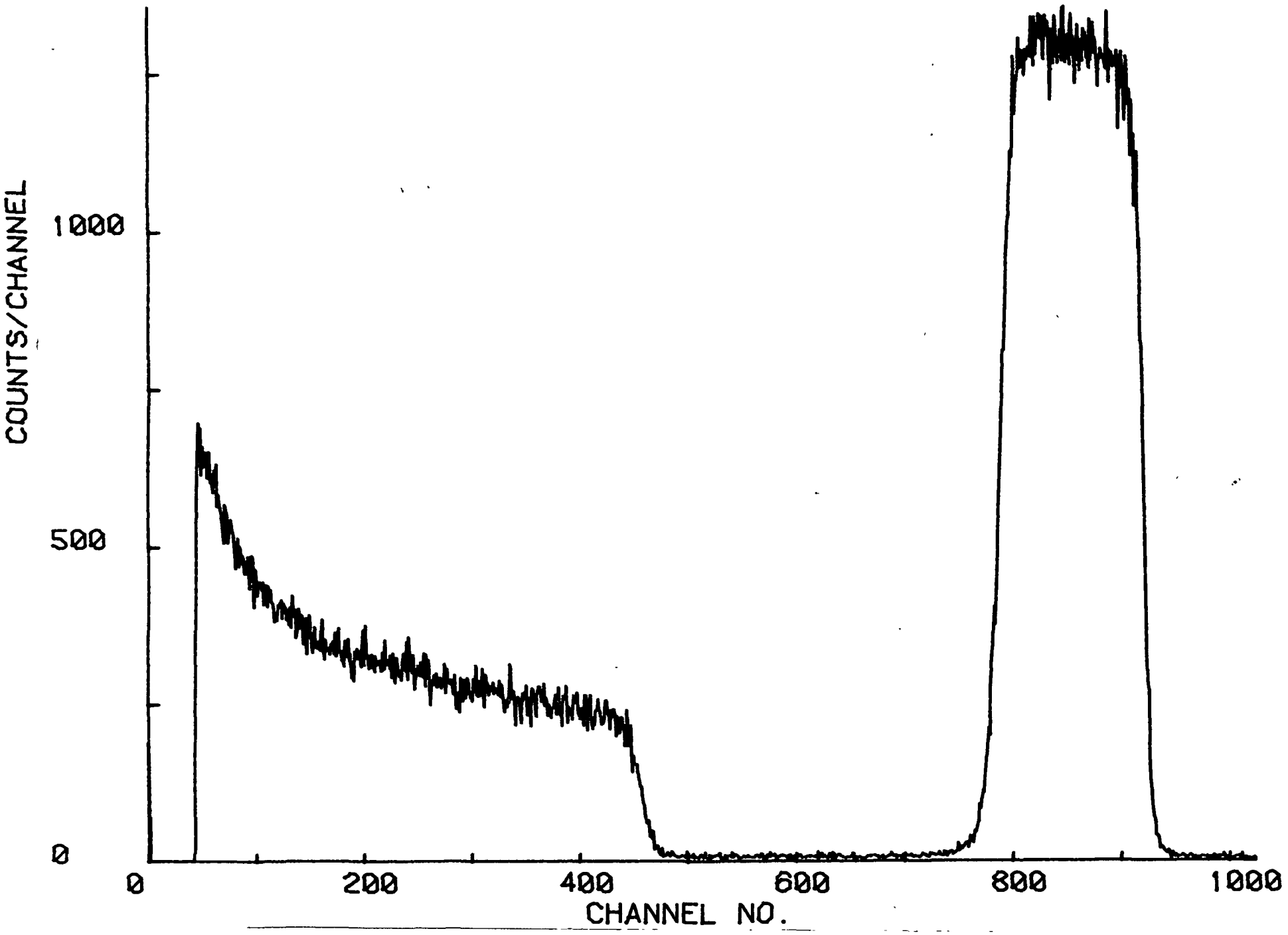

Fig. 49 Ag RBS Spectrum - Specimen B

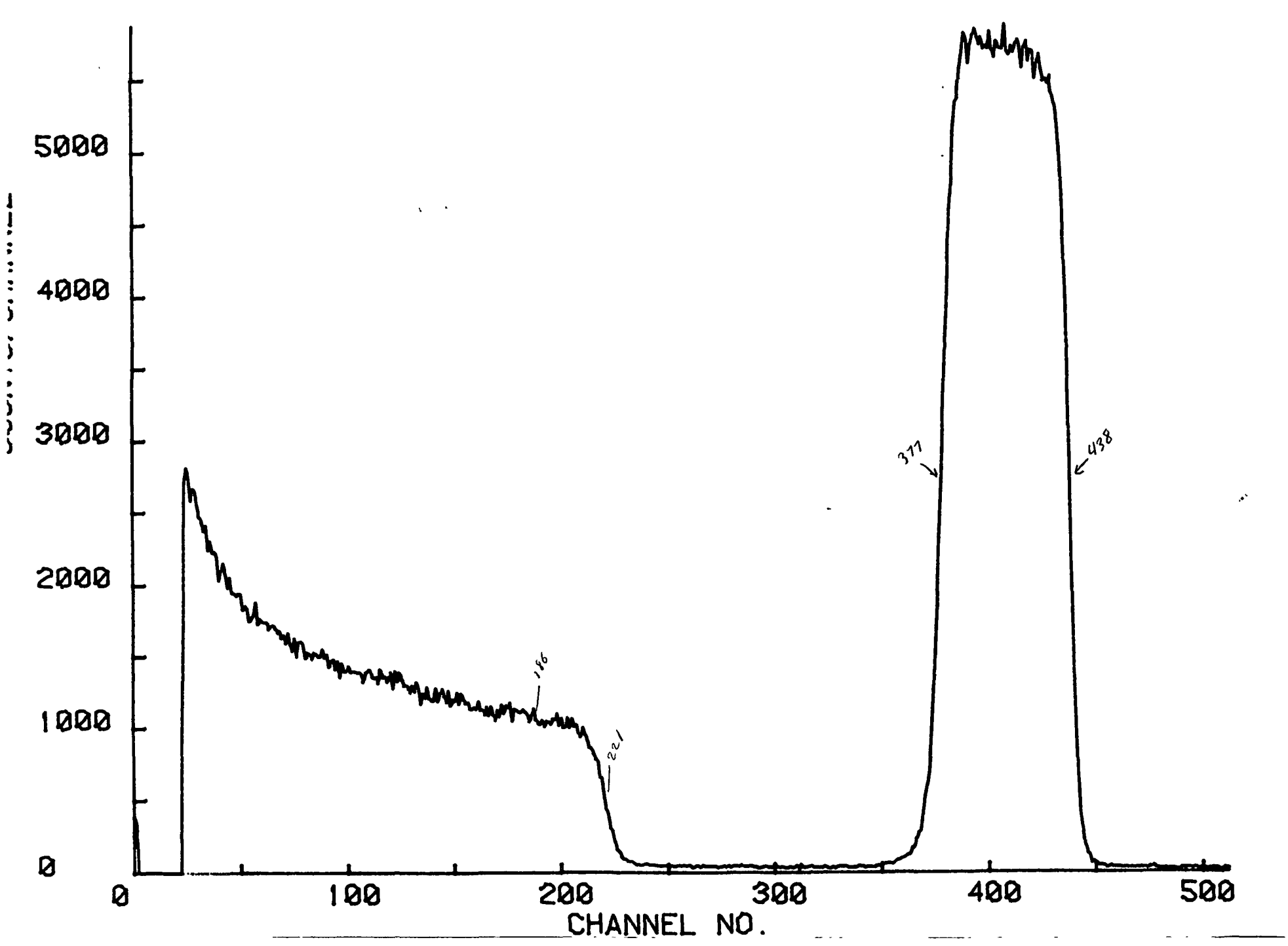

Fig. 50 Ag RBS Spectrum - Specimen C

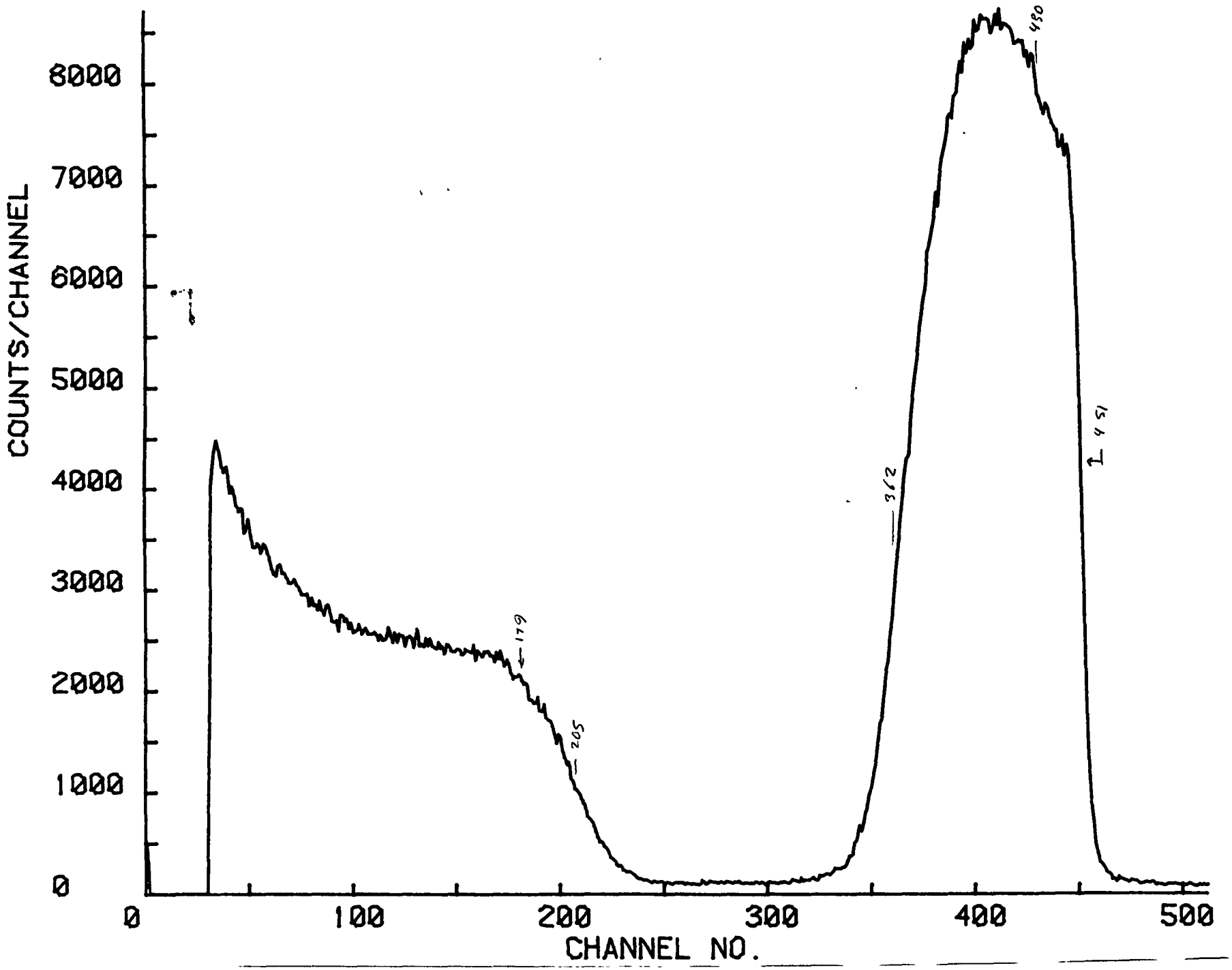

Fig. 51 Ag RBS Spectrum - Specimen F

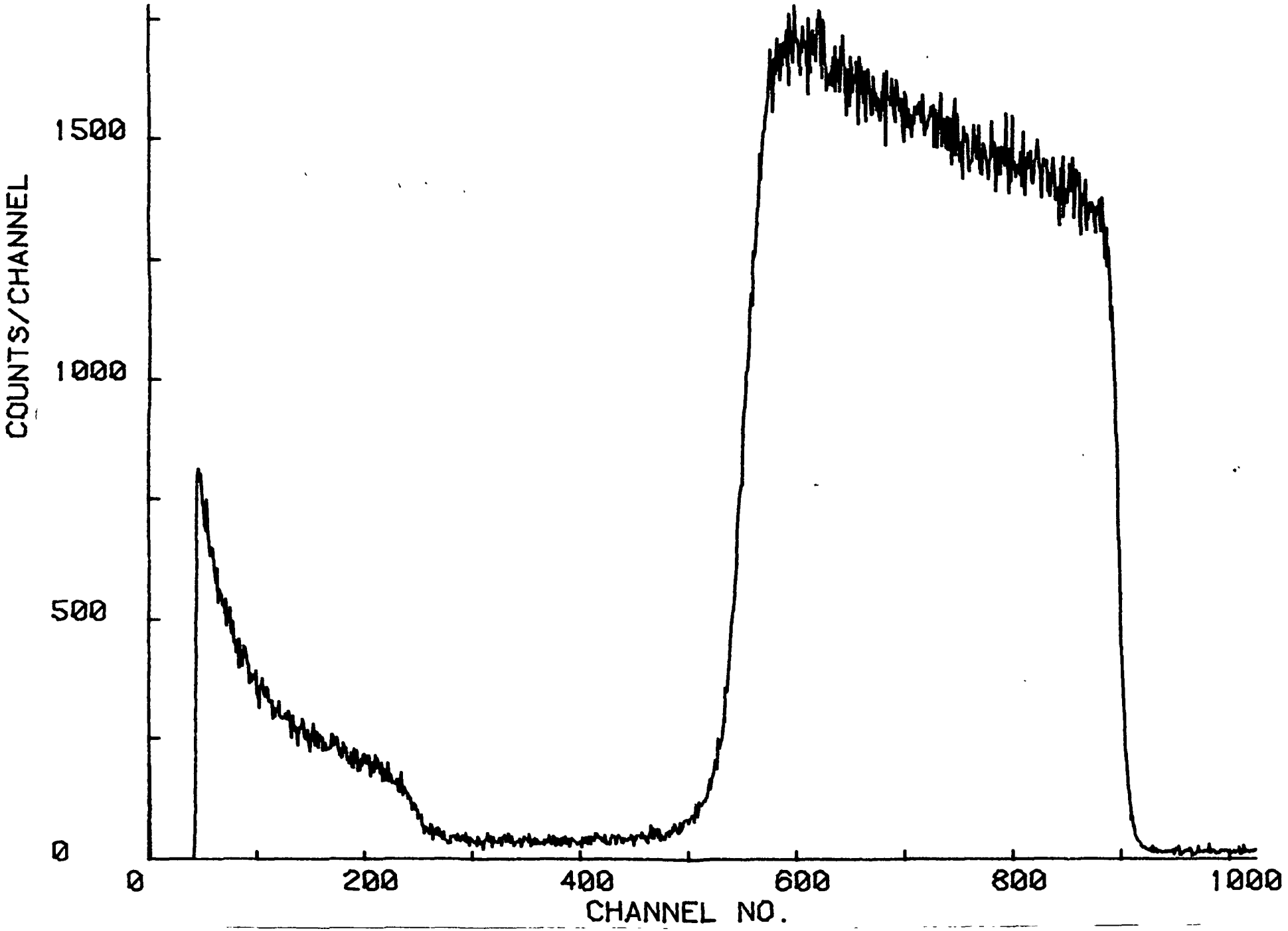

Fig. 52 Au RBS Spectrum - Specimen A

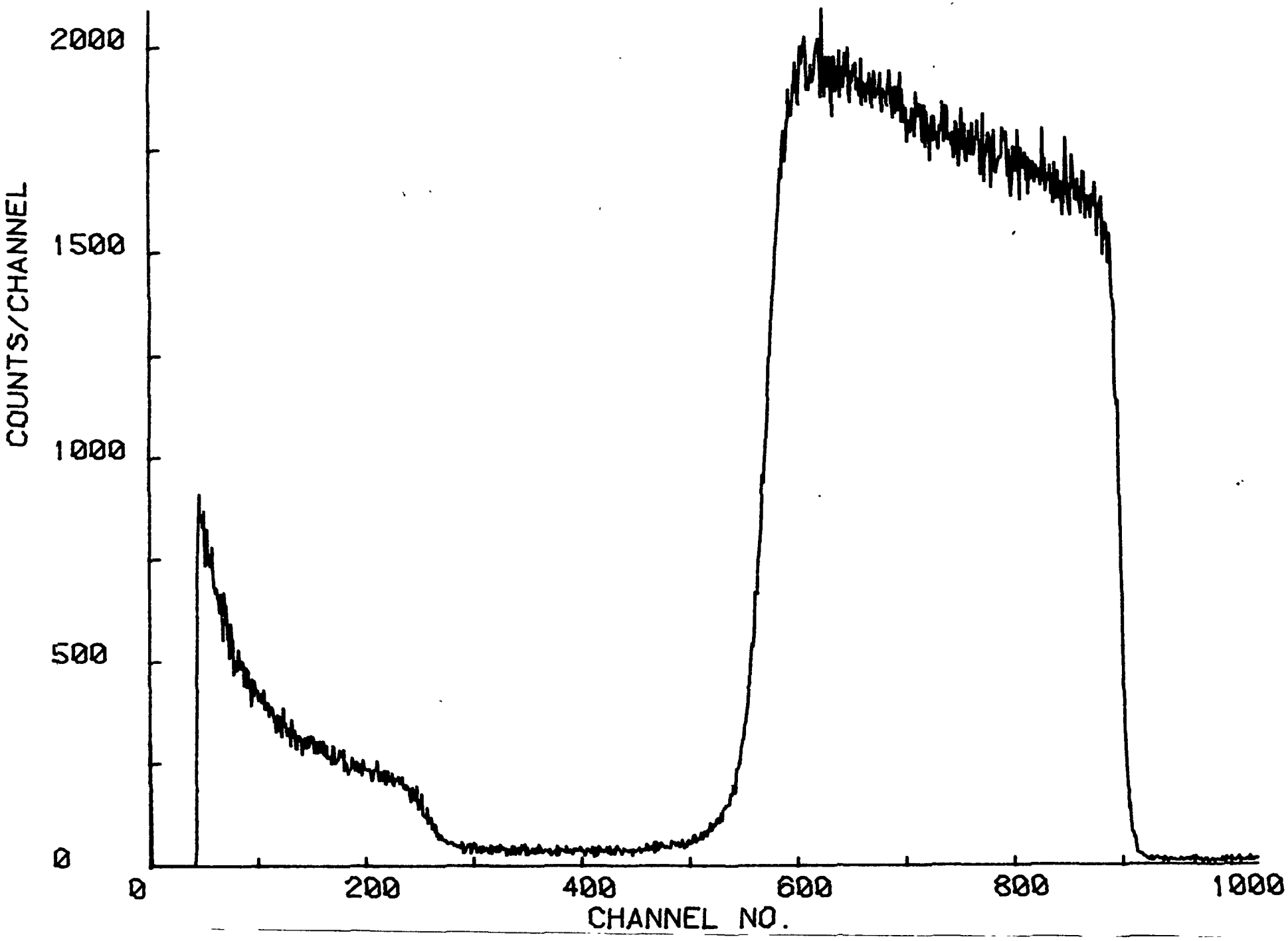

Fig. 53 Au RBS Spectrum - Specimen B

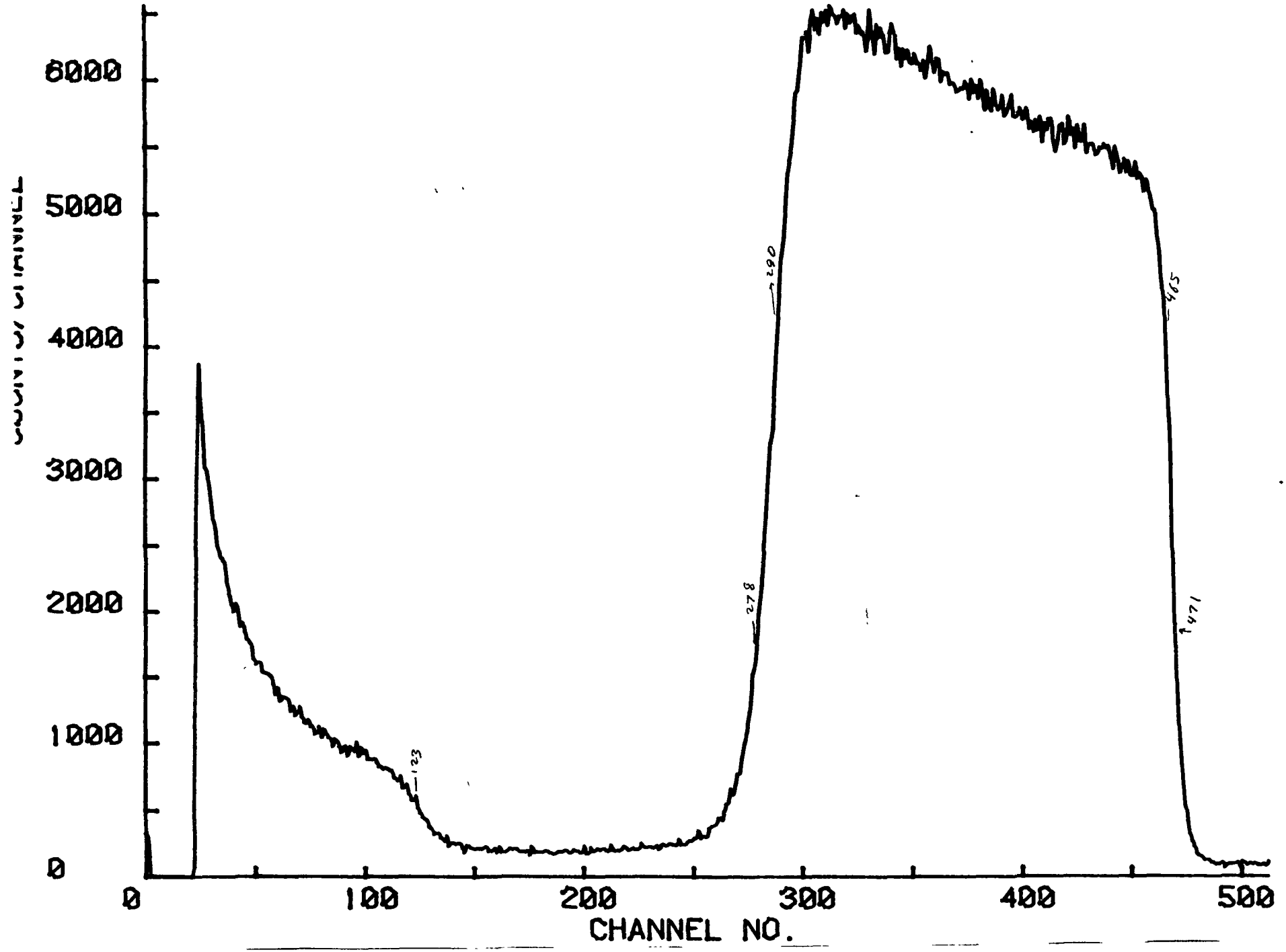

Fig. 54 Au RBS Spectrum - Specimen C

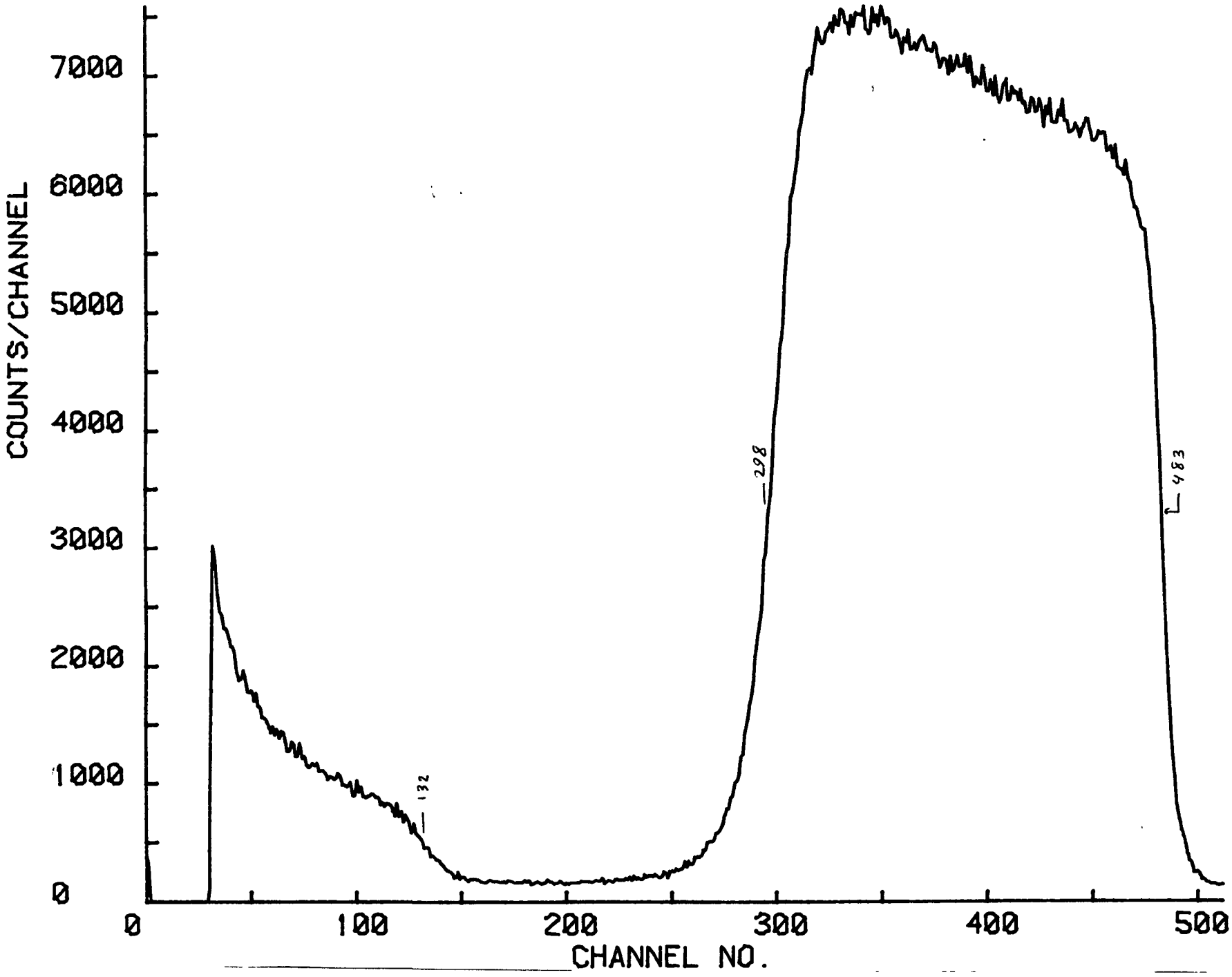

Fig. 55 Au RBS Spectrum - Specimen F

Pd. 6061.- A

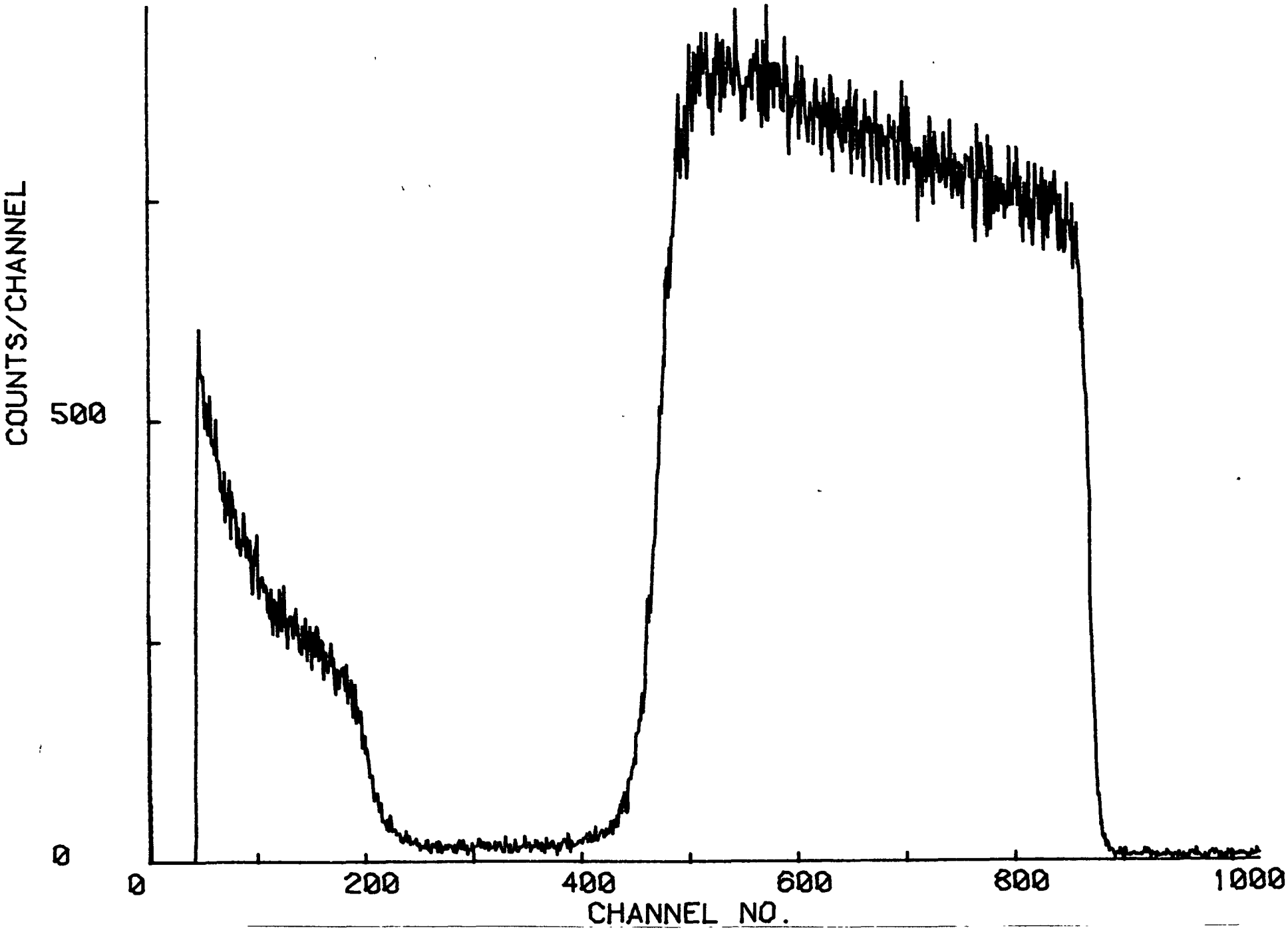

Fig. 56 Pd RBS Spectrum - Specimen A

Pd 6061-B

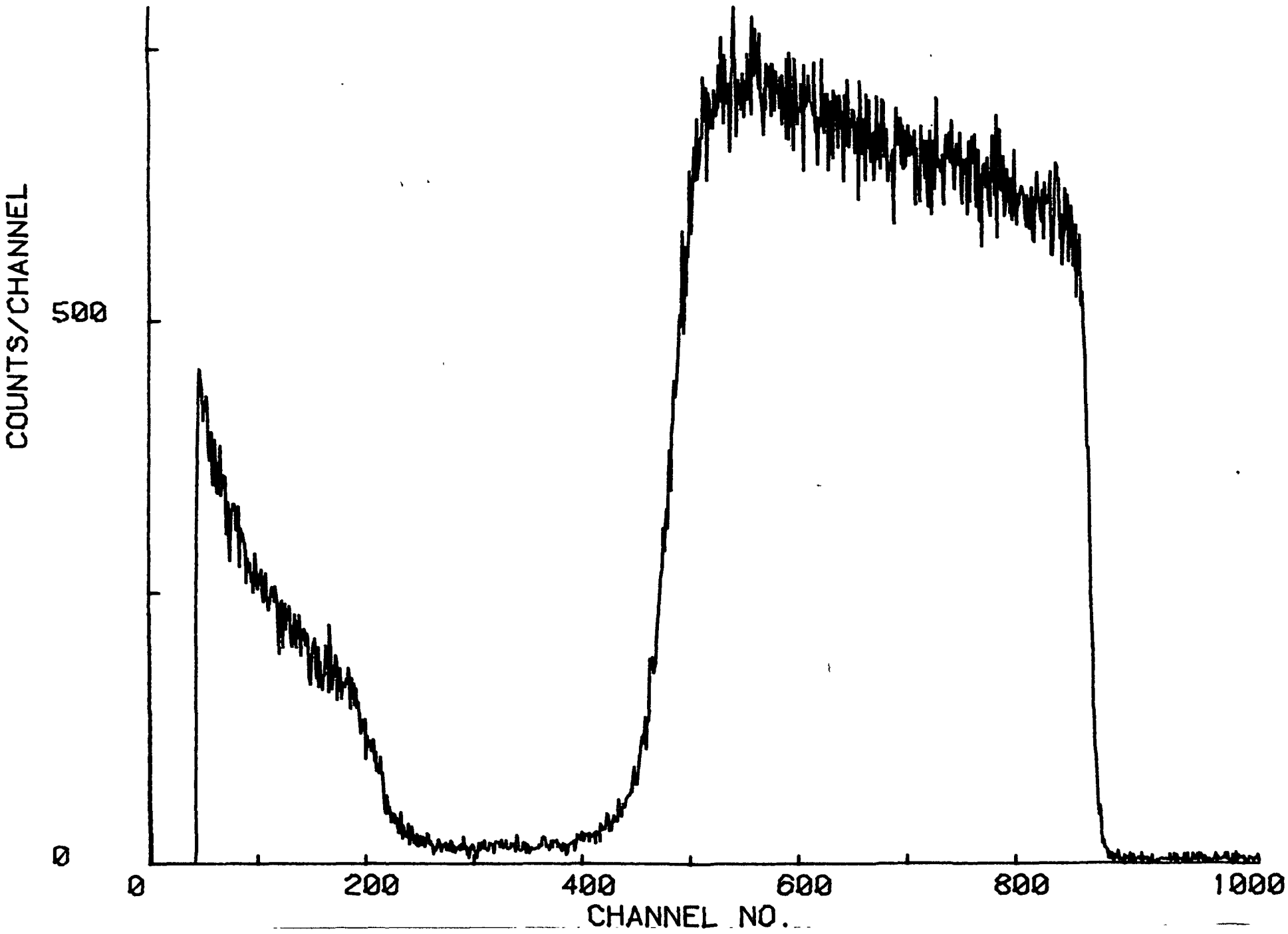

Fig. 57 Pd RBS Spectrum - Specimen B

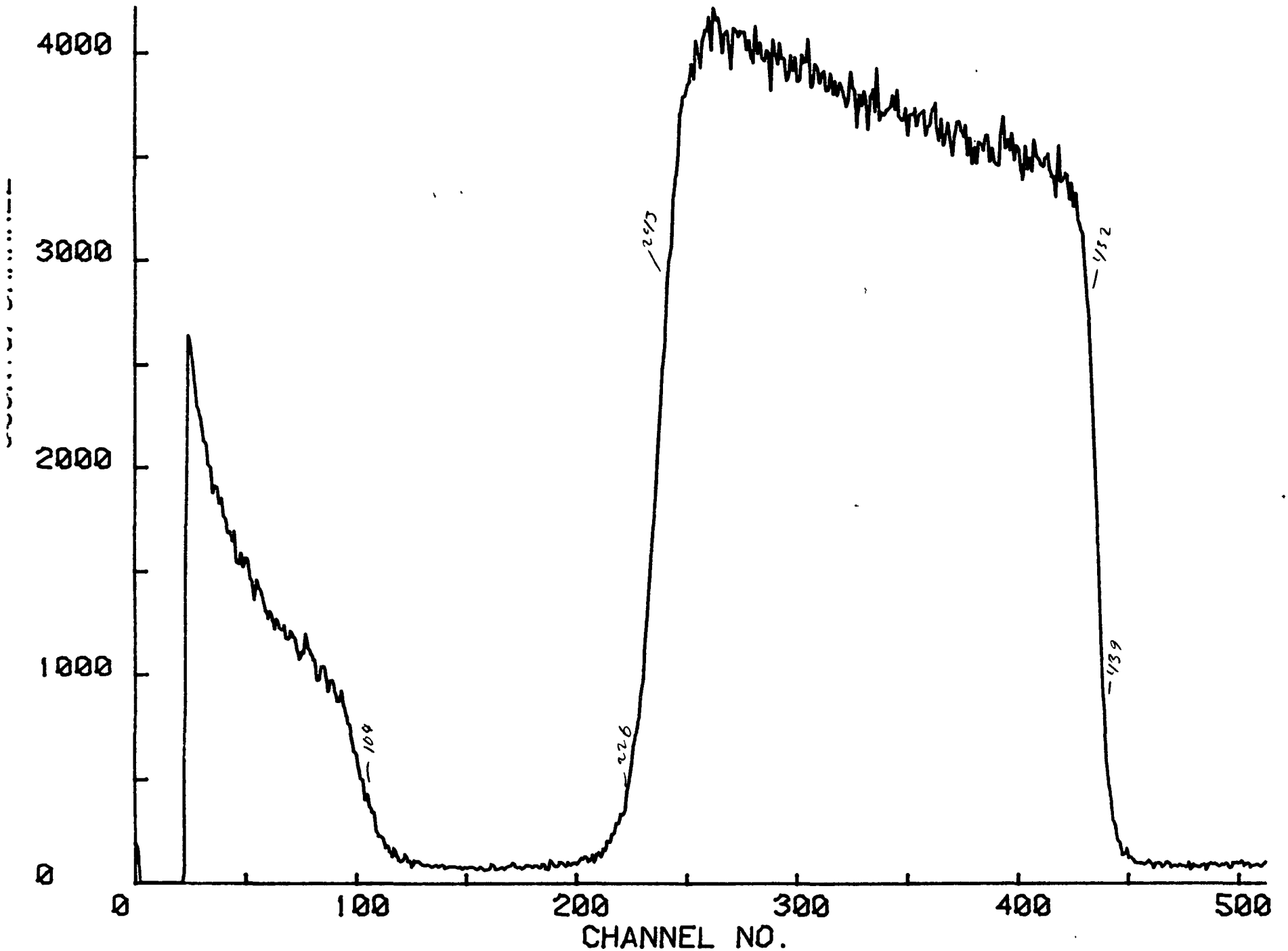

Fig. 58 Pd RBS Spectrum - Specimen C

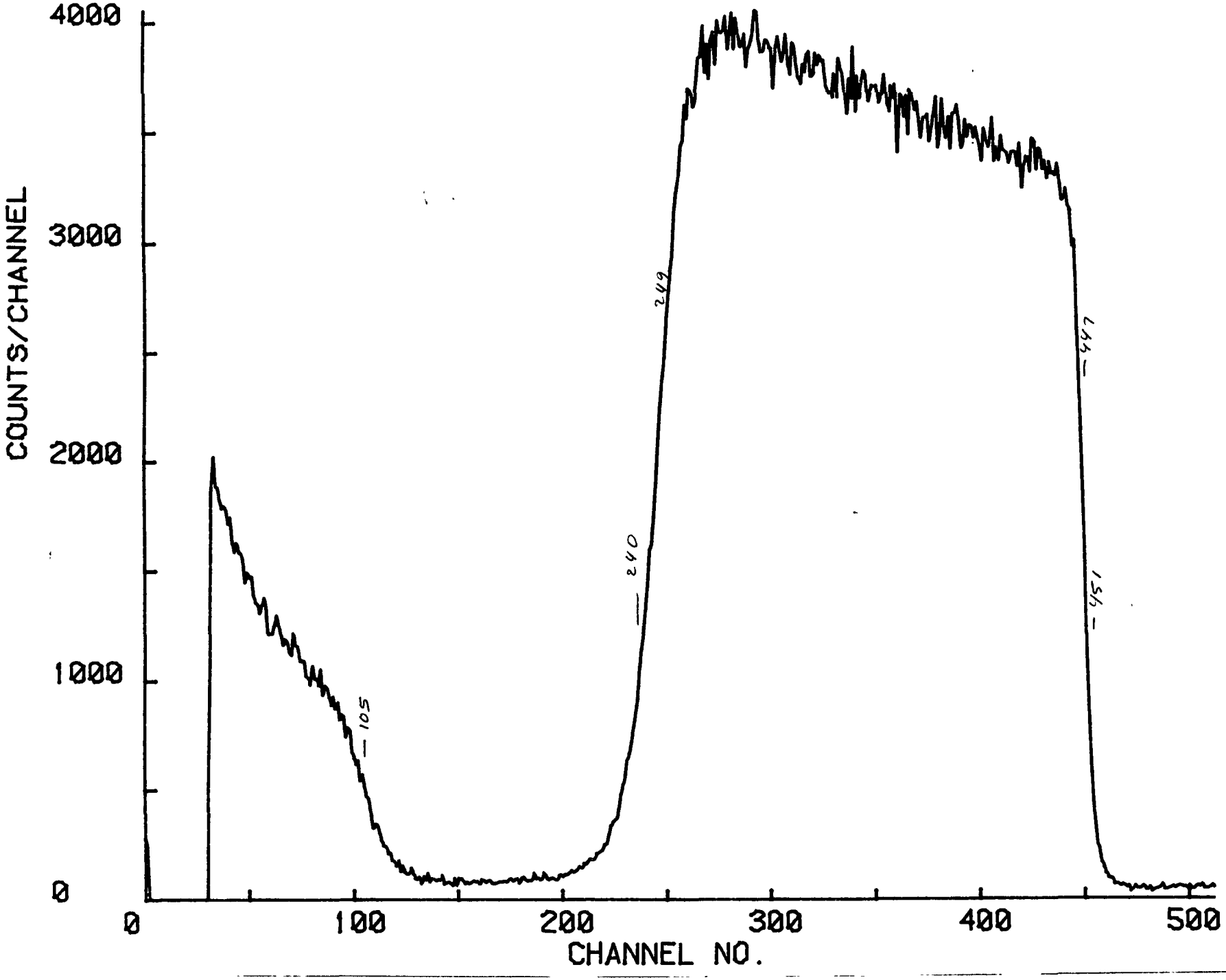

Fig. 59 Pd RBS Spectrum - Specimen F

pt - 6061 - A

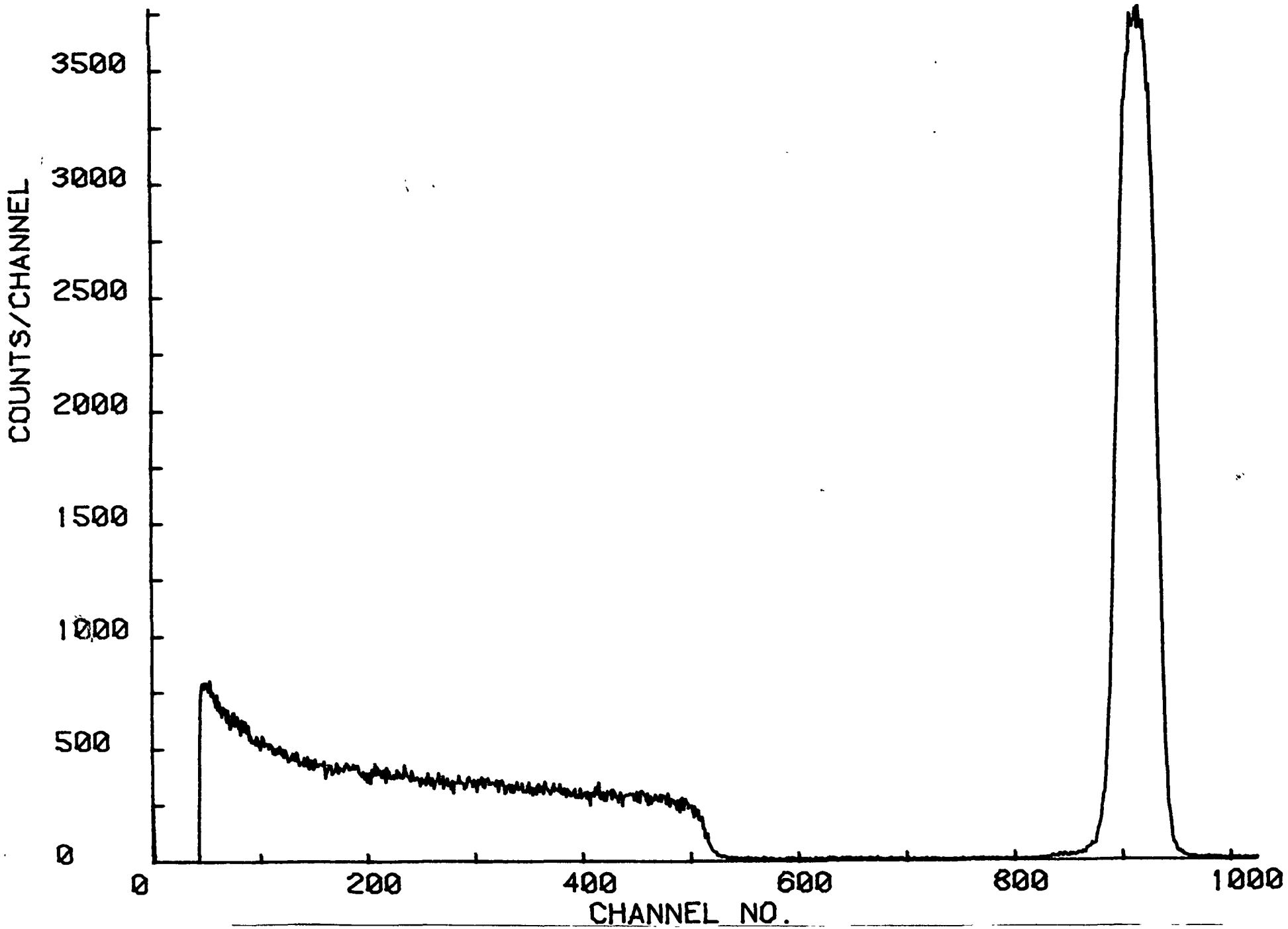

Fig. 60 Pt RBS Spectrum - Specimen A

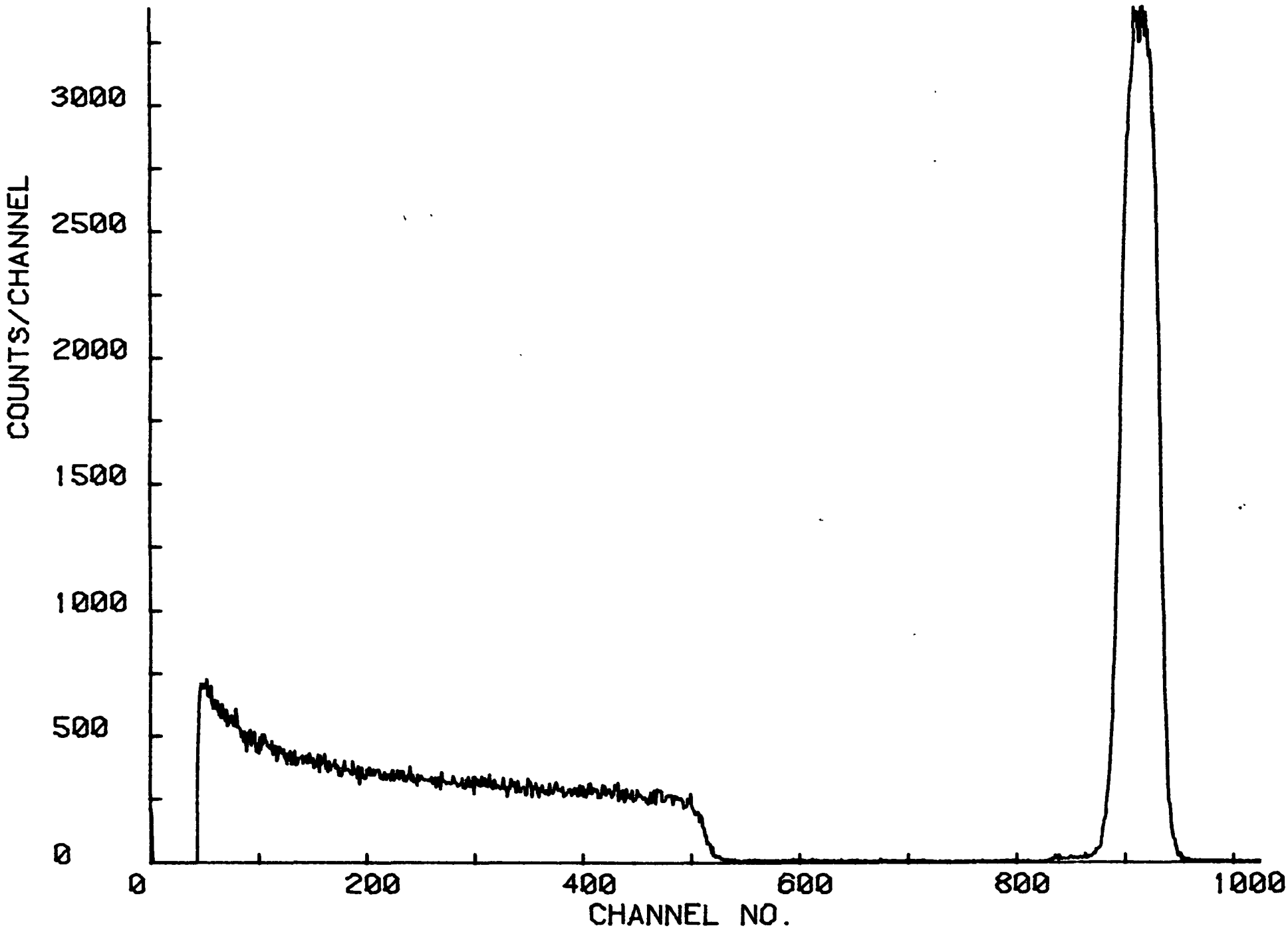

Fig. 61 Pt RBS Spectrum - Specimen B

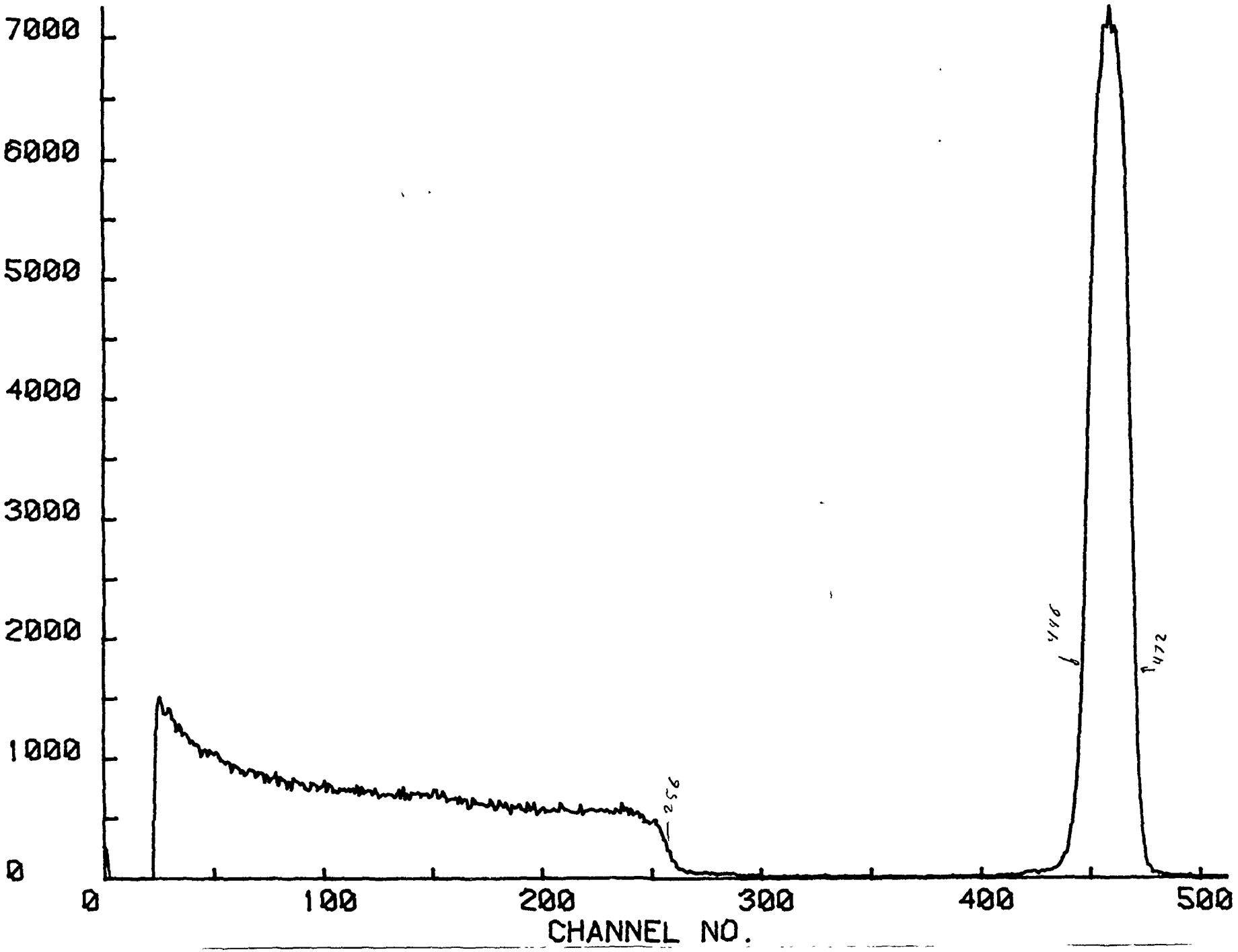

Fig. 62 Pt RBS Spectrum - Specimen C

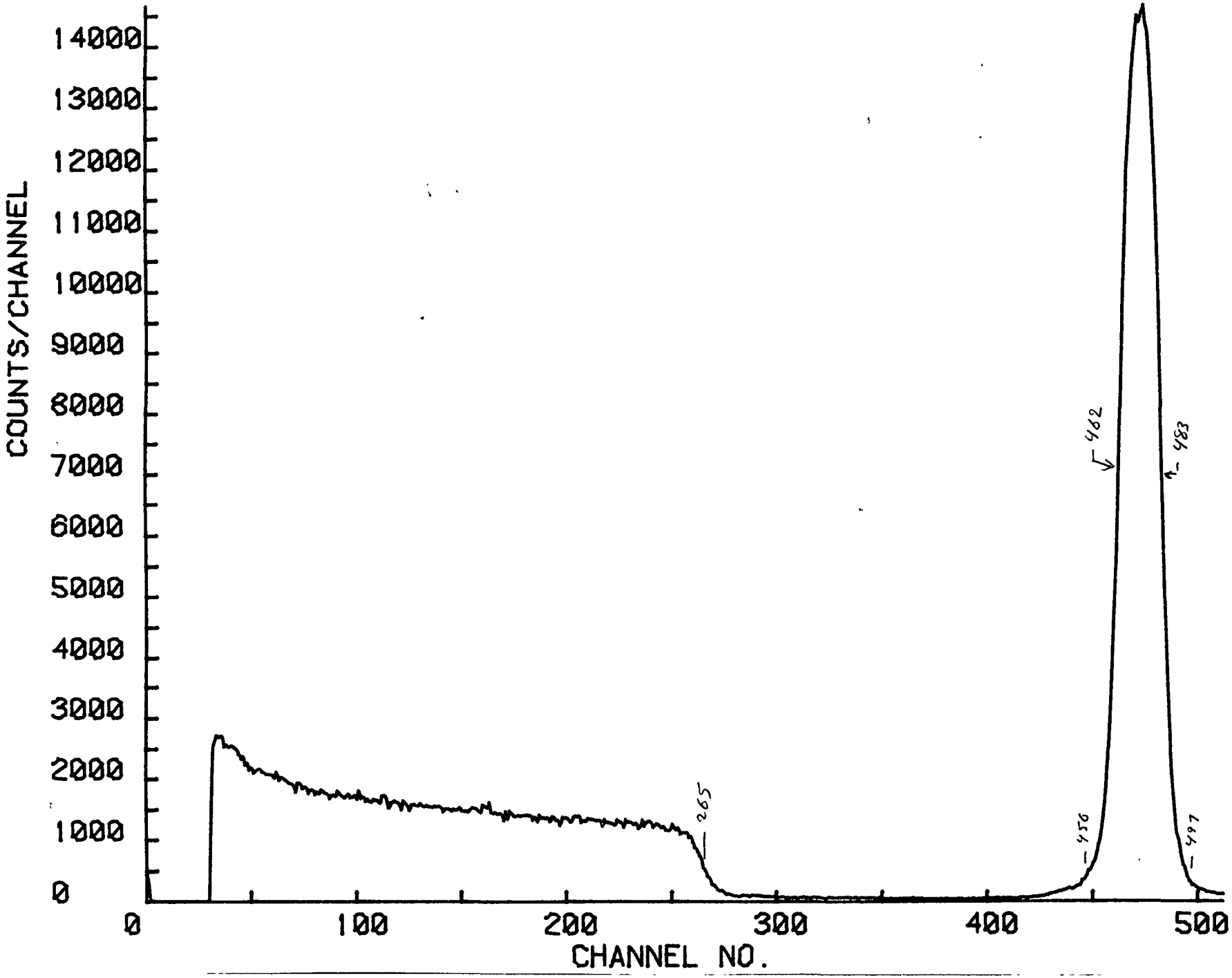

Fig. 63 Pt RBS Spectrum - Specimen F

Ni 6061 - A

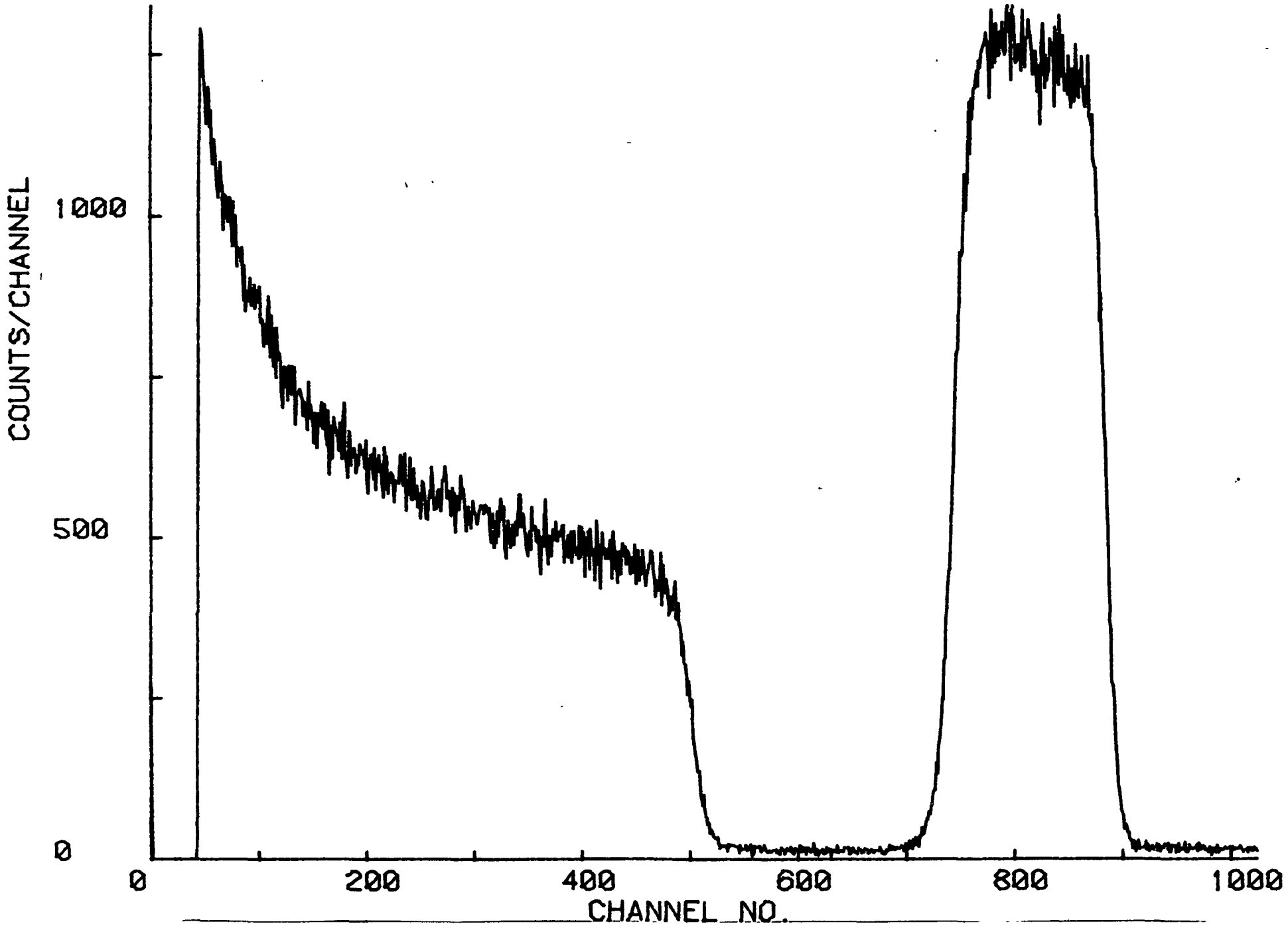

Fig. 64 Ni RBS Spectrum - Specimen A

Ni 6061 -B

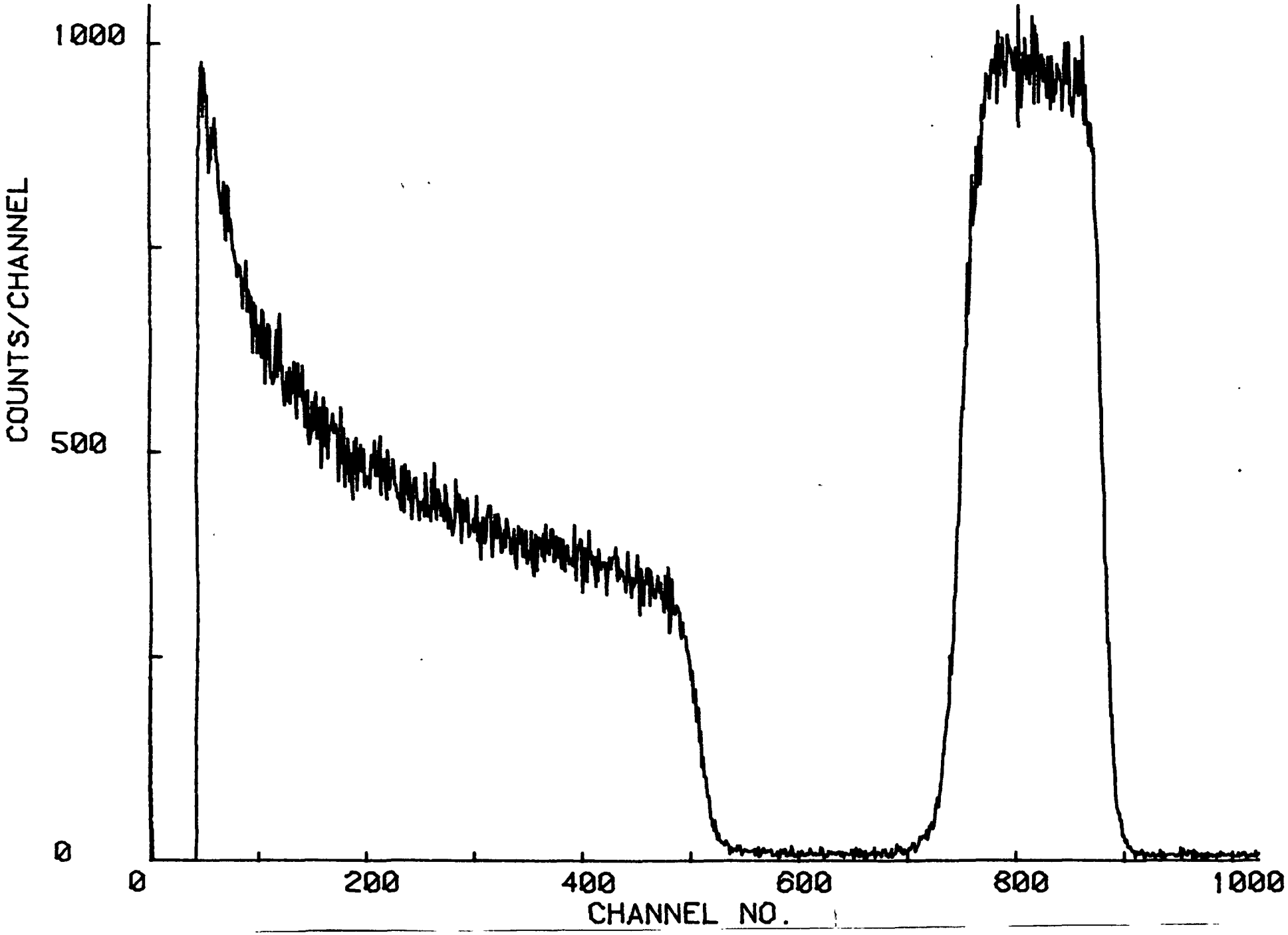

Fig. 65 Ni RBS Spectrum - Specimen B

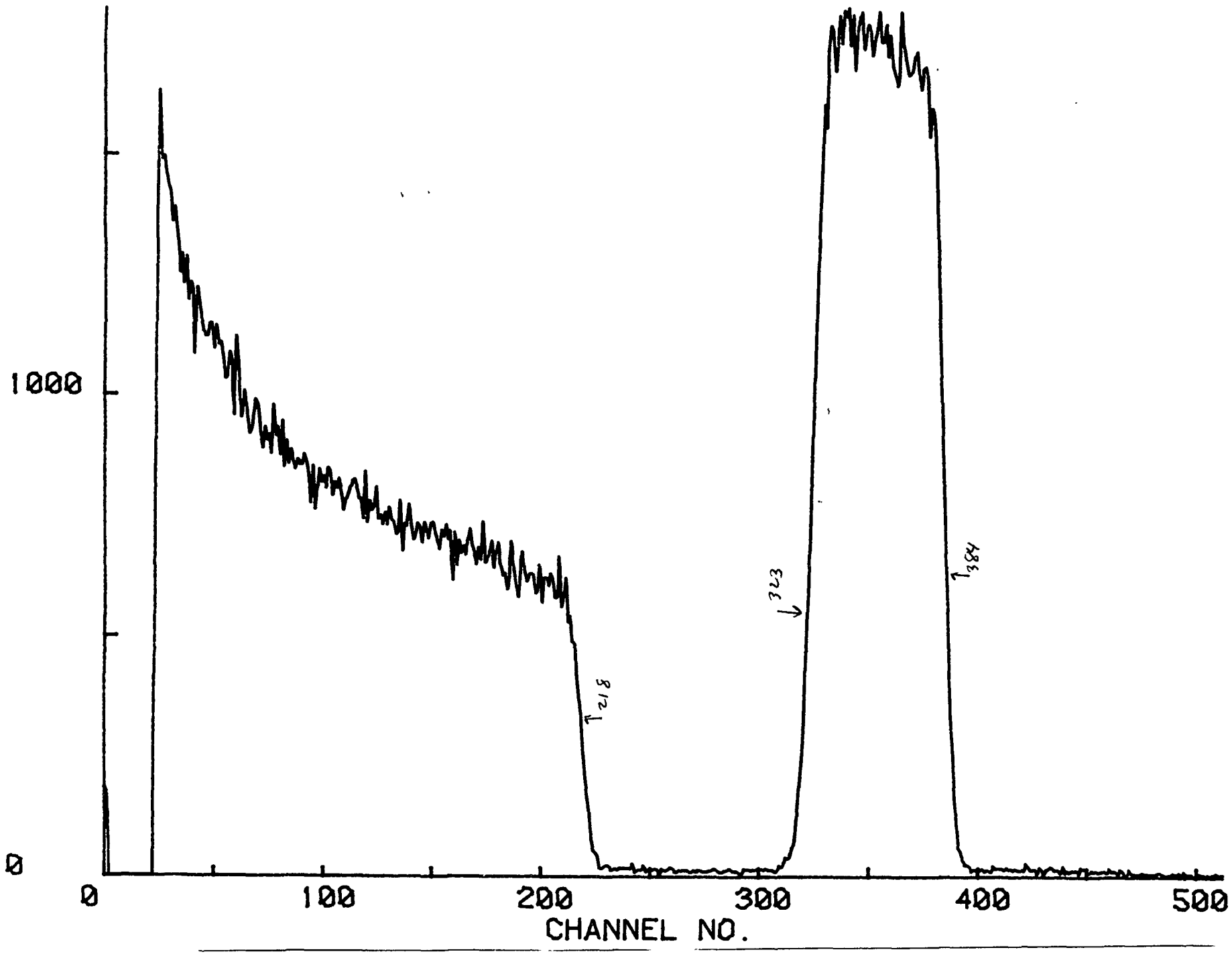

Fig. 66 Ni RBS Spectrum - Specimen C

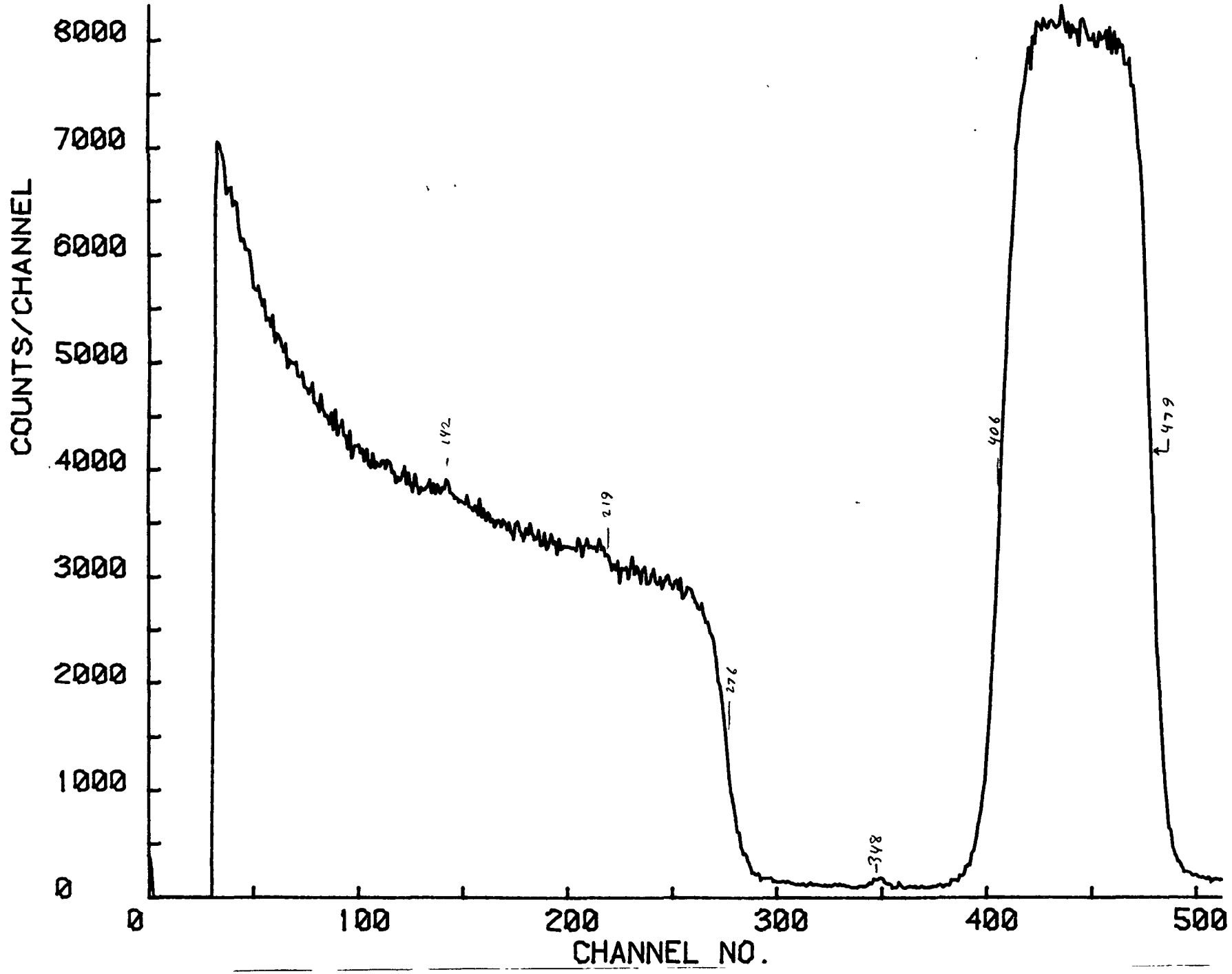

Fig. 67 Ni RBS Spectrum - Specimen F

Cu 303 - A

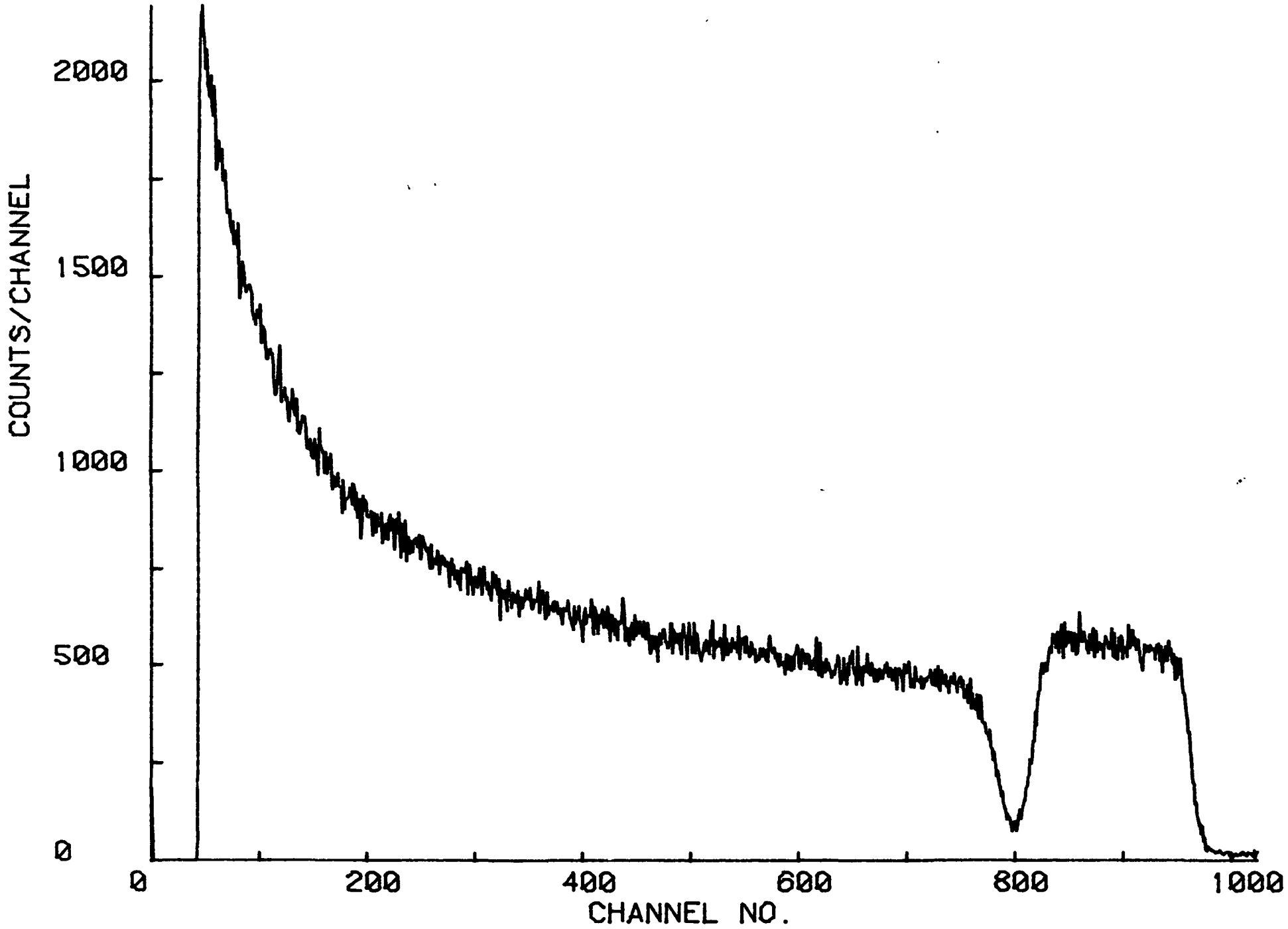

Fig. 68 Cu RBS Spectrum - Specimen A

Cu 303-B

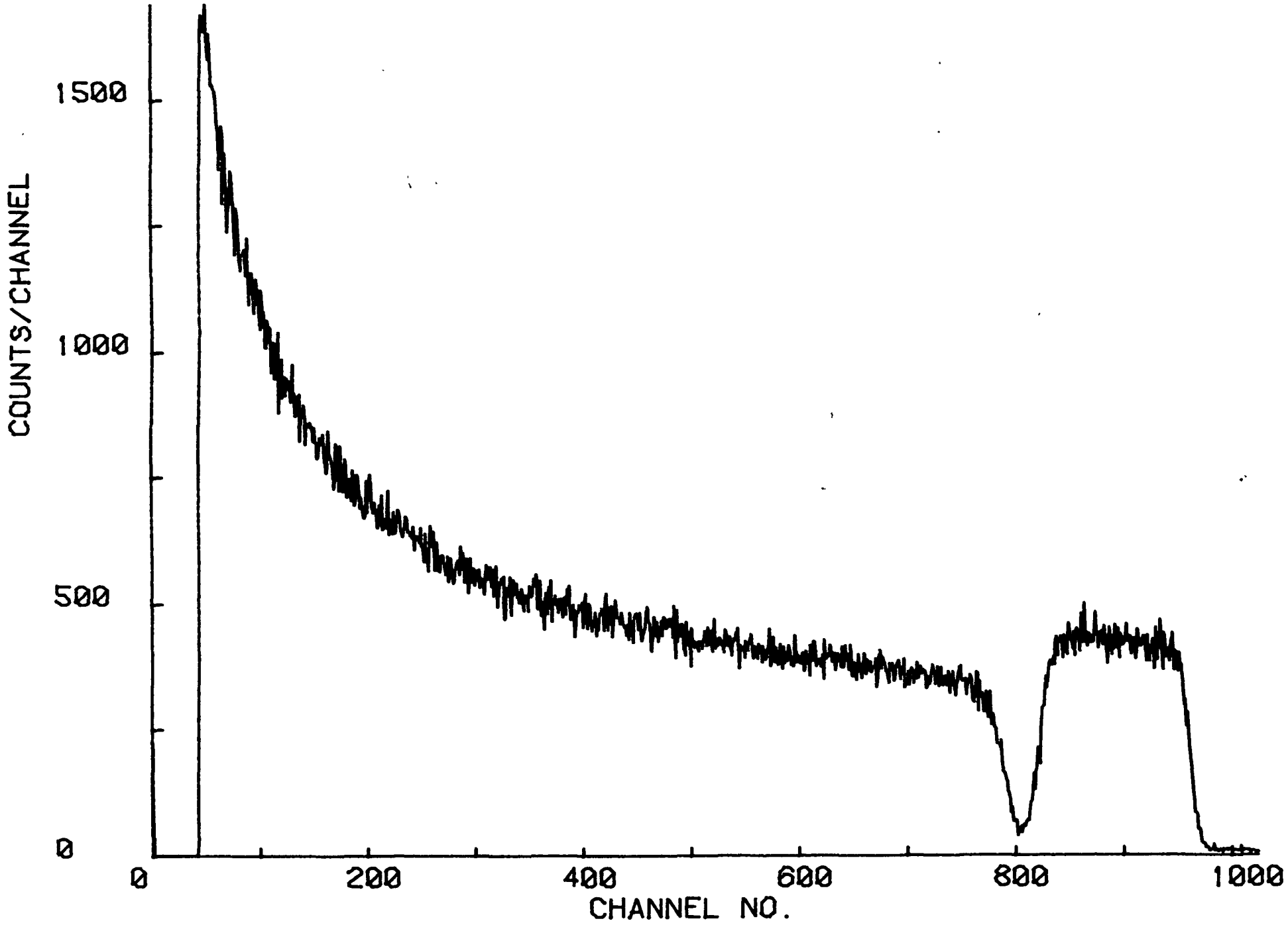

Fig. 69 Cu RBS Spectrum - Specimen B

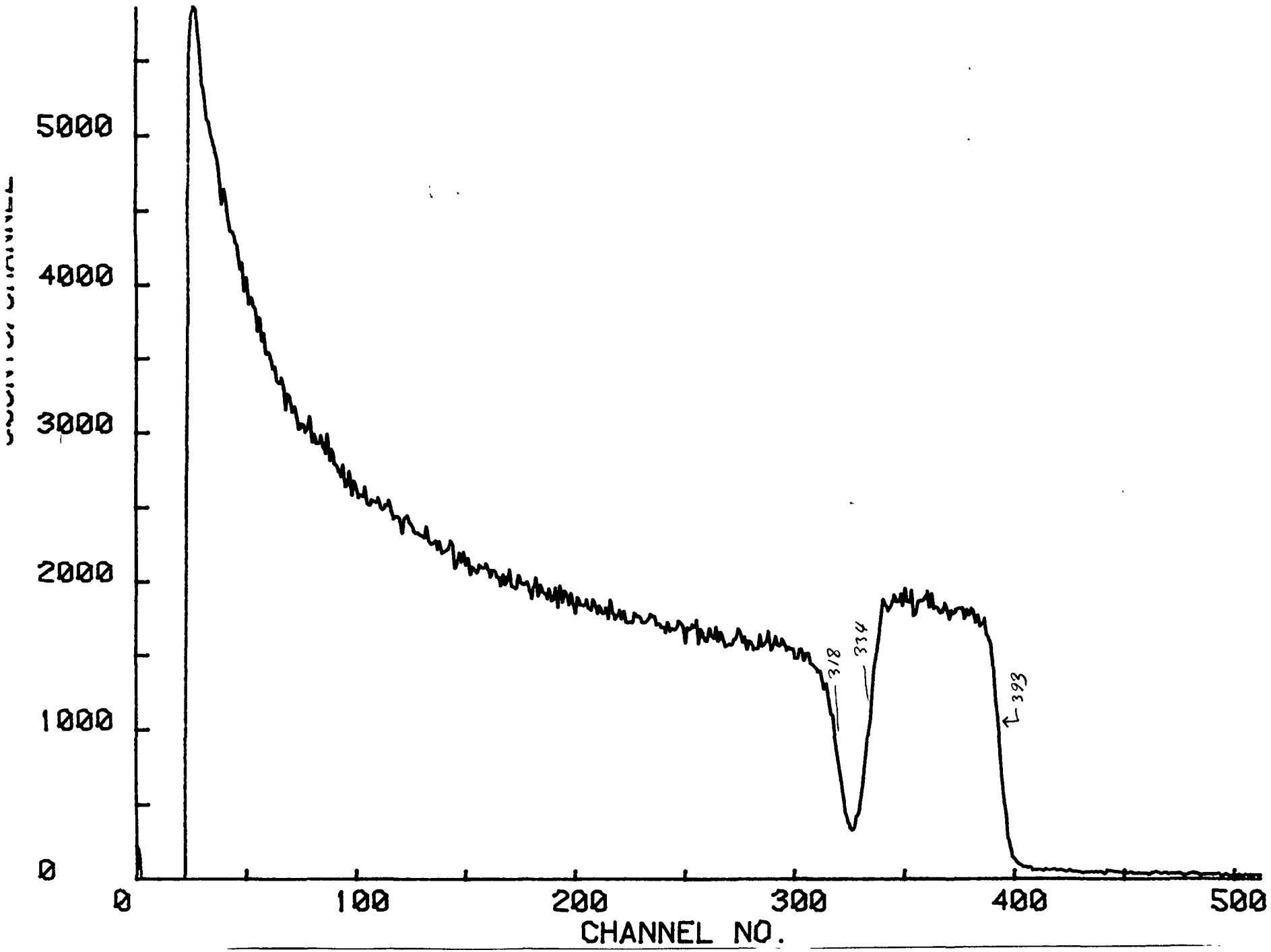

Fig. 70 Cu RBS Spectrum - Specimen C

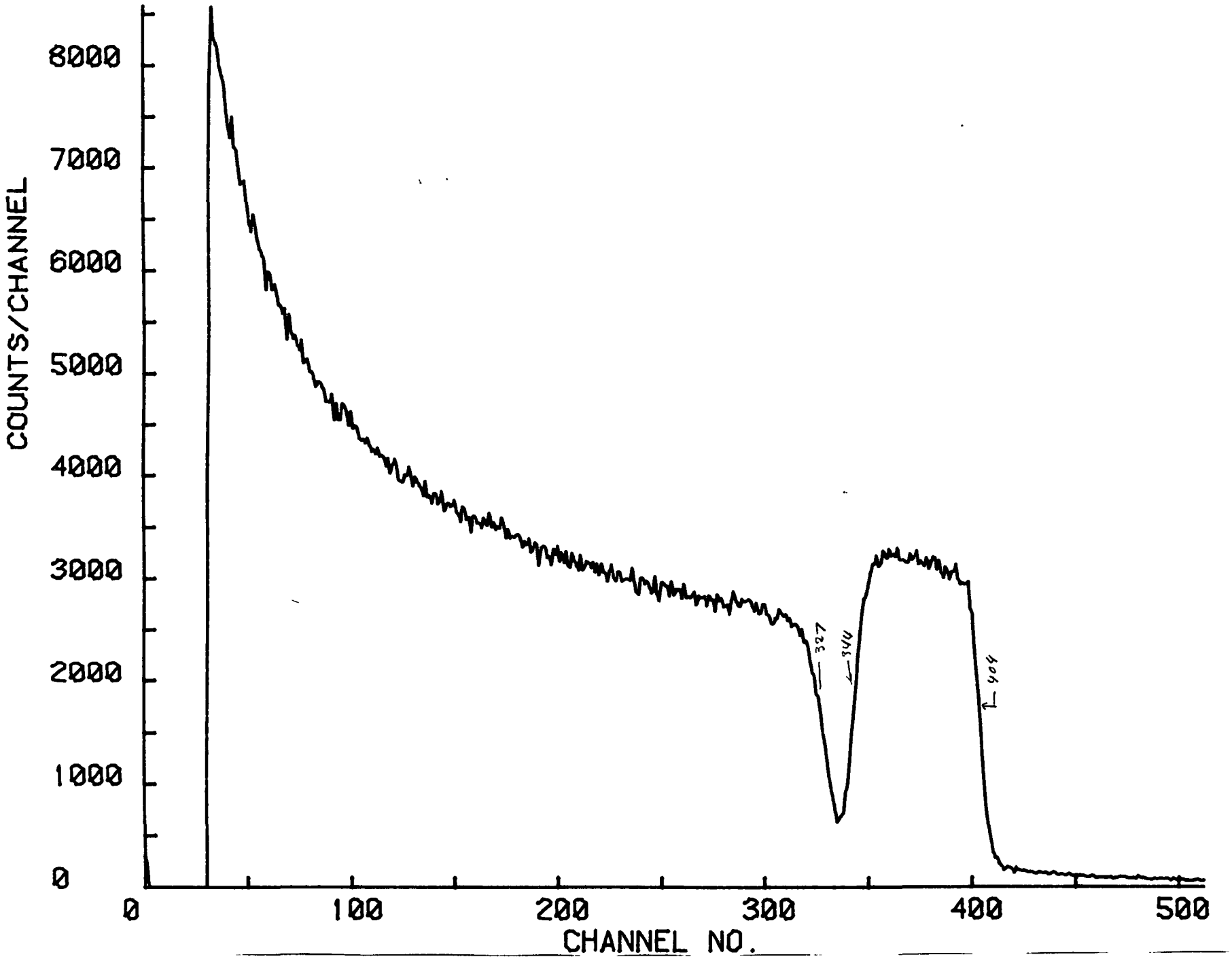

Fig. 71 Cu RBS Spectrum - Specimen F

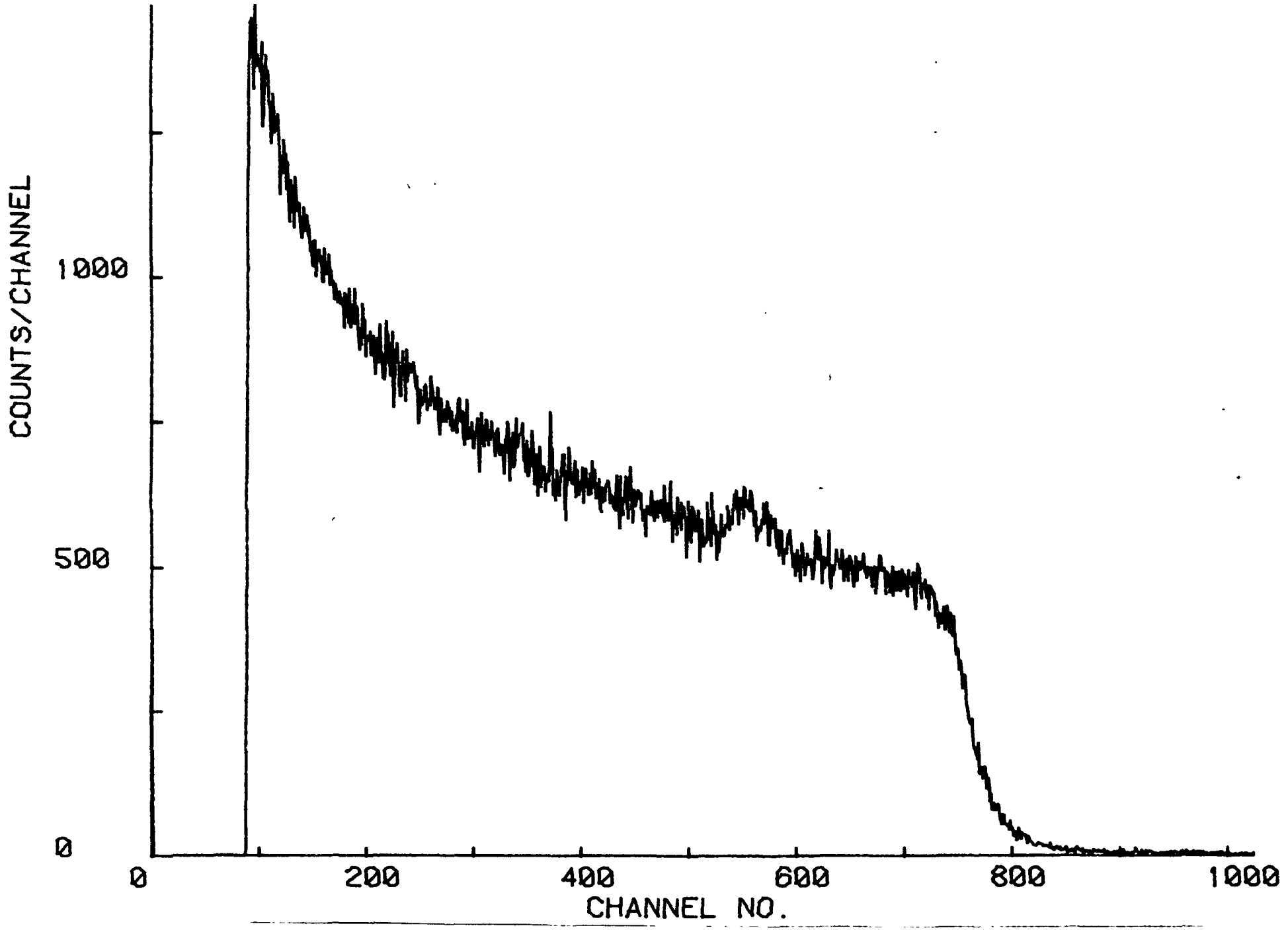

Fig. 72 Al RBS Spectrum - Specimen A

Al 303-B

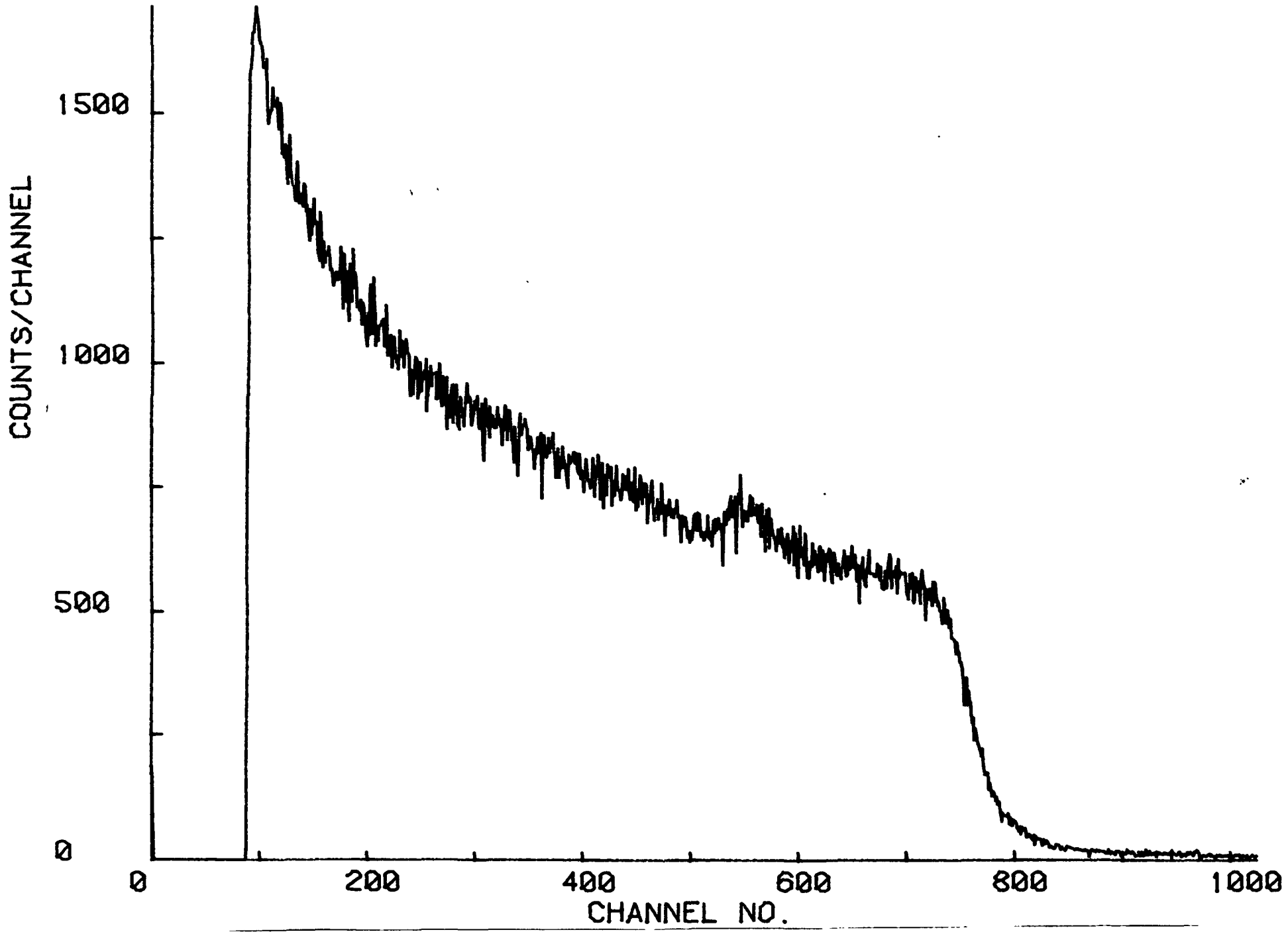

Fig. 73 Al RBS Spectrum - Specimen B

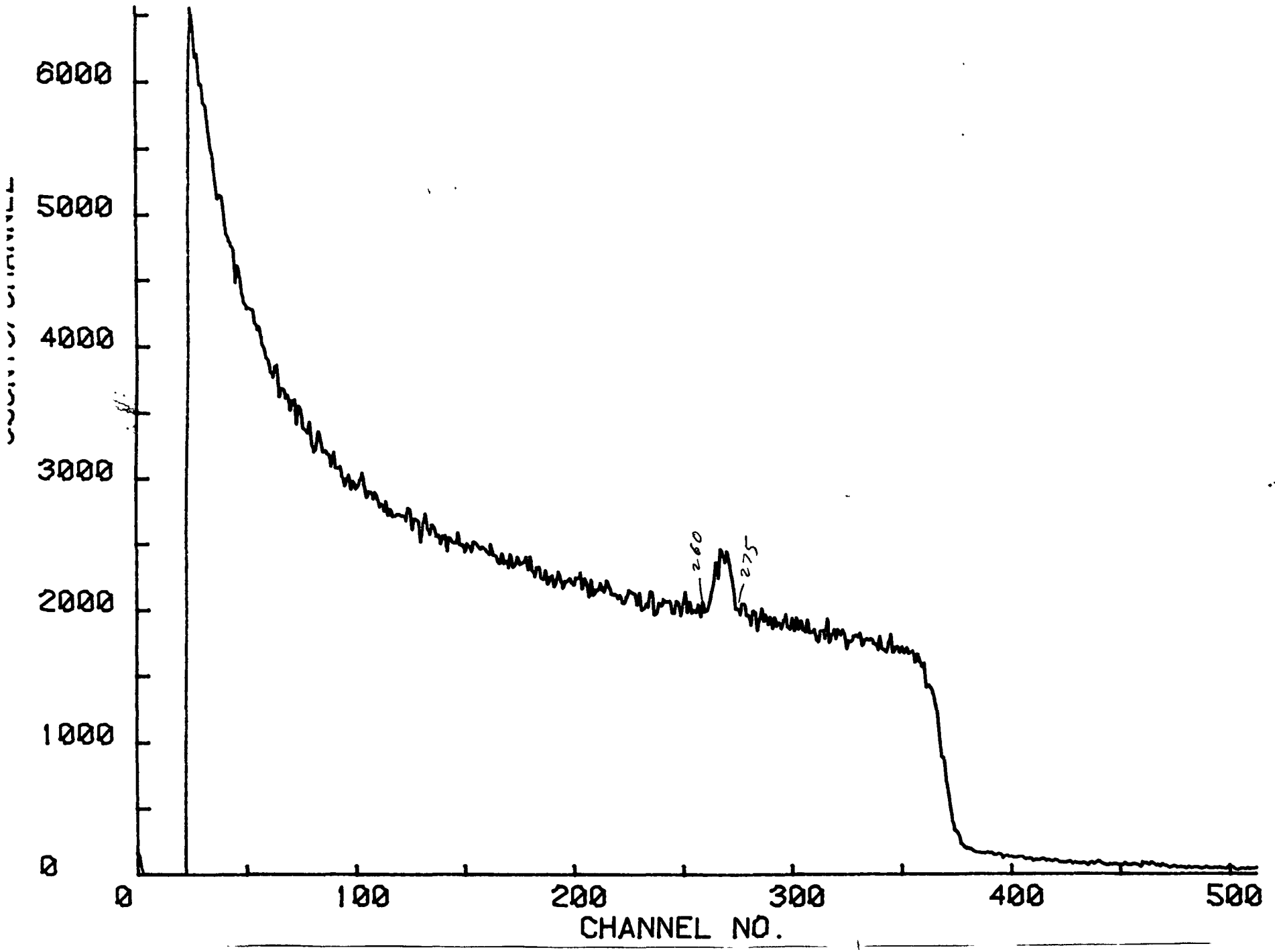

Fig. 74 Al RBS Spectrum - Specimen C

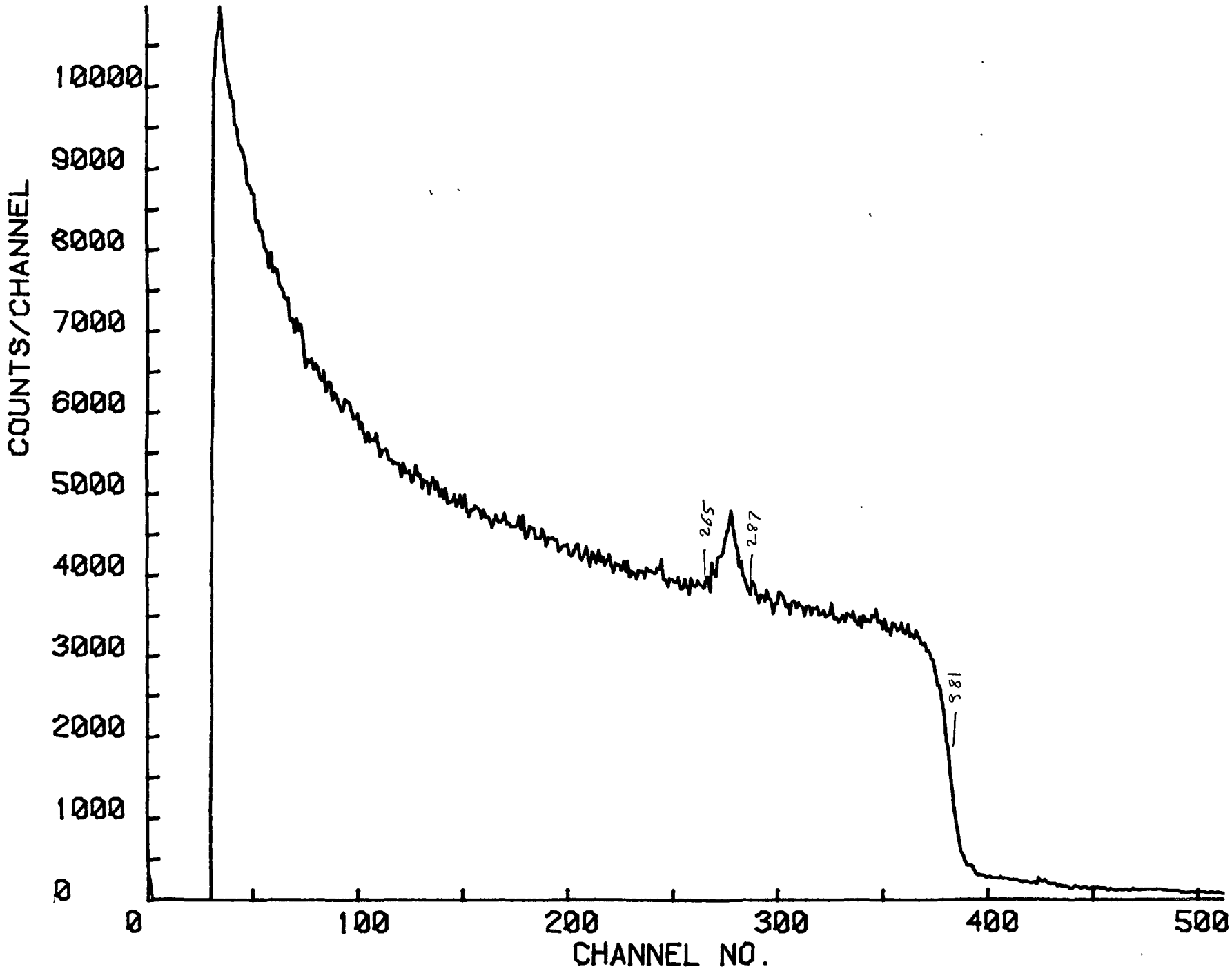

Fig. 75 Al RBS Spectrum - Specimen F

Cr - 2219 - A

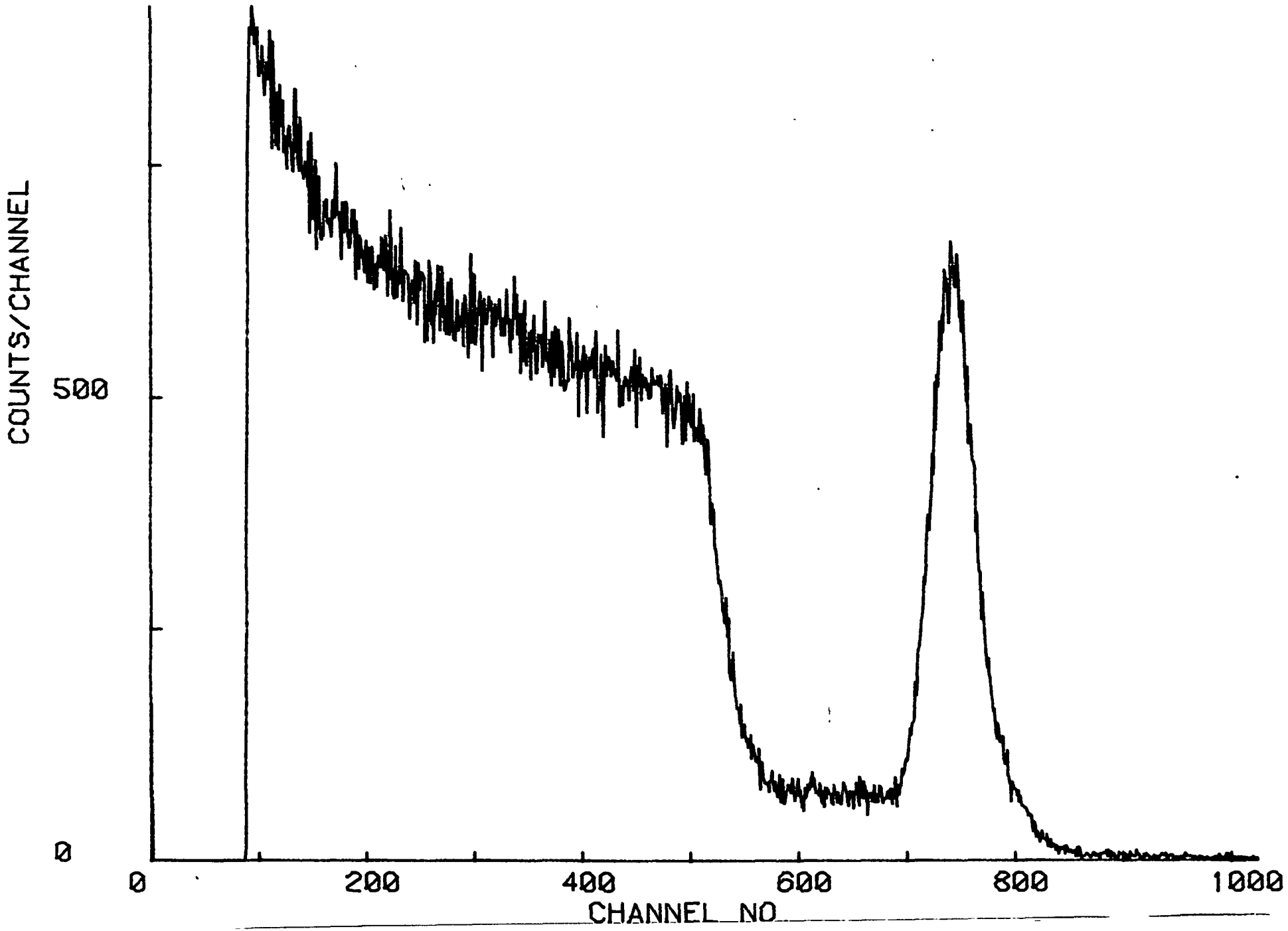

Fig. 76 Cr RBS Spectrum - Specimen A

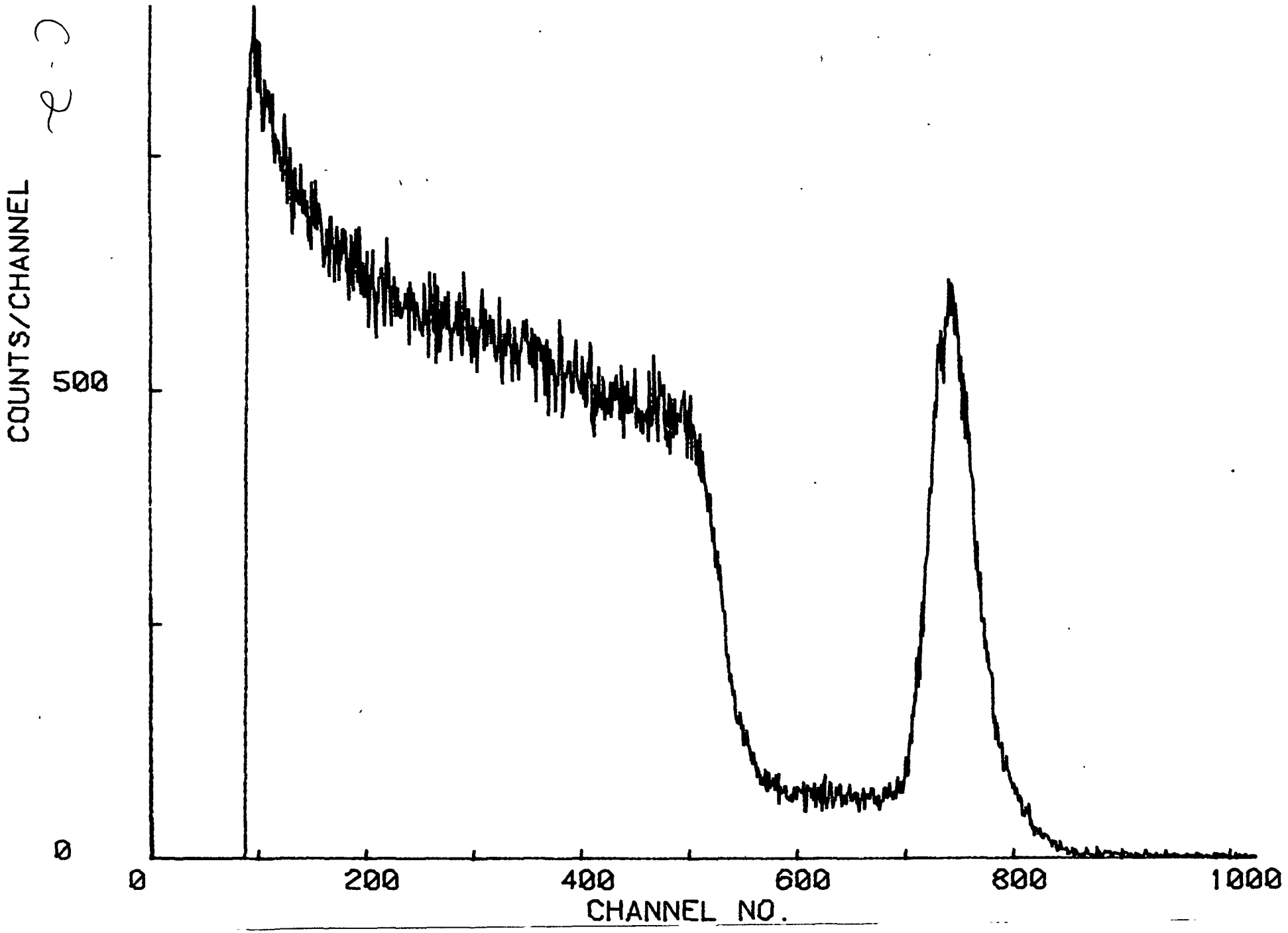

Fig. 77 Cr RBS Spectrum - Specimen B

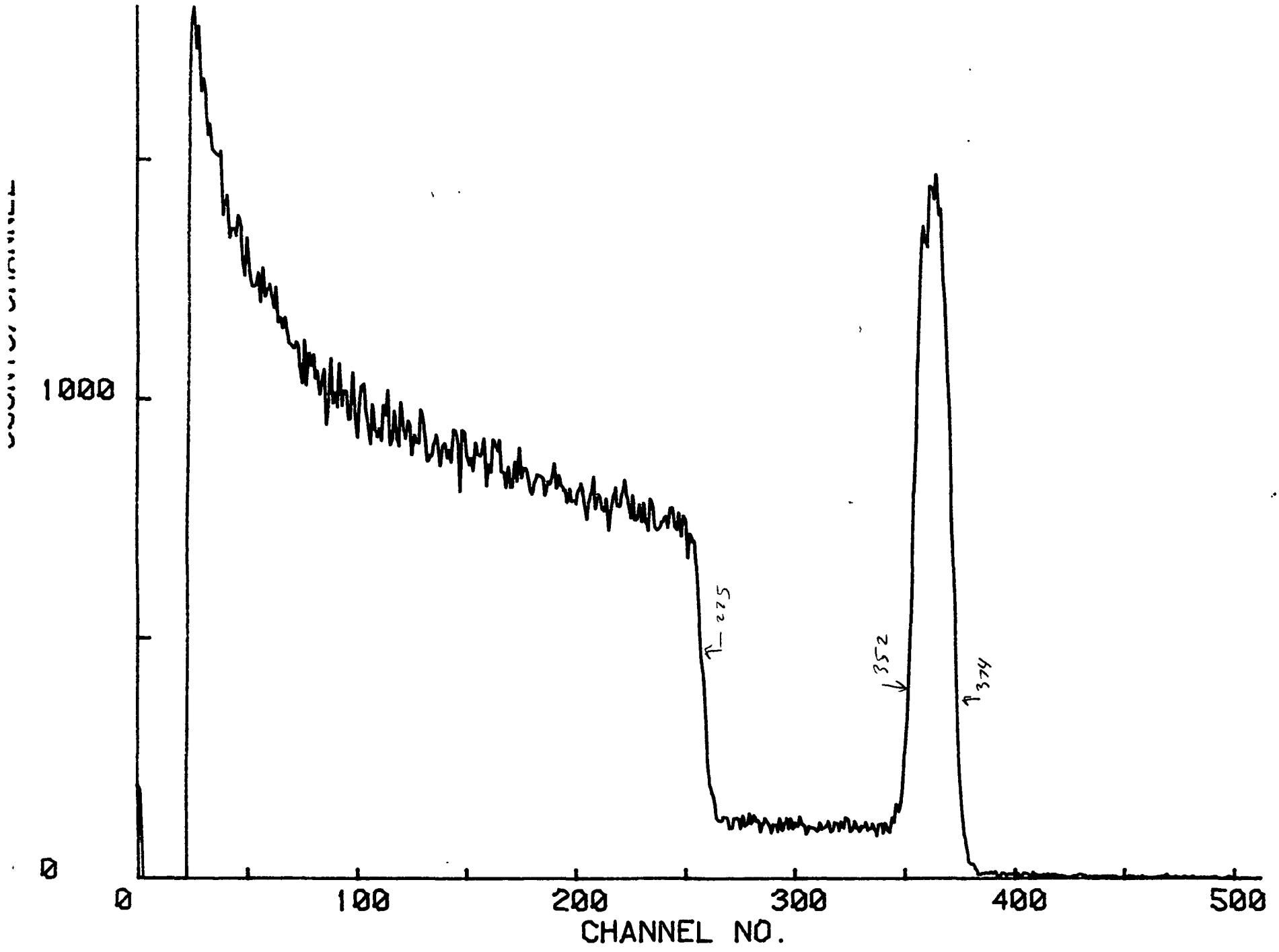

Fig. 78 Cr RBS Spectrum - Specimen C

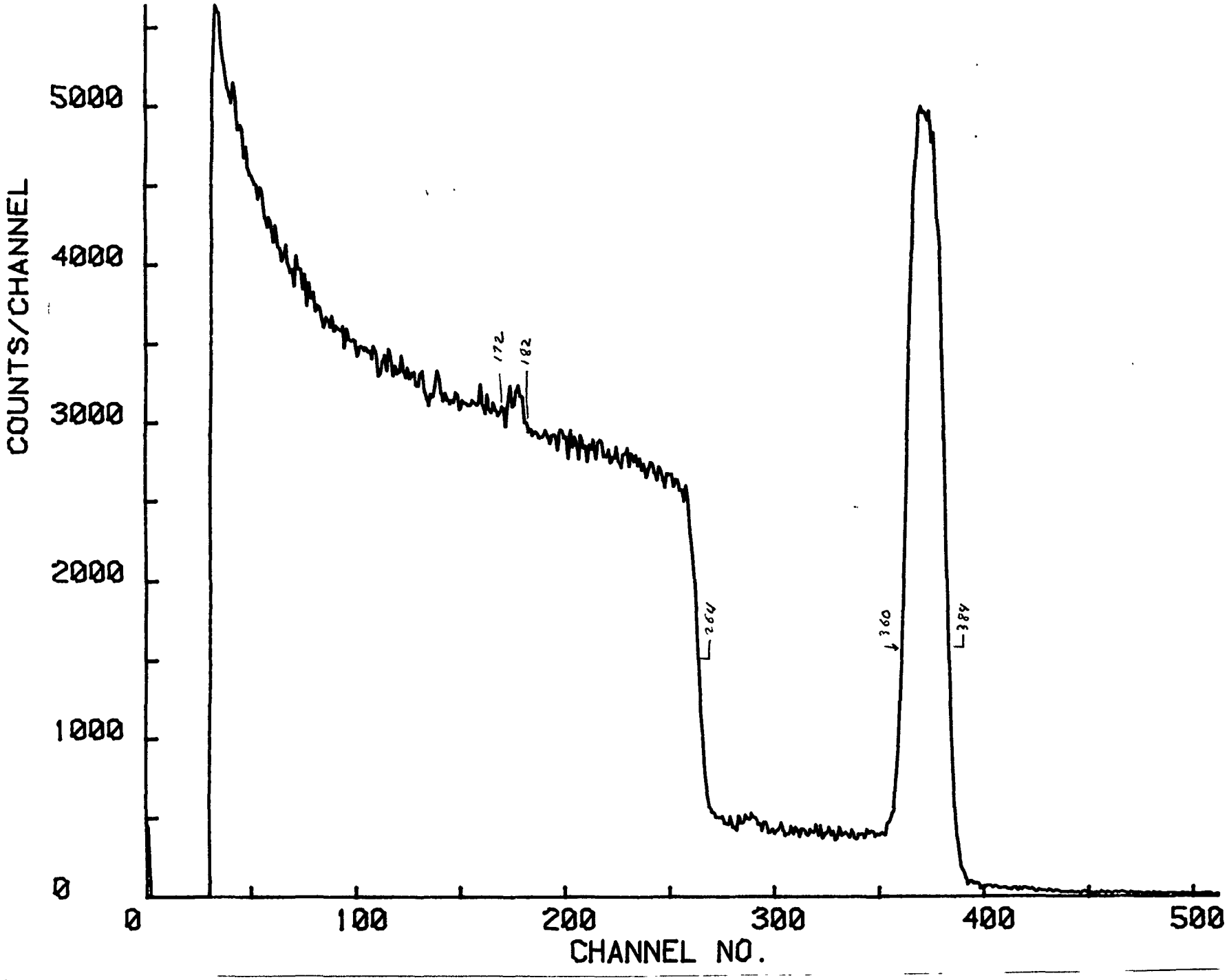

Fig. 79 Cr RBS Spectrum - Specimen F

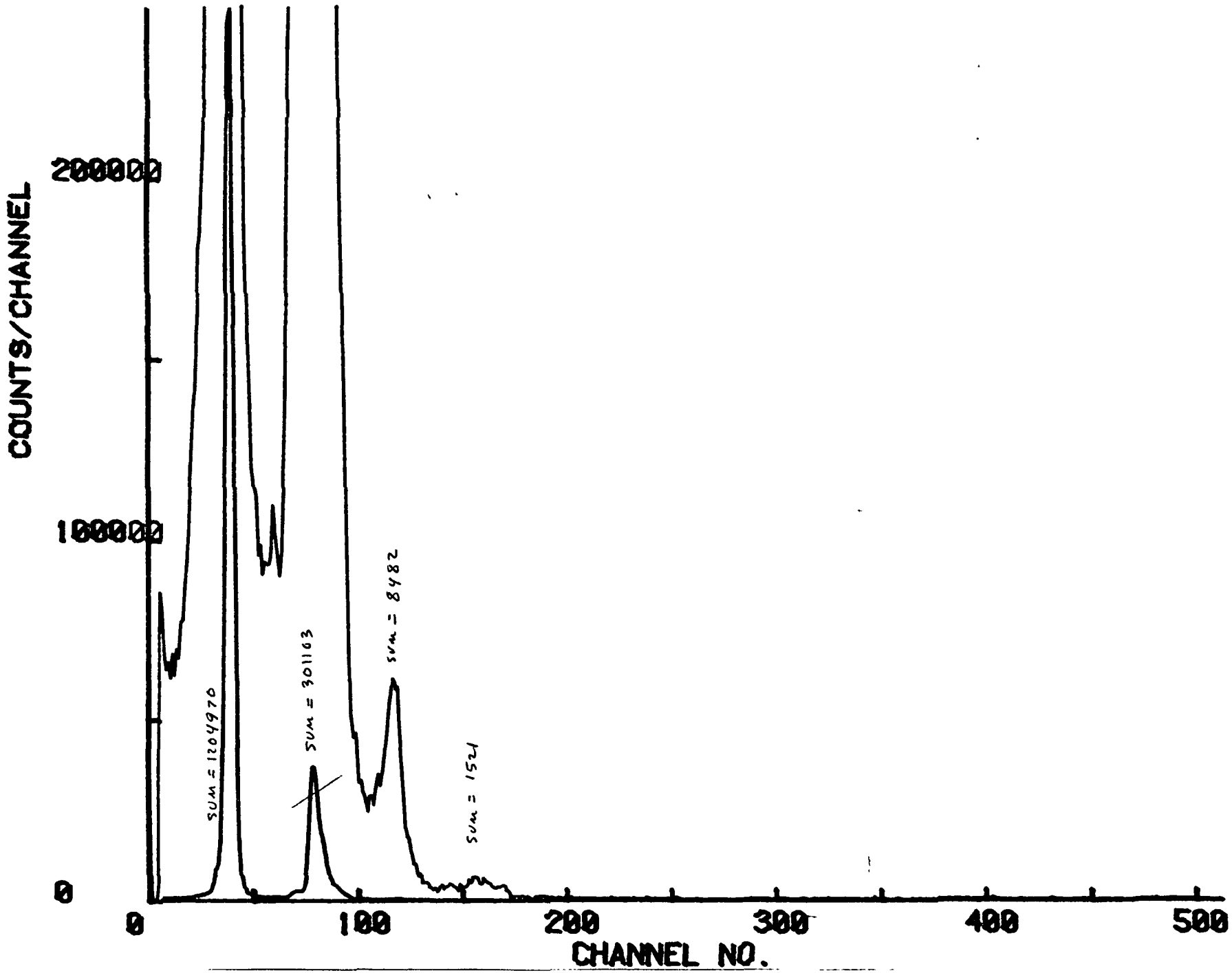

Fig. 80 Ag PIXE Spectrum - Specimen C

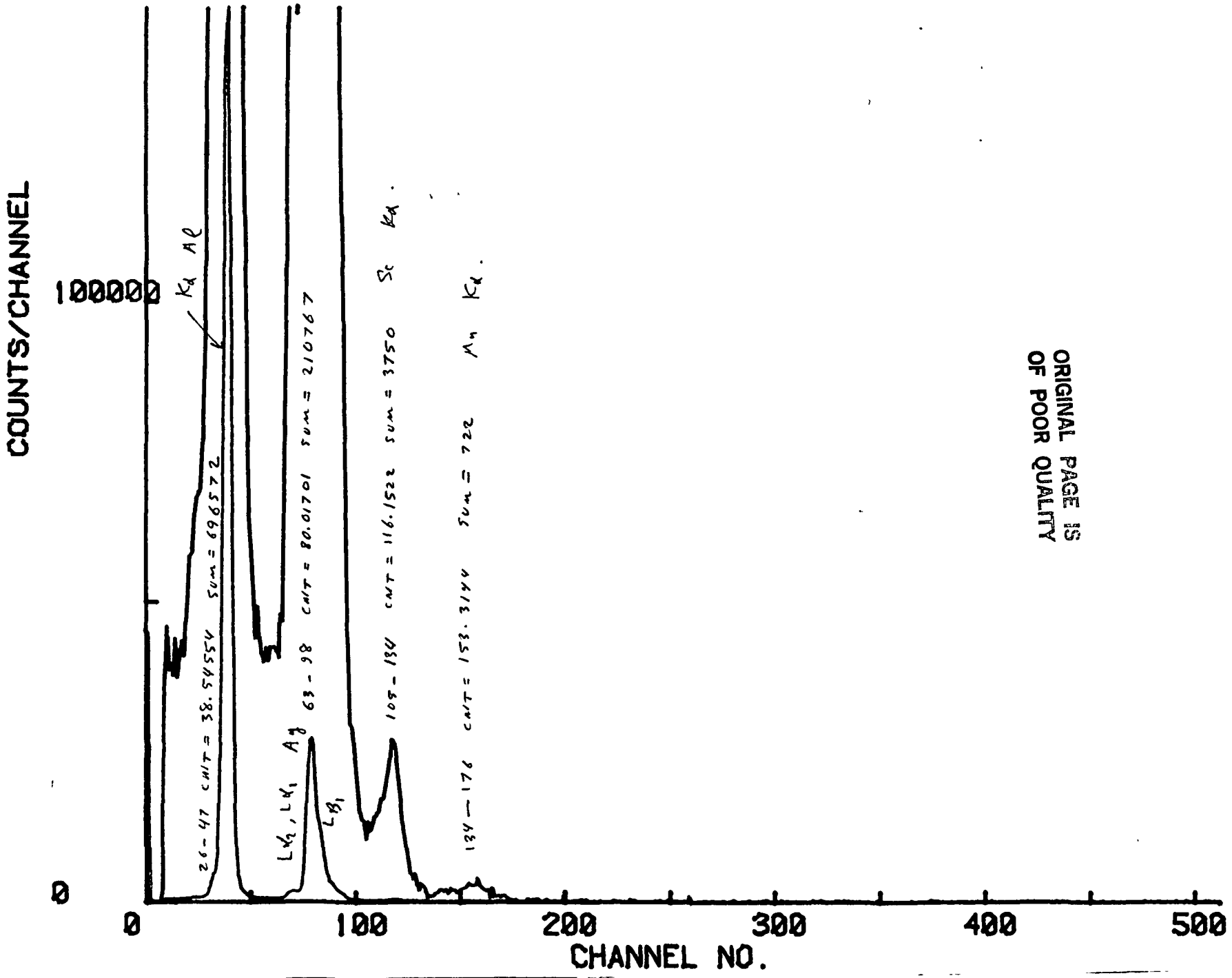

Fig. 81 Ag PIXE Spectrum - Specimen F

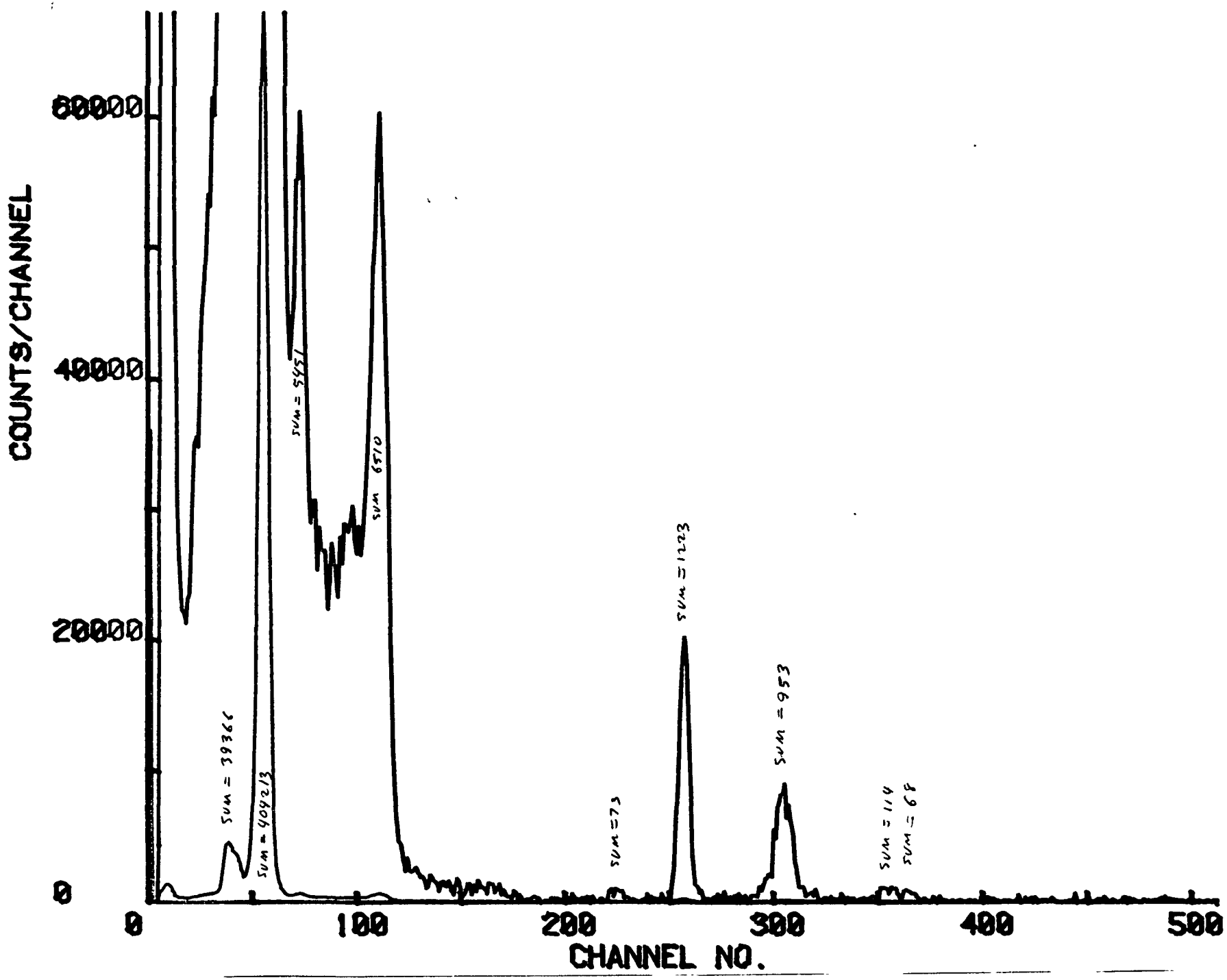

Fig. 82 Au PIXE Spectrum - Specimen C

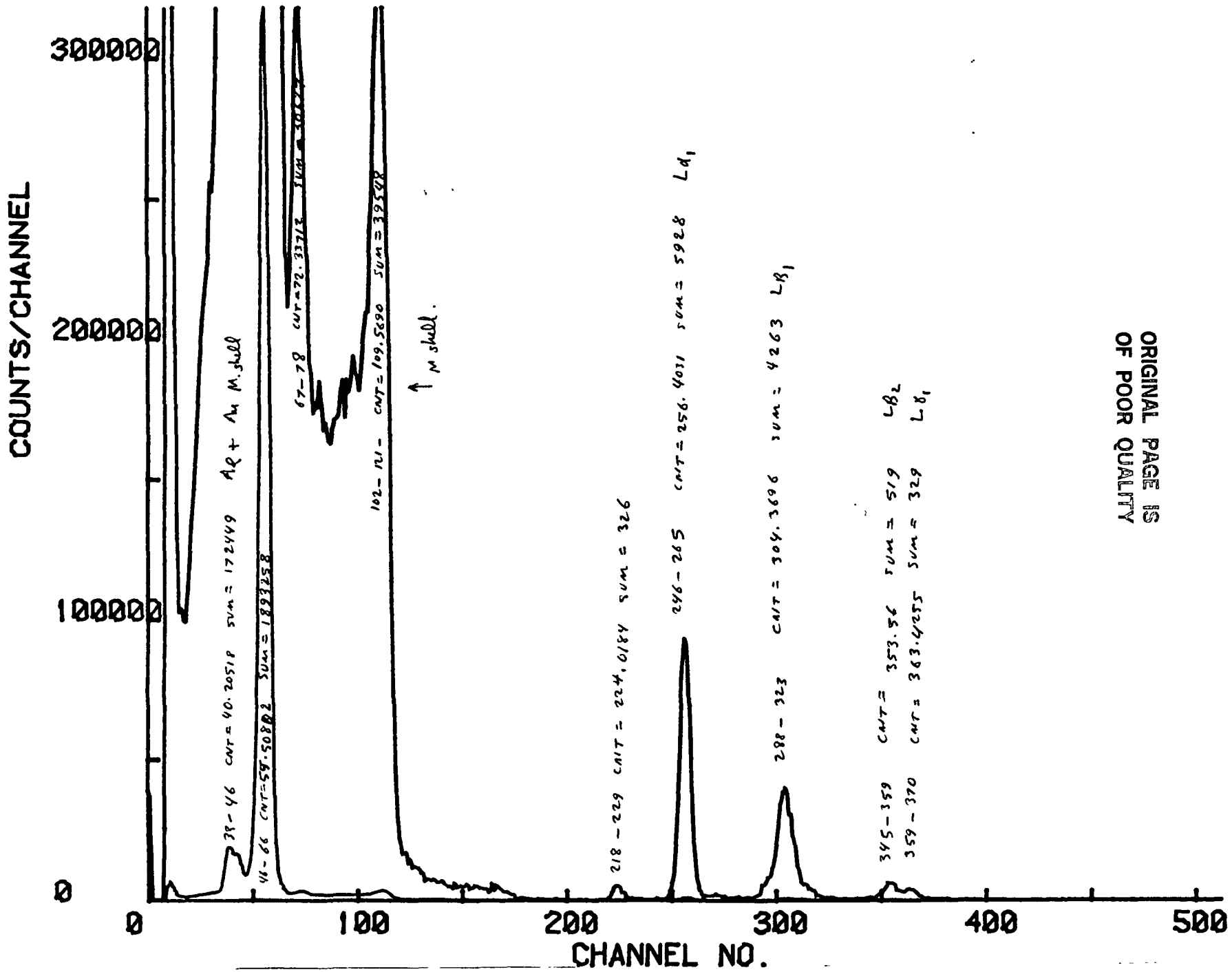

Fig. 83 Au PIXE Spectrum - Specimen F

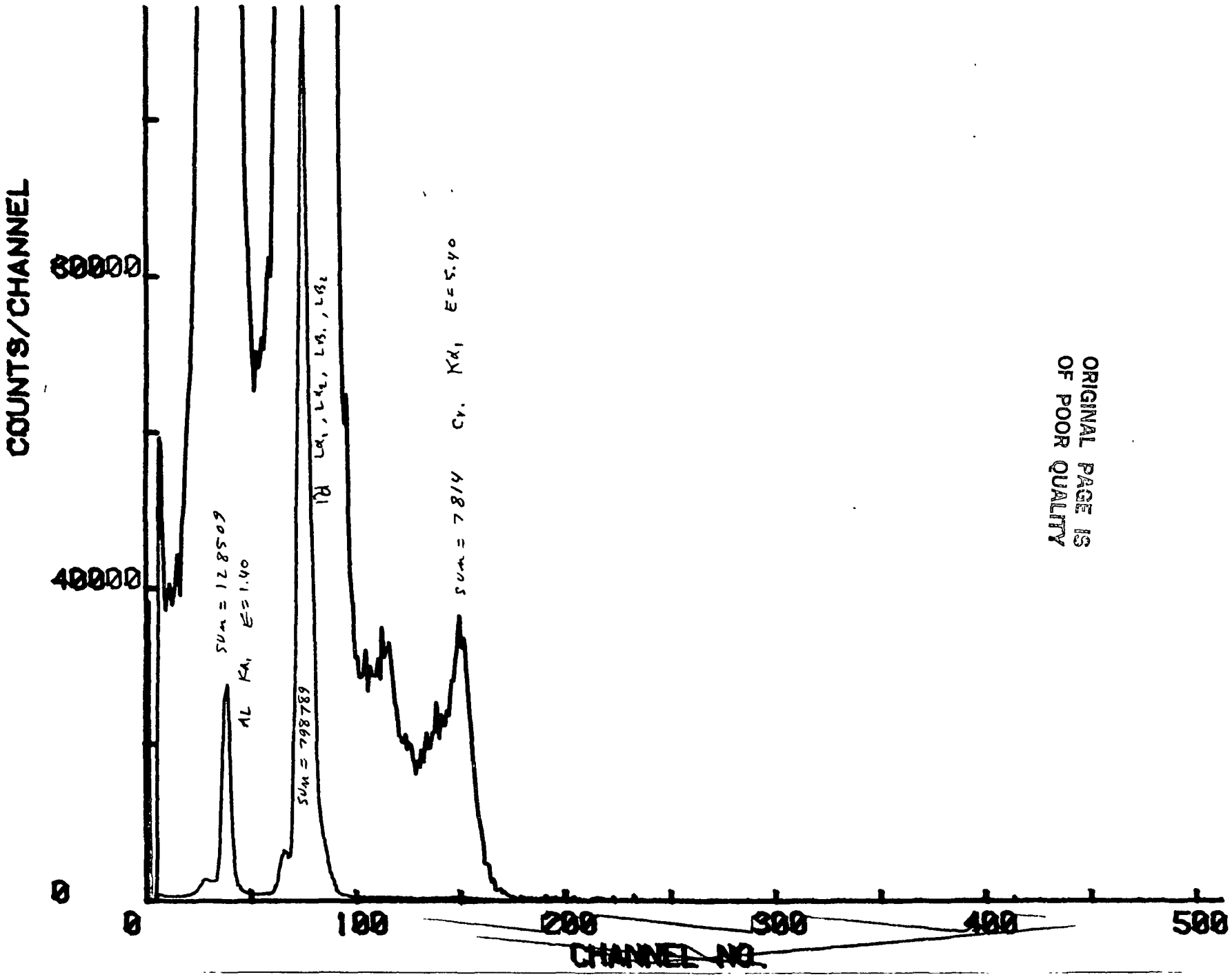

Fig. 84 Pd PIXE Spectrum - Specimen C

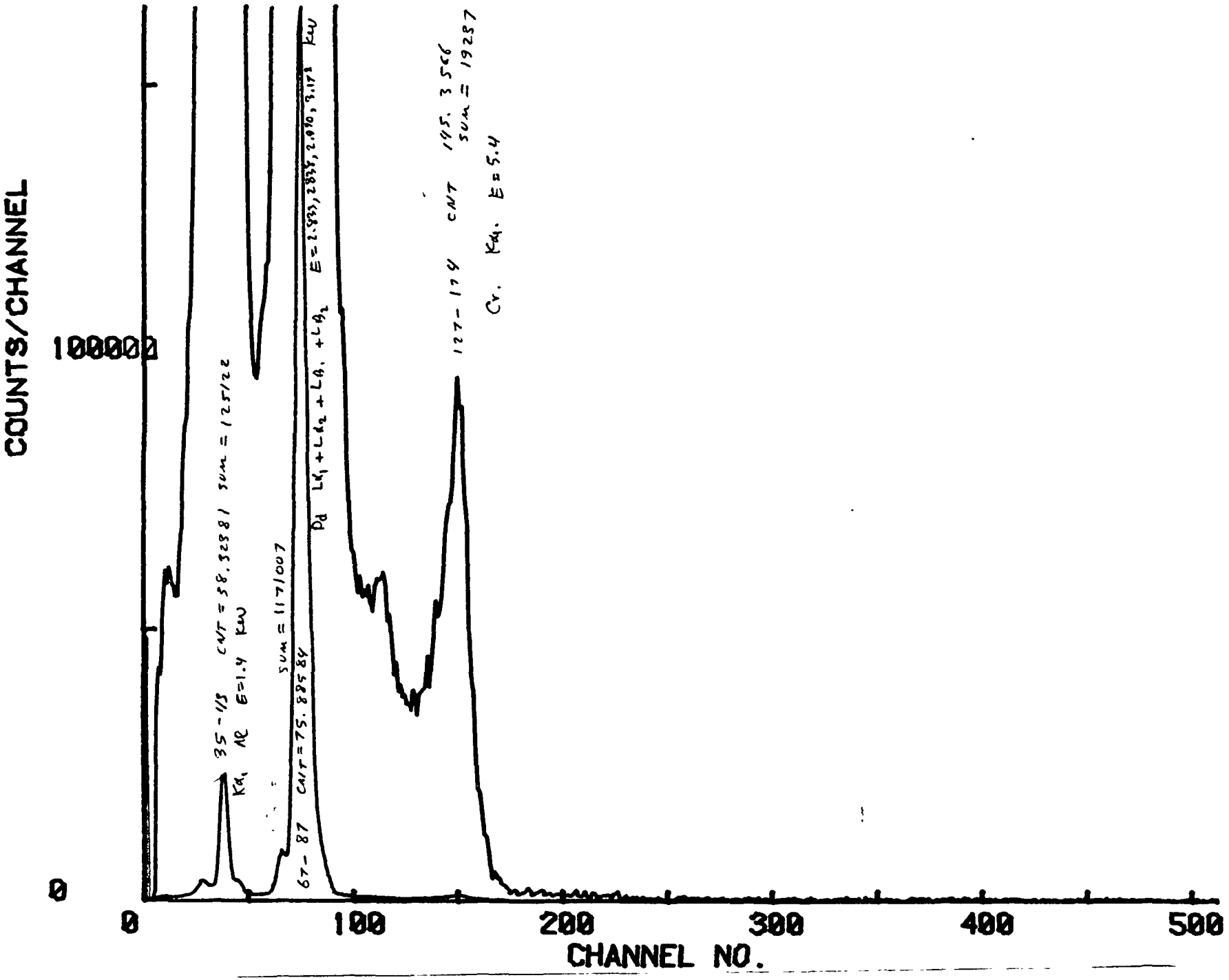

Fig. 85 Pd PIXE Spectrum - Specimen F

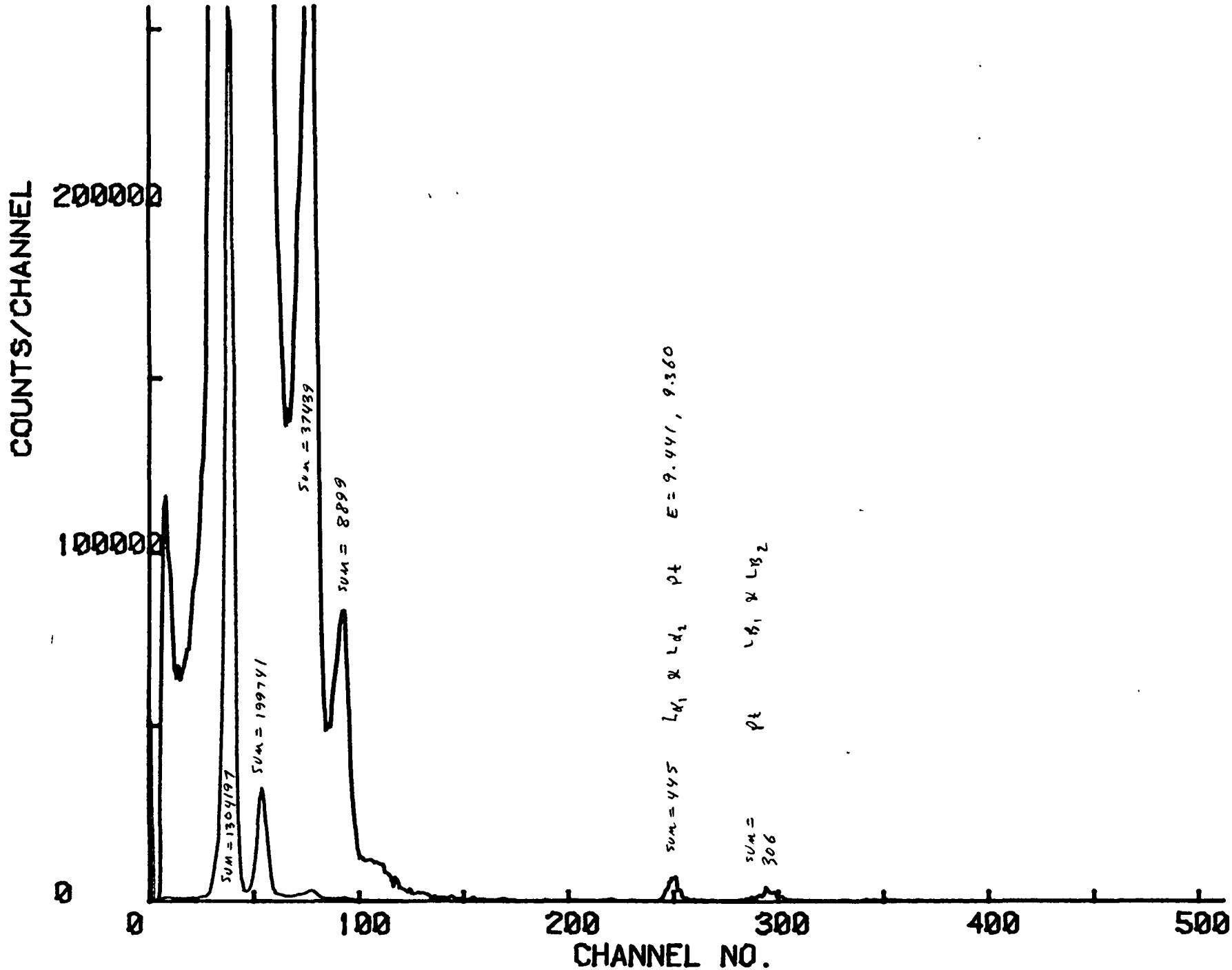

Fig. 86 Pt PIXE Spectrum - Specimen C

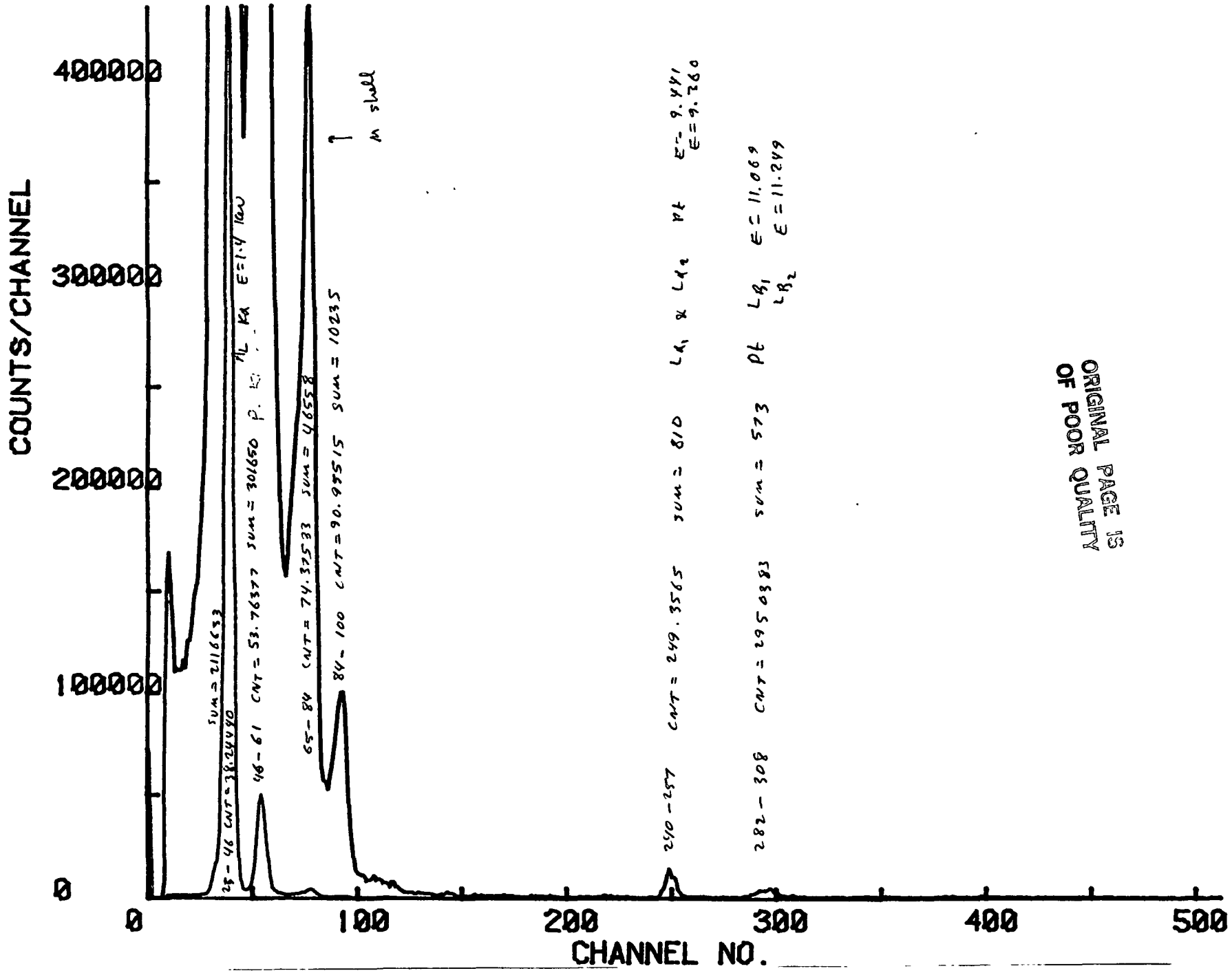

Fig. 87 Pt PIXE Spectrum - Specimen F

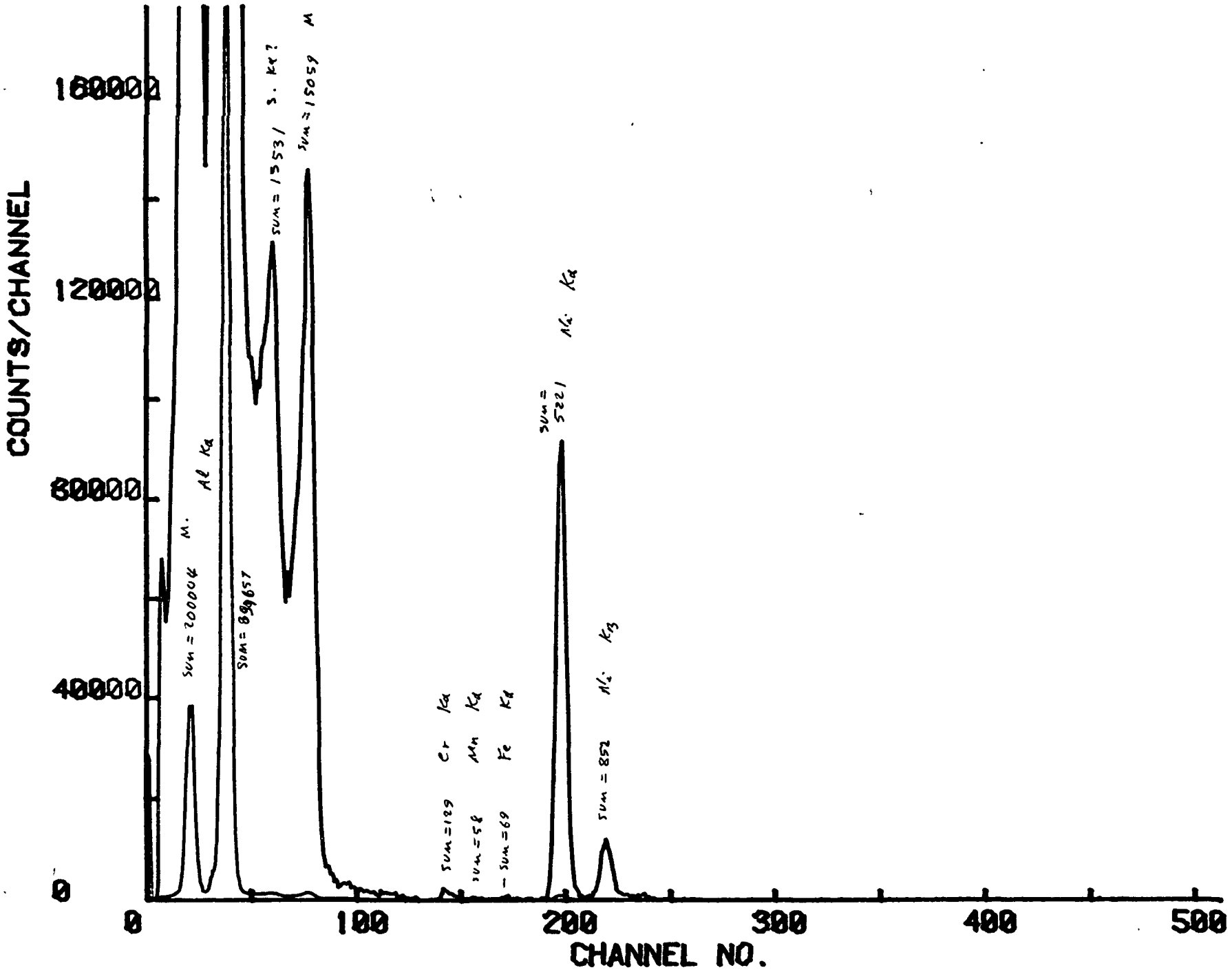

Fig. 88 Ni PIXE Spectrum - Specimen C

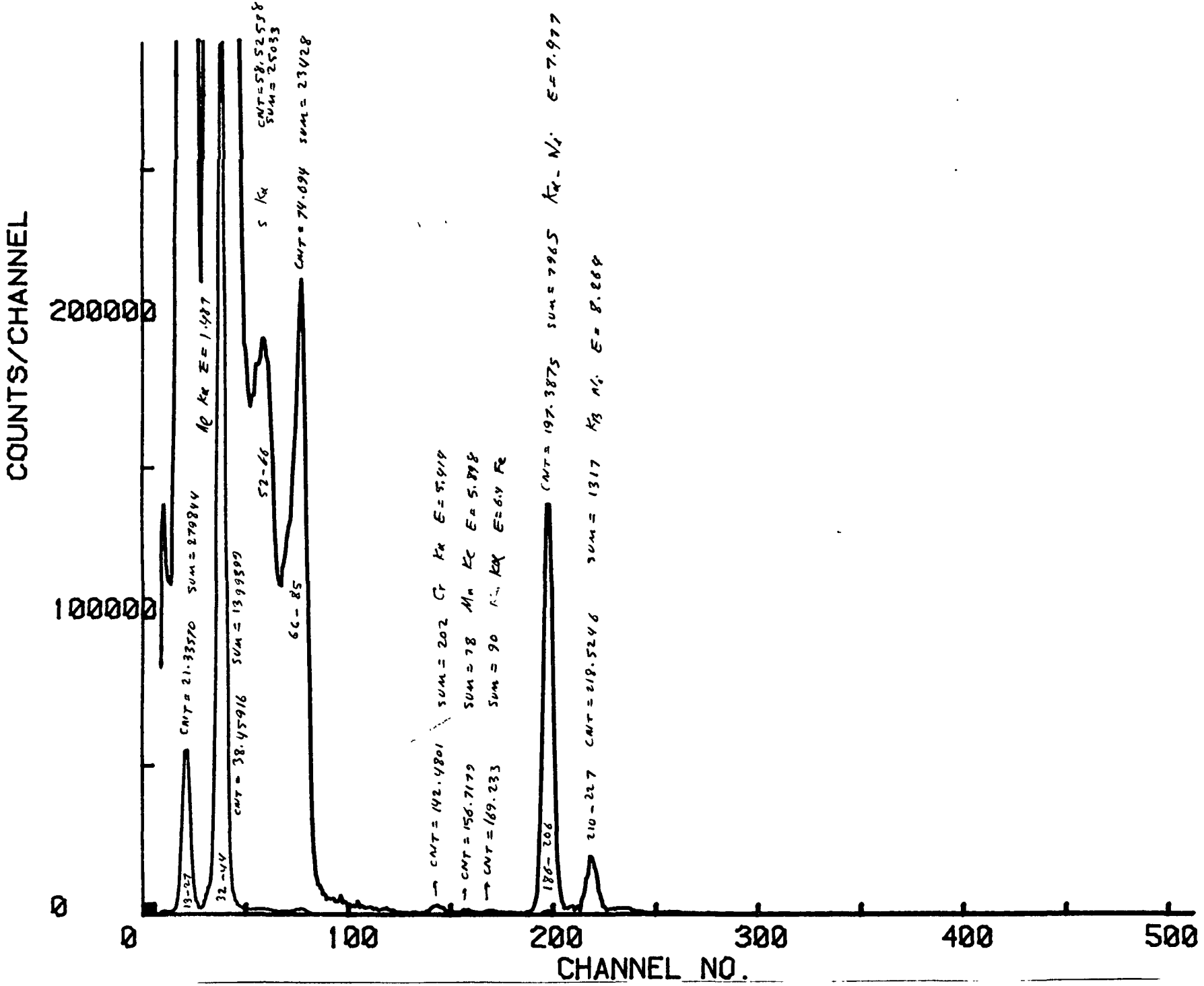

Fig. 89 Ni PIXE Spectrum - Specimen F

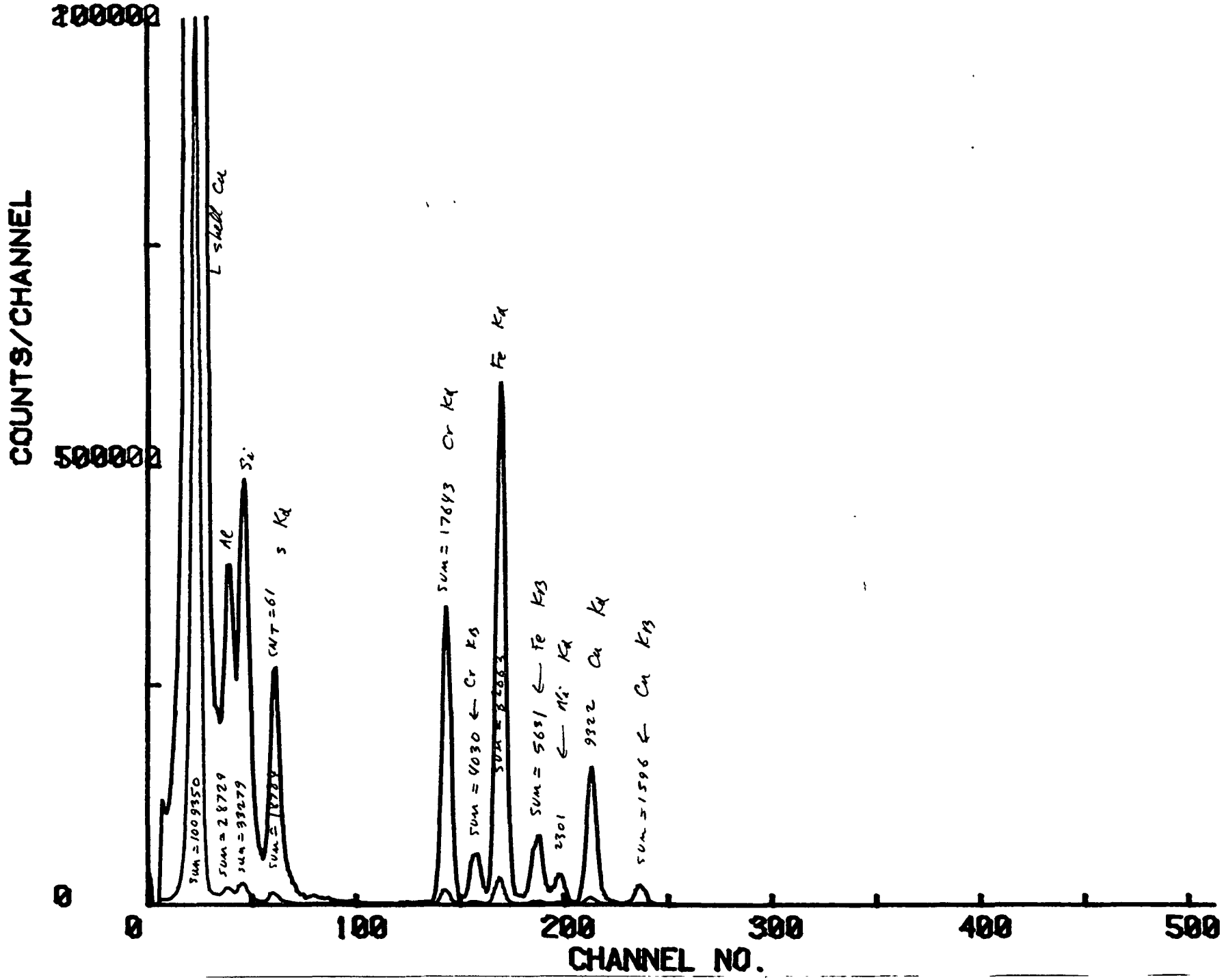

Fig. 90 Cu PIXE Spectrum - Specimen C

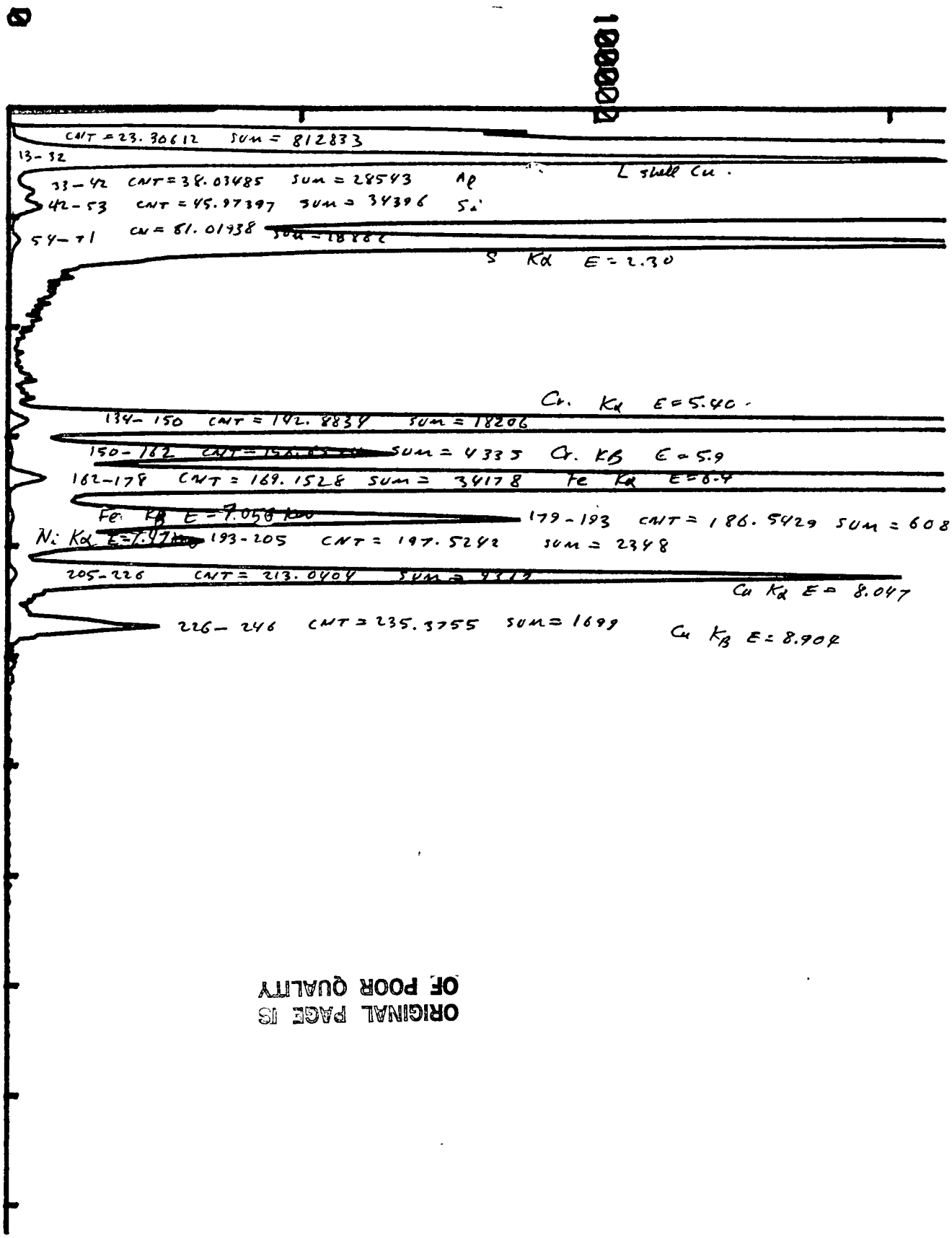

Fig. 91 Cu PIXE Spectrum - Specimen F

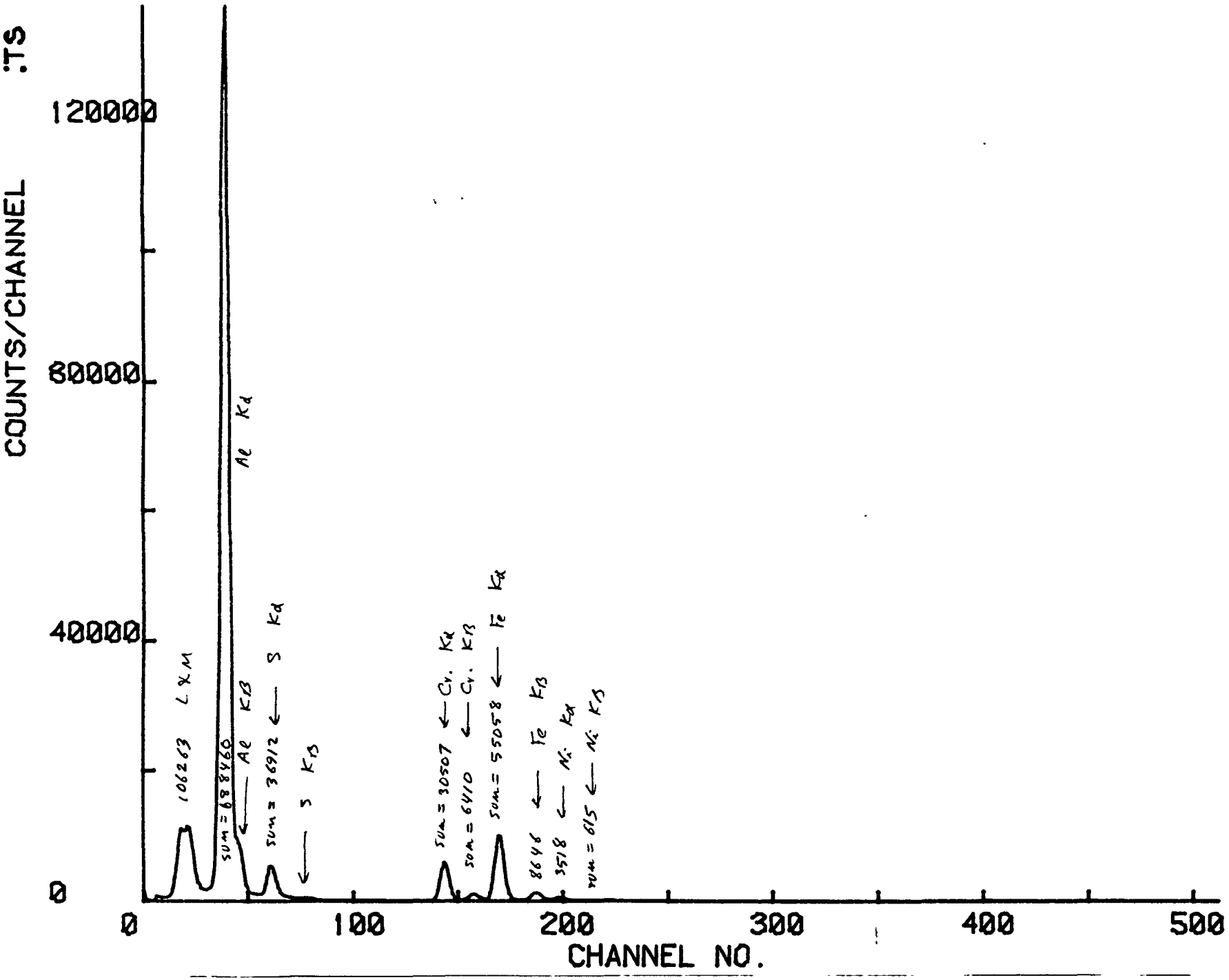

Fig. 92 Al PIXE Spectrum - Specimen C

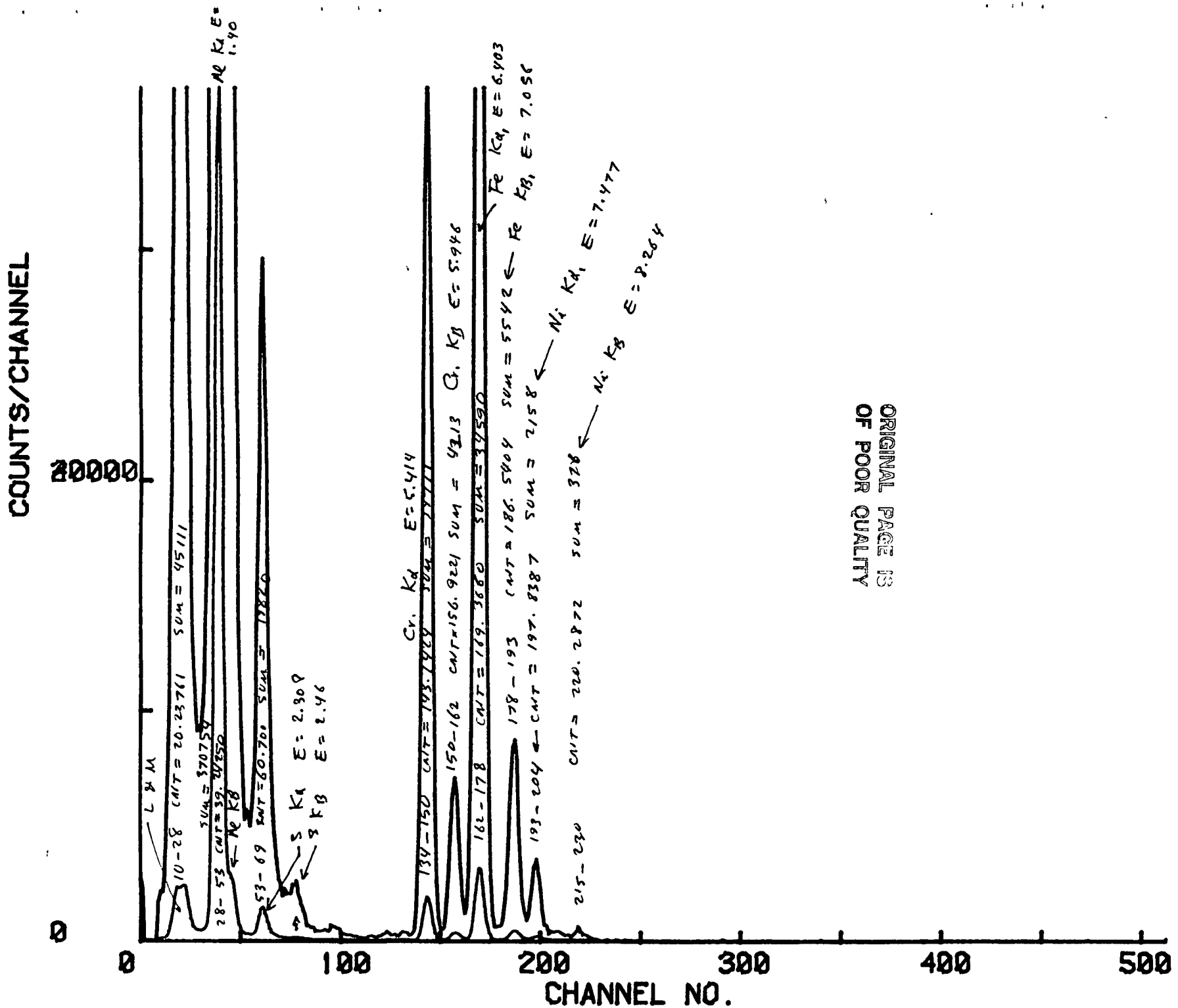

ORIGINAL PAGE IS
OF POOR QUALITY

Fig. 93 Al PIXE Spectrum - Specimen F

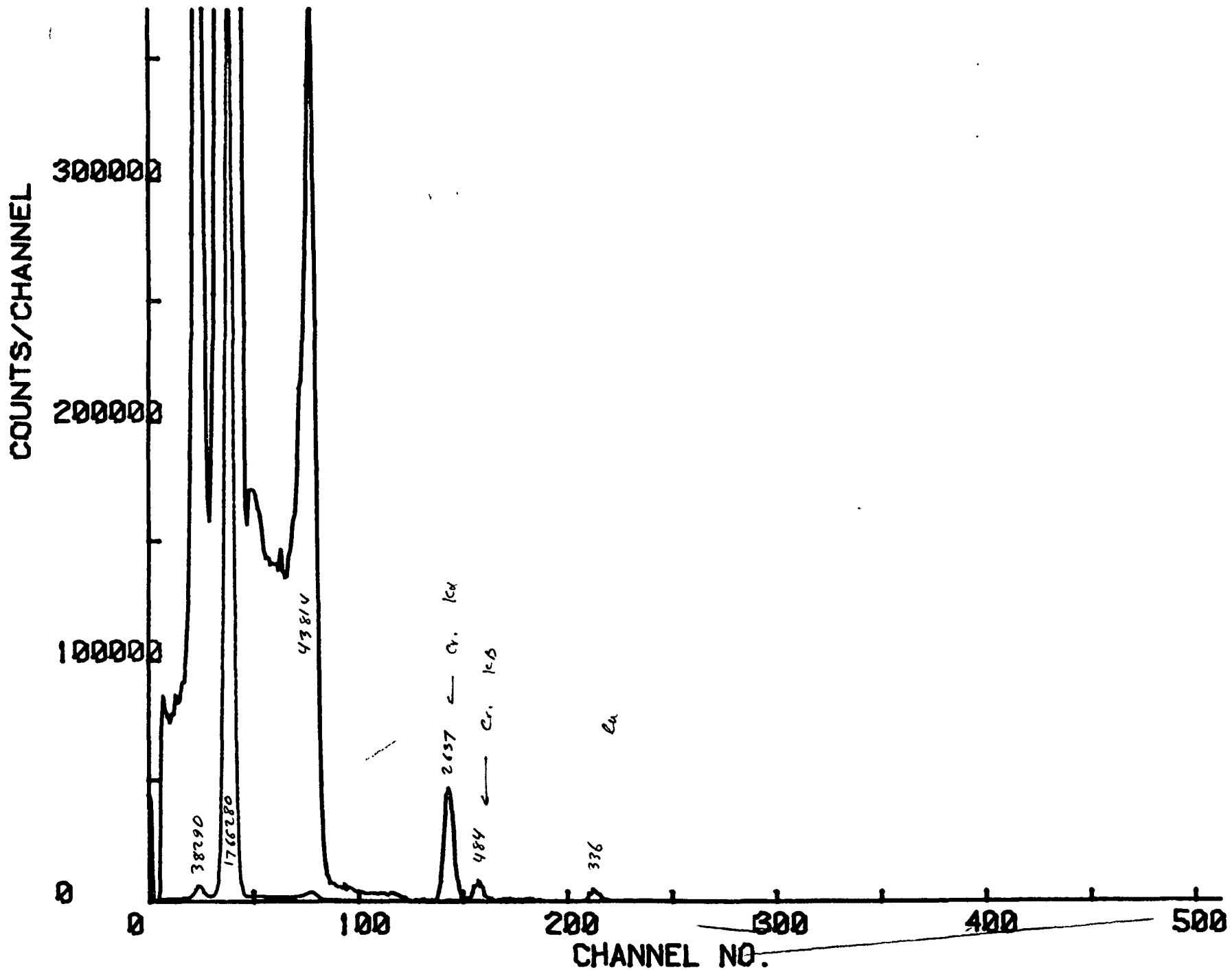

Fig. 94 Cr PIXE Spectrum - Specimen C

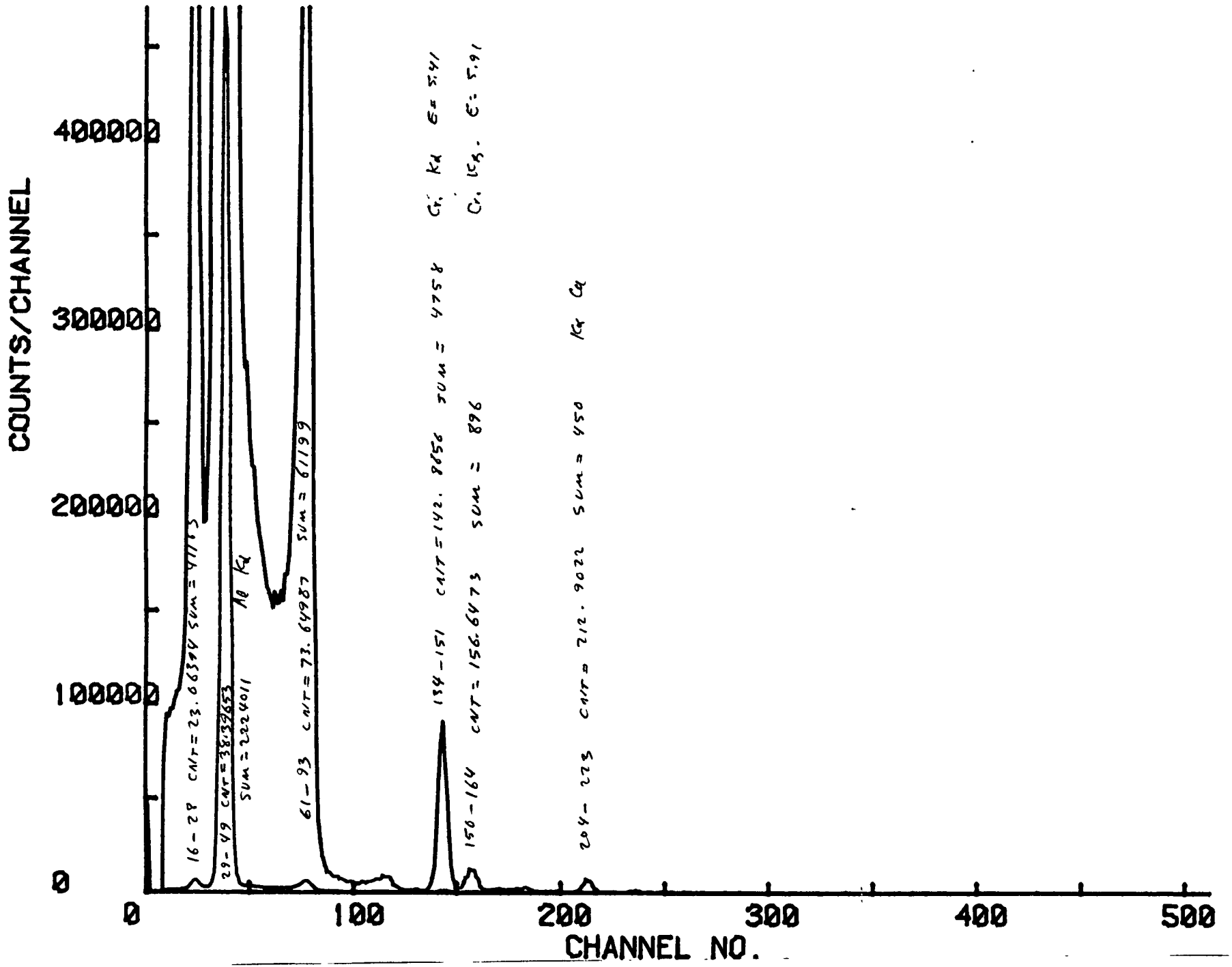

Fig. 95 Cr PIXE Spectrum - Specimen F

Fe55 calibration

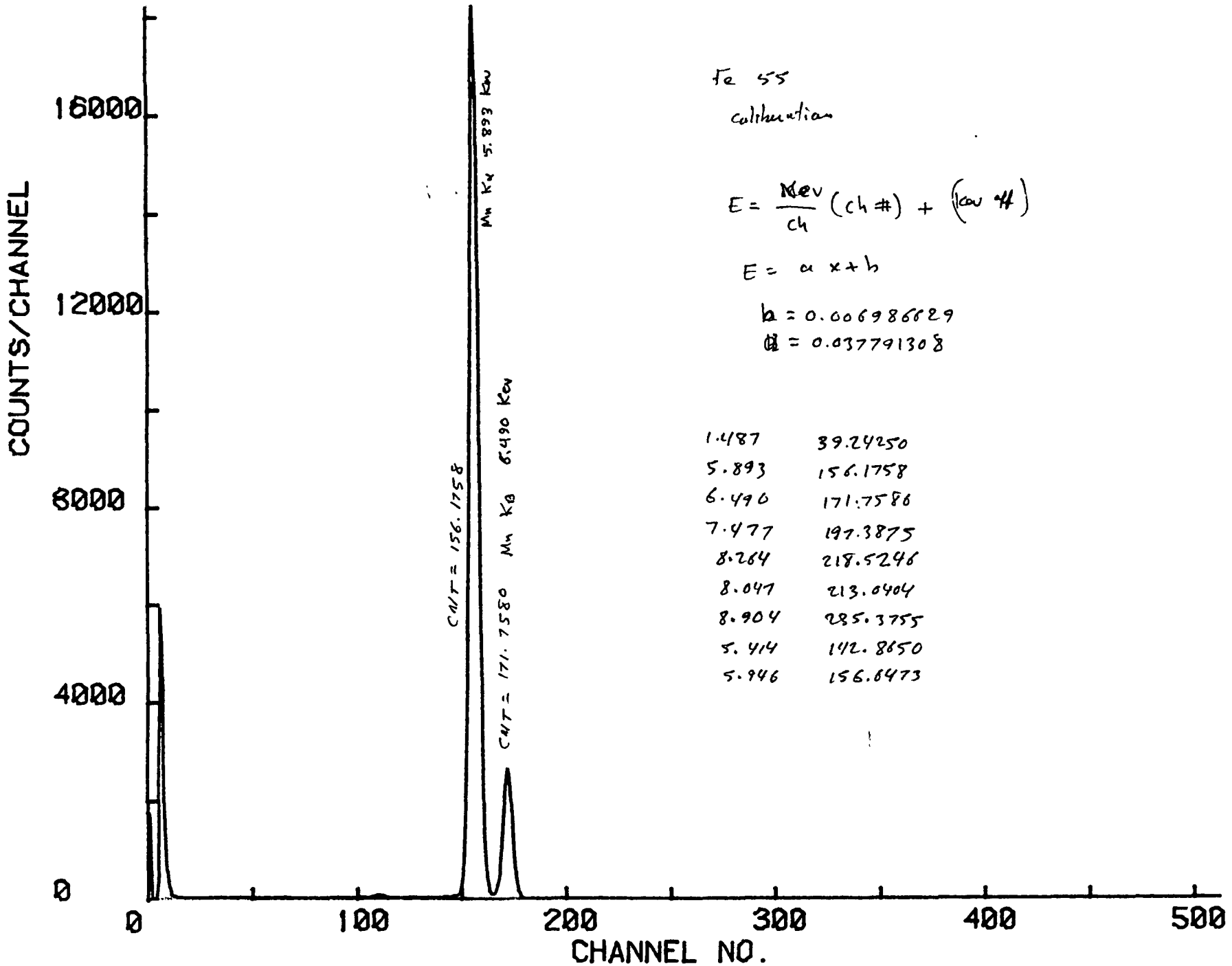

Fe 55
calibration

$$E = \frac{\text{Kev}}{ch}(ch\#) + (\text{Kev } 0)$$

$$E = ax + b$$

b = 0.006986829
a = 0.037791308

1.487	39.24250
5.893	156.1758
6.490	171.7586
7.477	197.3875
8.264	218.5246
8.047	213.0404
8.904	235.3755
5.414	142.8650
5.946	156.6473

Fig. 96 Iron Calibration PIXE Spectrum

Table 1

ELLIPSOMETER DATA ON EVAPORATED METALS

Specimen, Thickness (nominal), & the Substrate	Data Point,	Before Flight n	Before Flight k	After Flight n	After Flight k
Ag (2000 Å) on 6061 T6 Al	A.1a	0.5107	3.2876	0.2907	3.1972
	A.1b	0.5142	3.2885	0.2874	3.1946
	A.2a	0.5067	3.2629	0.2857	3.2054
	A.2b	0.5071	3.2644	0.2823	3.2028
	B.1a	0.2361	3.5285	1.9270	1.5010
	B.1b	0.2363	3.5303	1.9307	1.4958
	B.2a	0.2458	3.5206	1.9319	1.4963
	B.2b	0.2442	3.5225	1.9308	1.4939
Au (5000 Å) on 6061 T6 Al	A.1a	0.4955	2.4255	0.5025	2.3958
	A.1b	0.4951	2.4191	0.5041	2.3976
	A.2a	0.4800	2.3873	0.5024	2.3820
	A.2b	0.4818	2.3858	0.5014	2.3822
	B.1a	0.4999	2.4440	0.5615	2.2713
	B.1b	0.5004	2.4461	0.5630	2.2729
	B.2a	0.4971	2.4370	0.5352	2.2144
	B.2b	0.4987	2.4388	0.5360	2.2172
Pd (5000 Å) on 6061 T6 Al	A.1a	1.6781	3.2789	1.6877	3.1213
	A.1b	1.6815	3.2827	1.6890	3.1201
	A.2a	1.6816	3.2459	1.6976	3.1339
	A.2b	1.6756	3.2446	1.7186	3.1605
	B.1a	1.6368	3.1840	1.4505	2.8146
	B.1b	1.6392	3.1841	1.4478	2.8203
	B.2a	1.6406	3.1653	1.4373	2.8030
	B.2b	1.6408	3.1630	1.4334	2.8028
Pt (500 Å) on 6061 T6 Al	A.1a	2.2334	2.6452	2.1549	2.6887
	A.1b	2.2424	2.6427	2.1549	2.6832
	A.2a	2.2261	2.6414	2.1577	2.6866
	A.2b	2.2273	2.6420	2.1581	2.6887
	B.1a	2.1611	3.2019	1.8115	3.1422
	B.1b	2.1600	3.2035	1.8103	3.1434
	B.2a	2.1278	3.2276	1.8162	3.1538
	B.2b	2.1253	3.2281	1.8091	3.1519
Ni (2000 Å) on 6061 T6 Al	A.1a	1.8451	2.8488	1.7183	2.9088
	A.1b	1.8460	2.8455	1.7215	2.9097
	A.2a	1.8748	2.8692	1.7150	2.9165
	A.2b	1.8759	2.8701	1.7192	2.9183
	B.1a	1.8350	2.8343	1.8177	2.2375
	B.1b	1.8350	2.8322	1.8162	2.2379
	B.2a	1.8310	2.8944	1.8229	2.2426
	B.2b	1.8289	2.8968	1.8236	2.2417

Table 1 (continued)

ELLIPSOMETER DATA ON EVAPORATED METALS

Specimen, Thickness (nominal), & the Substrate	Data Point,	Before Flight n	Before Flight k	After Flight n	After Flight k
Cu (2000 A) on 303 stainless steel	A.1a	0.9028	2.5370	0.9379	2.3463
	A.1b	0.9033	2.5381	0.9378	2.3486
	A.2a	0.9280	2.5715	0.9331	2.3487
	A.2b	0.9269	2.5720	0.9327	2.3477
	B.1a	0.9468	2.5995	0.6282	1.8977
	B.1b	0.9510	2.6000	0.6363	1.9071
	B.2a	0.9509	2.6052	0.7431	1.9822
	B.2b	0.9509	2.6052	0.7415	2.0117
Al (500 A) on 303 stainless steel	A.1a	0.9953	5.6940	1.6199	5.1394
	A.1b	1.0139	5.7003	1.6246	5.1405
	A.2a	1.0053	5.6867	1.4739	4.8619
	A.2b	1.0054	5.6744	1.6275	5.1387
	B.1a	1.0007	5.3867	1.4225	4.3317
	B.1b	1.0052	5.3889	1.4261	4.3325
	B.2a	0.9894	5.3312	1.4139	4.3221
	B.2b	0.9972	5.3322	1.4117	4.3234
Cr (500 A) on 2219-T87 Al	A.1a	2.9355	2.9470	2.7999	3.1743
	A.1b	2.9300	2.9457	2.8037	3.1756
	A.2a	2.9406	2.9330	2.8191	3.1669
	A.2b	2.9469	2.9388	2.8252	3.1551
	B.1a	2.9232	2.9506	2.4469	2.5845
	B.1b	2.9322	2.9527	2.4392	2.5851
	B.2a	2.9237	2.9486	2.4344	2.5781
	B.2b	2.9168	2.9534	2.4338	2.5796

Table 2

RUTHERFORD BACKSCATTERING DATA

Metal Specimen		Before Flight L (A)		After Flight L (A)	B/A	F/C
Ag	B	2325	F	3214	1.00	1.42
	A	2325	C	2268		
Ni	B	1931	F	1906	0.99	0.96
	A	1951	C	1986		
Pd	B	6401	F	6368	1.01	0.98
	A	6342	C	6513		
Cu	B	2033	F	2107	0.96	0.99
	A	2115	C	2130		
Au	B	4994	F	5173	0.95	0.97
	A	5254	C	5310		
Cr	B	895	F	814	1.03	1.06
	A	870	C	766		
Pt	B	530	F	799	1.00	1.21
	A	529	C	660		
Al	B	-----		1095	-----	-----
	A	-----		1277		